PNNL-35037 Rev 0
EWG-RPT-043 Rev 0

Enhanced Hanford High-Fluoride Waste Glass Property Data Development: Phase 1

October 2023

RL Russell
D Kim
JD Vienna
JB Lang
S Baird
D Bellofotto
SE Sannoh
D Cutforth
B Westman

U.S. DEPARTMENT OF ENERGY

Prepared for the U.S. Department of Energy
under Contract DE-AC05-76RL01830

PACIFIC NORTHWEST NATIONAL LABORATORY
operated by
BATTELLE
for the
UNITED STATES DEPARTMENT OF ENERGY
under Contract DE-AC05-76RL01830

Printed in the United States of America

Available to DOE and DOE contractors from the
Office of Scientific and Technical Information,
P.O. Box 62, Oak Ridge, TN 37831-0062;
ph: (865) 576-8401
fax: (865) 576-5728
email: reports@adonis.osti.gov

Available to the public from the National Technical Information Service
5301 Shawnee Rd., Alexandria, VA 22312
ph: (800) 553-NTIS (6847)
email: orders@ntis.gov <https://www.ntis.gov/about>
Online ordering: http://www.ntis.gov

PNNL-35037 Rev 0
EWG-RPT-043 Rev 0

Enhanced Hanford High-Fluoride Waste Glass Property Data Development: Phase 1

October 2023

RL Russell
D Kim
JD Vienna
JB Lang
S Baird
D Bellofotto
SE Sannoh
D Cutforth
B Westman

Prepared for
the U.S. Department of Energy
under Contract DE-AC05-76RL01830

Pacific Northwest National Laboratory
Richland, Washington 99354

Executive Summary

This study focused on investigating the effects of fluorine concentration on simulated high-level waste glass properties to eventually establish a fluorine limit (as a single-component or multiple-component constraint) for glass formulations for high-fluoride Hanford wastes. This is a first step to provide data to understand the impacts of changing flowsheets on the mission duration and extent. A test matrix of 20 high-fluoride glasses was generated, and the chemical compositions were measured. The following properties were measured and tested against current model predictions: crystal formation after centerline canister cooling, crystallinity as a function of temperature, density, viscosity, electrical conductivity, toxic leaching characteristics using the toxicity characteristic leach profile (TCLP), product consistency using the product consistency test (PCT), and SO_3 solubility.

Overall, current models failed to adequately predict most of the properties, possibly due to differences in compositional space used to generate the models and the current test matrix. Additional work is needed to more accurately assess the impacts of high-fluoride wastes on Hanford processing, including additional data collection over a broader composition region and model development for the key models of interest such as PCT and TCLP.

Acknowledgments

The authors gratefully acknowledge the financial support provided by the U.S. Department of Energy Office of River Protection Waste Treatment and Immobilization Plant Project, managed by Tom Fletcher, with technical oversight by Albert Kruger.

The authors thank Madison Hsieh of Savannah River National Laboratory for her help in the analysis and testing of the glasses. We also thank Tongan Jin (PNNL) for his technical review, Matt Wilburn (PNNL) for his editorial review, and David MacPherson, Cassie Martin, and Chrissy Charron (PNNL) for programmatic support during the conduct of this work.

Acronyms and Abbreviations

ARG-1	Analytical Reference Glass-1
CCC	canister centerline cooling (heat treatment)
CF	crystal fraction
cTCLP	measured concentration of element in toxicity characteristic leaching procedure solution
DFHLW	Direct Feed High-Level Waste
DFLAW	Direct Feed Low-Activity Waste
DIW	deionized water
DWPF	Defense Waste Processing Facility
DOE	U.S. Department of Energy
EC	electrical conductivity
EPA	U.S. Environmental Protection Agency
η1150	viscosity at 1150 °C
HLW	high-level waste
IC	ion chromatography
ICP-OES	inductively coupled plasma – optical emission spectroscopy
KH	potassium hydroxide digestion
LAW	low-activity waste
LM	lithium metaborate/tetraborate fusion
NIST	National Institute of Standards and Technology
NQAP	Nuclear Quality Assurance Program
ORP	Office of River Protection
PCT	product consistency test
PF	sodium peroxide fusion
PNNL	Pacific Northwest National Laboratory
QA	quality assurance
RCRA	Resource Conservation and Recovery Act
rTCLP	normalized release of element in toxicity characteristic leaching procedure
SRNL	Savannah River National Laboratory
SSM	sulfur saturated melt
S/V	surface area-to-solution volume
TL	liquidus temperature
TM	melting temperature
TCLP	toxicity characteristic leaching procedure
UTS	Universal Treatment Standards
VFT	Vogel-Fulcher-Tamman

WTP	Waste Treatment and Immobilization Plant
XRD	X-ray diffraction

Contents

Figures

Tables

1.0 Introduction

The U.S. Department of Energy (DOE) Office of River Protection (ORP) requested that Pacific Northwest National Laboratory (PNNL) provide expert evaluation and experimental work in support of the River Protection Project vitrification technology development (DOE 2012). The long-term objective of this work is to expand the Hanford Site waste glass database and property-composition models to cover the balance of the Hanford Site tank waste treatment and immobilization mission.

This report presents the glass compositions and glass property data developed in the Hanford high-level waste (HLW) glass region of high fluoride. When the data development effort for enhanced Hanford waste glasses (EWGs) is complete, enhanced waste glass property models will be developed. Section 1.1 summarizes the background of high-fluoride waste and glass. Section 1.2 summarizes the high-fluoride waste glass composition region and test matrix tested in this study. Section 1.3 documents the quality assurance (QA) program used in performing the work discussed in this report.

1.1 Background

To begin the treatment of the nuclear waste as soon as possible, ORP is considering implementing a sequenced approach for vitrification of low-activity waste (LAW) and HLW at the Hanford Site. The sequenced approach includes Direct Feed Low-Activity Waste (DFLAW). One possible option for HLW startup includes a Direct Feed High-Level Waste (DFHLW) flowsheet in which Hanford tank waste is immobilized in the HLW Facility at the Hanford Waste Treatment and Immobilization Plant (WTP) prior to the implementation of a pretreatment process. If brought into practice, the WTP Pretreatment Facility would be bypassed, which would mean that the ultrafiltration and caustic leaching operations would either not be performed or would be replaced by an interim pretreatment function (Geeting and Hallen 2005; McGinnis et al. 1999). The proposed changes in the processing of both LAW and HLW streams are likely to affect the downstream vitrification operations. One potential major challenge in DFHLW feed compared to pretreated feed is expected high concentration of fluoride salts (Goel et al. 2019). Fluorine may promote salt accumulation in the melter (in concert with sulfate, chromate, phosphate, molybdate, etc.) or crystallize as alkali or alkaline-earth fluorides (Vienna et al. 2009).

Wastes generated from the stripping of zircaloy cladding from fuel rods by dissolving them in NH_4F/NH_4NO_3 solutions via the Zirflex process followed by neutralization with NaOH are rich in F-containing salts (Reynolds et al. 2014). For example, unwashed solids from tanks AW-103 and AW-105 contain up to 20 wt% F (Hanford 2020).

The current waste processing plan is to wash this waste with water to dissolve the soluble fluoride salts. However, unwashed solids will be treated under the DFHLW flowsheet, resulting in significantly elevated F concentrations in DFHLW glasses.

There is minimal literature addressing the problem of fluoride limit in HLW glass, and therefore it is important to understand the factors controlling the fluoride solubility in HLW glasses and to develop a model constraining the fluoride loading in DFHLW glasses (Jin et al. 2020). This data is also needed to develop a minimal impact flowsheet for DFLAW processing without risk of significant technical challenges in HLW processing.

1.2 Waste Glass Composition Region and Test Matrix

This section discusses the development of the experimental glass composition region and test matrix for the high-fluoride concentration waste glasses to be tested.

The preliminary projected compositions of the directly fed high-fluoride waste were provided by Washington River Protection Solutions for two tanks containing high amounts of fluoride (AW-103 and AW-105) that were planned to be under-washed (sufficient to remove nitrate, nitrite, chloride, and inorganic carbon as well as some sodium from the waste, without significant F removal). The tank waste compositions are listed in Table 1.1. The waste composition was normalized to sum to 1 after removing the radioactive UO_3 component.

Table 1.1. Composition (mass fraction) of Waste Batches Used for High-Fluoride Waste Glass Formulations

Component	AW-103	AW-105
Al_2O_3	0.0121	0.0821
CaO	0.0010	0.0027
Cr_2O_3	0.0008	0.0041
F	0.2015	0.1121
Fe_2O_3	0.0035	0.0071
K_2O	0.0028	0.0161
MnO	0.0000	0.0045
Na_2O	0.3587	0.5142
P_2O_5	0.0020	0.0073
SiO_2	0.0090	0.0091
SO_3	0.0004	0.0109
ZrO_2	0.4083	0.2298
SUM	1.0000	1.0000

Glass formulation calculations were performed using the existing glass property models given in Vienna et al. (2016) for spinel liquidus temperature (T_L) and viscosity at 1150 °C (η_{1150}) and in Piepel et al. (2008) for product consistency test (PCT) responses. Because none of the existing models are valid for the glass composition region being explored in this study, the predicted properties by these models were used as general guidance only. Table 1.2 summarizes the lower and upper bounds of component concentrations in the glasses resulting from the glass formulation efforts. The components listed in Table 1.2 include those that are high in waste and/or are expected to limit the waste loading in glass (Al_2O_3, F, K_2O, Na_2O, and ZnO, ZrO_2, and others) and the glass-forming additive components (B_2O_3, CaO, Li_2O, and SiO_2).

Table 1.2. Lower and Upper Bound of Component Concentrations (mass fraction) in the High-Fluoride Waste Glasses

Component	Lower Bound (wt%)	Upper Bound (wt%)
Al_2O_3	1.8	10.0
B_2O_3	4.0	12.0
CaO	0.0	6.0
F	2.0	7.0
K_2O	0.0	1.6
Li_2O	0.0	6.0
Na_2O	12.0	24.0
SiO_2	35.0	53.0
ZnO	0.0	4.0
ZrO_2	4.0	13.5
Others [(a)]	0.2	1.4

(a) The Others component was composed of the following mixture of five minor components (expressed as wt%): Cr_2O_3 = 0.2, Fe_2O_3 = 0.4, MnO = 0.2, P_2O_5 = 0.3, and SO_3 = 0.4.

A space-filling technique was used with JMP version 13.0 (SAS Institute Inc. 2016) software to generate a test matrix of 20 glasses. This experimental design was chosen to spread the 11 components that were selected to vary throughout the Hanford high-fluoride waste composition region as evenly as possible. The 20 high-fluoride waste glasses comprising the test matrix are listed in Table 1.3.

This report summarizes the experimental methods to fabricate, heat treat, and test the 20-glass high-fluoride waste test matrix prepared at PNNL. Measured properties relating to glass performance and processing are described in this report and are provided in appendices.

Table 1.3. Targeted Compositions (mass fractions) for the High-Fluoride Waste Glasses

	Glass ID									
Component	HFG1-01	HFG1-02	HFG1-03	HFG1-04	HFG1-05	HFG1-06	HFG1-07	HFG1-08	HFG1-09	HFG1-10
Al_2O_3	0.09700	0.07942	0.03863	0.01884	0.03808	0.05564	0.09919	0.03079	0.05755	0.06204
B_2O_3	0.06973	0.05870	0.08435	0.09263	0.09734	0.06076	0.11383	0.04531	0.04304	0.10087
CaO	0.00826	0.02795	0.02191	0.05393	0.00303	0.01368	0.00042	0.04168	0.05262	0.03353
Cr_2O_3	0.00091	0.00085	0.00079	0.00128	0.00193	0.00106	0.00042	0.00180	0.00183	0.00027
F	0.05322	0.06007	0.05231	0.03096	0.03773	0.05056	0.04376	0.06523	0.06761	0.04255
Fe_2O_3	0.00182	0.00171	0.00158	0.00256	0.00387	0.00212	0.00084	0.00360	0.00365	0.00054
K_2O	0.01554	0.01001	0.00763	0.01497	0.00244	0.01174	0.01263	0.01343	0.00359	0.00812
Li_2O	0.05594	0.01758	0.00057	0.00664	0.02668	0.03415	0.00497	0.00463	0.03823	0.02846
MnO	0.00091	0.00085	0.00079	0.00128	0.00193	0.00106	0.00042	0.00180	0.00183	0.00027
Na_2O	0.13834	0.15530	0.16652	0.23277	0.22362	0.22984	0.18857	0.23412	0.17422	0.19718
P_2O_5	0.00137	0.00128	0.00118	0.00192	0.00290	0.00159	0.00063	0.00270	0.00274	0.00040
SiO_2	0.43738	0.52836	0.48259	0.45880	0.43486	0.45732	0.47500	0.41598	0.46894	0.35312
SO_3	0.00182	0.00171	0.00158	0.00256	0.00387	0.00212	0.00084	0.00360	0.00365	0.00054
ZnO	0.03471	0.01333	0.03226	0.03366	0.00720	0.00446	0.01038	0.00953	0.03896	0.03851
ZrO_2	0.08305	0.04289	0.10733	0.04720	0.11452	0.07392	0.04812	0.12580	0.04156	0.13360
Total	1.00000	1.00000	1.00000	1.00000	1.00000	1.00000	1.00000	1.00000	1.00000	1.00000

Table 1.3. (cont.)

	Glass ID									
Component	HFG1-11	HFG1-12	HFG1-13	HFG1-14	HFG1-15	HFG1-16	HFG1-17	HFG1-18	HFG1-19	HFG1-20
Al_2O_3	0.07773	0.02737	0.08557	0.02526	0.05051	0.08682	0.04933	0.05277	0.08812	0.09885
B_2O_3	0.09465	0.06902	0.08105	0.04945	0.08532	0.04257	0.04044	0.11800	0.08301	0.04540
CaO	0.00080	0.05939	0.03619	0.05743	0.04619	0.05811	0.03772	0.00488	0.04524	0.02087
Cr_2O_3	0.00169	0.00032	0.00165	0.00056	0.00177	0.00139	0.00076	0.00062	0.00032	0.00118
F	0.06968	0.06699	0.04568	0.04479	0.02125	0.02189	0.02547	0.03882	0.05659	0.02717
Fe_2O_3	0.00337	0.00065	0.00330	0.00113	0.00355	0.00278	0.00152	0.00124	0.00064	0.00236
K_2O	0.00897	0.00642	0.00510	0.00118	0.01440	0.01310	0.00197	0.00389	0.01147	0.00027
Li_2O	0.01484	0.04750	0.05915	0.01504	0.04016	0.05842	0.05394	0.04910	0.01305	0.04243
MnO	0.00169	0.00032	0.00165	0.00056	0.00177	0.00139	0.00076	0.00062	0.00032	0.00118
Na_2O	0.17683	0.12645	0.12167	0.22035	0.15702	0.20316	0.17748	0.12936	0.22557	0.23821
P_2O_5	0.00253	0.00049	0.00247	0.00085	0.00266	0.00209	0.00114	0.00093	0.00048	0.00177
SiO_2	0.39540	0.47255	0.48981	0.48453	0.50110	0.37396	0.44712	0.50397	0.38764	0.40989
SO_3	0.00337	0.00065	0.00330	0.00113	0.00355	0.00278	0.00152	0.00124	0.00064	0.00236
ZnO	0.02463	0.00136	0.01750	0.01367	0.00551	0.00041	0.02795	0.02317	0.03063	0.03868
ZrO_2	0.12384	0.12052	0.04593	0.08409	0.06523	0.13114	0.13288	0.07138	0.05625	0.06940
Total	1.0000	1.0000	1.0000	1.00000	1.00000	1.00000	1.00000	1.00000	1.00000	1.00000

1.3 Quality Assurance

This work was performed in accordance with the PNNL Nuclear Quality Assurance Program (NQAP). The NQAP complies with the DOE Order 414.1D, *Quality Assurance*, and 10 CFR 830 Subpart A, *Quality Assurance Requirements*. The NQAP uses NQA-1-2012, *Quality Assurance Requirements for Nuclear Facility Application*, as its consensus standard and NQA-1-2012, Subpart 4.2.1, as the basis for its graded approach to quality.

The NQAP works in conjunction with PNNL's laboratory-level Quality Management Program, which is based on the requirements as defined in DOE Order 414.1D, *Quality Assurance*, and 10 CFR 830, *Nuclear Safety Management*, Subpart A, Quality Assurance Requirements.

The work of this report was performed to the QA technology readiness level 4. This work was performed to support technology development. Data obtained may be used to support design input. Work and deliverables will comply with the PNNL NQAP QA Program for this grading level and any additional controls.

2.0 Test Methods

This section describes how the data was obtained for the 20 high-fluoride waste glasses described in Section 1.0. The descriptions include the methods for glass fabrication (Section 2.1), chemical composition analysis (Section 2.2), density determination (Section 2.3), secondary phase identification from canister centerline cooling (CCC) samples (Section 2.4), viscosity measurement (Section 2.5), electrical conductivity (EC) measurement (Section 2.6), crystal fraction (CF) and T_L determination (Section 2.7), PCT response (Section 2.8), toxicity characteristic leaching procedure (TCLP) measurement (Section 2.9), and sulfate solubility measurement for these test glasses (Section 2.10).

2.1 Glass Fabrication

Glass fabrication was performed according to the PNNL procedure *Glass Batching and Melting* (WFDL-GBM-1, Rev 2).[1] Single metal oxides, single metal carbonates, boric acid, and sodium salts (including NaF) were weighed out in the appropriate masses to form the target glass composition for each glass and then placed in a plastic bag. After thoroughly mixing in the plastic bag for at least 30 s and until uniform color developed, the powders were transferred into an agate milling chamber and milled for 2 min in the Angstrom vibratory mill. The powders were then transferred to a clean Pt-10%Rh (hereafter referred to as Pt-alloy) crucible for melting using a two-step melt process. The first melt was of the raw materials after mechanically mixing in an agate milling chamber. Initial melting was performed at a temperature of 1150 °C for 1 h for the compositions to melt and form glasses. A second melt of the glass at 1150 °C for 1 h was accomplished after the first melt was quenched and the glass was ground to a fine powder in a tungsten carbide milling chamber in the Angstrom vibratory mill.

Several of the glasses were opaque with brown stripes and others were clear with brown clouds in them. The morphology and color of each quenched glass are shown in Appendix A. Because of this, these glasses were analyzed by X-ray diffraction (XRD) to try to determine the cause of these responses; the results are shown in Appendix B. The primary crystals found were fluoride salts (LiF, NaF, and CaF_2). Eight glasses were found to be amorphous, and two glasses were not analyzed.

2.2 Chemical Analysis of Glass Composition

To confirm that the "as-fabricated" glasses corresponded to the specified target compositions, a representative sample of each glass was chemically analyzed at Savannah River National Laboratory (SRNL). Three preparation techniques, including sodium peroxide fusion (PF), lithium metaborate/tetraborate fusion (LM), and potassium hydroxide digestion (KH), were used to prepare the glass samples, in duplicate, for analysis.

Each of the duplicate samples was analyzed twice for each element of interest by inductively coupled plasma-optical emission spectroscopy (ICP-OES) and ion chromatography (IC), for a total of four measurements per element per glass. Glass composition standards were also intermittently prepared and analyzed to assess the performance of the ICP-OES and IC instruments over the course of these analyses. Specifically, several samples of the Analytical Reference Glass-1 (ARG-1) (Smith 1993) and several samples of the low-activity reference material (Ebert and Wolfe 1999) were included as part of the SRNL analytical plan. The preparation and measurement methods used for each of the reported glass analytes are listed in Table 2.1.

[1] Russell, RL. 2016. *Glass Batching and Melting.* WFDL-GBM-1, Rev. 2.

A detailed analysis of the chemical composition measurements is published elsewhere (Hsieh 2021a). A short summary of these analyses is included in Section 3.1.

Table 2.1. Preparation and Measurement Methods Used in Measuring Concentrations of the Analytes in the High-Fluoride Waste Glasses

Analyte	Preparation Method	Measurement Method
Al	LM	ICP-OES
B	PF	ICP-OES
Ca	LM	ICP-OES
Cr	LM	ICP-OES
F	KH	IC
Fe	LM	ICP-OES
K	LM	ICP-OES
Li	PF	ICP-OES
Mn	LM	ICP-OES
Na	LM	ICP-OES
P	LM	ICP-OES
Si	PF	ICP-OES
S	LM	ICP-OES
Zn	LM	ICP-OES
Zr	PF	ICP-OES

PF = peroxide fusion
LM = lithium metaborate/tetraborate fusion
KH = potassium hydroxide digestion
ICP-OES = inductively coupled plasma-optical emission spectrometry
IC = ion chromatography

2.3 Glass Density

The room temperature density of each glass was measured according to PNNL procedure, *Density Using a Gas Pycnometer* (EWG-OP-0045),[2] using a MicroMeritics AccuPyc II 1340 gas pycnometer (MicroMeritics, Norcross, GA) with approximately 1.0 to 1.5 g of glass pieces. The glass was loaded into a vial and placed within the instrument. The instrument then determined the density by the difference in amount of helium gas needed to fill the vial with and without the glass present. After five runs for each glass, the average glass densities were calculated. The pycnometer was calibrated before and after measurements for that day using a National Institute of Standards and Technology (NIST) traceable standard tungsten carbide ball. These results are discussed in Section 3.2.

2.4 Canister Centerline Cooling

A portion (~150 g) of each test glass was subjected to the simulated CCC temperature profile shown in Table 2.2 and Figure 2.1.

[2] Russell RL. 2017. *Density Using a Gas Pycnometer*. EWG-OP-0045, Rev. 0.0.

Table 2.2. CCC Heat Treatment Schedule

Segment	Start Time (min)	Start Temp (°C)	Rate (°C/min)	End Time (min)	End Temp (°C)
1	0	MT[(a)]	0.0	30	MT[(a)]
2	30	1150	-12.5	38	1050
3	38	1050	-1.5556	83	980
4	83	980	-0.8065	145	930
5	145	930	-0.5914	238	875
6	238	875	-0.3876	367	825
7	367	825	-0.2525	565	775
8	565	775	-0.2778	745	725
9	745	725	-0.3040	1814	400

(a) MT = Melt temperature for the glass being tested.

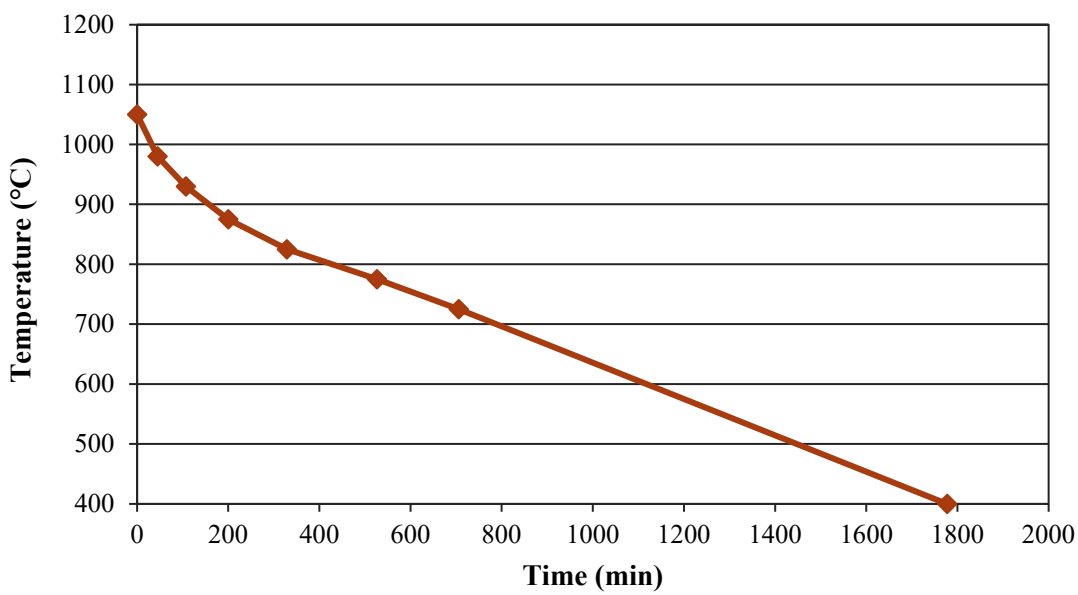

Figure 2.1. Plot of Temperature Schedule during CCC Treatment of Hanford High-Fluoride Glasses

This profile is the temperature schedule of CCC treatment for Hanford HLW glasses planned for use at the WTP[3] and modified by PNNL to include a 30-min soak at the glass melt temperature before the cooling began. Pieces of quenched glass, <3 cm in diameter, were placed in a Pt-alloy crucible and covered with a Pt-alloy lid. The glass samples were placed in a furnace preheated to the glass melting temperature of 1150 °C. After 30 min at the melting temperature, the furnace temperature was quickly dropped to 1050 °C and the cooling profile started. It progressed down to about 400 °C based on seven cooling segments shown in Table 2.2. The starting temperatures for the seven segments of cooling were 1050 °C, 980 °C, 930 °C, 875 °C, 825 °C, 775 °C, and 725 °C.

[3] Petkus LL. 2003. "Canister Centerline Cooling Data, Revision 1," to C.A. Musick, CCN: 074851, October 29, 2003, River Protection Project, Hanford Tank Waste Treatment and Immobilization Plant, Richland, Washington.

The amount and type of crystalline phases that formed during CCC treatment were analyzed by XRD according to Section 12.4.4 of the standard ASTM International procedure, *Standard Test Method for Determining Liquidus Temperature of Immobilized Waste Glasses and Simulated Waste Glasses* (ASTM C1720). Powdered glass samples were prepared using roughly 5 wt% CeO_2 as an internal standard phase with between 1 g and 2 g of powdered glass. Glass and CeO_2 were milled together for 1 min in a 10 cm^3 tungsten carbide disc mill. The powdered glass samples were loaded into XRD sample holders and scanned at a 0.015° 2θ step size, 1.5 s dwell time, from 5° to 75° 2θ scan range. XRD spectra were analyzed with TOPAS® 4.2 Software (Bruker AXS Inc., Madison, Wisconsin) for phase identification and Rietveld refinement to semi-quantify the amounts of crystal phases on some samples with high crystalline content. These results are discussed in Section 3.3.

2.5 Viscosity

The viscosities of the quenched glasses were measured as a functions of temperature using an automated Anton Paar FRS 1600 Furnace Rheometer System, according to the PNNL procedure *High-Temperature Viscosity Measurement Using Anton Paar FRS1600* (EWG-OP-0046, Rev. 0.0).[4] Approximately 200 g of each glass was first crushed in a tungsten carbide milling chamber for 0.05 min and about 25 to 30 mL, or ~70 g, of glass was placed into a Pt-alloy cylindrical cup. It was then heated to ~1150 °C and maintained until thermal equilibrium was reached. A Pt-alloy spindle was then lowered into the cup of molten glass. An initial torque reading (at a constant spindle speed) was taken at ~1150 °C with subsequent measurements at target temperatures of 1050 °C, 950 °C, 1150 °C, 1250 °C, and then 1150 °C at thermal equilibrium using a hysteresis approach. The hysteresis approach allows for the potential impacts of crystallization (at lower temperatures) to be assessed (via reproducibility), with duplicate measurements being taken at approximately melting temperature (T_M) and volatilization (at higher temperatures) minimized by measuring viscosity at temperatures above T_M as the final viscosity measurement(s). The soak time was 30 min at each temperature. Prior to quenched glass viscosity measurements, the rheometer was calibrated using a standard glass [Defense Waste Processing Facility (DWPF) Startup Frit] as discussed in the literature (Crum et al. 2012). These results are discussed in Section 3.4.

2.6 Electrical Conductivity

The ECs of the quenched glasses were measured with an Anton Paar FRS 1600 Furnace Rheometer System as the high-temperature furnace and a Solartron Analytical 1455 Cell Test System (Solartron Analytical, Oak Ridge, TN) impedance analyzer according to the PNNL procedure *High-Temperature Electrical Conductivity Measurement* (EWG-OP-0047, Rev. 0.0).[5] Platinum plates (1.3 in. long by 0.28 in. wide) were placed parallel to each other with a separation of 0.367 in. A 50-mL glass sample was used for conductivity measurement in a Pt-alloy crucible. Before measuring ECs of the test matrix glasses, calibration was conducted at room temperature with reference solutions of KCl (0.1 M and 1 M) by measuring the resistance values at three frequencies (1, 10, and 100 kHz). Four readings were taken at each frequency over a period of 2 to 5 min. The calibration was then checked with DWPF standard glass at the higher temperatures (Crum et al. 2012). The averaged values of the four readings were then used to calculate the cell constant. For glass measurement, the sample was first heated to melting temperature and the probe was slowly lowered into the molten glass to a depth of 12.7 mm. After the temperature was stabilized, a scan from 1 MHz to 0.1 Hz in 3 min was conducted and resistance at 1 kHz was used to calculate the EC. The glass was held for 10 min at each temperature before measurement for temperature stabilization. Then two scans were made for each temperature. The EC was measured at four different

[4] McCarthy, BM. 2017. *High-Temperature Viscosity Measurement Using Anton Paar FRS1600*. EWG-OP-0046, Rev. 0.0.
[5] McCarthy, BM. 2017. *High-Temperature Electrical Conductivity Measurement*. EWG-OP-0047, Rev. 0.0.

temperatures in a range around the melting temperature of the glass. These results are discussed in Section 3.5.

2.7 Liquidus Temperature and Equilibrium Crystal Fraction

Prior to measuring the CF, the furnace temperature accuracy was verified using ARG-1 glass (Smith 1993). Data measured and captured for the standard glass check was stored and maintained with the batch glass data.

The T_L and CF as a function of temperature were measured in Pt-alloy boats with tight-fitting lids (to minimize volatility) according to the standard ASTM International procedure *Standard Test Method for Determining Liquidus Temperature of Immobilized Waste Glasses and Simulated Waste Glasses* (ASTM C1720). The heat treatment times and temperatures are reported in Table 2.3. The samples were then cold water quenched to stop crystals from forming upon cooling.

Table 2.3. Heat Treatment Temperatures and Duration Used for CF and TL Measurements

Heat Treatment Temperatures and Duration	Glasses Tested
950 °C–24 h	All glasses
850 °C–48 h	All glasses except 16, 17, and 20
800 °C–72 h	All glasses except 16, 17, and 20
1150 °C–24 h	16, 17, and 20
1050 °C–24 h	16, 17, and 20
1000 °C–24 h	16, 17, and 20

The CF formed during heat treatment was analyzed by XRD according to Section 12.4.4 of the standard ASTM International procedure *Standard Test Method for Determining Liquidus Temperature of Immobilized Waste Glasses and Simulated Waste Glasses* (ASTM C1720). Powdered glass samples were prepared using 5 wt% CeO_2 as an internal standard phase with between 1.5 and 2.5 g of glass powder. Glass and CeO_2 were milled together for 2 min in a 10-cm^3 tungsten carbide disc mill. The powdered samples were loaded into XRD sample holders and scanned at a 0.04° 2θ step size, 4-s dwell time, from 10° to 70° 2θ scan range. XRD spectra were analyzed with TOPAS 4.2 Software (Bruker AXS Inc., Madison, Wisconsin) for phase identification and Rietveld refinement to semi-quantify the amounts of crystal phases on some samples with high crystalline content. These results are discussed in Section 3.6.

Attempts to measure the T_L of the test-matrix glasses were done using the *Crystal Fraction Extrapolation Method* in ASTM C1720, where T_L is calculated by extrapolating CF as a function of temperature to zero crystals. These results are discussed in Section 3.6.

2.8 Product Consistency Test

PCT responses were measured in triplicate for quenched and CCC samples of each glass using Method A of the standard ASTM International procedure *Standard Test Methods for Determining Chemical Durability of Nuclear, Hazardous, and Mixed Waste Glasses and Multiphase Glass Ceramics: The Product Consistency Test (PCT)* (ASTM C1285). Also included in the PCT experimental test matrix and tested in triplicate were the ARM-1 glass (Mellinger and Daniel 1984) and blanks. Glass samples were ground, sieved to −100 +200 mesh, washed, and prepared according to the standard ASTM C1285 Method A. The prepared glass was added to water in a 1.5 g to 15 mL ratio, resulting in a glass surface

area-to-volume (S/V) ratio of approximately 2000 m^{-1}. The vessels used were desensitized Type 304L stainless steel. The vessels were closed, sealed, and placed into an oven at 90 ± 2 °C for 7 days ± 3 h.

After the 7 days at 90 °C, the vessels were removed from the oven and allowed to cool to room temperature. The final mass of the vessel and the solution pH were recorded on a data sheet. Each test solution was then filtered through a 0.45-µm-size filter and acidified to 1 vol% using high-purity HNO_3 to assure that the cations present remained in solution. The resulting solutions were analyzed by SRNL for Si, Na, B, and Li. Samples of a multi-element, standard solution were also analyzed as a check on the accuracy of the ICP-OES. Normalized releases in g/L were calculated based on both target and measured compositions using the average of the logarithms of the leachate concentrations. Results from the PCT work are published elsewhere (Hsieh 2021c), and a short summary of these results is included in Section 3.7.

2.9 Toxicity Characteristic Leaching Procedure

The TCLP analyses were conducted at Southwest Research Institute on both quenched and CCC samples of all the high-fluoride matrix glasses. Glass samples in crushed form were extracted using U.S. Environmental Protection Agency (EPA) procedure SW-846 Method 1311 (EPA 1992a). Due to reduced sample masses (~25-50 g), Method 1311 was "modified," but the ratio of extraction fluid volume to sample weight remained the same as required in the method. Although no mercury was batched in the glasses, mercury extraction was performed using EPA SW-846 Method 7470A (EPA 1994). The remaining metals were extracted following EPA SW-846 Method 3010A (EPA 1992b) and were analyzed by ICP-OES. These results are discussed in Section 3.8.

2.10 Sulfur Solubility

Sulfur solubility was measured on the quenched glass samples. The procedure was developed by PNNL and can be found in Jin et al. (2019). There are three primary phases of testing with each glass: (1) saturation with sodium sulfate, (2) de-ionized water (DIW) wash, and (3) analysis.

Saturation of the glass with sodium sulfate was performed by taking 50 g of each glass, grinding it, and then sieving through a #120 sieve (125 µm). Then, 3.82 g of Na_2SO_4 per 50 g of glass was added to the sieved powdered glass to add 4 mass% SO_3 to the glass/salt system, and the combination was mixed for homogeneity. The mixture of baseline glass and Na_2SO_4 was melted at 1150 °C for 1 h in a Pt-alloy crucible with a tight-fitting lid. After melting, the mixture was poured onto a stainless-steel plate and quenched. The mixture was again mixed by crushing and sieving through a #120 sieve (125 µm) and placed back into the Pt-alloy crucible to melt at 1150 °C for 1 h the second time. After the second melting, the mixture was quenched by pouring onto a stainless-steel plate, mixed by crushing and sieving through a #120 sieve (125 µm), and melted under the same conditions for the third time. The glass, after three times re-melting and re-mixing, was crushed and sieved through the #120 sieve (125 µm).

The sieved samples after the third melt were washed with DIW to remove excess salt prior to further analysis. This was done by adding 2 g of glass/salt mixture to a centrifuge filter in a centrifuge tube and adding 20 g of DIW to the tube. The tube was capped and shaken by hand for 2 min. Samples were then placed in a balanced centrifuge that was set to 3175 rpm for 5 min. The solution was decanted into a bottle through a low-density polyethylene filter after centrifuging. The filter was removed and then reinserted into the centrifuge tube. A second wash was performed following the same steps, and then the glass was weighed and dried at ≥ 80 °C overnight. To ensure there was enough sample for analysis, a fresh 2 g of the same glass was obtained, and the procedure described above was repeated and the glass and resulting solutions combined.

The washed and filtered glasses were then analyzed using ICP-OES and IC at SRNL. Also, a representative sample was taken from each of the wash solutions generated from the preparation of the sulfur saturated melt (SSM) samples. The sample was diluted according to expected concentrations of the species of interest in each of the solutions, and each sample was analyzed in triplicate by ICP-OES and IC at SRNL. Blanks and standards were used intermittently to assess the performance of each of the instruments and procedures. Methods of measurement are shown in Table 2.4.

Results from the SO_3 work are published elsewhere (Hsieh 2021b), and a short summary of these results is included and discussed in Section 3.9.

Table 2.4. Measurement Methods Used in Reporting the Concentrations of Each of the Analytes of the SSM Glasses and Wash Solutions (Hsieh 2021b)

Analyte	Measurement Method
Al	ICP-OES
B	ICP-OES
Ca	ICP-OES
Cr	ICP-OES
F^-	IC
Fe	ICP-OES
K	ICP-OES
Mn	ICP-OES
Na	ICP-OES
P	ICP-OES
PO_4^-	IC
S	ICP-OES
SO_4^{2-}	IC
Si	ICP-OES
Zn	ICP-OES
Zr	ICP-OES

3.0 Results and Discussion

This section describes the results for the chemical composition (Section 3.1), density (Section 3.2), CCC crystallinity (Section 3.3), viscosity (Section 3.4), EC (Section 3.5), CF and T_L (Section 3.6), PCT (Section 3.7), TCLP (Section 3.8), and sulfate solubility (Section 3.9) for the high-fluoride waste glasses studied.

3.1 Chemical Analysis of Glass Composition

The targeted and average measured component concentrations (wt%) in the quenched glasses are presented in Appendix B along with the percent differences. The composition analyses of the glass samples were performed as described in Section 2.2. All the measurements for each oxide in each glass were averaged to determine a representative chemical composition for each glass. The measured sum of oxides for all the glasses was within the interval of 97.3 to 102 wt%, indicating acceptable recovery of the glass components within ±5 wt%.

Based on the observations above, along with the overall analysis results shown in Appendix B, it was determined that the glasses had been batched correctly and the target values were used in the resulting calculations in this report. More details can be found in Hsieh (2021a).

3.2 Density

This section discusses the results of the glass density measurements obtained using the methods discussed in Section 2.3. The median of these 20 °C density values is 2.67 g/cm^3, with a minimum of 2.55 g/cm^3 and a maximum of 2.77 g/cm^3. The density of these high-fluoride waste glasses varies little – 60% of the glasses have density values between 2.62 and 2.70 g/cm^3 and are shown in Table 3.1. The glasses have a density less than 3.7 g/cm^3, meeting the WTP Contract Specification 2 (DOE 2000) for package dimension, weight, and void fraction limits.

There are two models used to predict the density, ρ, of HLW glasses: the specific volume-based density model (Vienna et al. 2009) and the molar-volume-based density model (Vienna et al. 2002). The specific volume-based density model predicts density by using the partial-specific volume of oxides according to the following formula:

$$\rho = \frac{1}{\sum_{i=1}^{N} v_i g_i} \tag{3.1}$$

where v_i is the partial-specific volume of the i-th glass component, g_i is the mass fraction of the i-th component, and N is the total number of glass components.

The molar-volume-based model predicts density using the following equation:

$$\rho = \frac{\sum_{i=1}^{N} M_i x_i}{V_i} \tag{3.2}$$

where x_i is the mole fraction of the i-th component and v_i is the partial molar volume of the i-th component as listed in Table S.5 of Vienna et al. (2002). In an ideal mixture, the molar volume of the mixture is given by the sum of partial molar volumes of the mixture constituents. Clearly, glass is not an ideal mixture; however, a model based on volume is more likely to be linear than one based on density.

This model tends to overpredict the density for all but one glass, indicating that the density model is not very accurate in this composition range. This is most likely due to the glass not being an ideal mixture and the molar volume being assumed to be constant irrespective of bonding environment.

Of the two models, the molar volume-based model showed the best fit, clustering closer to the 45-degree line and appearing to have a similar slope as the 45-degree line, whereas the partial-specific volume model clearly overestimated all the data except for two with a decidedly different linear slope (Figure 3.1). Among the 18 total components used to generate the molar-volume density model, only 13 were shared by the high-fluoride glass matrix. The Cr_2O_3, together with P_2O_5 and SO_3, was not included in the model but was present in the glass and ended up being included in the "Others" component. The molar-volume density model should be considered for interim use only because it was not developed according to the Nuclear Quality Assurance Requirements and Descriptions (Cook 2019). While it has the advantage of leading to a better understanding of the relation between the model coefficients and the effect of each component on glass structure, it would be best in the future to generate more data in the high-fluoride composition space and develop a new model to predict the glass density in this composition region.

Table 3.1. Measured Densities of High-Fluoride Waste Glasses

Glass ID	Measured Density (g/cm^3)	Glass ID	Measured Density (g/cm^3)
HFG1-01-1	2.64	HFG1-11	2.68
HFG1-02	2.55	HFG1-12	2.68
HFG1-03	2.68	HFG1-13	2.58
HFG1-04	2.68	HFG1-14	2.69
HFG1-05	2.68	HFG1-15	2.62
HFG1-06	2.63	HFG1-16	2.72
HFG1-07	2.56	HFG1-17	2.75
HFG1-08	2.76	HFG1-18	2.59
HFG1-09	2.64	HFG1-19	2.67
HFG1-10	2.77	HFG1-20	2.67

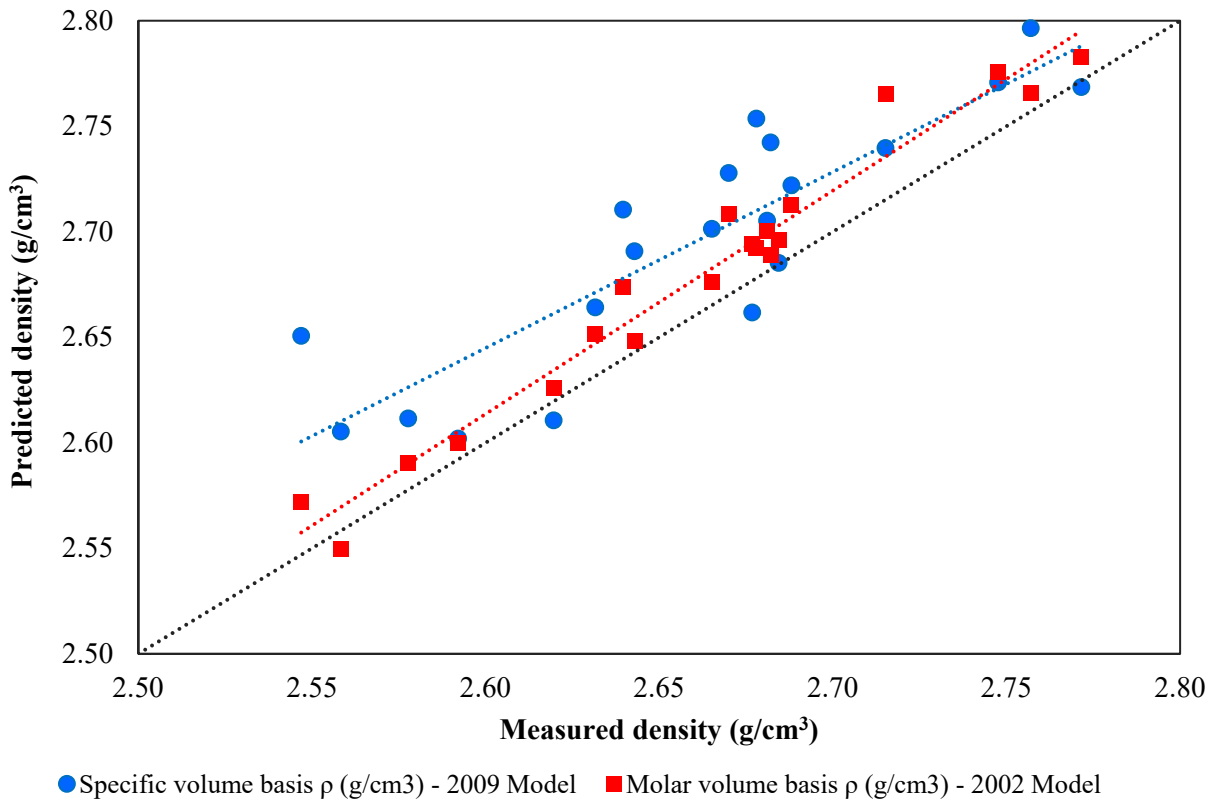

Figure 3.1. Predicted versus Measured Density for High-Fluoride Waste Glasses

3.3 Crystal Identification in Canister Centerline Cooling Glasses

This section presents and discusses the CF results from CCC glasses obtained using the methods discussed in Section 2.4. The crystal types and wt% crystallinity results are summarized in Table 3.2. XRD scans of CCC glass samples identified primarily fluoride salts crystalizing. Seven glasses were amorphous, and six glasses had crystal content of less than 5 mass%. Only one glass (HFG1-16) had a crystal content greater than 10 mass% and was almost completely crystallized, with several crystal types containing Zr and nepheline. Two glasses (HFG1-16 and HFG1-17) had Zr-containing phases. These glasses had concentrations of ZrO_2 >13 wt% and most likely were above the Zr solubility limit. Two glasses (HFG1-07 and HFG1-11) had a silica phosphate phase present. The crystals in the other glasses were a sodium, lithium, or calcium fluoride salt. All glass compositions with more than 5 wt% fluoride contained a fluoride salt. See Appendix D for photos of CCC-treated glasses and Appendix E for XRD spectra obtained from them.

Table 3.2. Weight Percent Crystallinity and Identification of Crystals by XRD in CCC-Treated Glasses

Glass ID	Starting CCC Temp (°C)	Wt% Crystallinity	Crystal Phase Identification
HFG1-01-1	1150	5.4	LiF
HFG1-02	1150	5.4 4.3	LiF CaF_2
HFG1-03	1150	5.3	CaF_2
HFG1-04	1150	0.0	Amorphous
HFG1-05	1150	0.0	Amorphous
HFG1-06	1150	0.0	Amorphous
HFG1-07	1150	0.3	SiP_2O_7
HFG1-08	1150	9.9	NaF
HFG1-09	1150	3.7 3.2	CaF_2 LiF
HFG1-10	1150	0.0	Amorphous
HFG1-11	1150	1.3 0.2	LiF SiP_2O_7
HFG1-12	1150	7.1 2.3	CaF_2 LiF
HFG1-13	1150	4.3	LiF
HFG1-14	1150	0.0	Amorphous
HFG1-15	1150	0.0	Amorphous
HFG1-16	1150	30.5 27.6 27.6 4.6 3.2	Nepheline Lithium Silicate $Na_4Zr_2(SiO_4)_3$ ZrO_2 Zirconium Silicon Oxide
HFG1-17	1150	3.1	ZrO_2
HFG1-18	1150	4.1	LiF
HFG1-19	1150	4.3	NaF
HFG1-20	1150	0.0	Amorphous

3.4 Viscosity

This section presents and discusses the viscosity results obtained using the methods discussed in Section 2.5. The results of the viscosity measurements are listed in Appendix F and summarized in Table 3.3.

Two model forms are widely used to fit viscosity-temperature data for each waste glass. The first model form is the Arrhenius equation [Eq. (3.3)]:

$$\ln(\eta) = A + \frac{B}{T_K} \tag{3.3}$$

where A and B are independent of temperature (T_K), which is in Kelvin (T(°C) + 273.15). The values for the A and B coefficients are shown in Table 3.4 for each glass. Table 3.4 summarizes the viscosity results at 1150 °C (η_{1150}) calculated using the Arrhenius equation [Eq. (3.3)] for the glasses.

The second model is the Vogel-Fulcher-Tamman (VFT) model [Eq. (3.4)]:

$$\ln(\eta) = E + \frac{F}{T_k - T_0} \tag{3.4}$$

where E, F, and T_0 are temperature independent and composition dependent coefficients and T_K is the temperature in Kelvin (T(°C) + 273.15). This model can be used to estimate the effect of temperature on viscosity over a wide range of temperatures for silicate-based glasses. Therefore, this model was also applied to the data for each glass; the E, F, and T_0 coefficients for each glass are shown in Table 3.4. Furthermore, Table 3.4 summarizes the viscosity results at 1150 °C (η_{1150}) calculated using the VFT equation [Eq. (3.4)] for the glasses.

Table 3.3. Measured ln η (Pa-s) Values versus Target Temperature (in the sequence of measurement) for the High-Fluoride Waste Glasses Tested

Target T, °C	1150	1050	950	1150	1200	1150
Glass ID	ln η (Pa-s)	ln η (Pa-s)	ln η (Pa-s)	ln η (Pa-s)	ln η (Pa-s)	ln η (Pa-s)
HFG1-01-1	1.394	2.236	3.329	1.405	1.141	1.476
HFG1-02	2.083	3.073	4.367	2.110	1.689	2.103
HFG1-03	2.370	3.580	5.158	2.380	1.872	2.389
HFG1-04	0.690	1.538	2.625	0.606	0.243	0.631
HFG1-05	NM	NM	NM	NM	NM	NM
HFG1-06	0.892	1.593	2.664	0.889	0.640	0.902
HFG1-07	1.988	2.927	4.204	1.981	1.603	2.000
HFG1-08	1.108	2.007	3.341	1.090	0.820	1.089
HFG1-09	0.993	1.714	2.794	1.005	0.798	1.022
HFG1-10	0.754	1.478	2.597	0.790	0.329	0.766
HFG1-11	1.275	2.200	3.478	1.308	0.926	1.324
HFG1-12	1.030	1.844	3.115	1.078	0.834	1.086
HFG1-13	1.326	2.130	3.267	1.319	1.052	1.335
HFG1-14	1.379	2.298	3.589	1.366	1.027	1.375
HFG1-15	1.425	2.302	3.509	1.427	1.106	1.436
HFG1-16	0.589	1.427	2.426	0.514	0.087	0.569
HFG1-17	1.280	2.468	3.703	1.320	0.800	1.269
HFG1-18	1.557	2.546	3.697	1.561	1.173	1.554
HFG1-19	1.848	2.138	2.513	2.066	2.060	2.107
HFG1-20	NM	NM	NM	NM	NM	NM

NM = not measured

Table 3.4. Fitted Coefficients of Arrhenius and VFT Models for Viscosity of High-Fluoride Waste Glasses Tested

	Arrhenius Coefficients		VFT Coefficients			Calculated η_{1150} (Pa-s)	
Glass ID	A (ln Pa-s)	B (ln Pa-s*K)	E (ln Pa-s)	F (ln Pa-s*K)	T_0 (K)	Arrhenius	VFT
HFG1-01-1	9.805	16011	-3.145	3128	740.2	4.245	4.200
HFG1-02	11.492	19352	-5.001	5862	597.4	8.216	8.145
HFG1-03	14.298	23746	-6.699	7743	570.1	10.891	10.781
HFG1-04	11.419	17165	-27.949	90249	-1732.3	1.902	1.918
HFG1-05	NM	NM	NM	NM	NM	NM	NM
HFG1-06	9.435	14722	-2.302	1798	861.2	2.483	2.453
HFG1-07	11.224	18817	-4.238	4746	661.0	7.376	7.304
HFG1-08	11.919	18571	-2.833	2184	869.6	3.095	3.044
HFG1-09	9.299	14706	-1.809	1466	904.8	2.814	2.774
HFG1-10	10.383	15829	-5.430	5335	557.4	2.094	2.080
HFG1-11	11.634	18420	-4.159	3825	722.2	3.704	3.662
HFG1-12	10.681	16760	-1.762	1358	944.8	2.990	2.937
HFG1-13	10.047	16218	-2.717	2510	803.9	3.852	3.805
HFG1-14	11.717	18655	-3.831	3494	752.3	4.019	3.968
HFG1-15	10.856	17510	-3.511	3347	746.5	4.252	4.202
HFG1-16	11.108	16574	42.130	1.80E+05	5741.8	1.712	1.740
HFG1-17	13.537	21114	-20.438	43628	-583.6	3.665	3.680
HFG1-18	11.358	18402	-7.901	10306	334.9	4.820	4.802
HFG1-19	0.494	3599	2.236	-4.981	1401.9	7.656	7.397
HFG1-20	NM	NM	NM	NM	NM	NM	NM

NM = not measured

Two models were used to predict the viscosities with measured values at 1150 ºC. The first model (Vienna et al. 2013) was developed for the target temperature of 1150 ºC only. It is a linear model with some selected binary terms for a total of 24 terms and the following form:

$$\ln(\eta_{1150}, Pa \cdot s) \sum_{i=1}^{p} h_i g_i + selected \left\{ \sum_{i=1}^{p-1} \sum_{j=1}^{p} h_{ij} g_i g_j \right\} \tag{3.5}$$

where p is the number of components modeled, h_i is the coefficient of the i-th glass component, g_i is the mass fraction of the i-th glass component, h_{ij} is the coefficient of the combined i-th and j-th components, and g_j is the mass fraction of the j-th HLW glass component.

The second model was developed by Vienna et al. (2016) in the form of the following linear equation:

$$\ln(\eta_{1150}, Pa \cdot s) = \sum_{i=1}^{q} b_i g_i \tag{3.6}$$

where b_i is the coefficient of the i-th HLW glass component, g_i is mass fraction of the i-th HLW glass component, and q is the number of HLW glass components in the model.

Figure 3.2 displays a plot of the ln (predicted η_{1150}) values against the ln (measured η_{1150}) values in Pa-s comparing the HLW viscosity model developed by Vienna et al. (2013) according to Eq. (3.5) and the HLW viscosity model developed by Vienna et al. (2016) according to Eq. (3.6) to the 45-degree line. The two models had similar fits to the data, with both underpredicting the viscosity, especially at lower values. At higher viscosities, there were a couple points overpredicted. This may be due to the Vienna et al. (2016) model being a linear model whereas the Vienna et al. (2013) model includes a binary term. This indicates that the data does not fit a linear model as well and binary terms need to be included. These models were also based on a wide composition range with several different components whereas this study was conducted on a tighter composition range with just higher fluoride in the glass and far fewer components.

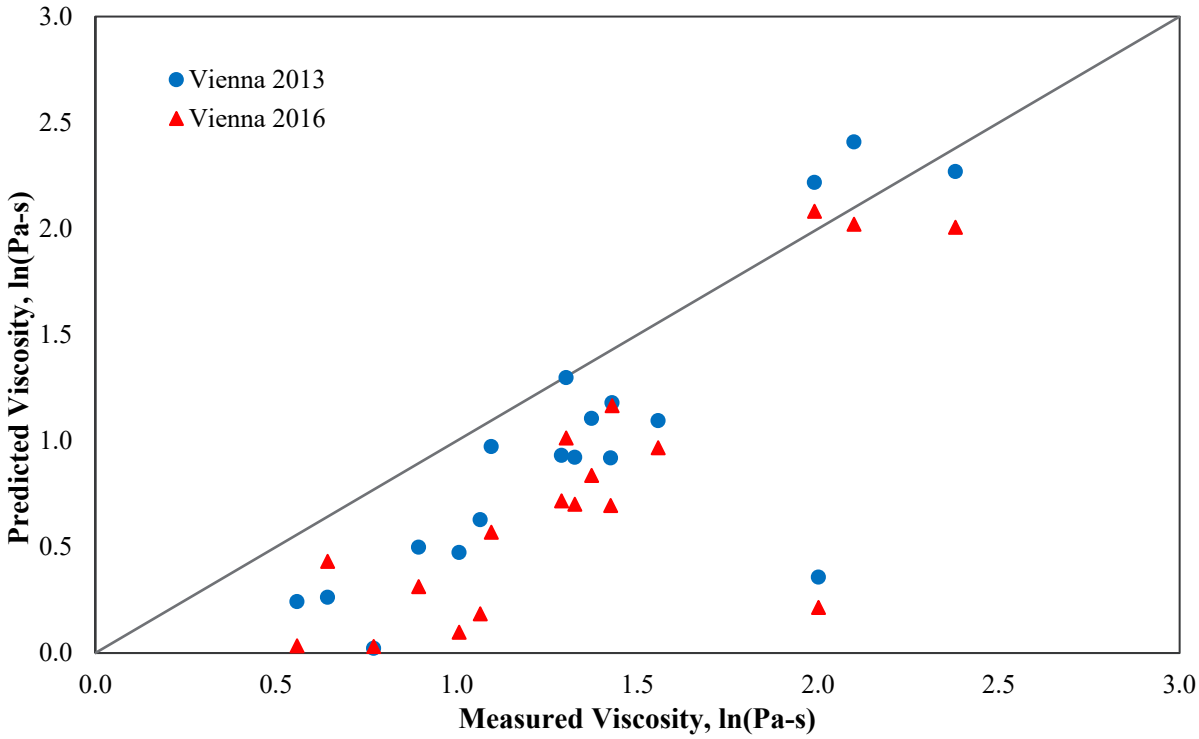

Figure 3.2. Predicted versus Measured Viscosity Data from Vienna (2013) and Vienna (2016) for High-Fluoride Waste Glasses

3.5 Electrical Conductivity

This section presents and discusses the EC results obtained using the methods discussed in Section 2.6. Table 3.5 lists the EC versus temperature data for each of the glasses and Appendix G shows the plots for the EC versus temperature data obtained from the EC experiments.

The Arrhenius equation [Eq. (3.7)] was used to fit ε-temperature data for each waste glass:

$$\ln(\varepsilon) = A + \frac{B}{T_K} \tag{3.7}$$

where A and B are temperature independent and composition dependent coefficients, and temperature (T_K) is in Kelvin [T(°C) + 273.15]. The values for the A and B coefficients obtained by fitting the

equation to the ε-temperature data for each glass (using least squares regression) are shown in Table 3.6 for each glass along with the calculated ε at 1150 °C (ε_{1150}) using Eq. (3.7) fit to each glass measured data.

Figure 3.3 shows the ln(ε) plot for predicted versus measured ε_{1150}, where the predicted values were produced by the modified Arrhenius equation parameters expanded as linear mixture models plus one alkali cross-product term (Vienna et al. 2009) following Eq. (3.8):

$$ln(\varepsilon_{1150}) = \sum_{i=1}^{N} b_i g_i + \left\{ \sum_{i=1}^{N} b_{ii} (g_i)^2 + \sum_{i=1}^{N-1} \sum_{<1}^{N} b_{ij}\, g_i g_j \right\} \tag{3.8}$$

where N is the number of components modeled, b_i is the coefficient of the i-th glass component, g_i is the mass fraction of the i-th glass component, b_{ii} and b_{ij} are the coefficients for the selected quadratic terms, and g_j is the mass fraction of j-th glass component.

This model was not very accurate as about half the glasses were overpredicted and half were underpredicted, with only three glasses near the 45° line. This could be because of the different glass composition region that the high-fluoride study explored compared to the composition region explored for the models. Therefore, a new model exploring a wider composition region would be useful to account for this data.

Table 3.5. Measured Electrical Conductivity (S/m) Values versus Temperatures for the High-Fluoride Glasses

Target T, °C	950	1200	1150	1050
Glass ID		Electrical Conductivity (S/m)		
HFG1-01-1	29.4	74.1	73.7	46.1
HFG1-02	12.7	22.8	19.6	16.8
HFG1-03	30.5	81.1	65.8	49.9
HFG1-04	67.7	129.7	118.3	94.6
HFG1-05	NM	NM	NM	NM
HFG1-06	11.5	63.0	57.4	32.9
HFG1-07	17.4	50.6	33.5	29.4
HFG1-08	NM	NM	NM	NM
HFG1-09	45.3	77.5	92.1	75.2
HFG1-10	28.2	56.9	53.6	47.7
HFG1-11	35.3	96.3	86.4	69.7
HFG1-12	16.4	22.1	27.2	25.6
HFG1-13	30.2	93.3	81.3	46.2
HFG1-14	20.3	28.0	27.8	23.4
HFG1-15	27.5	38.5	45.9	38.7
HFG1-16	NM	NM	NM	NM
HFG1-17	21.2	50.6	45.5	31.8
HFG1-18	23.1	45.3	43.2	34.1
HFG1-19	27.7	53.1	52.9	31.9
HFG1-20	NM	NM	NM	NM

NM = not measured

Table 3.6. Fitted Coefficients of the Arrhenius Model for Electrical Conductivity for the High-Fluoride Glasses

Glass ID	Arrhenius Coefficients		Calculated ε_{1150} (S/m)
	A, ln[S/m]	B, ln[(S-K)/m]	
HFG1-01-1	9.1988	-7100	67.3
HFG1-02	5.8441	-4031	20.3
HFG1-03	9.0658	-6869	69.4
HFG1-04	8.1055	-4741	118.4
HFG1-05	NM	NM	NM
HFG1-06	12.732	-12453	53.6
HFG1-07	8.4781	-6853	39.0
HFG1-08	NM	NM	NM
HFG1-09	7.4341	-4309	82.0
HFG1-10	7.4770	-4970	53.8
HFG1-11	9.4519	-7098	86.9
HFG1-12	4.9438	-2483	26.6
HFG1-13	10.261	-8417	77.2
HFG1-14	5.0269	-2466	27.0
HFG1-15	5.7315	-2869	41.1
HFG1-16	NM	NM	NM
HFG1-17	8.2825	-6389	44.4
HFG1-18	7.2042	-4930	40.3
HFG1-19	7.5625	-5253	48.0
HFG1-20	NM	NM	NM

NM = not measured

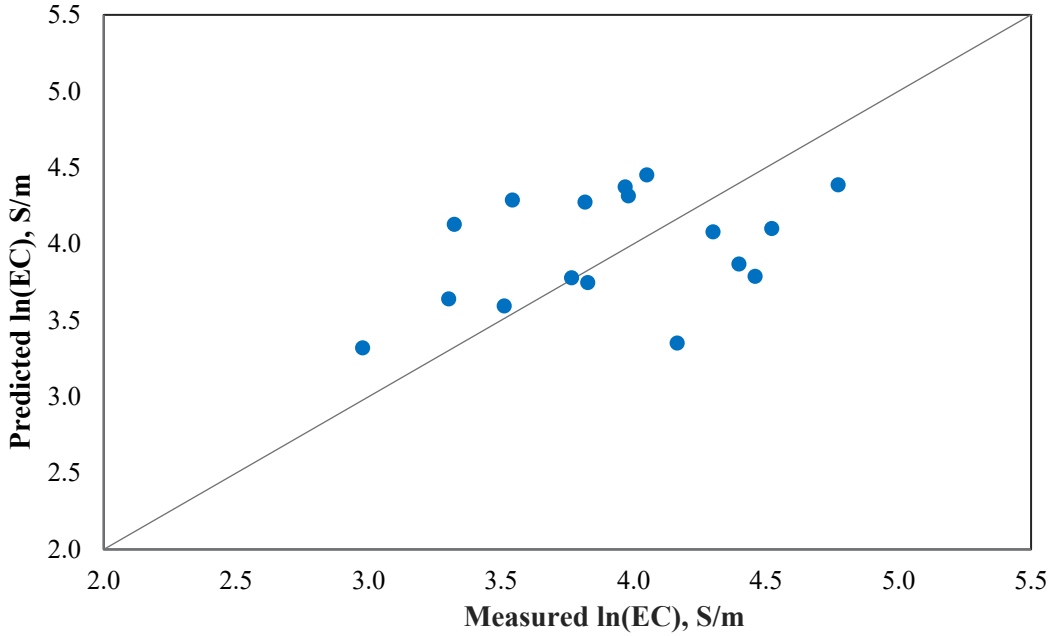

Figure 3.3. Predicted versus Measured Electrical Conductivity for High-Fluoride Waste Glasses

3.6 Crystal Fraction and Liquidus Temperature

This section presents and discusses the CF and T_L results obtained using the methods discussed in Section 2.7. See Appendix H for photos of CF heat-treated glasses at 950 °C and Appendix I for XRD spectra obtained from them.

All but four glasses had insufficient crystals to perform XRD analysis when treated at 950 °C for 24 h. The glasses with crystals at 950 °C for 24 h all contained silicates of either sodium or zirconium and sodium. A total of seven glasses contained silicates at different temperatures. A couple glasses contained some nepheline and a couple glasses contained zirconium oxide at lower temperatures. At 800 °C, two glasses had calcium fluoride form. The wt% total crystallinity ranged from 0 to 23.3 at various temperatures. These results are summarized in Table 3.7.

Only four glasses had enough crystals to obtain the T_L by extrapolating the CF as a function of temperature to zero crystals. These values are also shown in Table 3.7. The four glasses that contained > 12.5 wt% ZrO_2 each had T_L > 900 °C with Zr-containing phases of parakeldyshite or baddeleyite.

Table 3.7. Weight Percent Crystallinity and Identification of Crystals by XRD in Heat-Treated High-Fluoride Waste Glasses

Glass ID	Temp (°C)	Wt% Crystallinity	Crystal Phase Identification	Liquidus Temperature (°C)
HFG1-01-1	800	0	None	<800
	850	0		
	950	0		
HFG1-02	800	2.6	CaF_2	<850
	850	0	None	
	950	0	None	
HFG1-03	800	0.75	CaF_2	<850
	850	0	None	
	950	0	None	
HFG1-04	800	0	None	<800
	850	0		
	950	0		
HFG1-05	800	0.83, 0.60, 0.41	Na_2SiO_5, $Na_2ZrSi_2O_7$, $Na_2Si_4O_9$	<850
	850	0	None	
	950	0	None	
HFG1-06	800	0.29	$Na_2ZrSi_2O_7$	<850
	850	0	None	
	950	0	None	
HFG1-07	800	0	None	<800
	850	0		
	950	0		
HFG1-08	800		$Na_2ZrSi_2O_7$, Na_2SiO_5	1146
	850	5.2, 1.32.7, 1.9, 0.24	Na_2SiO_5, $Na_2ZrSi_2O_7$, Nepheline	
	950	2.0, 1.7, 0.07	Na_2SiO_5, $Na_2ZrSi_2O_7$, Nepheline	
HFG1-09	800	0	None	<800
	850	0		
	950	0		
HFG1-10	800	8.8, 2.8, 0.37	$Na_2ZrSi_2O_7$, Na_2SiO_5, Nepheline	<950
	850	6.9, 1.8, 0.2	$Na_2ZrSi_2O_7$, Na_2SiO_5, Nepheline	
	950	0	None	
HFG1-11	800	0	None	<800
	850	0		
	950	0		
HFG1-12	800	0	None	<800
	850	0		
	950	0		
HFG1-13	800	0	None	<800
	850	0		
	950	0		
HFG1-14	800	0	None	<800
	850	0		
	950	0		
HFG1-15	800	0	None	<800
	850	0		
	950	0		
HFG1-16	950	21, 2.1	$Na_4Zr_2(SiO_4)_3$, ZrO_2	1148
	1000	18, 2.1	$Na_4Zr_2(SiO_4)_3$, ZrO_2	
	1050	8.1, 5.3	$Na_4Zr_2(SiO_4)_3$, ZrO_2	
	1150	1.2, 6.6	$Na_4Zr_2(SiO_4)_3$, ZrO_2	
HFG1-17	950	12, 2.6, 0.42	$Na_2ZrSi_2O_7$, Na_2SiO_5, $Na_2Si_4O_9$	1066
	1000	2.2, 1.4, 1.2	ZrO_2, $Na_2ZrSi_2O_7$, $ZrSiO_4$	
	1050	4.0	ZrO_2	
	1150	4.9	ZrO_2	

Glass ID	Temp (°C)	Wt% Crystallinity	Crystal Phase Identification	Liquidus Temperature (°C)
HFG1-18	800 850 950	0 0 0	None	<800
HFG1-19	800 850 950	0 0 0	None	<800
HFG1-20	950 1000 1050 1150	3.0 0.24 4.0 0	$Na_4Zr_2(SiO_4)_3$ $Na_4Zr_2(SiO_4)_3$ $CaSi_2O_5$ None	1004

3.7 Product Consistency Test

This section presents and discusses the PCT results obtained using the methods discussed in Section 2.8. The PCTs were performed at PNNL and the PCT leachates were analyzed at SRNL (Hsieh 2021c) and are summarized in Table 3.8. The PCT results were normalized to the target values of the glasses.

The CCC heat treatment had only a slight to no impact on most of the PCT results. HFG1-16-CCC had a notably higher normalized release for all analytes than the quenched version and was higher than the DWPF-EA benchmark for all analytes (see Table 3.9). This glass had extensive crystallization after CCC treatment, which most likely made the glass less durable and able to leach. Both the quenched and the CCC values were higher than the DWPF-EA benchmark for all analytes in the HFG1-06 glass. The reason for this is not clear as the quenched glass was amorphous and the CCC glass had only slight crystallization. Further analyses would be necessary to identify the cause of the unusual behavior of this glass. However, this is outside the scope of the current task and would require a separate effort.

Table 3.8. PCT Normalized Concentration (NC) Release Results for High-Fluoride Glasses. Red values are above the PCT constraints for B, Li, or Na.

Glass ID	Type	B (g/L)	Na (g/L)	Li (g/L)	Si (g/L)
HFG1-01-1	Quenched	0.476	0.812	0.383	0.233
	CCC	0.461	1.81	11.2	0.244
HFG1-02	Quenched	0.310	0.595	<0.612	0.177
	CCC	0.334	1.24	10.2	0.179
HFG1-03	Quenched	0.356	0.522	<18.9	0.168
	CCC	0.445	0.637	<18.9	0.195
HFG1-04	Quenched	13.7	12.0	10.8	3.62
	CCC	11.0	8.96	7.85	3.20
HFG1-05	Quenched	7.96	6.18	3.92	0.858
	CCC	7.70	5.51	4.08	0.913
HFG1-06	Quenched	23.6	18.2	16.1	4.35
	CCC	25.0	18.3	18.0	3.64
HFG1-07	Quenched	3.43	2.28	<2.17	0.164
	CCC	2.45	1.68	<2.17	0.240
HFG1-08	Quenched	2.30	2.44	<2.32	0.509
	CCC	1.41	5.21	<2.32	0.363
HFG1-09	Quenched	0.768	1.52	0.491	0.434
	CCC	0.940	2.08	4.27	0.420
HFG1-10	Quenched	3.35	2.97	1.83	0.252
	CCC	3.23	2.62	1.89	0.258
HFG1-11	Quenched	1.60	1.30	0.744	0.132
	CCC	1.47	1.93	7.39	0.159
HFG1-12	Quenched	2.20	2.06	1.76	0.489
	CCC	3.92	3.60	5.05	0.826
HFG1-13	Quenched	0.540	0.698	0.541	0.224
	CCC	0.534	0.908	2.58	0.242
HFG1-14	Quenched	5.40	5.10	3.17	1.58
	CCC	5.61	4.99	3.38	1.67
HFG1-15	Quenched	4.08	3.56	3.56	1.12
	CCC	3.87	3.16	3.40	1.14
HFG1-16	Quenched	1.92	4.86	2.70	0.753
	CCC	29.7	22.4	14.2	1.82
HFG1-17	Quenched	0.843	1.89	0.685	0.355
	CCC	0.961	1.89	0.983	0.470
HFG1-18	Quenched	2.15	1.57	1.80	0.355
	CCC	1.27	1.04	1.69	0.366
HFG1-19	Quenched	3.12	2.82	1.35	0.326
	CCC	1.90	3.06	<0.825	0.283
HFG1-20	Quenched	1.63	3.17	0.561	0.564
	CCC	1.51	2.70	0.570	0.560

The DWPF-EA PCT releases are used to assess the durability of the samples and are given in Table 3.9. The WTP contract limits set by the DWPF-EA glass are reported as orange dashed lines in Figure 3.4, Figure 3.5, and Figure 3.6.

Table 3.9. WTP PCT Normalized Release Limits to HLW Glass (g/L)

Constraint Description	Value	Source
PCT normalized B release	NC_B <16.70 (g/L) ln(NC_B), g/L <2.82	DOE 2000
PCT normalized Li release	NC_{Li} <9.57 (g/L) ln($NC_{Li,}$), g/L <2.26	DOE 2000
PCT normalized Na release	NC_{Na} <13.35 (g/L) ln(NC_{Na}), g/L <2.59	DOE 2000

Overall, one quenched sample and two CCC samples exceeded the B NC_B constraint and the NC_{Na} constraint. Two quenched samples and four CCC samples exceeded the NC_{Li} release constraint.

Figure 3.4 to Figure 3.6 compare the PCT normalized releases of the quenched versus CCC glass samples. This shows that CCC didn't affect the PCT leaching of the glasses unless there were significant crystals present (>5 wt%). The main glass affected by CCC was HFG1-16, which was farthest from the 45-degree line and was almost completely crystalized after CCC and contained about 30% nepheline and several silicates (see Table 3.2).

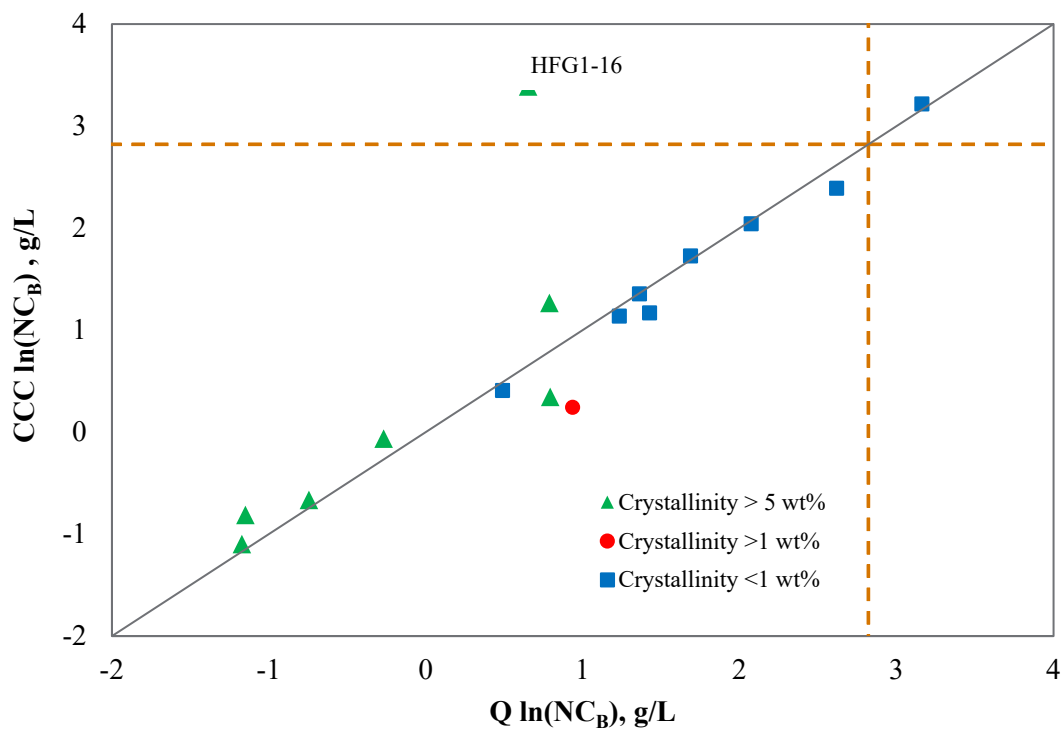

Figure 3.4. NC_B Release in Natural Logarithm Scale of Quenched versus CCC of High-Fluoride Glasses. Dashed orange lines are natural logarithm scale of the NC_B constraint in g/L.

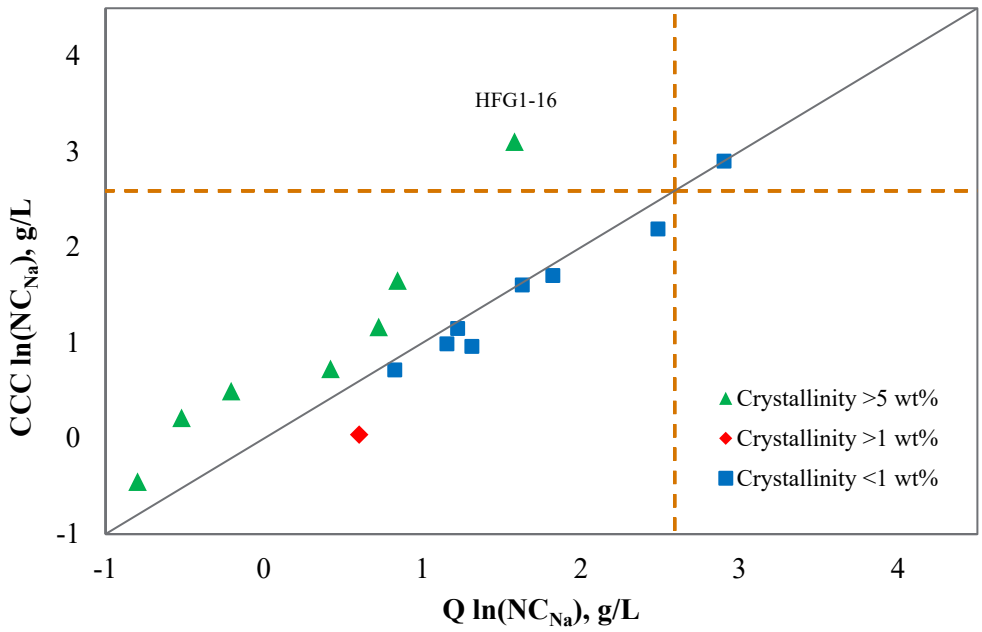

Figure 3.5. NC_{Na} Release in Natural Logarithm Scale of Quenched versus CCC of High-Fluoride Glasses. Dashed orange lines are natural logarithm scale of the NC_{Na} constraint in g/L.

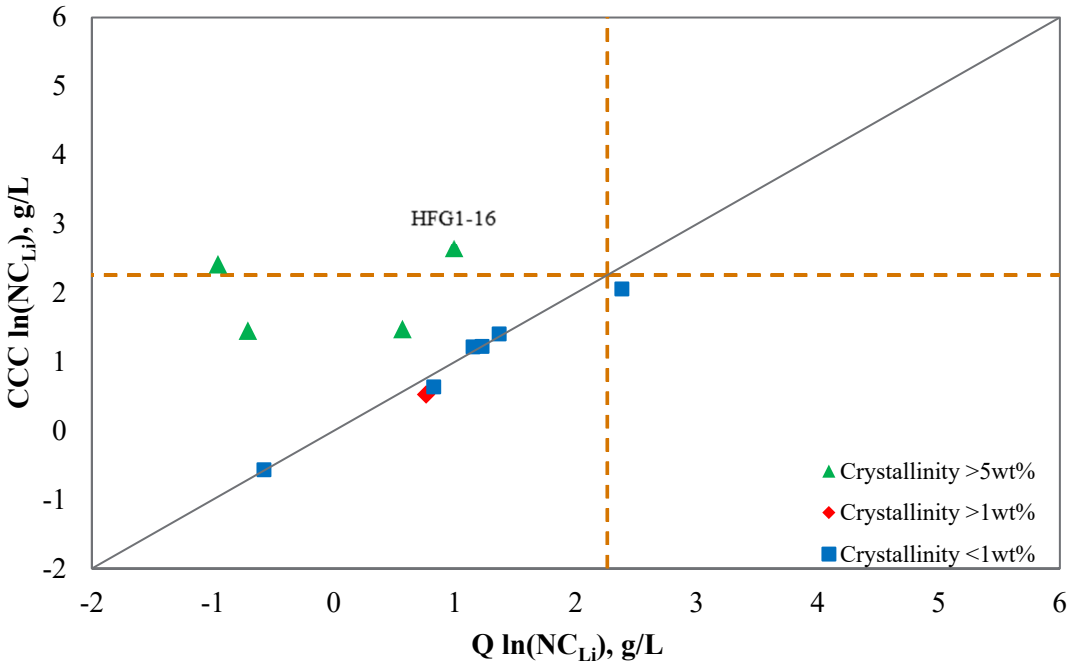

Figure 3.6. NC_{Li} Release in Natural Logarithm Scale of Quenched versus CCC of High-Fluoride Glasses. Dashed orange lines are natural logarithm scale of the NC_{Li} constraint in g/L.

Vienna et al. (2016) and Vienna et al. (2013) use the same model equation; however, they have different coefficients. The model equation is shown in Eq. (3.9).

$$ln[PCT] = \sum_{i=1}^{q} b_i g_i + b2_{Al_2O_3} g^2{}_{Al_2O_3} + b3_{Al_2O_3} g^3{}_{Al_2O_3} + b4_{Al_2O_3} g^4{}_{Al_2O_3} \quad (3.9)$$

where q is the number of HLW glass components in the model; b_i is the coefficient of the i-th component; g_i is the mass fraction of the i-th component; and $b2_{Al2O3}$, $b3_{Al2O3}$, and $b4_{Al2O3}$ are the coefficients for higher-order terms involving the mass fraction of Al_2O_3.

The results in natural logarithmic scale of predicted NL_B, NL_{Na} and NL_{Li}, by the model and the different coefficients versus the measured releases in natural logarithmic scale are shown in Figure 3.7, Figure 3.8, and Figure 3.9, respectively.

The 2013 model primarily overpredicts and the 2016 model primarily underpredicts the PCT release of all three elements of interest. With low PCT release of Li, the 2016 model overpredicts until about $ln(NL_{Li})$ of -0.50 g/m^2 (Figure 3.7 to Figure 3.9). It is not unexpected that neither provides highly accurate predictions because the composition boundaries used to develop both models are quite different from the one used in the current study.

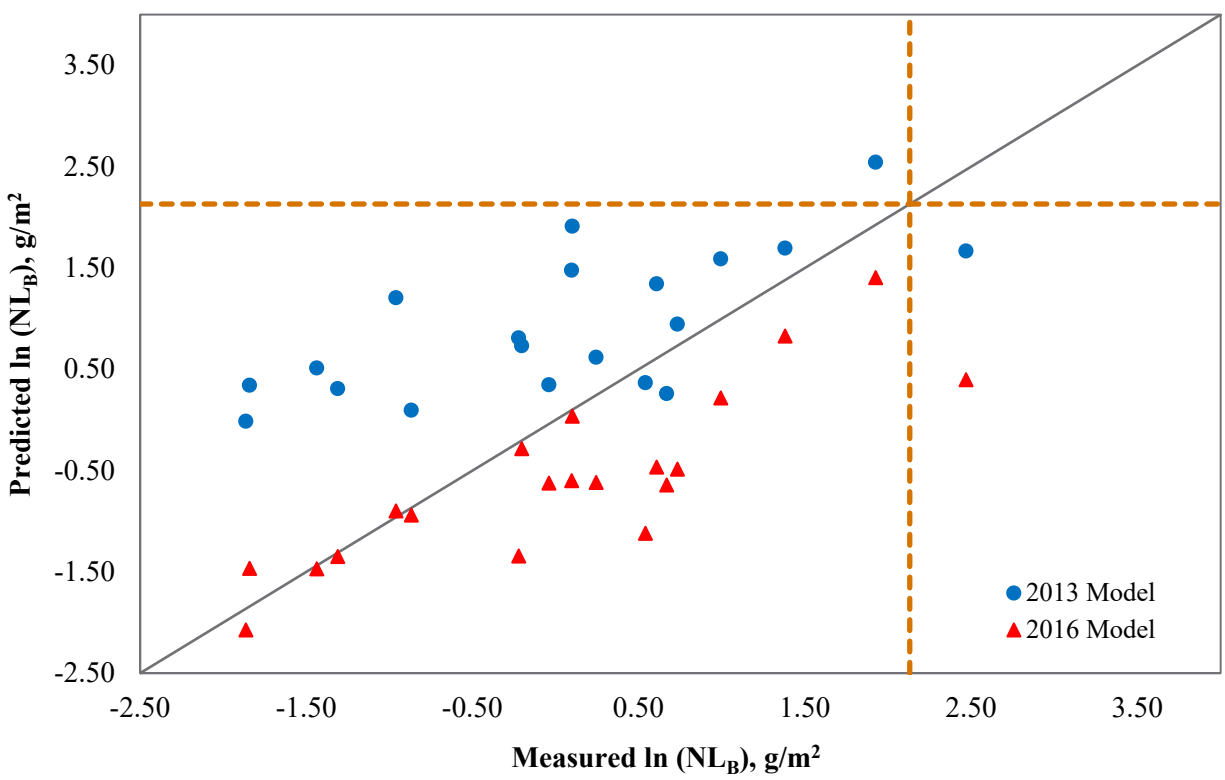

Figure 3.7. Natural Log Scale NL_B versus Predicted Releases using the 2013 Model and 2016 Model. The orange dotted lines are the natural logarithmic scale of the NL constraints.

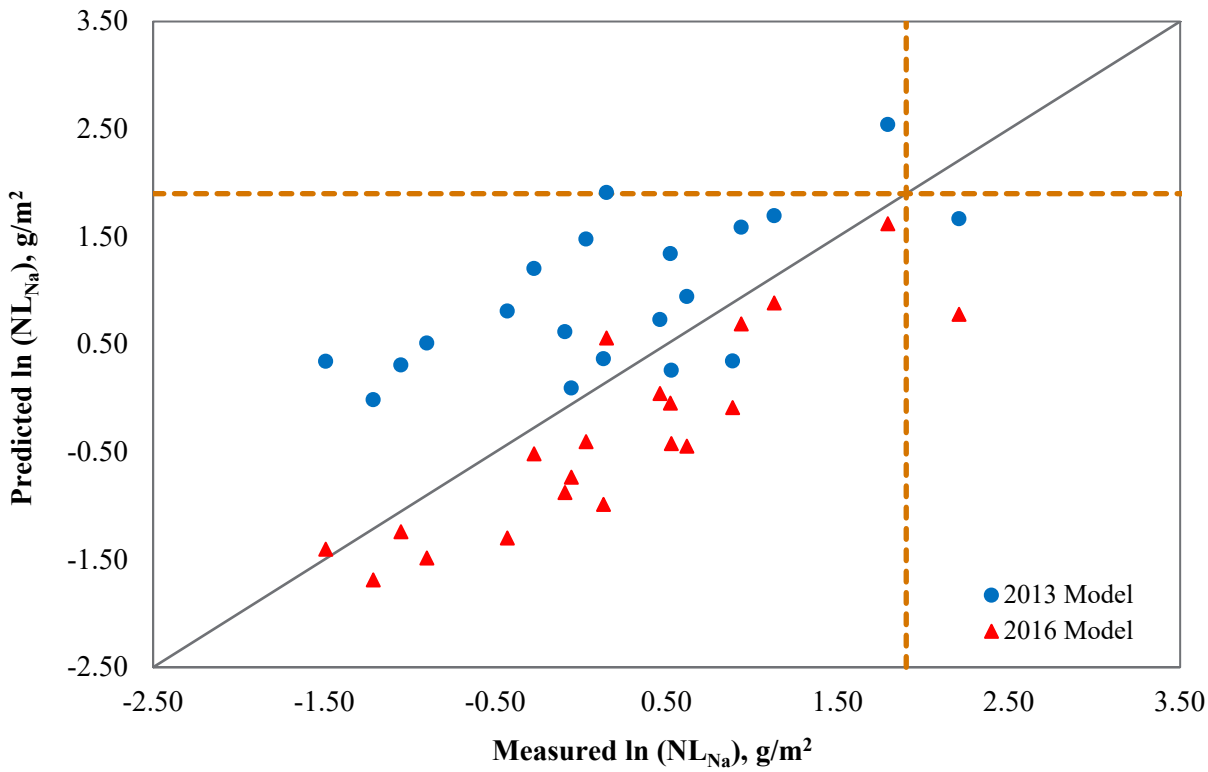

Figure 3.8. Natural Log Scale NL_{Na} versus Predicted Releases using 2013 Model and 2016 Model. The orange dotted lines are the natural logarithmic scale of the NL constraints.

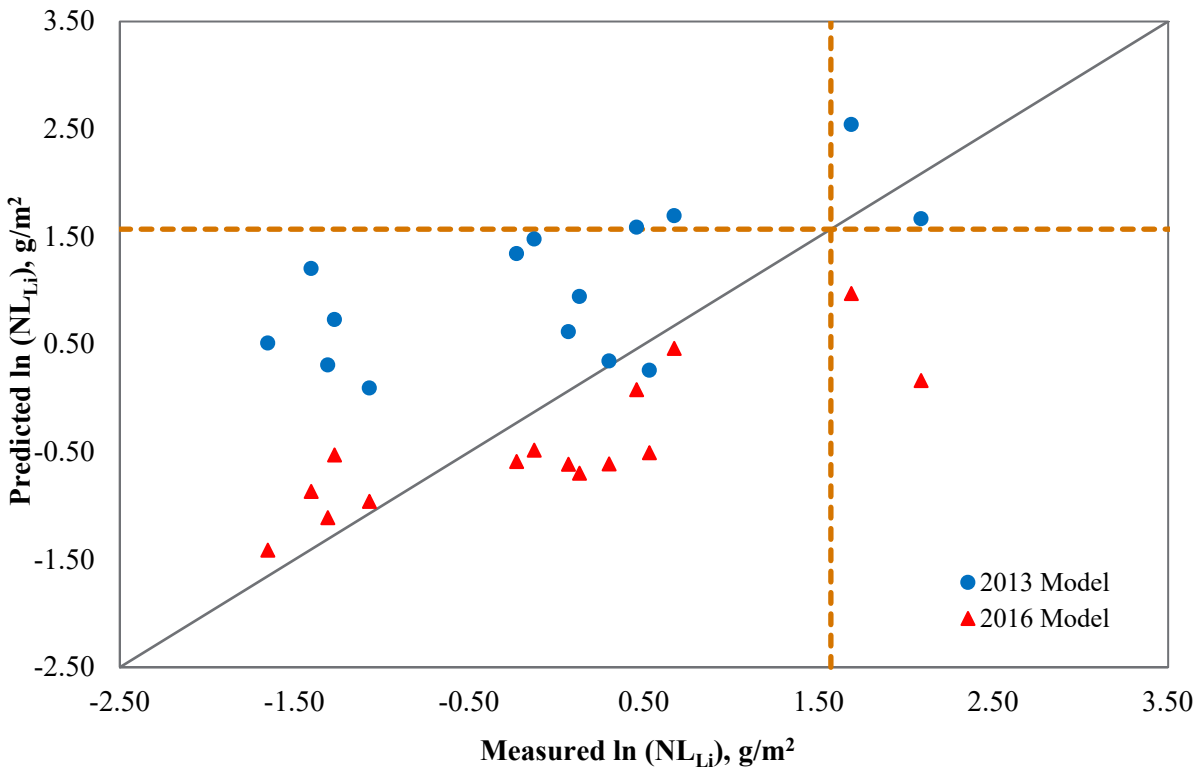

Figure 3.9. Natural Log Scale NL_{Li} versus Predicted Releases using 2013 Model and 2016 Model. The orange dotted lines are the natural logarithmic scale of the NL constraints.

3.8 Toxic Characterization Leaching Procedure

This section presents and discusses the TCLP results obtained using the methods discussed in Section 2.9. The TCLP results for quenched and CCC glasses are listed in Table 3.10 and Table 3.11, respectively. The Hanford HLW delisting limits, toxicity limits, and Universal Treatment Standards (UTS) limits as set by Resource Conservation and Recovery Act (RCRA) are listed in Table 3.12.

Only one CCC glass (HFG1-16-CCC) failed to pass the Cr Hanford HLW delisting limit of 4.95 mg/L. The other glasses passed the Hanford delisting limit for Cr. Chromium was the only component of the TCLP test that was present in these glasses.

Table 3.10. TCLP Results from the Quenched High-Fluoride Glasses

Sample ID	As (mg/L)	Ba (mg/L)	Cd (mg/L)	Cr (mg/L)	Pb (mg/L)	Hg (mg/L)	Se (mg/L)	Ag (mg/L)	B (mg/L)
HFG1-01-1	<0.0500	<0.100	<0.0100	0.0464	<0.0150	<0.001	<0.0500	<0.0200	1.81
HFG1-02	<0.0500	<0.100	<0.0100	[0.0133]	<0.0150	<0.001	<0.0500	<0.0200	0.503
HFG1-03	<0.0500	<0.100	<0.0100	[0.0182]	<0.0150	<0.001	<0.0500	<0.0200	0.919
HFG1-04	<0.0500	<0.100	<0.0100	0.313	<0.0150	<0.001	<0.0500	<0.0200	108
HFG1-05	<0.0500	<0.100	<0.0100	0.0798	<0.0150	<0.001	<0.0500	<0.0200	9.93
HFG1-06	<0.0500	<0.100	<0.0100	0.0782	<0.0150	<0.001	<0.0500	<0.0200	13.9
HFG1-07	<0.0500	<0.100	<0.0100	0.0280	<0.0150	<0.001	<0.0500	<0.0200	2.25
HFG1-08	<0.0500	<0.100	<0.0100	0.0383	<0.0150	<0.001	<0.0500	<0.0200	1.14
HFG1-09	<0.0500	<0.100	<0.0100	0.0711	<0.0150	<0.001	<0.0500	<0.0200	1.70
HFG1-10	<0.0500	<0.100	<0.0100	[0.0171]	<0.0150	<0.001	<0.0500	<0.0200	25.1
HFG1-11	<0.0500	<0.100	<0.0100	0.0402	<0.0150	<0.001	<0.0500	<0.0200	2.56
HFG1-12	<0.0500	<0.100	<0.0100	[0.0163]	<0.0150	<0.001	<0.0500	<0.0200	1.11
HFG1-13	<0.0500	<0.100	<0.0100	0.0346	<0.0150	<0.001	<0.0500	<0.0200	1.38
HFG1-14	<0.0500	<0.100	<0.0100	0.0245	<0.0150	<0.001	<0.0500	<0.0200	4.99
HFG1-15	<0.0500	<0.100	<0.0100	0.0336	<0.0150	<0.001	<0.0500	<0.0200	2.86
HFG1-16	<0.0500	<0.100	<0.0100	0.297	<0.0150	<0.001	<0.0500	<0.0200	16.5
HFG1-17	<0.0500	<0.100	<0.0100	[0.0173]	<0.0150	<0.001	<0.0500	<0.0200	1.01
HFG1-18	<0.0500	<0.100	<0.0100	[0.0116]	<0.0150	<0.001	<0.0500	<0.0200	1.73
HFG1-19	<0.0500	<0.100	<0.0100	0.0621	<0.0150	<0.001	<0.0500	<0.0200	43.3
HFG1-20	<0.0500	<0.100	<0.0100	0.0611	<0.0150	<0.001	<0.0500	<0.0200	4.11

[ ] = greater than limit of detection but less than the limit of quantitation

Table 3.11. TCLP Results from the CCC High-Fluoride Glasses

Sample ID	As (mg/L)	Ba (mg/L)	Cd (mg/L)	Cr (mg/L)	Pb (mg/L)	Hg (mg/L)	Se (mg/L)	Ag (mg/L)	B (mg/L)
HFG1-01-1	<0.0500	<0.100	<0.0100	0.148	<0.0150	<0.001	<0.0500	<0.0200	11.4
HFG1-02	<0.0500	<0.100	<0.0100	0.103	<0.0150	<0.001	<0.0500	<0.0200	1.25
HFG1-03	<0.0500	<0.100	<0.0100	[0.0177]	<0.0150	<0.001	<0.0500	<0.0200	0.813
HFG1-04	<0.0500	<0.100	<0.0100	0.796	<0.0150	<0.001	<0.0500	<0.0200	94.1
HFG1-05	<0.0500	<0.100	<0.0100	0.0821	<0.0150	<0.001	<0.0500	<0.0200	7.00
HFG1-06	<0.0500	<0.100	<0.0100	0.128	<0.0150	<0.001	<0.0500	<0.0200	12.9
HFG1-07	<0.0500	<0.100	<0.0100	[0.0141]	<0.0150	<0.001	<0.0500	<0.0200	1.61
HFG1-08	<0.0500	<0.100	<0.0100	0.868	<0.0150	<0.001	<0.0500	<0.0200	11.3
HFG1-09	<0.0500	<0.100	<0.0100	0.304	<0.0150	<0.001	<0.0500	<0.0200	2.84
HFG1-10	<0.0500	<0.100	<0.0100	[0.0139]	<0.0150	<0.001	<0.0500	<0.0200	10.9
HFG1-11	<0.0500	<0.100	<0.0100	0.222	<0.0150	<0.001	<0.0500	<0.0200	4.96
HFG1-12	<0.0500	<0.100	<0.0100	0.0238	<0.0150	<0.001	<0.0500	<0.0200	1.08
HFG1-13	<0.0500	<0.100	<0.0100	0.0295	<0.0150	<0.001	<0.0500	<0.0200	1.34
HFG1-14	<0.0500	<0.100	<0.0100	0.0279	<0.0150	<0.001	<0.0500	<0.0200	2.65
HFG1-15	<0.0500	<0.100	<0.0100	0.0446	<0.0150	<0.001	<0.0500	<0.0200	1.33
HFG1-16	<0.0500	<0.100	<0.0100	7.25	<0.0150	<0.001	<0.0500	<0.0200	471
HFG1-17	<0.0500	<0.100	<0.0100	0.0356	<0.0150	<0.001	<0.0500	<0.0200	1.17
HFG1-18	<0.0500	<0.100	<0.0100	[0.0182]	<0.0150	<0.001	<0.0500	<0.0200	1.63
HFG1-19	<0.0500	<0.100	<0.0100	0.212	<0.0150	<0.001	<0.0500	<0.0200	51.7
HFG1-20	<0.0500	<0.100	<0.0100	0.0528	<0.0150	<0.001	<0.0500	<0.0200	2.39

[ ] = greater than limit of detection but less than the limit of quantitation

Table 3.12. Waste Treatment and Immobilization Plant Delisting Limits (DOE 2006), and Resource Conservation and Recovery Act Toxicity and UTS Limits for TCLP (40 CFR 268. 2015)

Element	Ag	As	Ba	Cd	Cr	Hg	Pb	Se
WTP Delisting Limit (mg/L)	3.07	0.616	100	0.48	4.95	0.2	5	1
RCRA Toxicity Limit (mg/L)	5	5	100	1	5	0.2	5	1
RCRA UTS Limit (mg/L)	0.14	5	21	0.11	0.6	0.025	0.75	5.7

The normalized toxicity leaching behaviors of Cr are plotted versus those of B in Figure 3.10 and Figure 3.11. Chromium generally showed lower leaching behavior than that of B in both quenched and CCC glasses; however, the Cr leaching tended to increase after CCC treatment, bringing them closer to the 45-degree line. This indicates that the CCC causes Cr to leach to an extent closer to the glass in general, which may be caused by higher oxidation, which would increase solubility of Cr.

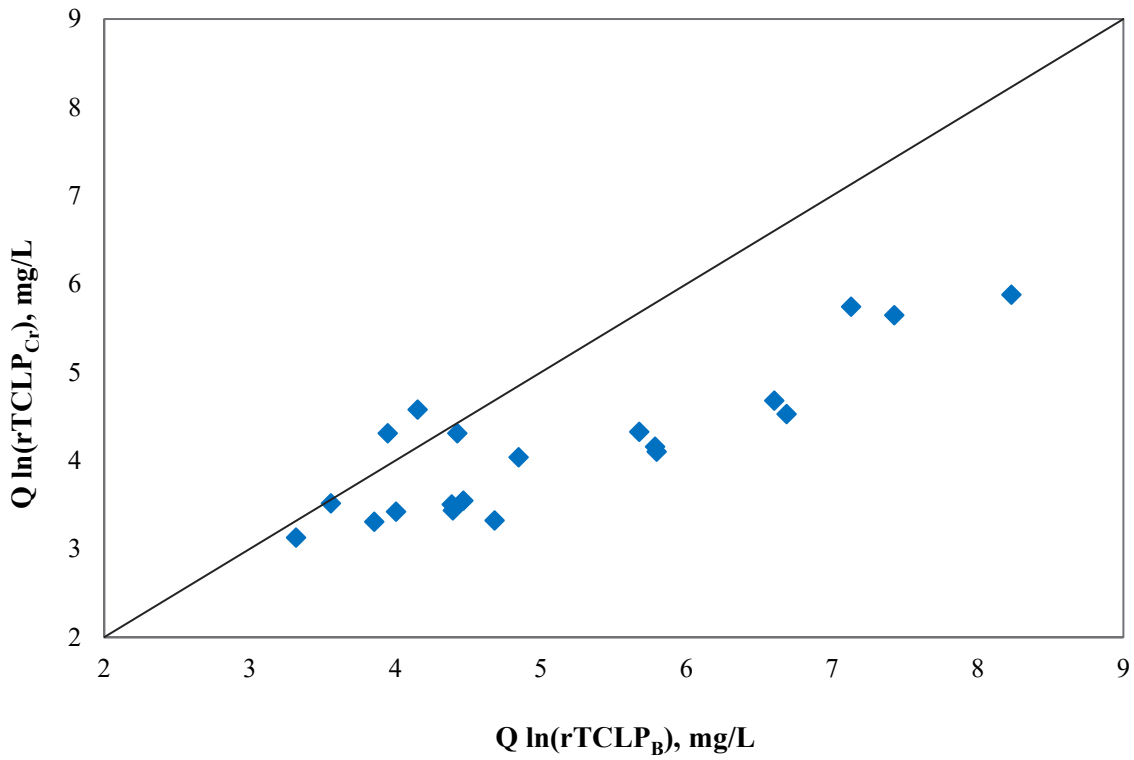

Figure 3.10. TCLP Releases (mg/L) of Cr Compared to B Releases (mg/L) for Quenched Samples of HLW Glasses in the High-Fluoride Study

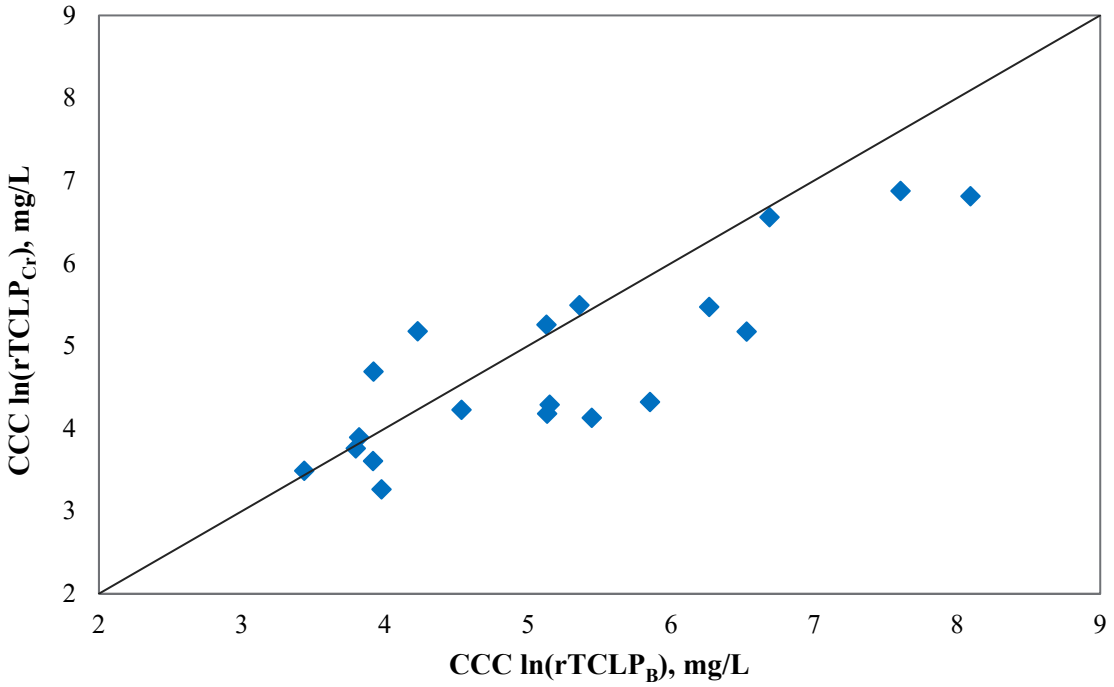

Figure 3.11. TCLP Releases (mg/L) of Cr Compared to B Releases (mg/L) for CCC Samples of HLW Glasses in the High-Fluoride Study

The glasses were divided into three groups depending on the quantity of crystals present, and the TCLP normalized release (rTCLP) of quenched versus CCC samples were plotted. Figure 3.12 and Figure 3.13 report the $rTCLP_B$ and $rTCLP_{Cr}$ results, respectively. In both plots, most of the samples lay near the 45-degree line until the crystal content exceeds 5 wt%, indicating that the quantity of crystals formed after CCC does affect TCLP behavior. Of the 20 glasses, only four were significantly affected by CCC for B release: HFG1-01-1, HFG1-02, HFG1-08, and HFG1-16. CCC slightly improved the $rTCLP_B$ performances of four glasses: HFG1-10, HFG1-14, HFG1-15, and HFG1-20 (Figure 3.12). The $rTCLP_{Cr}$ increased after CCC in seven glasses (HFG1-01-1, HFG1-02, HFG1-08, HFG1-09, HFG1-11, HFG1-16, and HFG1-19) and decreased in one glass (HFG1-07) (Figure 3.13). The TCLP concentration releases for both B and Cr showed the same glass behaviors as the rTCLP releases and therefore are not shown here.

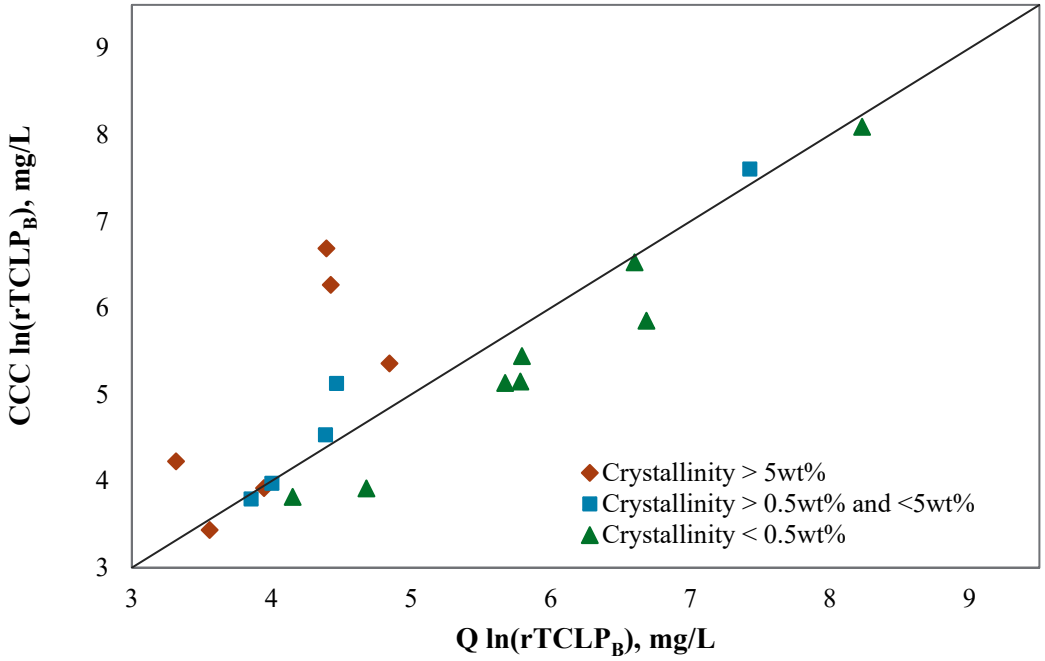

Figure 3.12. Quenched versus CCC rTCLPB Natural Logarithmic Scale of High-Fluoride HLW Glasses

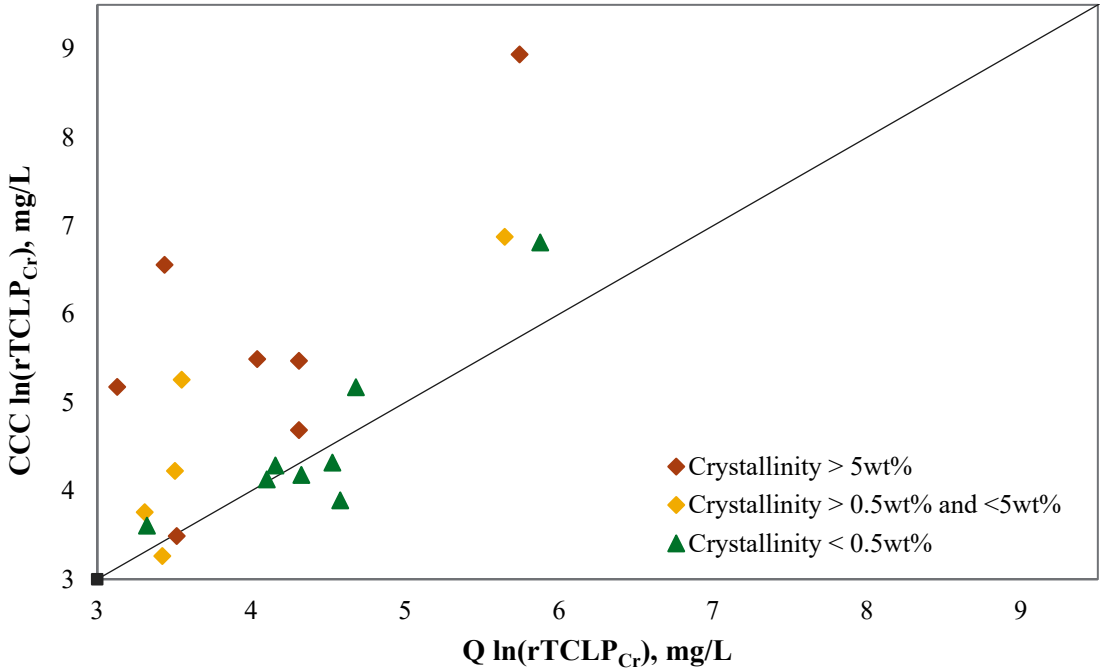

Figure 3.13. Quenched versus CCC rTCLP$_{Cr}$ Natural Logarithmic Scale of High-Fluoride HLW Glasses

The TCLP results were compared with predictions from two current models of Kim and Vienna (2002) and Vienna et al. (2009). The 2003 model approach is that the rTCLP values for elements of interest are calculated assuming they are the same as $rTCLP_B$, which is a reasonable assumption for congruent components but conservative for other elements such as Cr. Studies have demonstrated that Cr leaches from the glass at a lower rate than B, thus justifying the use of TCLP models based uniquely on B release to safely predict delisting HLW glasses (Kim and Vienna 2003). Similar to previous observations reported in the literature, TCLP normalized Cr releases of the current high-fluoride samples were lower than B releases (Figure 3.10).

In Kim and Vienna (2003), TCLP releases of the element of interest (c_i, mg/L) can be calculated based on its elemental mass fraction (f_i) as:

$$ln[r_B] = \sum_{i=1}^{N} r_{B,i}\, x_i \qquad (3.10)$$

$$c_i = r_B f_i$$

where $r_{B,i}$ is the model coefficient for the i-th component and x_i is the mole fraction of the i-th component in the glass. The coefficients of the Kim and Vienna (2003) model were derived from about 250 glasses.

The second TCLP model from Vienna et al. (2009) was generated with 291 data compositions based on older WTP baseline data, which focused on lower waste loadings (i.e., no high-fluoride glasses) using a stepwise regression method allowing only first-order terms:

$$c_r = N_{TCLP} f_r = f_r exp\left[\sum_{n=1}^{N} b_{NTCLP,i} x_i\right] \qquad (3.11)$$

where c_r is the TCLP response of each RCRA element (mg/L) and f_r is the mass fraction of the r-th element in the glass.

The normalized measured versus predicted $TCLP_B$ and $TCLP_{Cr}$ releases of quenched glasses are plotted in Figure 3.14. The model appears to underpredict $TCLP_B$ response at higher concentrations and overpredict $TCLP_B$ response at lower concentration (Figure 3.14, top). The underpredicting of the $TCLP_B$ response at higher concentrations could be explained by the conservative nature of the modeling approach. Only one glass was underpredicted for $TCLP_{Cr}$. At lower concentrations, the model overpredicted, with several glasses in the middle being predicted fairly well (Figure 3.14, bottom). Overall, the model does not appear to predict either elemental TCLP well, and one reason may be the difference in the compositional boundary of the current high-fluoride HLW glass matrix versus the ones used to develop the model. This indicates that a new model with wider compositional boundaries could be useful to obtain more accurate predictions.

Figure 3.15 shows the normalized quenched glasses measured versus predicted B (top) and Cr (bottom) TCLP releases using the 2009 model. Generally, the 2009 model tends to underpredict the B release more significantly than the 2003 model at high composition (Figure 3.15, top). However, it predicts the B release fairly well at low concentrations and then tends to limit the ln(predicted concentration) to ~5 mg/L. Comparing the predicted versus measured $TCLP_{Cr}$ concentration using the 2009 model shows that it will overpredict the Cr release at lower concentrations and slightly underpredict at higher concentrations (Figure 3.15, bottom).

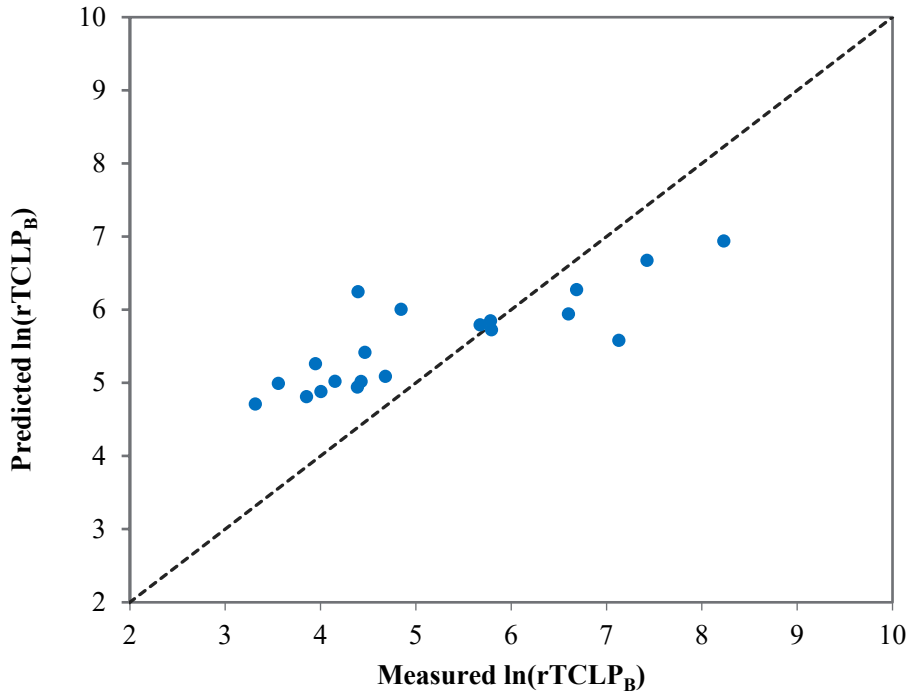

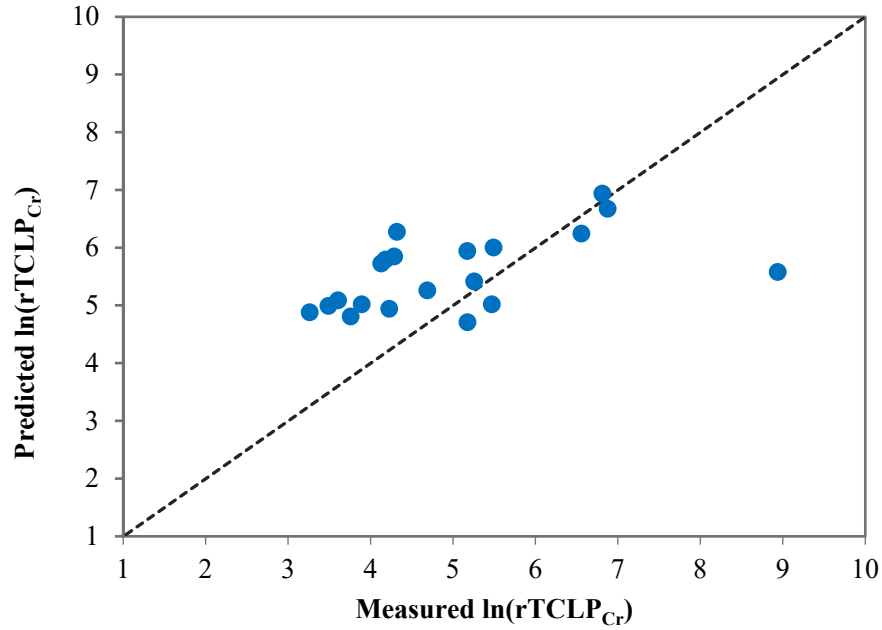

Figure 3.14. Measured versus Predicted TCLP Normalized Releases in Natural Log Scale for B (B, top) and Cr (Cr, bottom) (Kim and Vienna [2003] Model)

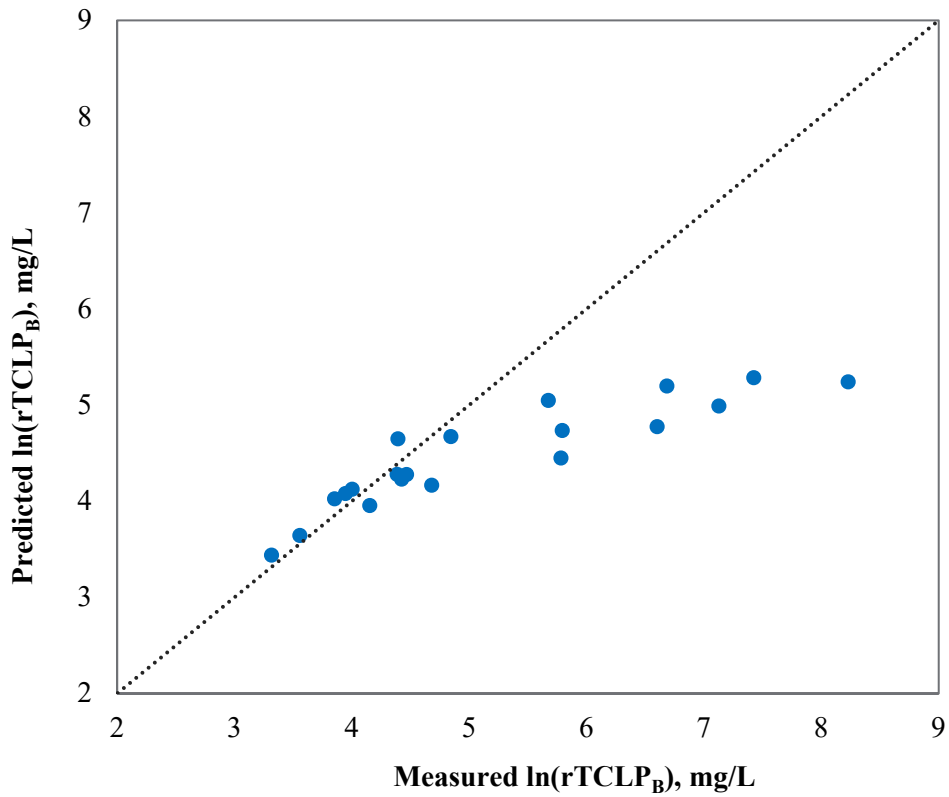

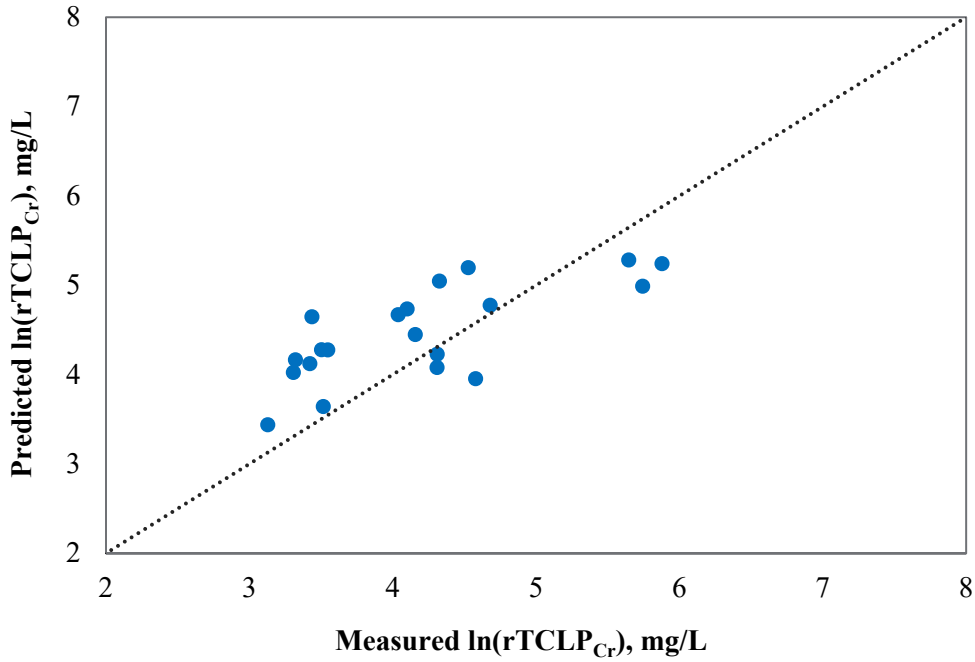

Figure 3.15. Measured versus Predicted Normalized TCLP Releases in Natural Logarithmic Scale for B (B, top) and Cr (Cr, bottom) of High-Fluoride HLW Glasses (Vienna et al. [2009] Model)

The purpose of this comparison was to assess how well the current models would predict TCLP results for the HLW glasses in this high-fluoride study. The Vienna et al. (2009) model was developed for the purpose of assessing the volume of HLW waste to be produced over the course of the WTP mission. Hence, that model was not intended for direct comparison to the various measured TCLP elemental releases from an experimental study (like the high-fluoride study). Therefore, in the future, new separate models for each of the important TCLP normalized elemental releases will need to be developed to account for the new data on high-fluoride glasses as well as all increased elements in higher waste loading glasses.

3.9 Sulfur Solubility

Sulfur solubility (i.e., the saturated SO_3 concentrations) of each glass was determined experimentally by measuring SO_3 retention after saturation as discussed in Section 2.10. These results are shown in Table 3.13. The SO_3 solubility (i.e., the saturated SO_3 concentrations) was between ~0.7 and ~2.1 wt%.

All measurements for each oxide for each glass were averaged to determine a representative chemical composition for the SSM version of each glass. A sum of oxides was also computed for each glass based on the averaged, measured values. These values are shown in Appendix J. Comparisons of the overall analyzed glass compositions after normalization of the baseline and sulfur-saturated glass samples showed that after the sulfur-saturation, other major glass components only have negligible changes except for F, which has high volatilization during multiple times of melting and/or extraction into the salt. K_2O also decreases, possibly be due to being washed out in the salt phase. All measurements for each analyte for each wash solution were averaged to determine a representative chemical composition for each solution; these were reported by Hsieh (2021b) and are given in Appendix J.

Table 3.13. Target and Saturated Concentrations of SO_3 in High-Fluoride Glasses

	SO_3 wt%		
Sample ID	Target Baseline	Measured Baseline	Sulfate-saturated
HFG1-01-1	0.182	0.186	0.891
HFG1-02	0.171	0.137	0.795
HFG1-03	0.158	<0.150	0.695
HFG1-04	0.256	0.241	2.123
HFG1-05	0.387	0.381	1.443
HFG1-06	0.212	0.209	1.612
HFG1-07	0.084	<0.125	0.728
HFG1-08	0.360	0.355	1.212
HFG1-09	0.365	0.359	1.524
HFG1-10	0.054	<0.125	1.266
HFG1-11	0.337	0.313	0.717
HFG1-12	0.065	<0.125	1.313
HFG1-13	0.330	0.297	1.187
HFG1-14	0.113	0.137	1.667
HFG1-15	0.355	0.330	1.846
HFG1-16	0.278	0.291	1.889
HFG1-17	0.152	0.166	1.452
HFG1-18	0.124	<0.136	1.019
HFG1-19	0.064	<0.125	1.522
HFG1-20	0.236	0.264	1.613

The chemical analyses data of the sulfur-saturated glasses has been used to evaluate the empirical mixture models for SO_3 solubility model (Vienna et al. 2013). This empirical model recommended a combined LAW and HLW SO_3 solubility model based on the data available at the time. This produced the model predicting SO_3 solubility shown in Eq. (3.12):

$$w_{SO_3}^{Pred} = \sum_{i=1}^{q} s_i n_i + \text{selected}\left\{\sum_{i=1}^{q} s_{ii} n_i^2 + \sum_{j=1}^{q-1}\sum_{k=j+1}^{q} s_{jk} n_j n_k\right\} \tag{3.12}$$

where

$w_{SO_3}^{Pred}$ = the predicted SO_3 solubility (in wt%)
q = the number of components in the waste glass except for SO_3
n_i = normalized (after removing SO_3) mass fraction of the ith component
s_i = coefficient of the ith component
s_{ii} = coefficient for the ith component squared
s_{jk} = coefficient for the jth and kth components cross-product

In this preliminary model, only Li_2O has a squared term (s_{ii}); there are no cross-product terms (s_{jk}). However, crucible tests performed since that model was generated showed it significantly underpredicted the measured SO_3 solubility model for HLW glasses. Although the model was found to be conservative, a more accurate model was desired and there were enough differences between the LAW and HLW feed composition that separate models were needed. The latest model (Vienna et al. 2016) is shown in Eq. (3.13):

$$w_{SO_3}^{Pred} = \sum_{i=1}^{q} s_i n_i \tag{3.13}$$

When comparing the measured SO_3 solubility with the predicted SO_3 solubility, both models were found to underpredict the SO_3 solubility of the glasses (Figure 3.16). There are most likely two reasons for this. One reason is that both models were formed with a dataset that provides incomplete coverage of the current component ranges. The other reason is that the models were formed from a dataset where the glasses were not sulfur saturated in the same method, which caused a statistically significant offset between the SO_3 saturation methods (Skidmore et al. 2018) used in the current study and the SO_3 melter tolerance used to generate the models. The previous samples in the dataset were prepared by one-time mixing and melting of the glasses with Na_2SO_4, which could not fully saturate the glass and achieve the true SO_3 solubility. On the other hand, the three times mixing and melting sulfur-saturation method used in this work (see Section 2.10) can fabricate glasses fully saturated by SO_3 and determine the true SO_3 solubility of the glass (Jin et al. 2019; Skidmore et al. 2019). Therefore, these models need to be modified using this new experimentally determined SO_3 solubility data to improve the empirical model for SO_3 solubility.

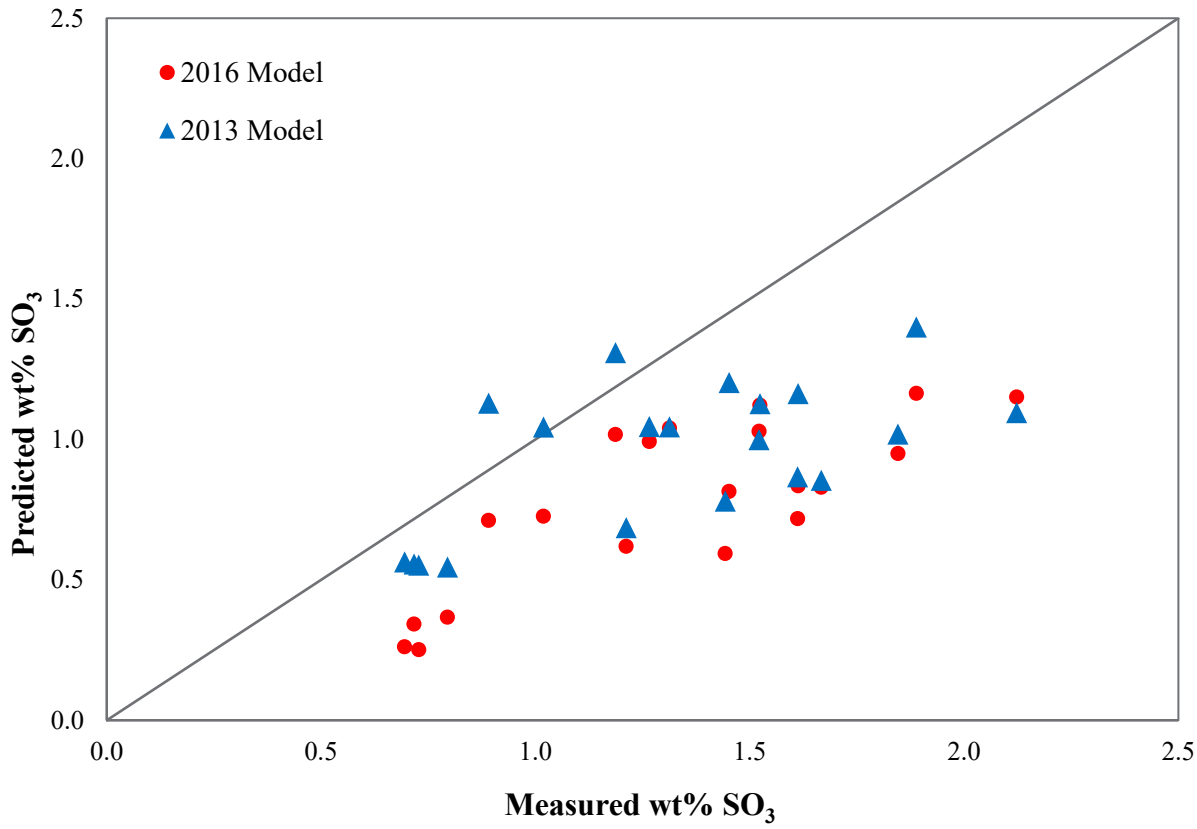

Figure 3.16. Predicted versus Measured SO_3 Solubility for High-Fluoride HLW Glasses

4.0 Summary

This study was aimed at investigating the effects of fluoride concentration on simulated HLW glass properties to eventually establish a fluoride limit (as a single-component constraint or a multiple-component constraint) for glass formulation for high-fluoride Hanford wastes.

A text matrix of 20 high-fluoride glasses was generated. Their chemical compositions were measured. The following properties were measured and tested against the current model predictions: crystal formation after CCC, CF as a function of temperature, density, viscosity, EC, TCLP, PCT, and SO_3 solubility.

The XRD scans of CCC glass samples identified primarily fluoride salts (LiF, NaF, and CaF_2). Seven samples had no crystals and six glasses had crystal content of less than 5 mass%. Only one glass (HFG1-16) had a crystal content greater than 10 mass% and contained silicates, ZrO_2, and nepheline. Two glasses (HFG1-16 and HFG1-17) had Zr containing phases. These glasses had compositions of ZrO_2 >13 wt% and most likely were above the Zr solubility limit.

The mode of these 20 density values was 2.68 g/cm^3, with a minimum of 2.55 g/cm^3 and a maximum of 2.77 g/cm^3. The density of these waste glasses varied little – 60% of the glasses have density values between 2.62 and 2.70 g/cm^3. The molar volume-based model showed the best fit, clustering closer to the 45-degree line and appearing to have a similar slope as the 45-degree line, whereas the partial-specific volume model clearly overestimated all the data except for two with a decidedly different linear slope. However, it would be best in the future to generate more data in the high-fluoride composition space and develop a new model to predict the glass density in this composition region.

Viscosity at 1150 °C ranged from 1.71 to 10.89 Pa·s. The two current viscosity models (Vienna et al. 2013, 2016) were applied to the current matrix. The two models had similar fits to the data, with both underpredicting the viscosity, especially at lower values. At higher viscosities, there were a couple points overpredicted. This may be due to the Vienna et al. (2016) model being a linear model whereas the Vienna et al. (2013) model includes a binary term. This indicates that the data does not fit a linear model as well and binary terms need to be included. These models were also based on a wide composition range with several different components whereas this study was conducted on a tighter composition range with just higher fluoride in the glass and far fewer components.

The measured EC at 1150 °C was between 19.6 and 92.1 S/m. The EC model (Vienna et al. 2009) was not very accurate as eight glasses were overpredicted and six were underpredicted, with only three glasses near the 45-degree line. This could be because of the different glass composition region that the high-fluoride study explored compared to the composition region explored for the models. Therefore, a new model exploring a wider composition region would be useful to account for this data.

In measuring the CF of the glasses by holding them at 950 °C for 24 ± 2 h, all but four glasses had insufficient crystals to perform XRD analysis when treated at 950 °C. Therefore, the temperature was lowered to 850 °C and 800 °C. Two glasses formed CaF_2 and two glasses formed $Na_2ZrSi_2O_7$. The rest remained amorphous. For the four glasses that crystals were measured at 950 °C, the temperature was increased to 1050 °C and 1150 °C. They all form a sodium zirconium silicate or zirconium oxide.

Normalized PCT releases for B, Na and Li were measured. Overall, 5% quenched and 10% CCC samples exceeded the limit. No significant effect of CCC heat treatment was observed on PCT except for one glass, HFG1-16. The content of crystals after CCC in this glass was over 90%. This glass also failed the

PCT after CCC, indicating that the crystals reduced the durability of the glass. When applying the two current models (Vienna et al. 2013, 2016) to predict a normalized PCT and B, Na, and Li releases, the 2013 model appeared to overpredict the property and the 2016 model appeared to underpredict the property (from Figure 3.9 to Figure 3.11). This is expected due to the difference in compositional space between data used to generate the models and the current matrix.

TCLP concentrations (cTCLP) for both quenched and CCC glasses were measured. Only one CCC glass (HFG1-16-CCC) failed to pass the Cr Hanford delisting limit of 4.95 mg/L. This is most likely due to the crystal content of the glass (~93%) decreasing the durability. The other glasses passed the Hanford delisting limit for Cr. Chromium was the only component of the TCLP test that was present in these glasses. As for PCT, crystallinity content after CCC appeared to be the cause of the behavior.

The Kim and Vienna (2003) model approach for TCLP is that the rTCLP values for elements of interest are calculated assuming they are the same as $rTCLP_B$. This assumption is reasonable for congruent components but has a conservative effect on other elements such as chromium. The Vienna et al. (2009) model uses a stepwise regression allowing only first order terms. However, the current models were generated using a very different compositional space. Indeed, both the Kim and Vienna (2003) and the Vienna et al. (2009) models failed to predict the rTCLP response of the current high-fluoride HLW glass matrix by underpredicting at lower rTCLP values and overpredicting at higher values. The purpose of this comparison was to assess how well the current models would predict TCLP results for the HLW glasses in this high fluoride study. In the future, new separate models for each of the important TCLP normalized elemental releases will need to be developed to account for the new data on high-fluoride glasses as well as all increased elements in higher waste loading glasses.

Sulfur solubility (i.e., the saturated SO_3 concentrations) was measured for each glass. The SO_3 solubility (i.e., the saturated SO_3 concentrations) was between 0.7 and 2.1 wt% for all glasses. The SO_3 solubility model (Vienna et al. 2013) to predict SO_3 melter tolerance was applied as well as the latest model (Vienna et al. 2016). When comparing the measured SO_3 solubility with the predicted SO_3 solubility, both models were found to underpredict the SO_3 solubility of the glasses. Therefore, these models need to be modified using this new experimentally determined SO_3 solubility data to improve the empirical model for SO_3 solubility in HLW glasses.

Additional work is needed to accurately assess the impacts of high-fluoride wastes on Hanford waste processing, including additional data collection over a broader composition region (including higher F content) and model development for the key models of interest such as PCT and TCLP.

5.0 References

40 CFR 268. "Land Disposal Restrictions." *Code of Federal Regulations*.

ASTM C1285, *Standard Test Methods for Determining Chemical Durability of Nuclear, Hazardous, and Mixed Waste Glasses and Multiphase Glass Ceramics: The Product Consistency Test (PCT)*. ASTM International, West Conshohocken, PA.

ASTM C1720, *Standard Test Method for Determining Liquidus Temperature of Immobilized Waste Glasses and Simulated Waste Glasses.* ASTM International, West Conshohocken, PA.

Cook KM. 2019. *Nuclear Quality Research Program Manual*. PNNL-SA-115260, Pacific Northwest National Laboratory, Richland, WA.

Crum JV, TB Edwards, RL Russell, PJ Workman, MJ Schweiger, RF Schumacher, DE Smith, DK Peeler, and JD Vienna. 2012. "DWPF Startup Frit Viscosity Measurement Round Robin Results." *Journal of the American Ceramic Society* 95(7):2196-2205.

DOE. 2000. *Design, Construction, and Commissioning of the Hanford Tank Waste Treatment and Immobilization Plant*. Contract DE-AC27-01RV14136, as amended, U.S. Department of Energy, Office of River Protection, Richland, WA.

DOE. 2006. *Petition to Delist Immobilized High-Level Waste Generated at the Waste Treatment and Immobilization Plant*. Contract DE-AC27-01RV14136, as amended, U.S. Department of Energy, Office of River Protection, Richland, WA.

DOE. 2012. Memorandum, "Enhanced WTP Glass Composition Envelope Development," to C. Swan. Inter-Entity Work Order M0ORV00020, October 18, 2012, U.S. Department of Energy, Office of River Protection, Richland, WA.

DOE Order 414.1D, *Quality Assurance*. U.S. Department of Energy, Washington, D.C.

Ebert, W.L. and S.F. Wolfe. 1999. *Round-robin Testing of a Reference Glass for Low-Activity Waste Forms*. ANL-99/22, Argonne National Laboratory, Argonne, IL.

EPA. 1992a. *Toxicity Characteristic Leaching Procedure.* SW 846 Method 1311, Rev. 0, U. S. Environmental Protection Agency, Washington, D.C.

EPA. 1992b. *Acid Digestion of Aqueous Samples and Extracts for Total Metals for Analysis by FLAA or ICP Spectroscopy.* SW 846 Method 3010A, Rev. 1, U. S. Environmental Protection Agency, Washington, D.C.

EPA. 1994. *Mercury in Liquid Waste (Manual Cold-Vapor Technique).* SW 846 Method 7470A, Rev. 1, U. S. Environmental Protection Agency, Washington, D.C.

Geeting JGH and RT Hallen. 2005. "Filtration, washing, and caustic leaching of Hanford tank AZ-101 sludge." *Separation Science Technology* 40:1-15.

Goel A, JS McCloy, R Pokorny, and AA Kruger. 2019. "Challenges with vitrification of Hanford High-Level Waste (HLW) to borosilicate glass—An overview." *Journal of Crystalline Solids: X* 4:100033.

Hanford. 2020. *Best Basis Inventory*. https://twins.hanford.gov/twinsdata, Retrieved August 14, 2020.

Hsieh M. 2021a. *Composition Measurements of the HFG1 Glasses*. SRNL-STI-2021-00147, Rev. 0, Savannah River National Laboratory, Aiken, SC.

Hsieh M. 2021b. *Characterization of the Sulfur-Saturated Melt Versions of the HFG1 Study Glasses*. SRNL-STI-2021-00149, Rev. 0, Savannah River National Laboratory, Aiken, SC.

Hsieh M. 2021c. *Product Consistency Test Results for the HFG1 Glasses*. SRNL-STI-2021-00148, Rev. 0, Savannah River National Laboratory, Aiken, SC.

Jin T, DS Kim, LP Darnell, BL Weese, NL Canfield, M Bliss, MJ Schweiger, JD Vienna, and AA Kruger. 2019. "A Crucible Salt Saturation Method for Determining Sulfur Solubility in Glass Melt." *International Journal of Applied Glass Science* 10:92-102.

Jin T, JD Vienna, D-S Kim, and MS Fountain. 2020, *Fluorine Limits and Impacts in High-Level Waste Glass Compositions*. PNNL-30072, Rev. 0 RPT-OSIF-013, Rev. 0, Pacific Northwest Laboratory, Richland, WA.

Kim DS and JD Vienna. 2002. *Model for TCLP Releases from Waste Glasses*. PNNL-14061, Pacific Northwest National Laboratory, Richland, WA.

McGinnis CP, TD Welch, and RD Hunt. 1999. "Caustic leaching of high-level radioactive tank sludge: a critical literature review." *Separation Science Technology* 34:1479-1494.

Mellinger GB and JL Daniel. 1984. *Approved Reference and Testing Materials for Use in Nuclear Waste Management Research and Development Programs*. PNL-4955-2, Pacific Northwest Laboratory, Richland, WA.

NQA-1-2012, *Quality Assurance Requirements for Nuclear Facility Application*. American Society of Mechanical Engineers, New York, NY.

Piepel GF, SK Cooley, A Heredia-Langner, SM Landmesser, WK Kot, H Gan, and IL Pegg. 2008. *IHLW PCT, VHT, Viscosity, and Electrical Conductivity Model Development*. VSL-07R1240-4, Rev. 0, Vitreous State Laboratory, The Catholic University of America, Washington, D.C.

Reynolds JG, HJ Huber, GA Cooke, and JA Pestovich. 2014. "Solid-phase zirconium and fluoride species in alkaline zircaloy cladding waste at Hanford." *Journal of Hazardous Materials* 278:203-210.

Skidmore, C. H., J. D. Vienna, T. Jin, D. Kim, B. A. Stanfill, K. M. Fox, and A. A. Kruger. 2019. Sulfur solubility in low activity waste glass and its correlation to melter tolerance. "International Journal of Applied Glass Science" (10):558-68.

Smith GL. 1993. *Characterization of Analytical Reference Glass-1 (ARG-1)*. PNL-8992, Pacific Northwest Laboratory, Richland, WA.

Vienna, JD, DS Kim, and P Hrma. 2002. *Database and Interim Glass Property Models for Hanford HLW and LAW Glasses*. PNNL-14060, Pacific Northwest National Laboratory, Richland, WA.

Vienna JD, A Fluegal, DS Kim, and P Hrma. 2009. *Glass Property Data and Models for Estimating High-Level Waste Glass Volume*. PNNL-18501, Pacific Northwest National Laboratory, Richland, WA.

Vienna JD, DC Skorski, D Kim, J Matyas. 2013. *Glass Property Models and Constraints for Estimating Glass to be Produced at Hanford by Implementing Current Advanced Glass Formulation Efforts.* PNNL-22631, Rev. 1, ORP-58289, Pacific Northwest National Laboratory, Richland, WA.

Vienna JD, GF Piepel, DS Kim, JV Crum, CE Lonergan, BA Stanfill, BJ Riley, SK Cooley, and T Jin. 2016. *2016 Update of Hanford Glass Property Models and Constraints for Use in Estimating the Glass Mass to be Produced at Hanford by Implementing Current Enhanced Glass Formulation Efforts*. PNNL-25835, Pacific Northwest National Laboratory, Richland, WA.

Appendix A – Morphology/Color of Each Quenched Glass

The photos in this appendix show each glass after melting in a Pt-alloy crucible twice at the specified melt temperature.

(a) Photograph of Poured Glass HFG1-01 Morphology

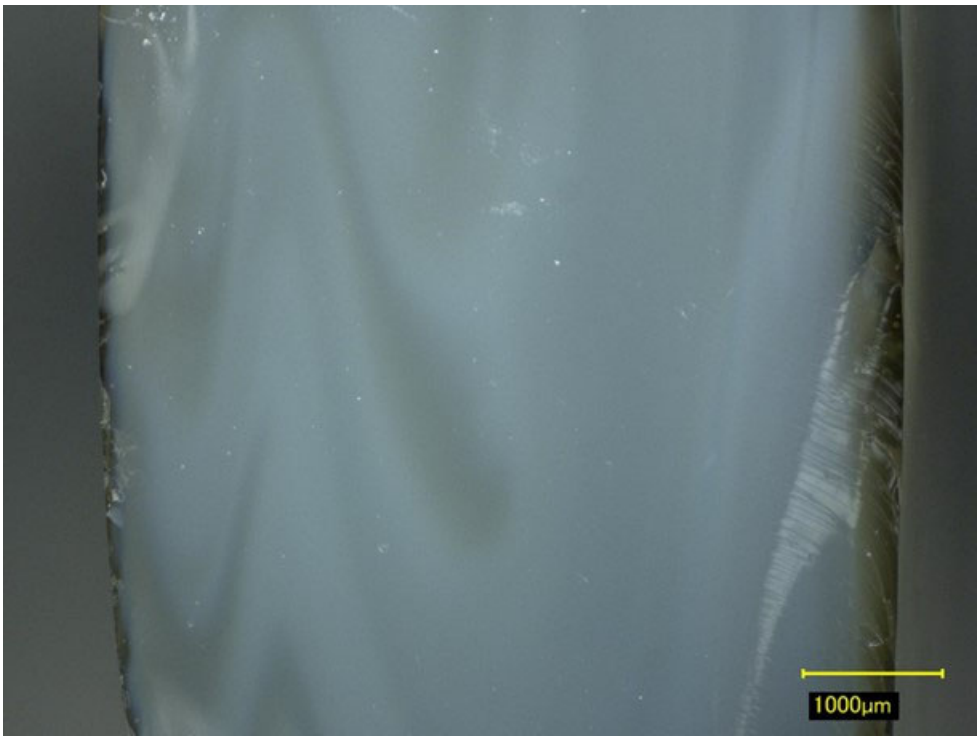

(b) Optical Micrograph of Glass HFG1-01 Morphology Magnified 50X

Figure A.1. Photograph and Optical Micrograph of Glass HFG1-01 Morphology of Second Melt at 1150 °C for 1 h

(a) Photograph of Poured Glass HFG1-02 Morphology

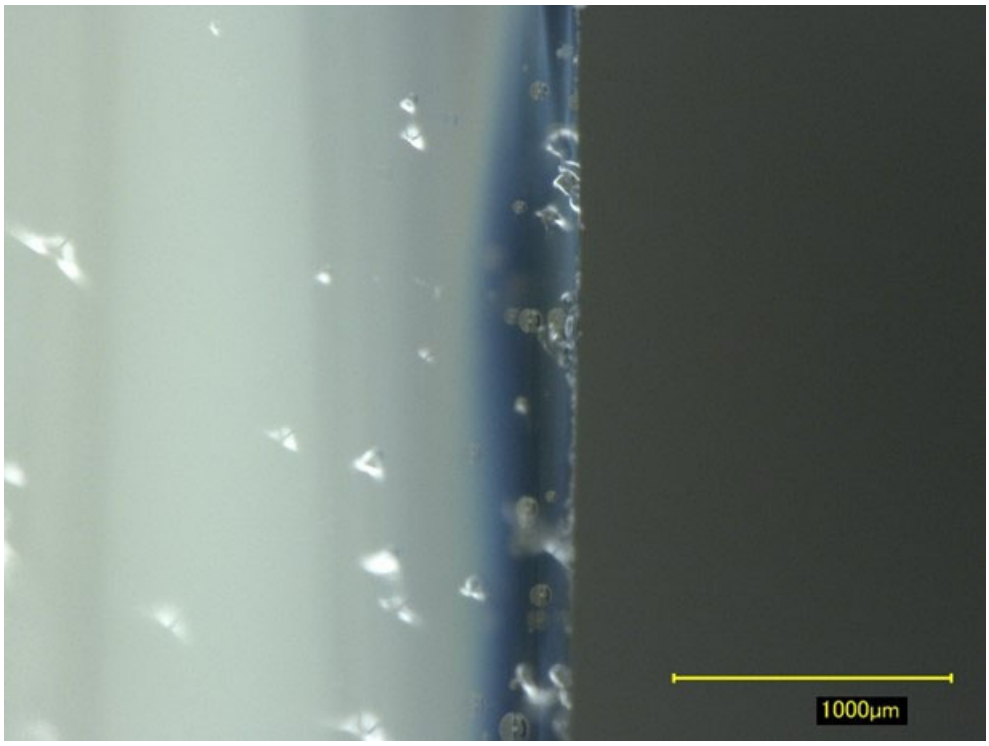

(b) Optical Micrograph of Glass HFG1-02 Morphology Magnified 100X

Figure A.2. Photograph and Optical Micrograph of Glass HFG1-02 Morphology of Second Melt at 1150 °C for 1 h

(a) Photograph of Poured Glass HFG1-03 Morphology

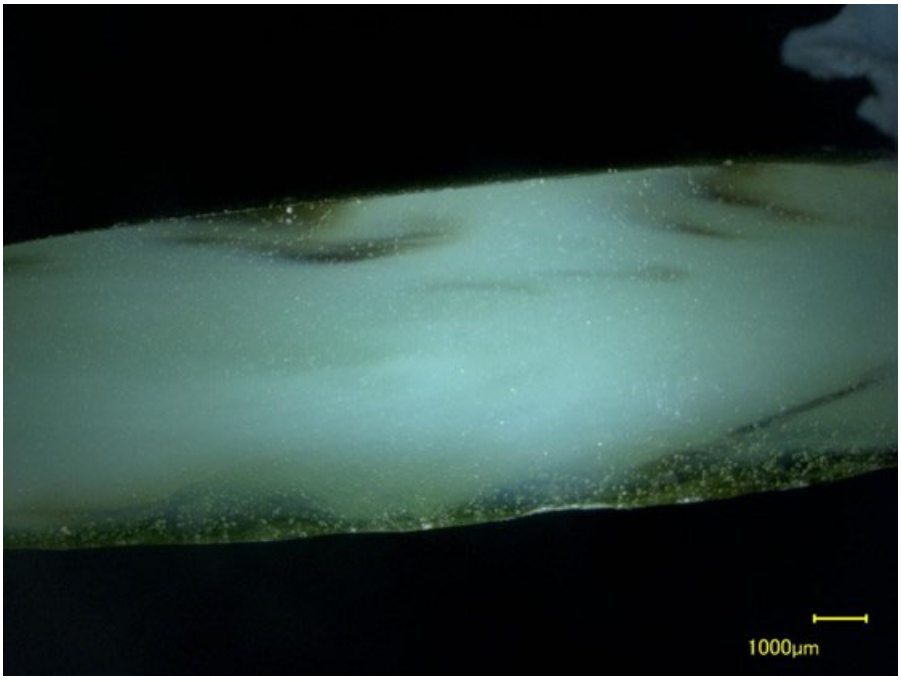

(b) Optical Micrograph of Glass HFG1-03 Morphology Magnified 20X

Figure A.3. Photograph and Optical Micrograph of Glass HFG1-03 Morphology of Second Melt at 1150 °C for 1 h

Figure A.4. Photograph of Glass HFG1-04 Morphology of Second Melt at 1150 °C for 1 h

(a) Photograph of Poured Glass HFG1-05 Morphology

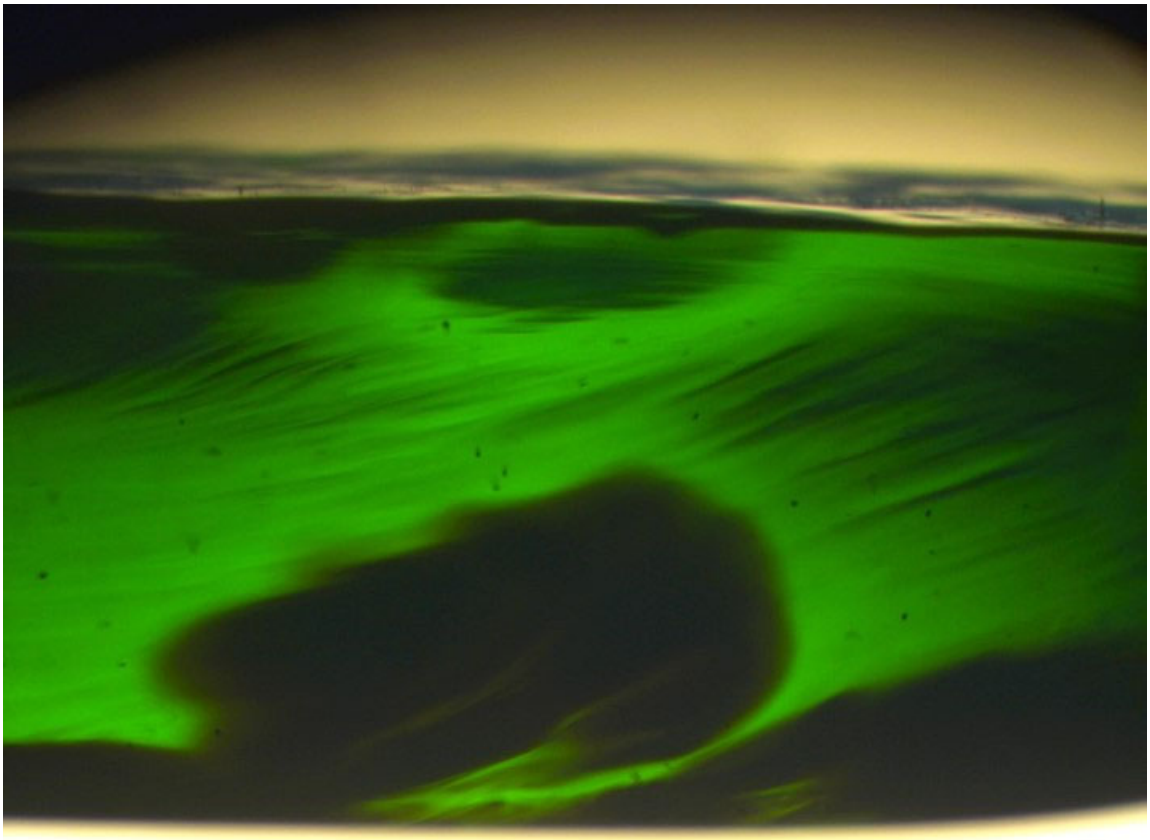

(b) Optical Micrograph of Glass HFG1-05 Morphology Magnified

Figure A.5. Photograph and Optical Micrograph of Glass HFG1-05 Morphology of Second Melt at 1150 °C for 1 h

(a) Photograph of Poured Glass HFG1-06 Morphology

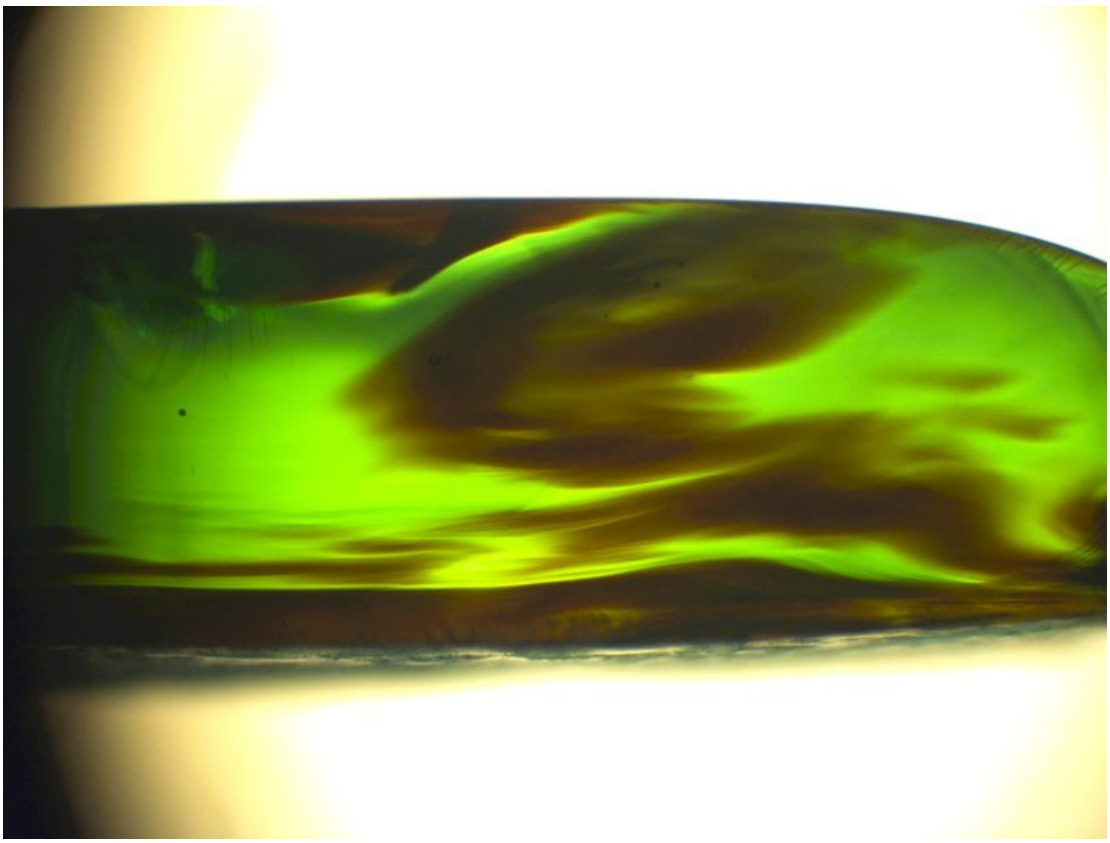

(b) Optical Micrograph of Glass HFG1-06 Morphology Magnified

Figure A.6. Photograph and Optical Micrograph of Glass HFG1-06 Morphology of Second Melt at 1150 °C for 1 h

Figure A.7. Photograph of Glass HFG1-07 Morphology of Second Melt at 1150 °C for 1 h

(a) Photograph of Poured Glass HFG1-08 Morphology

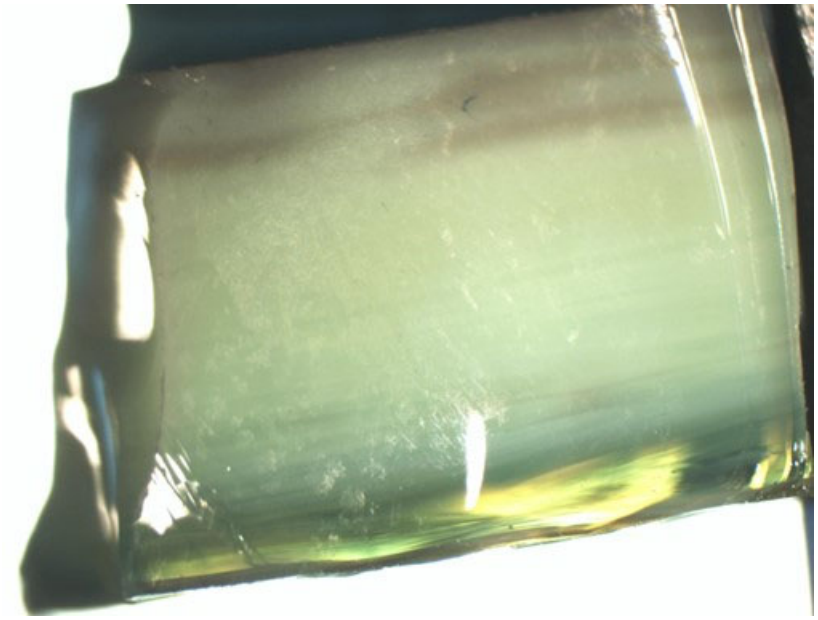

(b) Optical Micrograph of Glass HFG1-08 Morphology Magnified

Figure A.8. Photograph and Optical Micrograph of Glass HFG1-08 Morphology of Second Melt at 1150 °C for 1 h

Figure A.9. Photograph of Glass HFG1-09 Morphology of Second Melt at 1150 °C for 1 h

Figure A.10. Photograph of Glass HFG1-10 Morphology of Second Melt at 1150 °C for 1 h

(a) Photograph of Poured Glass HFG1-11 Morphology

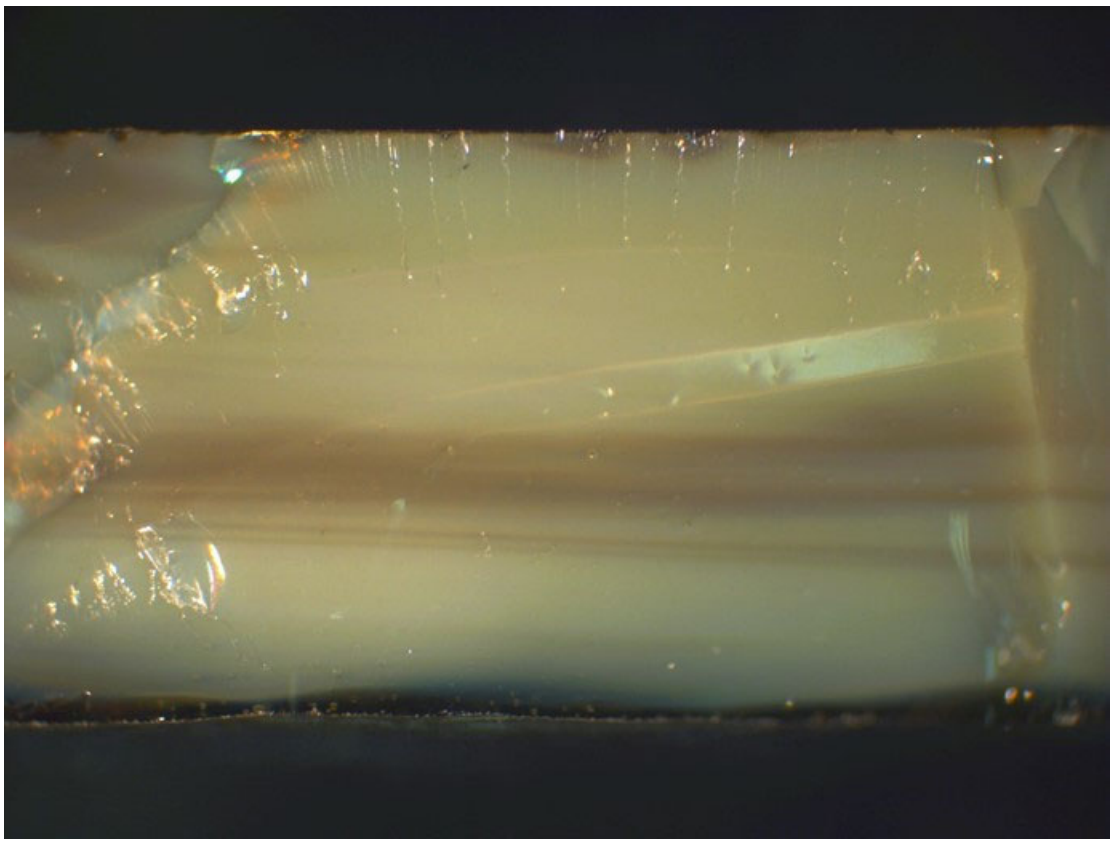

(b) Optical Micrograph of Glass HFG1-11 Morphology Magnified

Figure A.11. Photograph and Optical Micrograph of Glass HFG1-11 Morphology of Second Melt at 1150 °C for 1 h

Figure A.12. Photograph of Glass HFG1-12 Morphology of Second Melt at 1150 °C for 1 h

Figure A.13. Photograph of Glass HFG1-13 Morphology of Second Melt at 1150 °C for 1 h

Figure A.14. Photograph of Glass HFG1-14 Morphology of Second Melt at 1150 °C for 1 h

Figure A.15. Photograph of Glass HFG1-15 Morphology of Second Melt at 1150 °C for 1 h

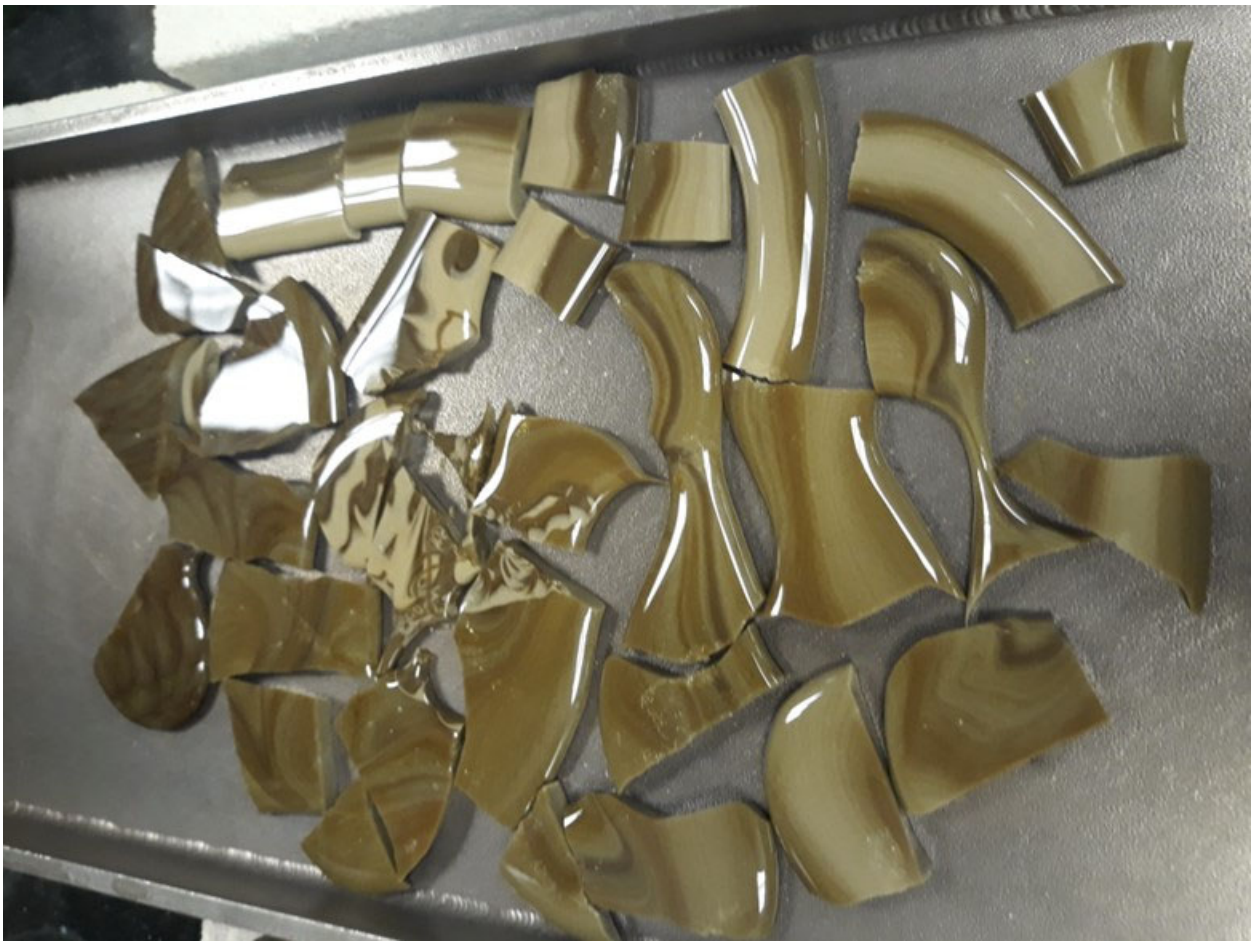

Figure A.16. Photograph of Glass HFG1-16 Morphology of Second Melt at 1150 °C for 1 h

Figure A.17. Photograph of Glass HFG1-17 Morphology of Second Melt at 1150 °C for 1 h

Figure A.18. Photograph of Glass HFG1-18 Morphology of Second Melt at 1150 °C for 1 h

Figure A.19. Photograph of Glass HFG1-19 Morphology of Second Melt at 1150 °C for 1 h

Figure A.20. Photograph of Glass HFG1-20 Morphology of Second Melt at 1150 °C for 1 h

Appendix B – XRD of Quenched Glasses

This appendix shows the X-ray diffraction (XRD) plots of the high-fluoride glasses after melting and quenching. These glasses were found to range from being amorphous to developing crystals of fluoride salts as shown by the following plots.

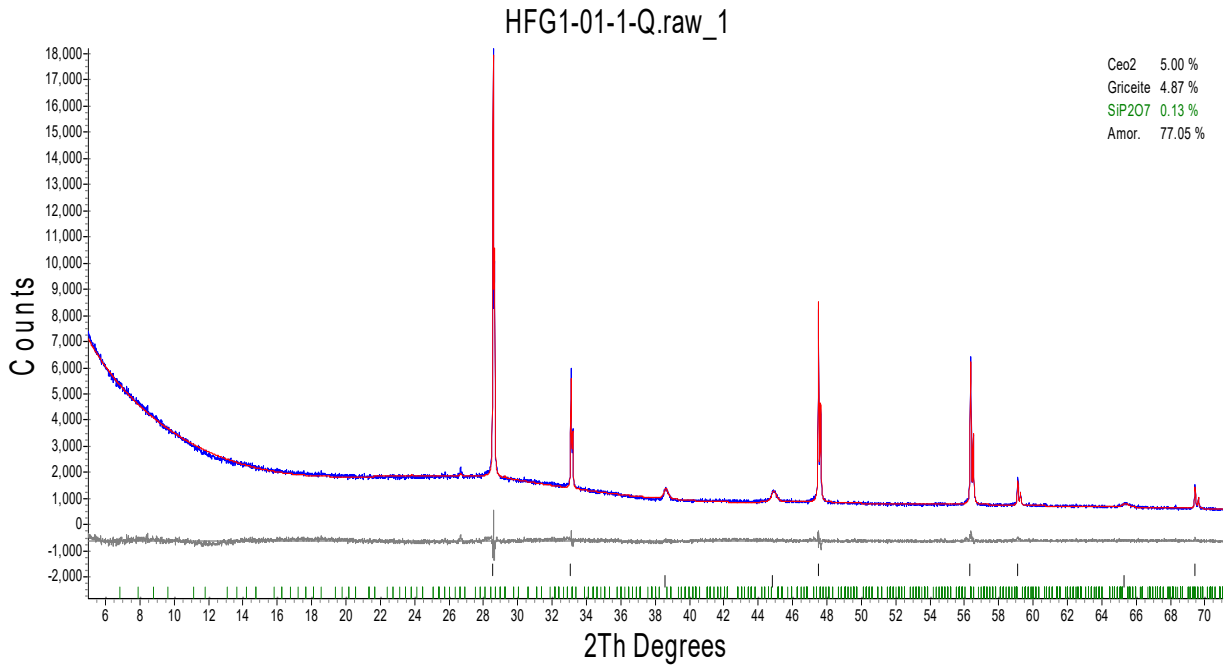

Phase Name	Wt% of Spiked	Wt% in Spiked Sample	Wt% in Original Sample
CeO_2	5.000	5.000	0.000
LiF	0.000	4.874	5.131
SiP_2O_7	0.000	0.131	0.138

Figure B.1. XRD Spectrum of Quenched Glass HFG1-01-1

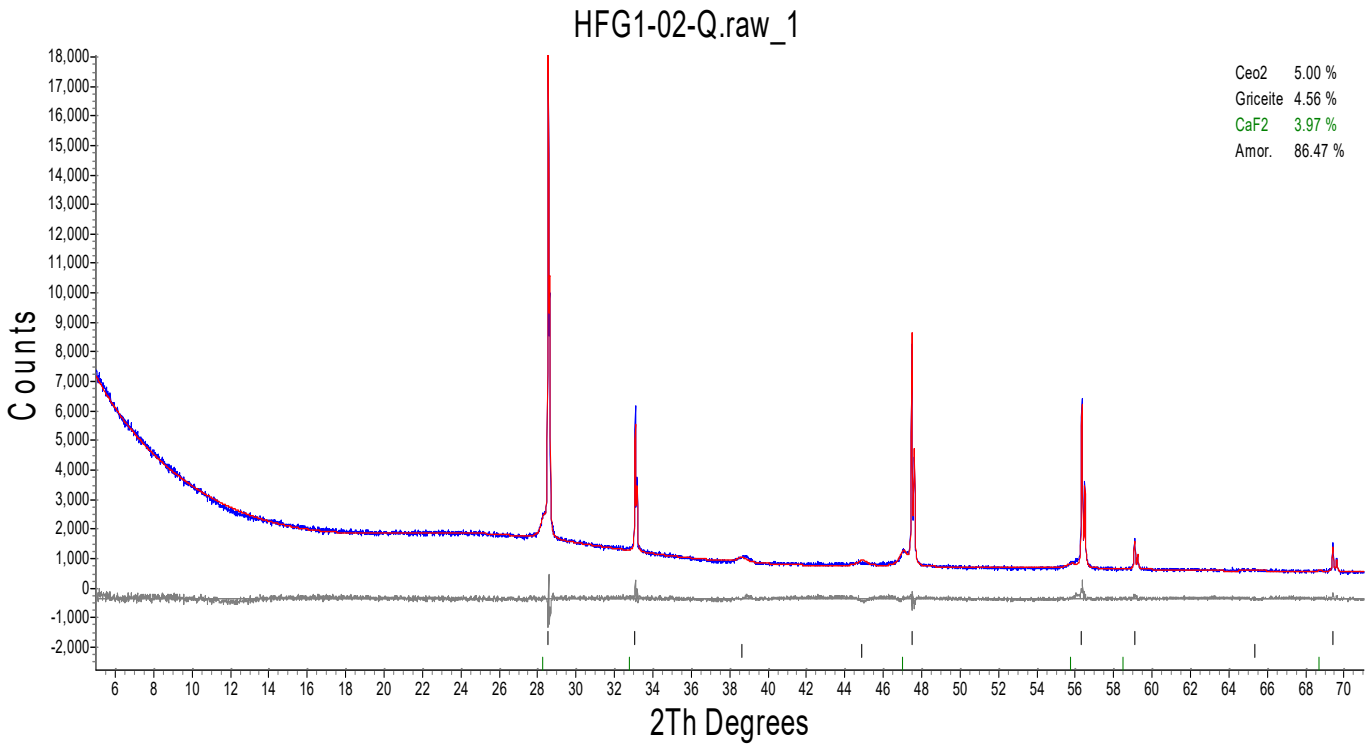

Phase Name	Wt% of Spiked	Wt% in Spiked Sample	Wt% in Original Sample
CeO_2	5.000	5.000	0.000
LiF	0.000	4.561	4.801
CaF_2	0.000	3.971	4.180

Figure B.2. XRD Spectrum of Quenched Glass HFG1-02

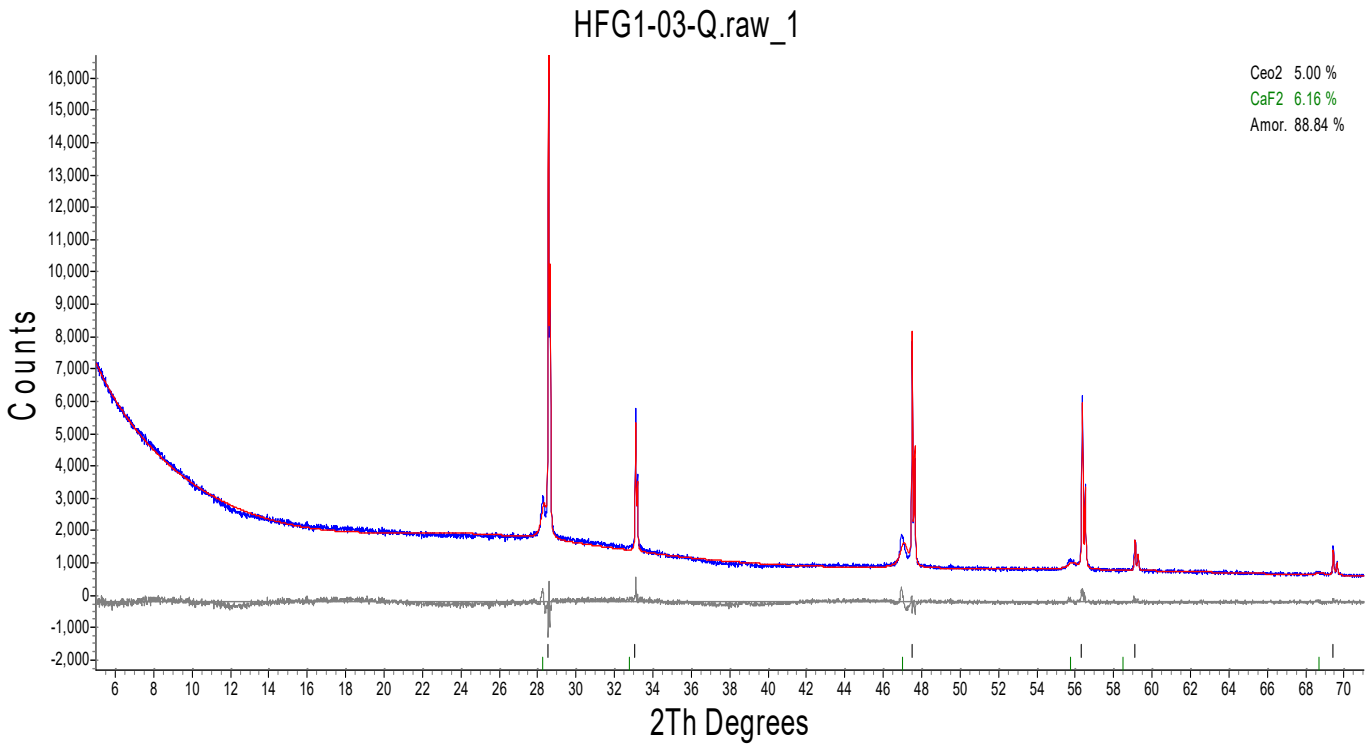

Phase Name	Wt% of Spiked	Wt% in Spiked Sample	Wt% in Original Sample
CeO_2	5.000	5.000	0.000
CaF_2	0.000	6.163	6.488

Figure B.3. XRD Spectrum of Quenched Glass HFG1-03

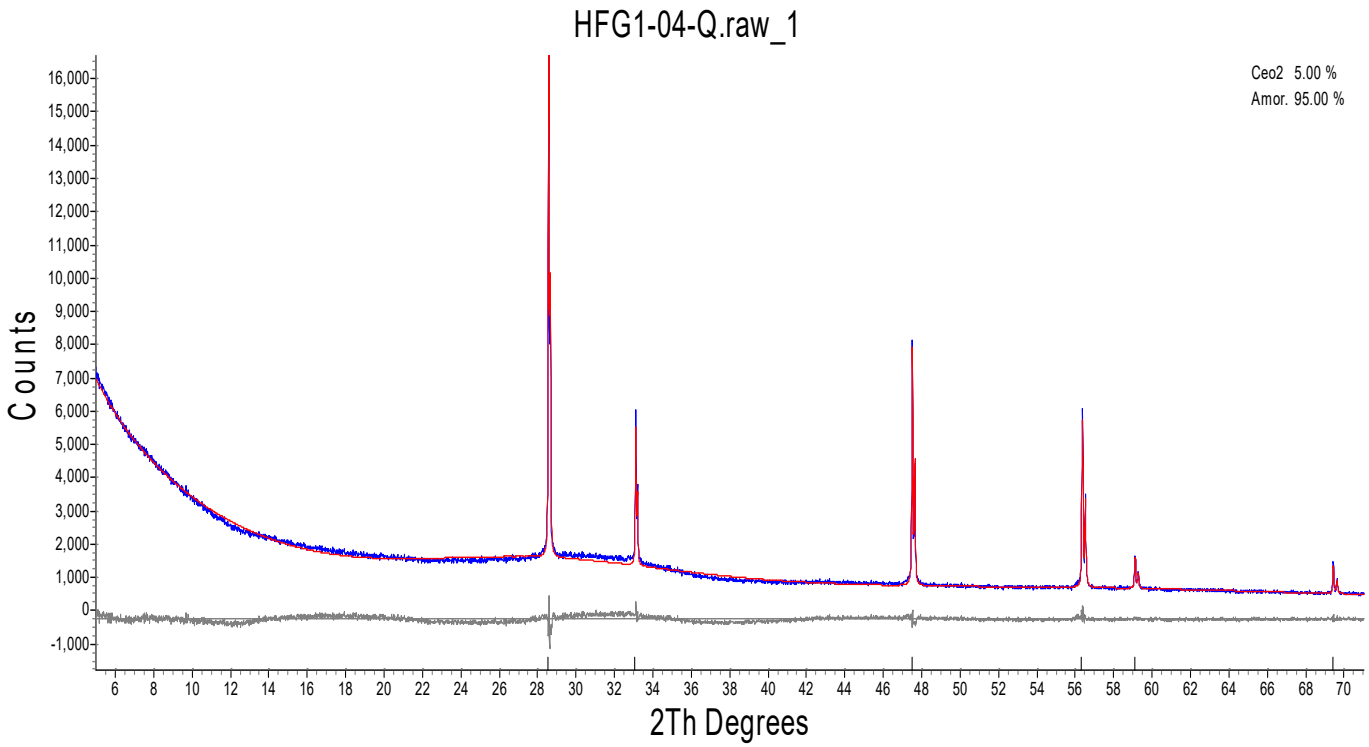

Figure B.4. XRD Spectrum of Quenched Glass HFG1-04

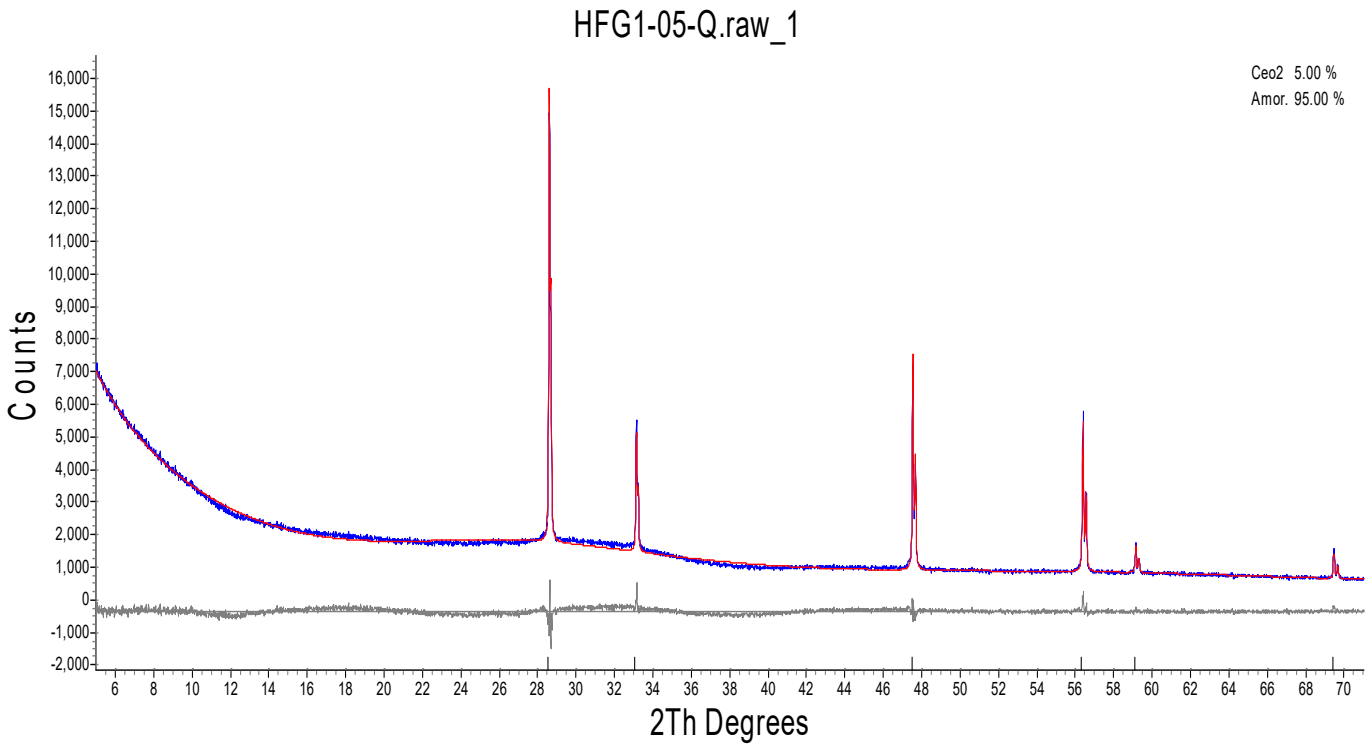

Figure B.5. XRD Spectrum of Quenched Glass HFG1-05

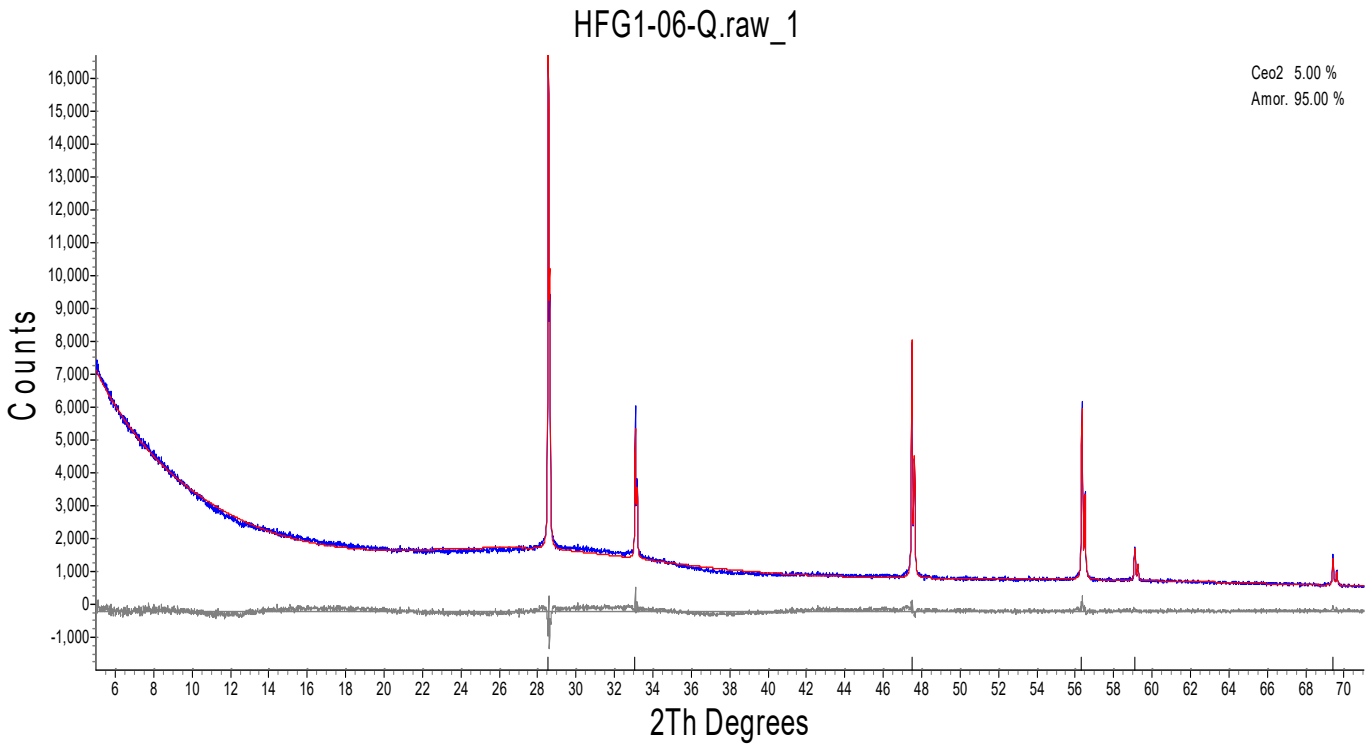

Figure B.6. XRD Spectrum of Quenched Glass HFG1-06

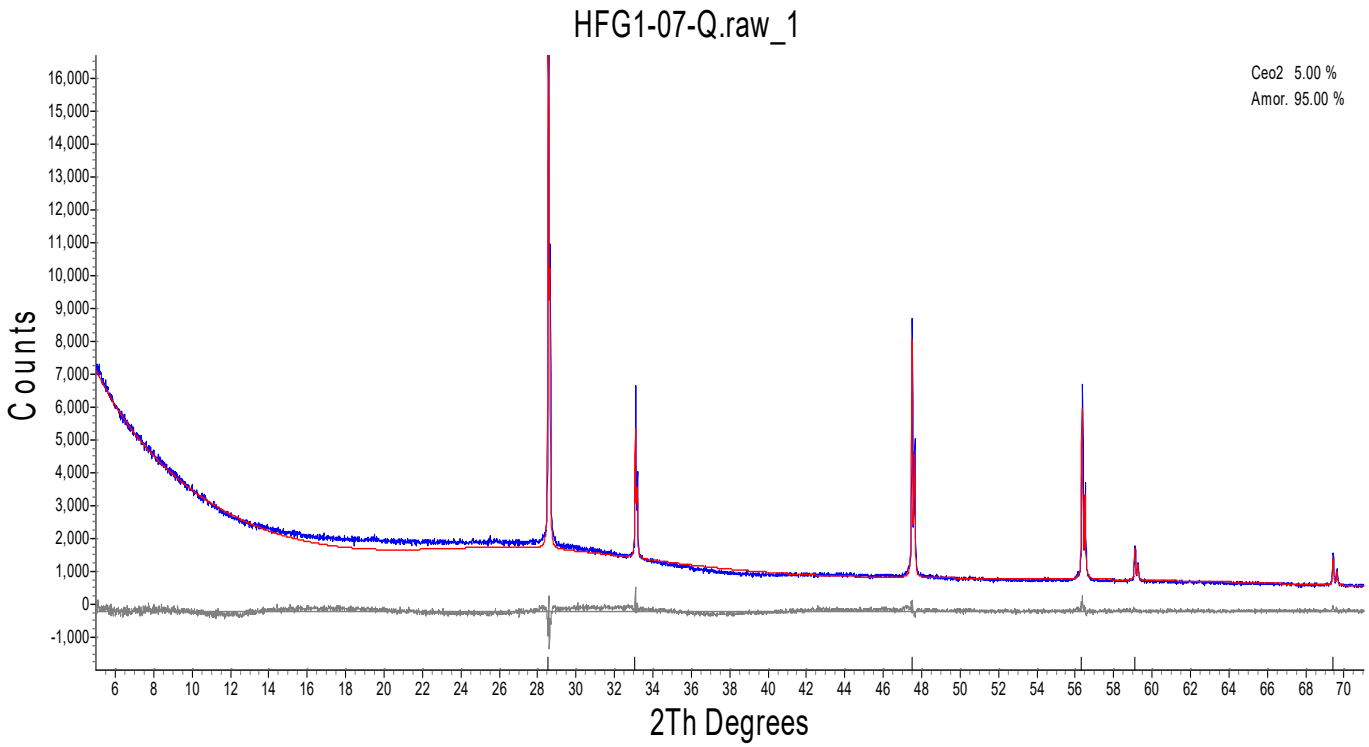

Figure B.7. XRD Spectrum of Quenched Glass HFG1-07

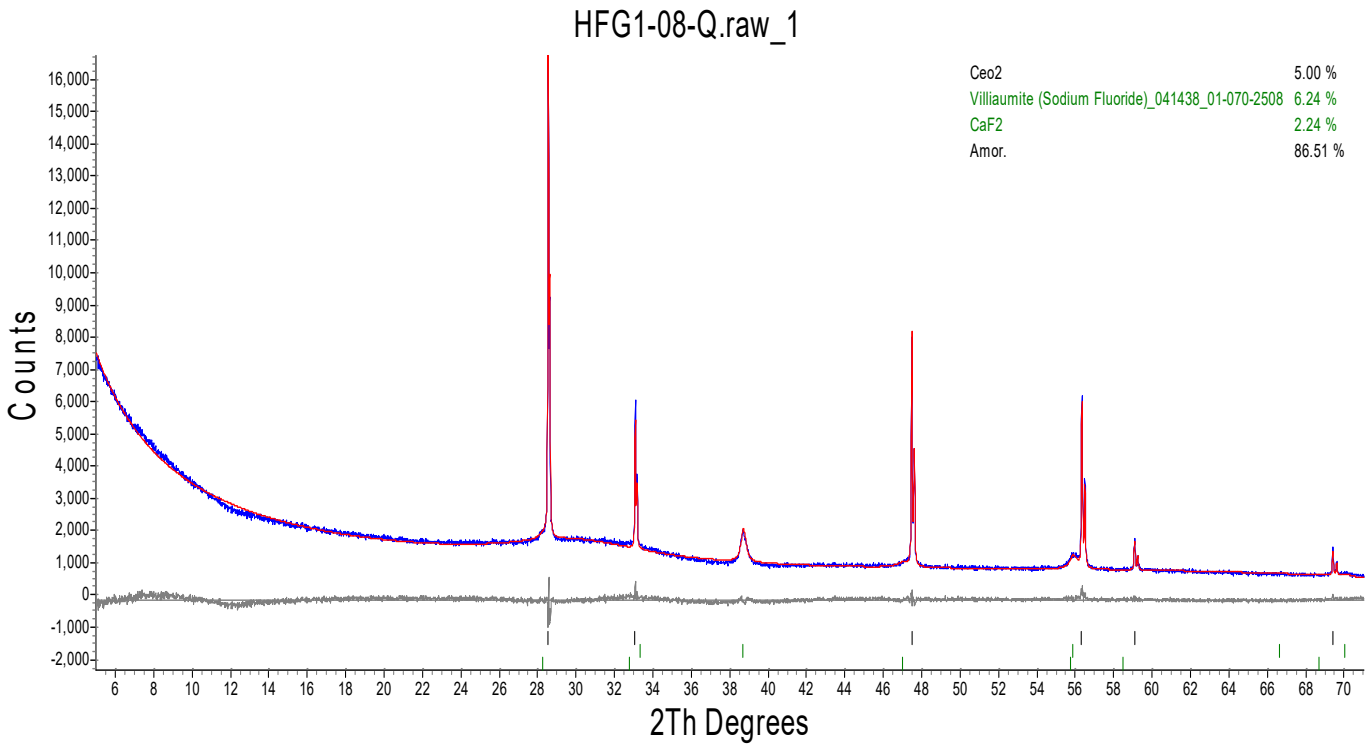

Phase Name	Wt% of Spiked	Wt% in Spiked Sample	Wt% in Original Sample
CeO_2	5.000	5.000	0.000
NaF	0.000	6.244	6.573
CaF_2	0.000	2.243	2.361

Figure B.8. XRD Spectrum of Quenched Glass HFG1-08

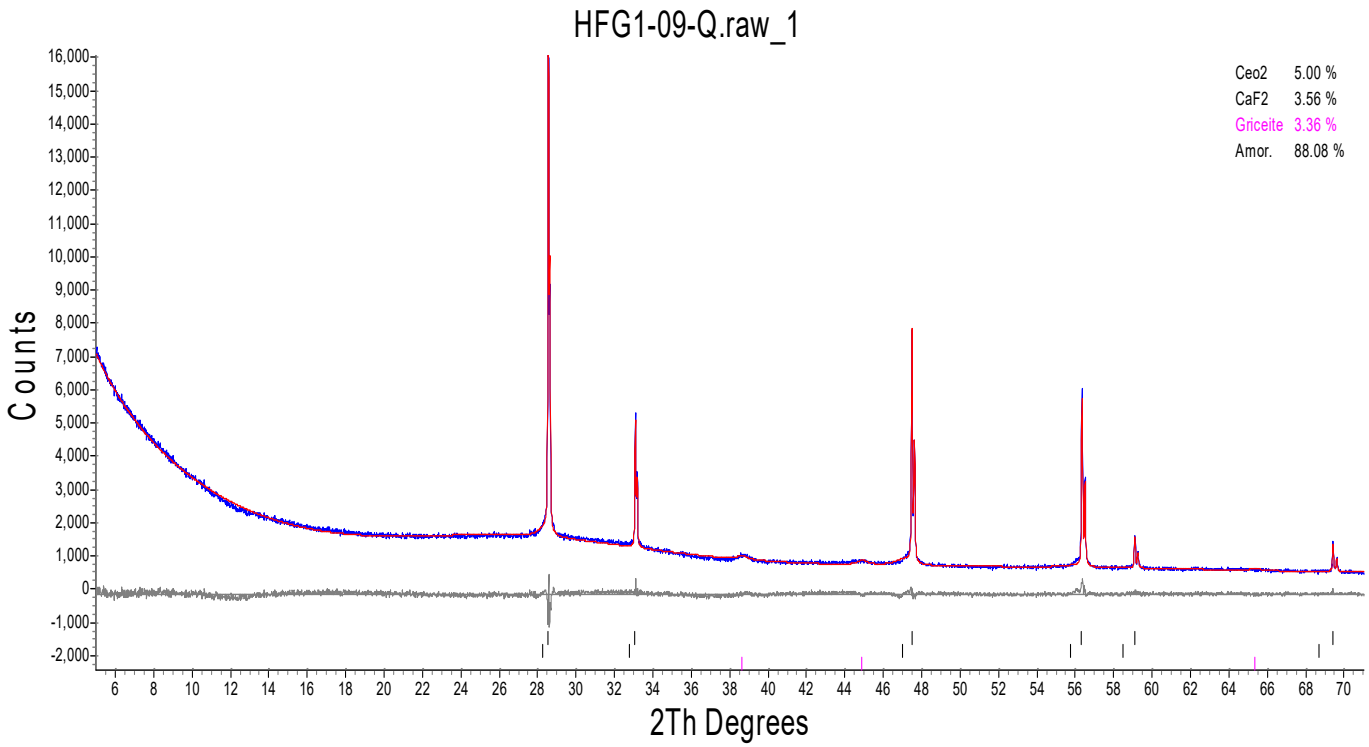

Phase Name	Wt% of Spiked	Wt% in Spiked Sample	Wt% in Original Sample
CeO_2	5.000	5.000	0.000
CaF_2	0.000	3.560	3.747
LiF	0.000	3.358	3.534

Figure B.9. XRD Spectrum of Quenched Glass HFG1-09

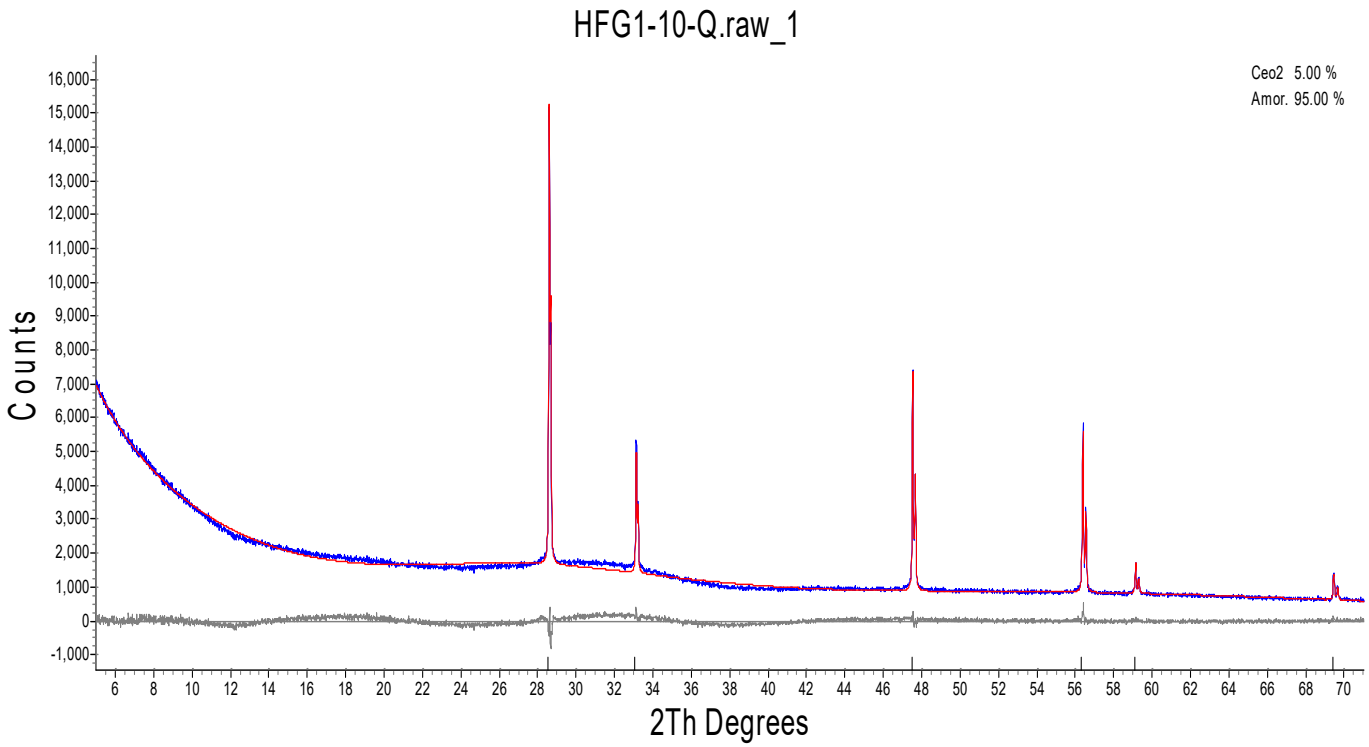

Figure B.10. XRD Spectrum of Quenched Glass HFG1-10

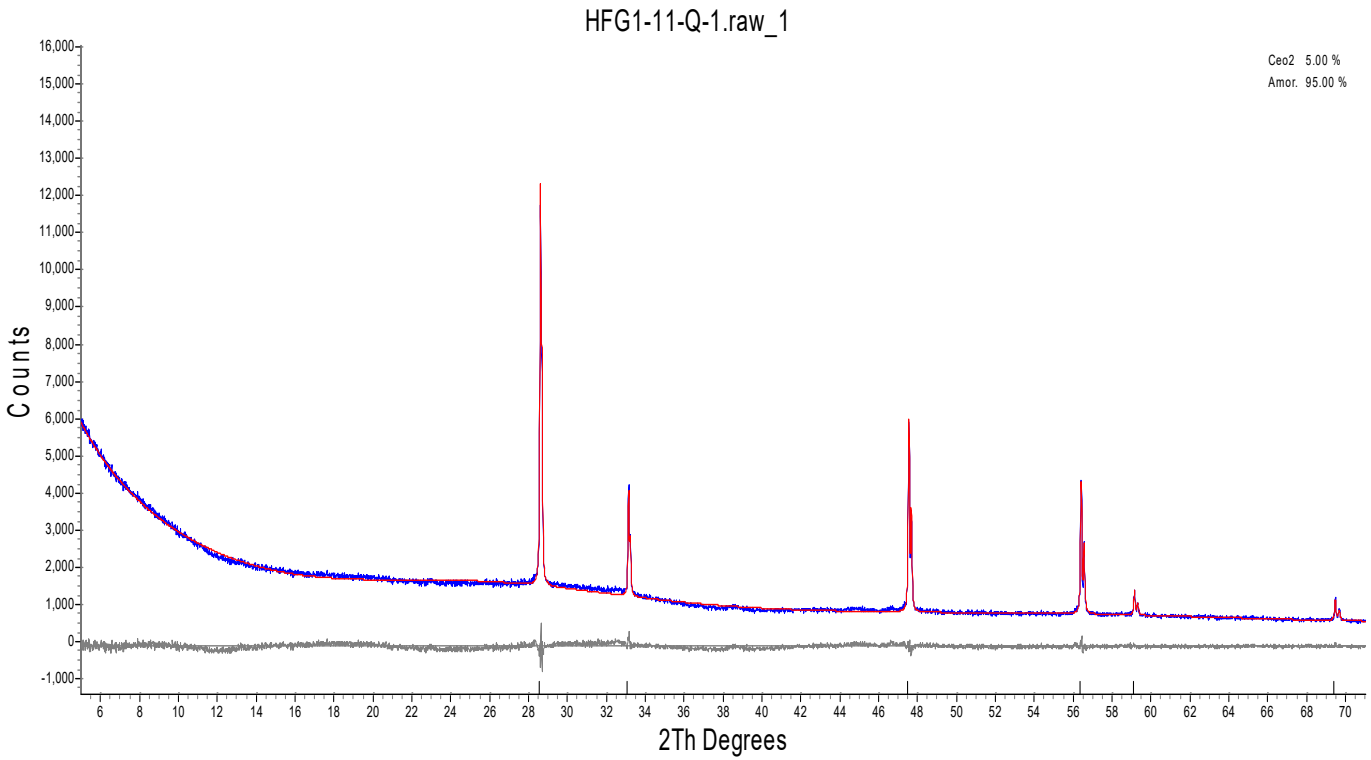

Figure B.11. XRD Spectrum of Quenched Glass HFG1-11

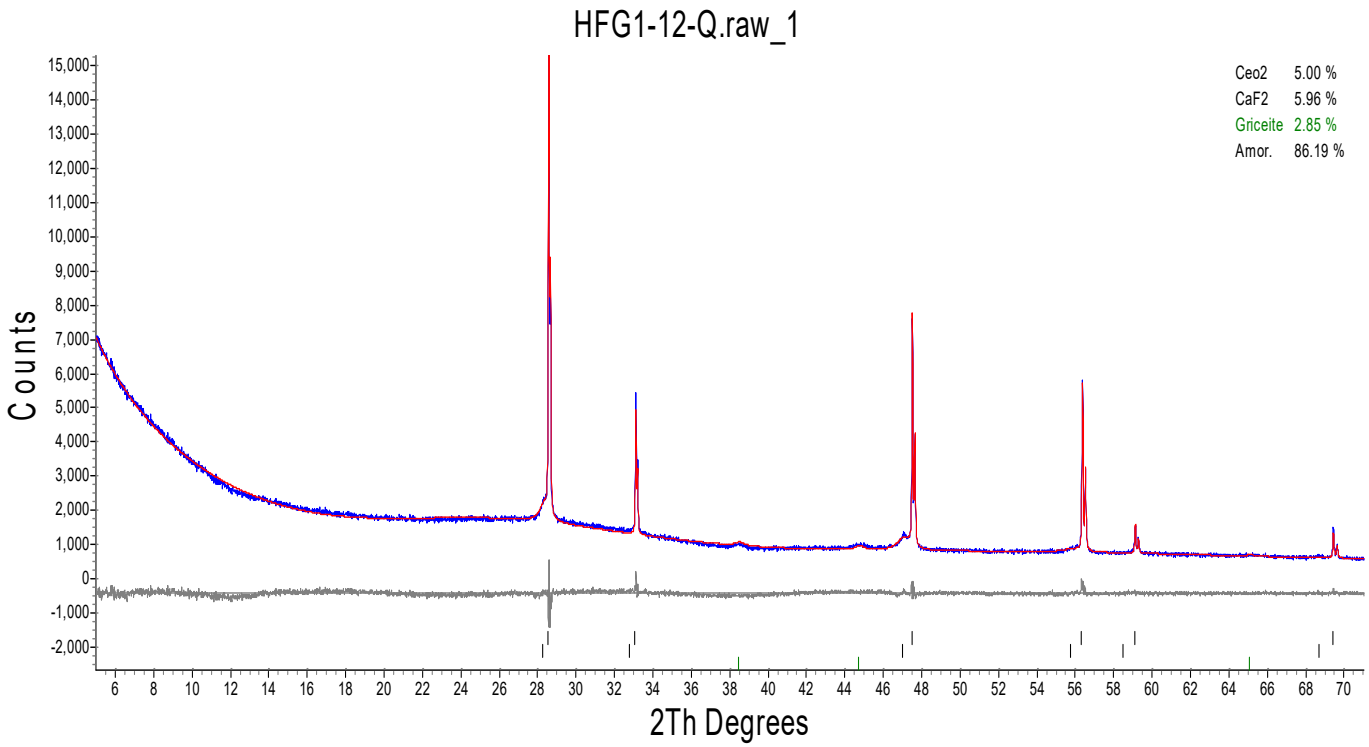

Phase Name	Wt% of Spiked	Wt% in Spiked Sample	Wt% in Original Sample
CeO_2	5.000	5.000	0.000
CaF_2	0.000	5.964	6.278
LiF	0.000	2.846	2.996

Figure B.12. XRD Spectrum of Quenched Glass HFG1-12

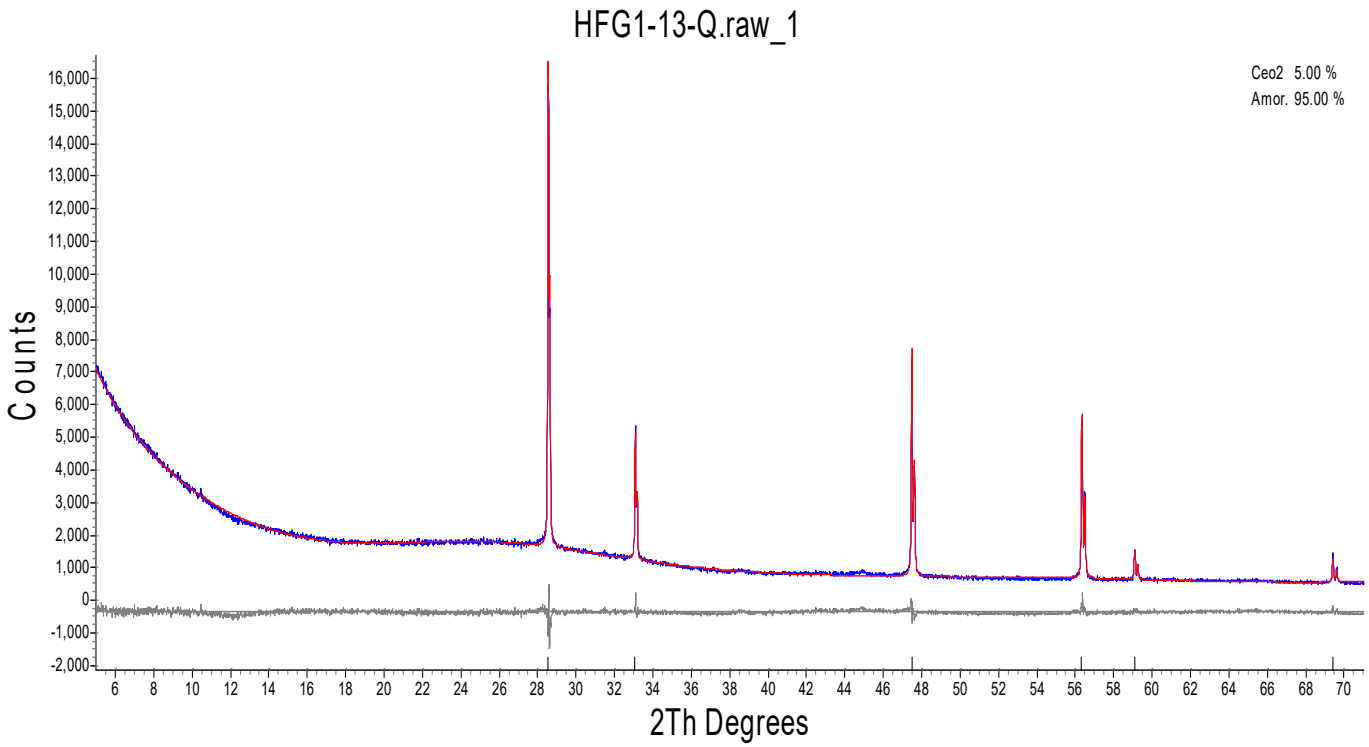

Figure B.13. XRD Spectrum of Quenched Glass HFG1-13

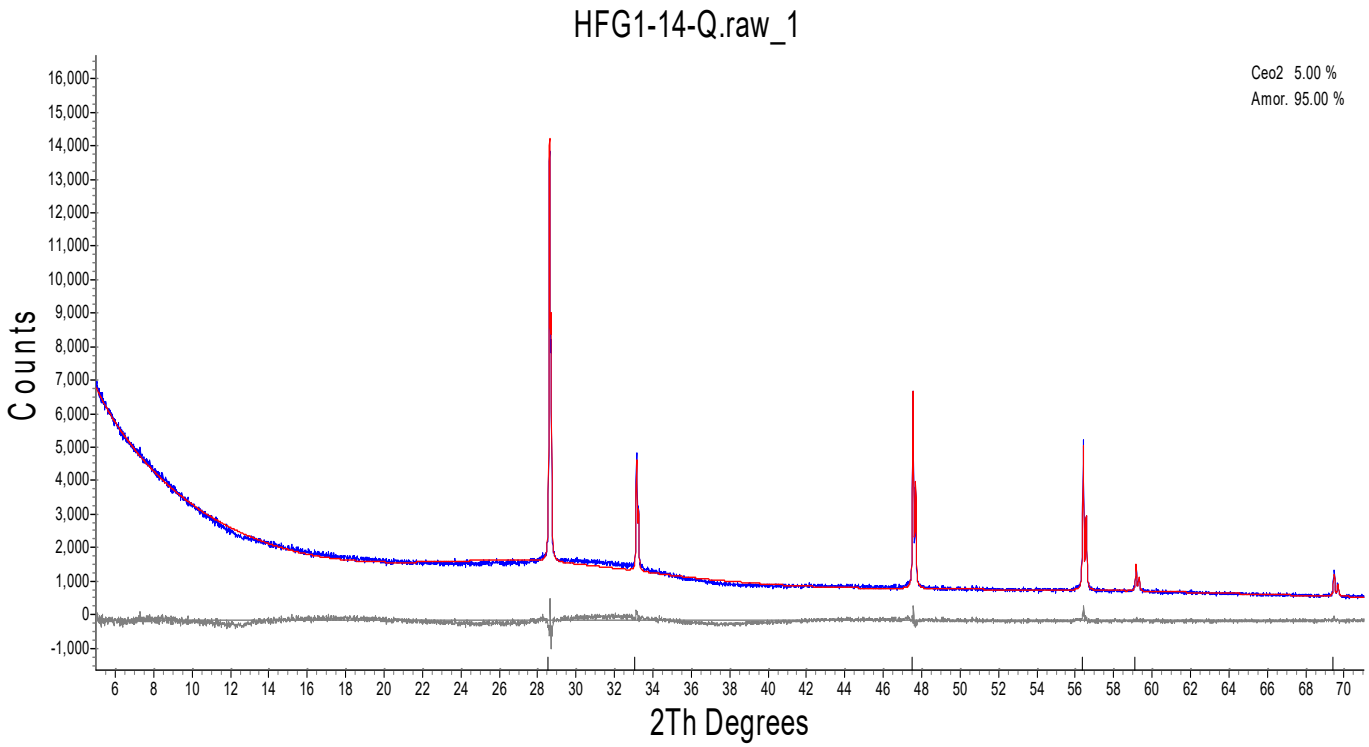

Figure B.14. XRD Spectrum of Quenched Glass HFG1-14

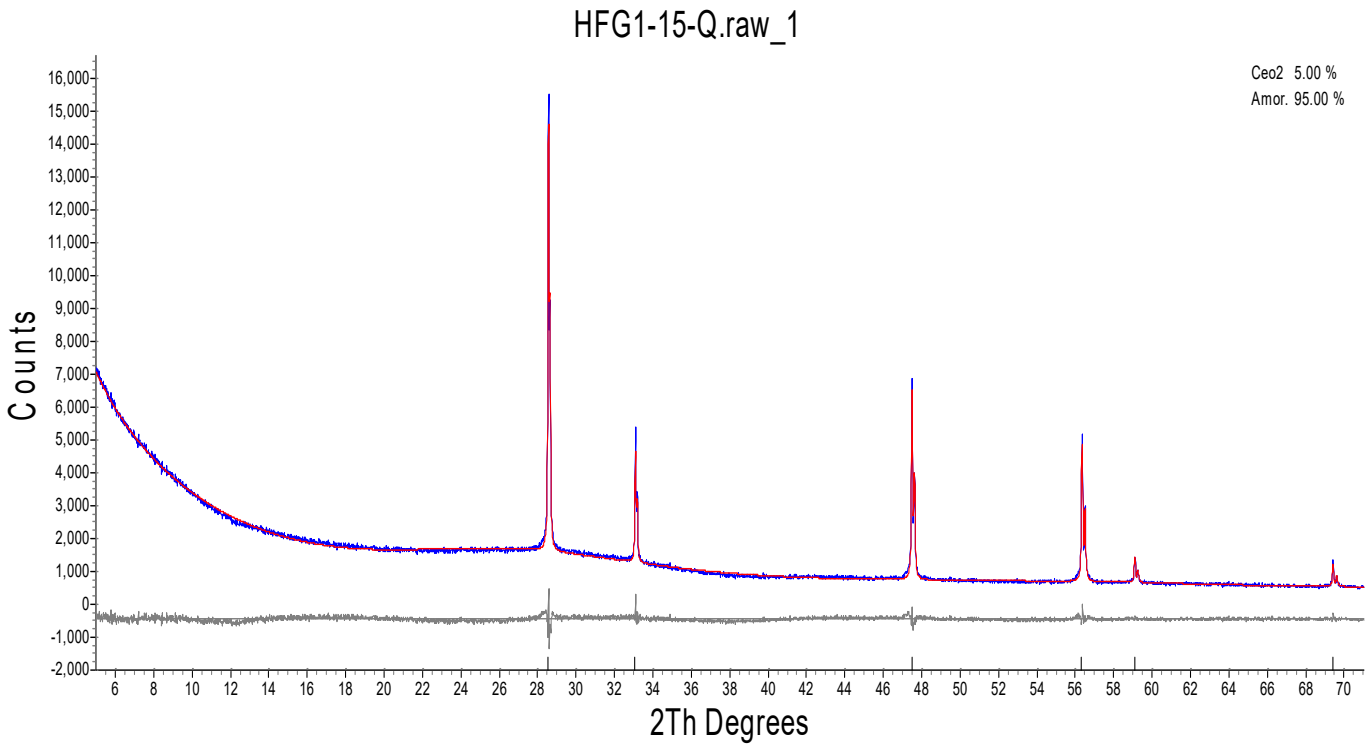

Figure B.15. XRD Spectrum of Quenched Glass HFG1-15

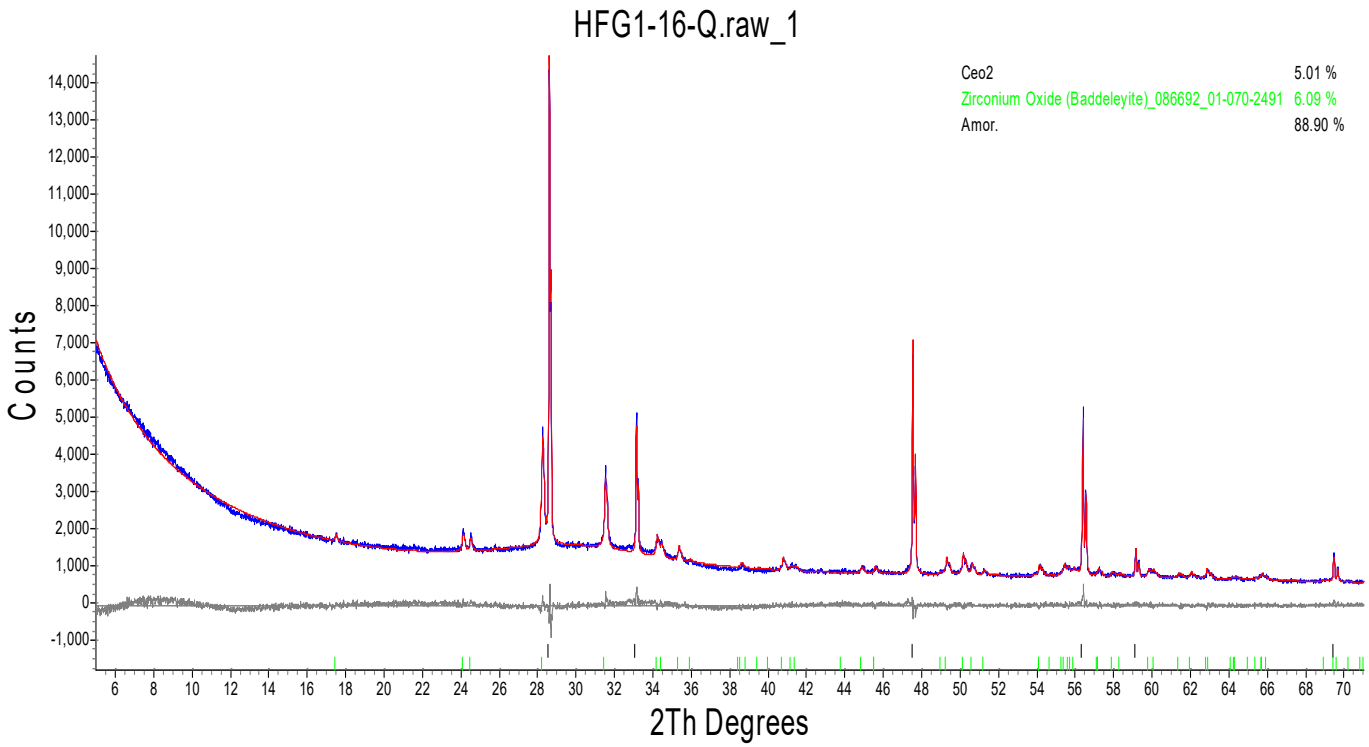

Phase Name	Wt% of Spiked	Wt% in Spiked Sample	Wt% in Original Sample
CeO_2	5.009	5.009	0.000
Baddeleyite (ZrO_2)	0.000	6.090	6.411

Figure B.16. XRD Spectrum of Quenched Glass HFG1-16

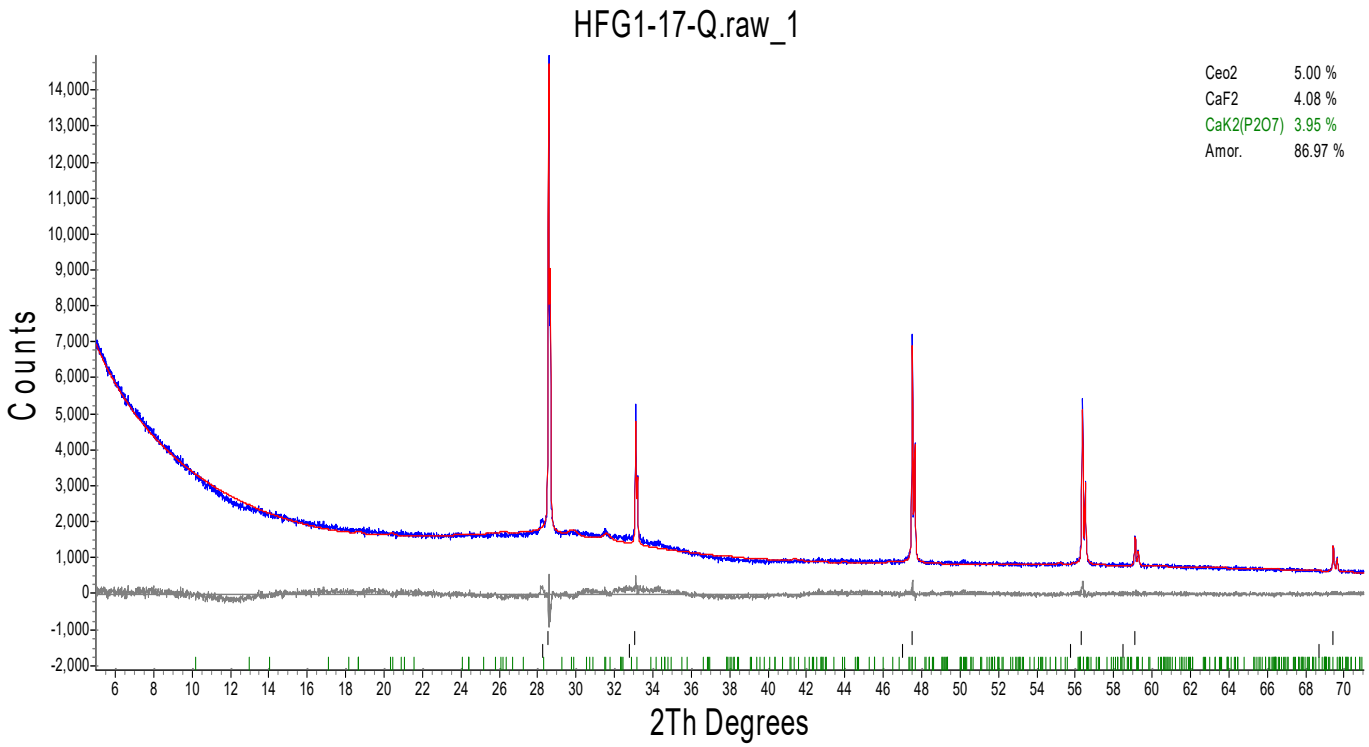

Phase Name	Wt% of Spiked	Wt% in Spiked Sample	Wt% in Original Sample
CeO_2	5.000	5.000	0.000
CaF_2	0.000	4.085	4.300
$CaK_2(P_2O_7)$	0.000	3.946	4.153

Figure B.17. XRD Spectrum of Quenched Glass HFG1-17

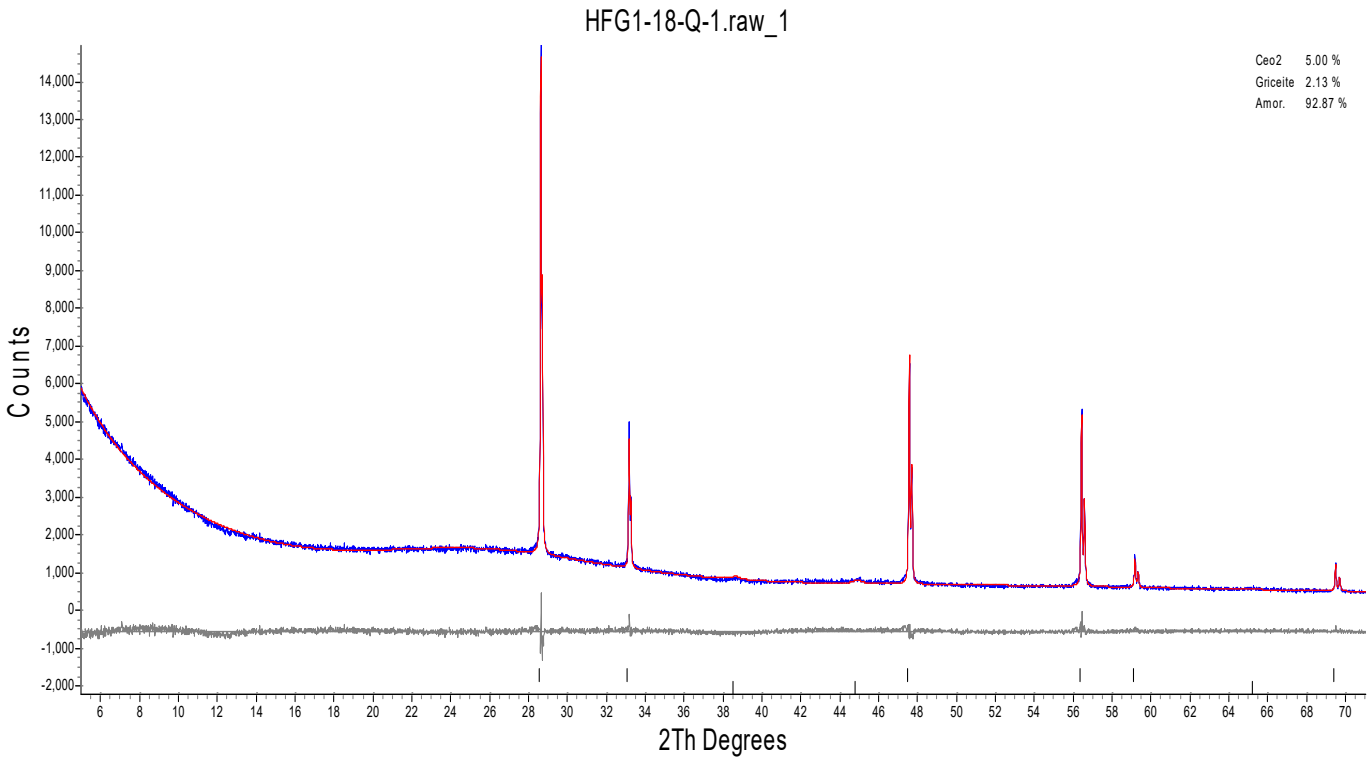

Phase Name	Wt% of Spiked	Wt% in Spiked Sample	Wt% in Original Sample
CeO_2	5.000	5.000	0.000
LiF	0.000	2.127	2.239

Figure B.18. XRD Spectrum of Quenched Glass HFG1-18

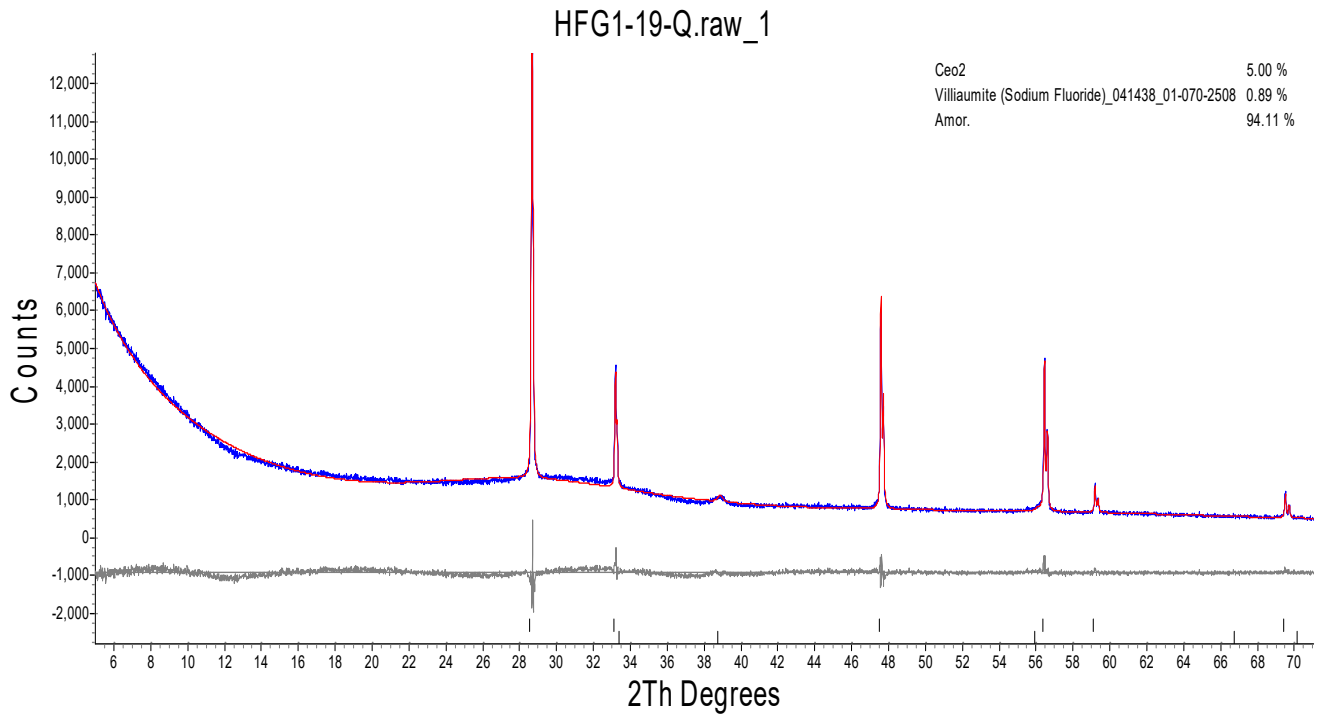

Phase Name	Wt% of Spiked	Wt% in Spiked Sample	Wt% in Original Sample
CeO_2	5.000	5.000	0.000
NaF	0.000	0.886	0.932

Figure B.19. XRD Spectrum of Quenched Glass HFG1-19

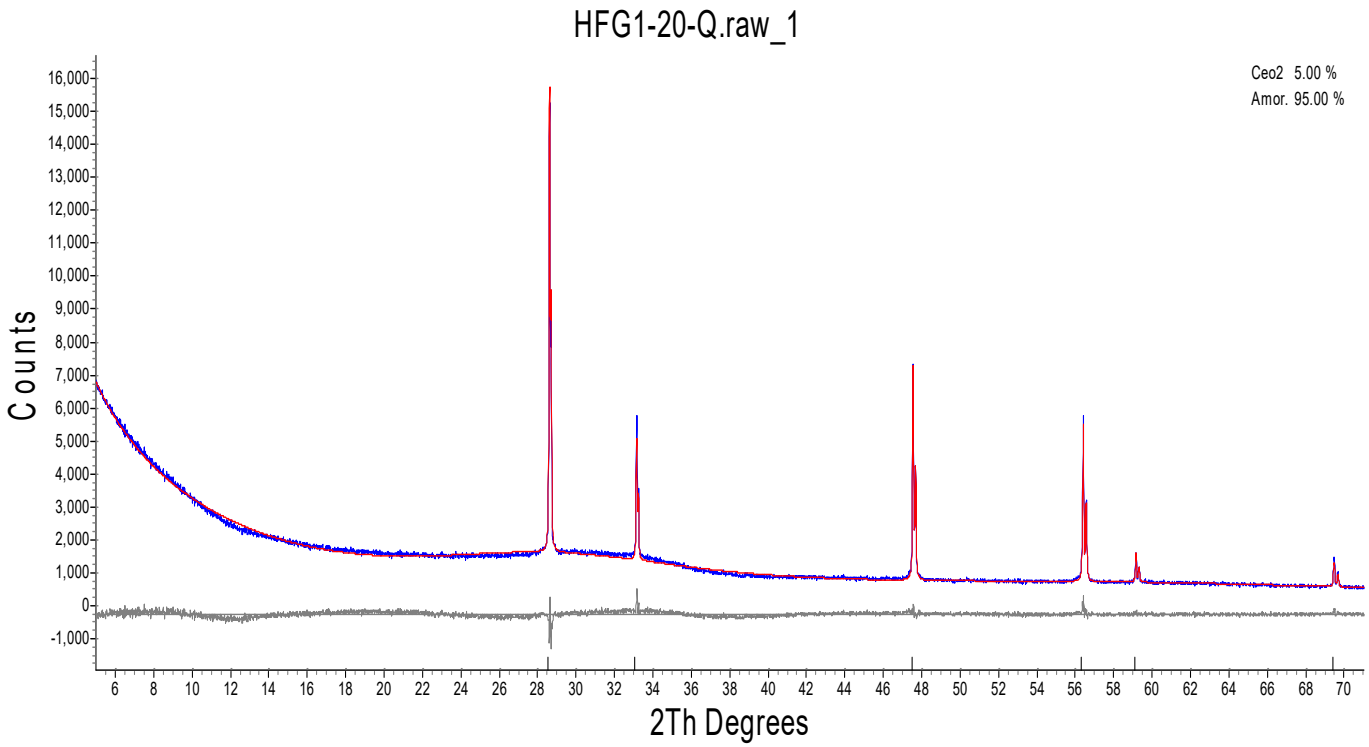

Figure B.20. XRD Spectrum of Quenched Glass HFG1-20

Appendix C – Analyzed High-Fluoride Glass Compositions

The data in this appendix compares the targeted glass compositions with the analyzed glass compositions and their percent differences. There appeared to be overall agreement in all samples and the targeted compositions are adequate for use in future work to develop property-composition models.

Table C.1. Comparison of Targeted and Analyzed High-Fluoride Glass Compositions

Glass ID	HFG1-01-1			HFG1-02			HFG1-03			HFG1-04		
Component	Targeted (wt%)	Analyzed (wt%)	% Diff	Targeted (wt%)	Analyzed (wt%)	% Diff	Targeted (wt%)	Analyzed (wt%)	% Diff	Targeted (wt%)	Analyzed (wt%)	% Diff
Al_2O_3	9.700	9.339	-3.72	7.942	7.893	-0.61	3.863	3.817	-1.20	1.884	1.956	3.79
B_2O_3	6.973	6.722	-3.61	5.870	5.723	-2.49	8.435	8.179	-3.04	9.263	9.032	-2.50
CaO	0.826	0.822	-0.48	2.795	2.991	7.00	2.191	2.165	-1.19	5.393	5.723	6.12
Cr_2O_3	0.091	<0.146	--	0.085	<0.146	--	0.079	<0.146	--	0.128	<0.146	--
F	5.322	4.703	**-11.64**	6.007	5.165	**-14.02**	5.231	4.513	**-13.74**	3.096	2.763	**-10.76**
Fe_2O_3	0.182	0.190	4.26	0.171	0.186	8.64	0.158	0.166	5.00	0.256	0.272	6.15
K_2O	1.554	1.298	**-16.47**	1.001	1.109	**10.88**	0.763	0.808	5.98	1.497	1.358	-9.29
Li_2O	5.594	5.764	3.04	1.758	1.830	4.11	0.057	<0.215	--	0.664	0.683	2.94
MnO	0.091	<0.129	--	0.085	<0.129	--	0.079	<0.129	--	0.128	<0.129	--
Na_2O	13.834	13.750	-0.61	15.530	14.909	-4.00	16.652	17.052	2.40	23.277	22.916	-1.55
P_2O_5	0.137	<0.229	--	0.128	<0.229	--	0.118	<0.229	--	0.192	<0.229	--
SiO_2	43.738	44.551	1.86	52.836	52.627	-0.40	48.259	48.134	-0.26	45.880	45.139	-1.61
SO_3	0.182	0.186	2.12	0.171	0.137	**-19.88**	0.158	<0.150	--	0.256	0.241	-6.07
ZnO	3.471	3.327	-4.15	1.333	1.344	0.836	3.226	3.121	-3.24	3.366	3.333	-0.98
ZrO_2	8.305	8.270	-0.42	4.289	4.387	2.28	10.733	10.600	-1.23	4.720	4.758	0.81
Total	100.000	98.921	-1.08	100.000	98.301	-1.70	100.000	98.555	-1.44	100.000	98.172	-1.83

Table C.1. (cont.)

Glass ID	HFG1-05			HFG1-06			HFG1-07			HFG1-08		
Component	Targeted (wt%)	Analyzed (wt%)	% Diff	Targeted (wt%)	Analyzed (wt%)	% Diff	Targeted (wt%)	Analyzed (wt%)	% Diff	Targeted (wt%)	Analyzed (wt%)	% Diff
Al_2O_3	3.808	3.774	-0.89	5.564	5.428	-2.46	9.919	9.504	-4.18	3.079	3.278	6.46
B_2O_3	9.734	9.289	-4.57	6.076	5.941	-2.23	11.383	11.125	-2.27	4.531	4.403	-2.83
CaO	0.303	0.338	**11.55**	1.368	1.377	0.67	0.042	<0.140	--	4.168	4.523	8.53
Cr_2O_3	0.193	0.176	-8.92	0.106	<0.146	--	0.042	<0.146	--	0.180	0.163	-9.42
F	3.773	3.443	-8.75	5.056	4.820	-4.66	4.376	4.008	-8.42	6.523	6.253	-4.14
Fe_2O_3	0.387	0.379	-2.00	0.212	0.212	-0.15	0.084	<0.143	--	0.360	0.371	2.94
K_2O	0.244	0.279	**13.99**	1.174	1.221	4.01	1.263	1.007	**-20.26**	1.343	1.258	-6.29
Li_2O	2.668	3.046	**14.20**	3.415	4.048	**18.54**	0.497	0.580	**16.76**	0.463	0.500	7.91
MnO	0.193	0.186	-3.80	0.106	<0.129	--	0.042	<0.129	--	0.180	0.183	1.76
Na_2O	22.362	21.534	-3.70	22.984	23.320	1.47	18.857	18.535	-1.71	23.412	22.748	-2.84
P_2O_5	0.290	0.260	**-10.29**	0.159	<0.229	--	0.063	<0.229	--	0.270	0.253	-6.44
SiO_2	43.486	42.465	-2.35	45.732	44.551	-2.58	47.500	46.423	-2.27	41.598	41.930	0.80
SO_3	0.387	0.381	-1.35	0.212	0.209	-1.52	0.084	<0.125	--	0.360	0.355	-1.34
ZnO	0.720	0.682	-5.39	0.446	0.433	-2.80	1.038	0.999	-3.79	0.953	0.964	1.06
ZrO_2	11.452	11.131	-2.81	7.392	7.298	-1.27	4.812	4.768	-0.90	12.580	12.519	-0.49
Total	100.000	97.363	-2.64	100.000	98.950	-1.05	100.000	96.949	-3.05	100.000	99.699	-0.30

Table C.1. (cont.)

Glass ID	HFG1-09			HFG1-10			HFG1-11			HFG1-12		
Component	Targeted (wt%)	Analyzed (wt%)	% Diff	Targeted (wt%)	Analyzed (wt%)	% Diff	Targeted (wt%)	Analyzed (wt%)	% Diff	Targeted (wt%)	Analyzed (wt%)	% Diff
Al_2O_3	5.755	5.565	-3.30	6.204	6.028	-2.84	7.773	7.846	0.94	2.737	2.806	2.52
B_2O_3	4.304	4.089	-5.00	10.087	9.740	-3.44	9.465	9.273	-2.03	6.902	6.697	-2.97
CaO	5.262	5.153	-2.07	3.353	3.344	-0.27	0.080	<0.140	--	5.939	5.866	-1.23
Cr_2O_3	0.183	0.244	**33.33**	0.027	<0.146	--	0.169	0.183	8.28	0.032	<0.146	--
F	6.761	6.445	-4.67	4.255	4.090	-3.88	6.968	6.683	-4.09	0.099	6.215	-7.22
Fe_2O_3	0.365	0.364	-0.27	0.054	<0.143	--	0.337	0.356	5.64	0.065	<0.143	--
K_2O	0.359	0.386	7.52	0.812	0.872	7.39	0.897	0.983	9.59	0.642	0.678	5.61
Li_2O	3.823	3.859	0.94	2.846	3.143	**10.44**	1.484	1.560	5.12	4.750	4.898	3.12
MnO	0.183	0.175	-4.37	0.027	<0.129	--	0.169	0.174	2.96	0.032	<0.129	--
Na_2O	17.422	17.996	3.29	19.718	19.445	-1.38	17.683	17.221	-2.61	12.645	13.092	3.35
P_2O_5	0.274	<0.229	--	0.040	<0.229	--	0.253	0.240	-5.14	0.049	<0.229	--
SiO_2	46.894	45.835	-2.26	35.312	34.871	-1.25	39.540	39.631	0.23	47.255	46.583	-1.42
SO_3	0.365	0.359	-1.64	0.054	<0.125	--	0.337	0.313	-7.12	0.065	<0.125	--
ZnO	3.896	3.731	-4.24	3.851	3.694	-4.08	2.463	2.493	1.22	0.136	0.134	-1.47
ZrO_2	4.156	4.177	0.51	13.360	13.055	-2.28	12.384	12.441	0.46	12.052	12.029	-0.19
Total	100.002	98.608	-1.39	100.000	99.055	-0.94	100.002	99.535	-0.47	100.000	99.771	-0.23

Table C.1. (cont.)

Glass ID	HFG1-13			HFG1-14			HFG1-15			HFG1-16		
Component	Targeted (wt%)	Analyzed (wt%)	% Diff	Targeted (wt%)	Analyzed (wt%)	% Diff	Targeted (wt%)	Analyzed (wt%)	% Diff	Targeted (wt%)	Analyzed (wt%)	% Diff
Al_2O_3	8.557	8.389	-1.96	2.526	2.589	2.49	5.051	4.998	-1.05	8.682	8.366	-3.64
B_2O_3	8.105	8.380	3.39	4.945	4.999	1.09	8.532	8.235	-3.48	4.257	4.049	-4.89
CaO	3.619	3.753	3.70	5.743	5.737	-0.10	4.619	4.852	5.04	5.811	5.698	-1.94
Cr_2O_3	0.165	<0.146	--	0.056	<0.146	--	0.177	0.155	**-12.43**	0.139	<0.146	--
F	4.568	4.215	-7.73	4.479	4.318	-3.59	2.125	1.958	-7.86	2.189	2.173	-0.73
Fe_2O_3	0.330	0.329	-0.30	0.113	<0.143	--	0.335	0.355	5.97	0.278	0.293	5.40
K_2O	0.510	0.587	**15.10**	0.118	0.164	**38.98**	1.440	1.316	-8.61	1.310	0.973	**-25.73**
Li_2O	5.915	6.486	9.65	1.504	1.652	9.84	4.016	4.193	4.41	5.842	5.942	1.71
MnO	0.165	0.161	-2.42	0.056	<0.129	--	0.177	0.172	-2.82	0.139	0.142	2.16
Na_2O	12.167	11.249	-7.54	22.035	21.501	-2.42	15.702	15.064	-4.06	20.316	19.647	-3.29
P_2O_5	0.247	<0.235	--	0.085	<0.229	--	0.266	0.247	-7.14	0.209	<0.229	--
SiO_2	48.981	51.076	4.28	48.453	49.418	1.99	50.110	49.257	-1.70	37.396	37.117	-0.75
SO_3	0.330	0.297	**-10.00**	0.113	0.137	**21.24**	0.355	0.330	-1.49	0.278	0.291	4.68
ZnO	1.750	1.715	-2.00	1.367	1.316	-3.73	0.551	0.541	-1.81	0.041	<0.124	--
ZrO_2	4.593	4.620	0.59	8.409	8.385	-0.29	6.523	6.322	-3.08	13.114	12.076	-7.92
Total	100.002	100.637	1.63	100.002	100.862	0.86	99.959	97.994	-1.97	100.001	97.266	-2.73

Table C.1. (cont.)

Glass ID	HFG1-17			HFG1-18			HFG1-19			HFG1-20		
Component	Targeted (wt%)	Analyzed (wt%)	% Diff	Targeted (wt%)	Analyzed (wt%)	% Diff	Targeted (wt%)	Analyzed (wt%)	% Diff	Targeted (wt%)	Analyzed (wt%)	% Diff
Al_2O_3	4.933	4.899	-0.60	5.277	5.069	-3.94	8.812	8.791	-0.24	9.885	9.325	-5.67
B_2O_3	4.044	3.950	-2.32	11.800	11.543	-2.18	8.301	8.179	-1.47	4.540	4.299	-5.31
CaO	3.772	3.760	-0.32	0.488	0.489	0.20	4.524	4.845	7.10	2.087	2.032	-2.64
Cr_2O_3	0.076	<0.146	--	0.062	<0.146	--	0.032	<0.146	--	0.118	<0.167	--
F	2.547	2.463	-3.30	3.882	3.538	-8.86	5.659	5.410	-4.40	2.717	2.683	-1.25
Fe_2O_3	0.152	0.161	5.92	0.124	<0.143	--	0.064	<0.143	--	0.236	0.236	0.00
K_2O	0.197	0.235	**19.29**	0.389	0.407	4.63	1.147	1.176	2.53	0.027	<0.120	--
Li_2O	5.394	6.050	**12.16**	4.910	5.178	5.46	1.305	1.385	6.13	4.243	4.317	1.74
MnO	0.076	<0.129	--	0.062	<0.129	--	0.032	<0.129	--	0.118	<0.129	--
Na_2O	17.748	17.153	-3.35	12.936	12.958	0.17	22.557	22.141	-1.84	23.821	23.994	0.73
P_2O_5	0.114	<0.229	--	0.093	<0.229	--	0.048	<0.229	--	0.177	<0.229	--
SiO_2	44.712	44.141	-1.28	50.397	50.648	0.50	38.764	39.631	2.24	40.989	40.165	-2.01
SO_3	0.152	0.166	9.21	0.124	<0.136	--	0.064	<0.125	--	0.236	0.264	**11.86**
ZnO	2.795	2.676	-4.26	2.317	2.244	-3.15	3.063	3.075	0.39	3.868	3.725	-3.70
ZrO_2	13.288	12.828	-3.46	7.138	7.065	-1.02	5.625	5.663	0.68	6.940	6.768	-2.48
Total	100.000	98.986	-1.01	99.999	99.921	-0.08	99.997	101.067	1.07	100.002	98.453	-1.55

Appendix D – Canister Centerline Cooling (CCC) Glass Photographs

This appendix contains photos of glasses after they were CCC treated beginning at the glass melting temperature of 1150 °C. Each showed different responses to the CCC treatment as indicated by these photos.

Figure D.1. Photograph of Glass HFG1-01-1 after CCC

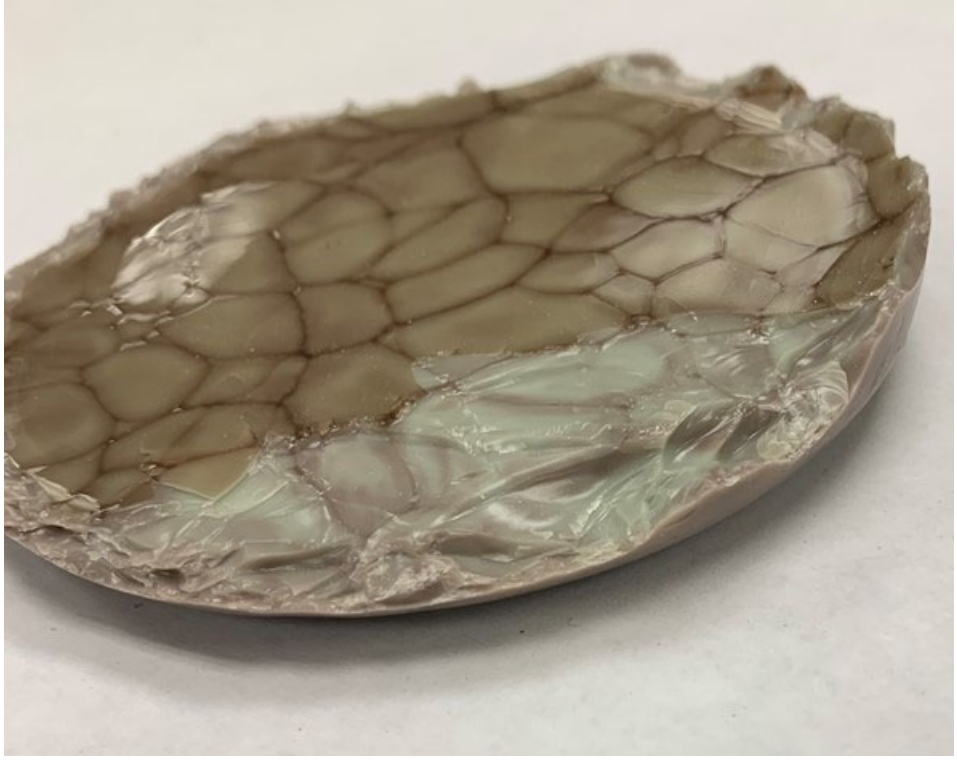

Figure D.2. Photograph of Glass HFG1-02 after CCC

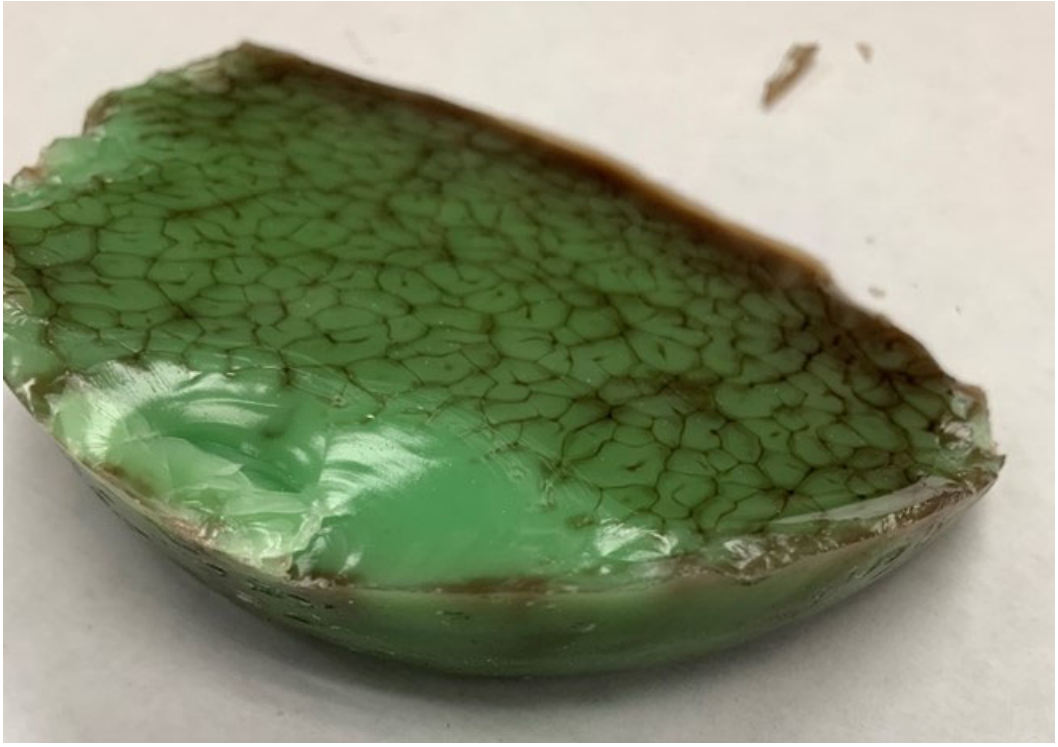

Figure D.3. Photograph of Glass HFG1-03 after CCC

Figure D.4. Photograph of Glass HFG1-04 after CCC

Figure D.5. Photograph of Glass HFG1-05 after CCC

Figure D.6. Photograph of Glass HFG1-06 after CCC

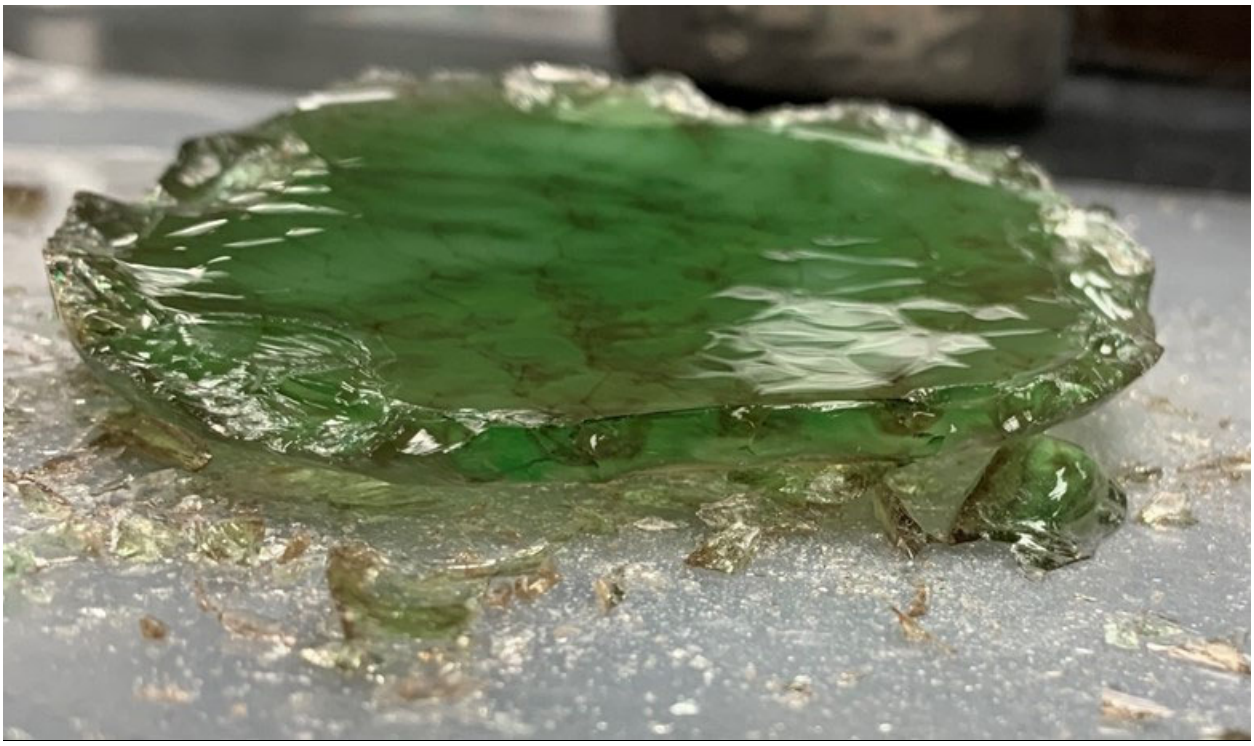

Figure D.7. Photograph of Glass HFG1-07 after CCC

Figure D.8. Photograph of Glass HFG1-08 after CCC

Figure D.9. Photograph of Glass HFG1-09 after CCC

Figure D.10. Photograph of Glass HFG1-10 CCC

Figure D.11. Photograph of Glass HFG1-11 CCC

Figure D.12. Photograph of Glass HFG1-12 after CCC

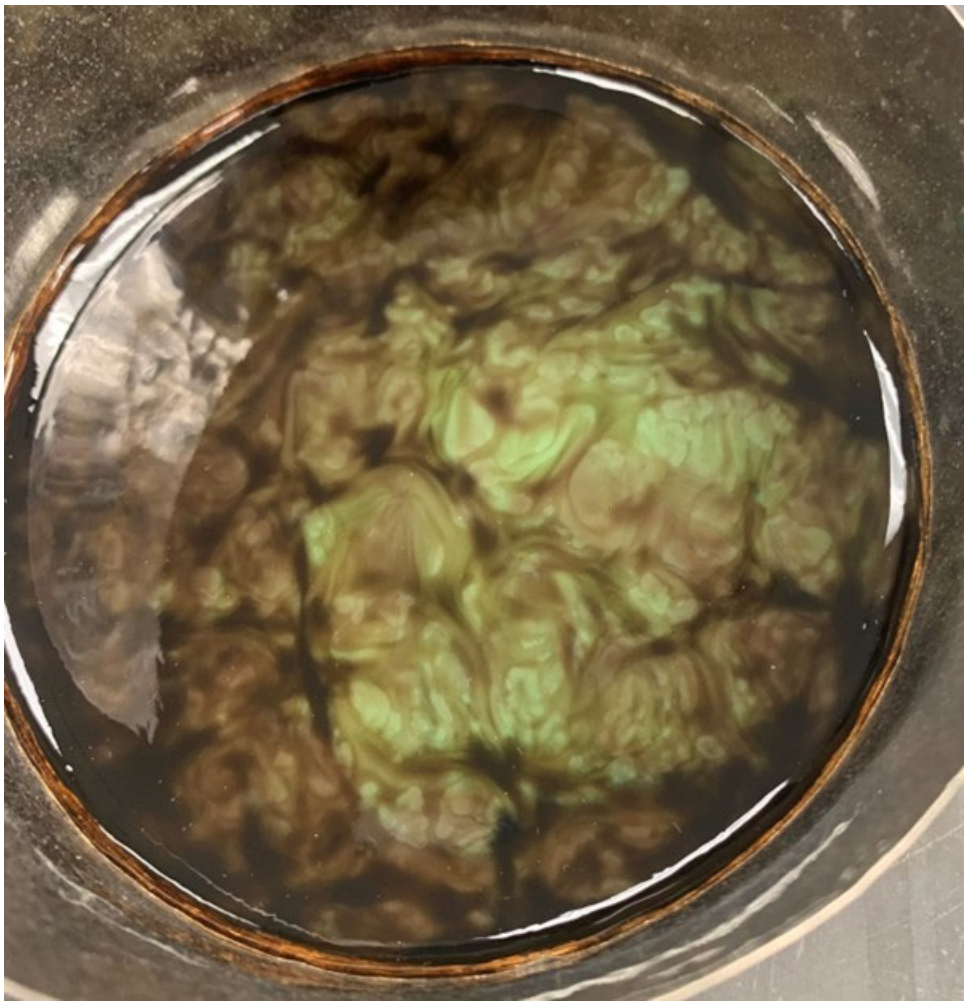

Figure D.13. Photograph of Glass HFG1-13 after CCC

Figure D.14. Photograph of Glass HFG1-14 after CCC

Figure D.15. Photograph of Glass HFG1-15 after CCC

Figure D.16. Photograph of Glass HFG1-16 after CCC

Figure D.17. Photograph of Glass HFG1-17 after CCC

Figure D.18. Photograph of Glass HFG1-18 after CCC

Figure D.19. Photograph of Glass HFG1-19 after CCC

Figure D.20. Photograph of Glass HFG1-20 after CCC

Appendix E – XRD of Canister Centerline Cooling (CCC) Treated Glasses

This appendix shows the X-ray diffraction (XRD) plots of the high-fluoride glasses after CCC treating. These glasses show primarily fluoride salts or remaining amorphous.

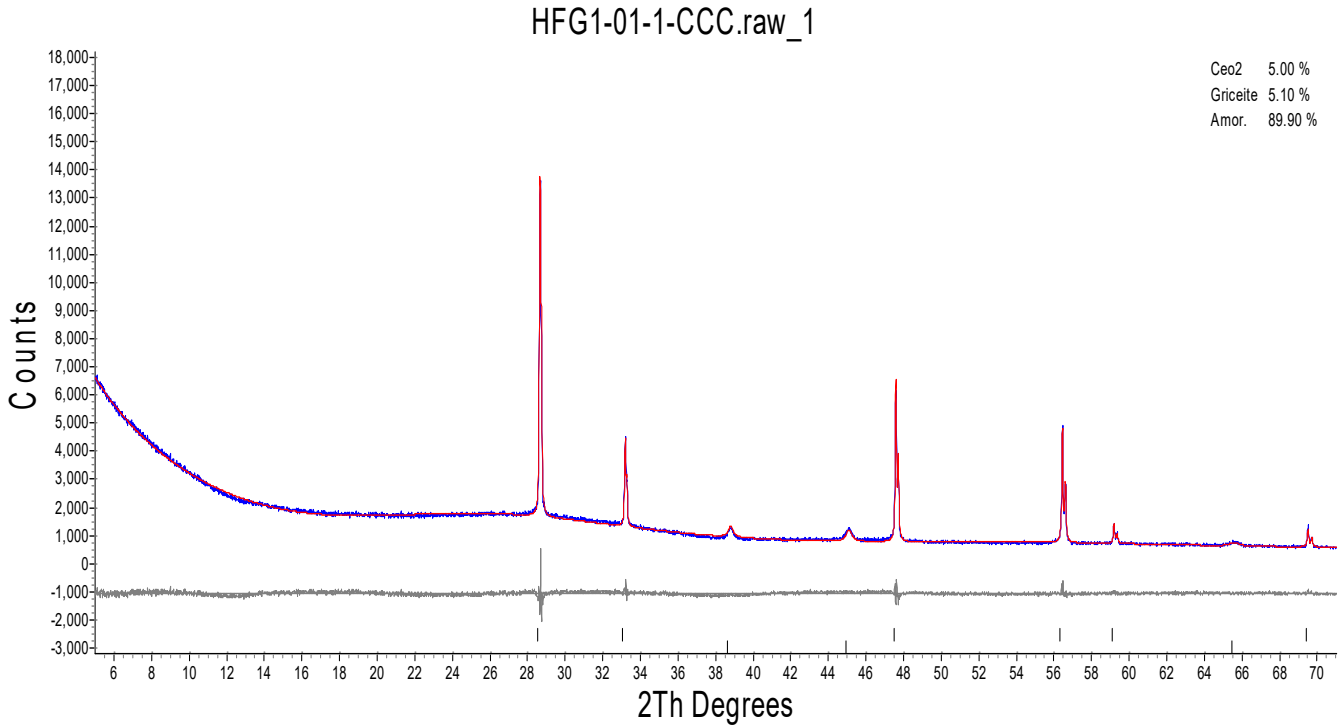

Phase Name	Wt% of Spiked	Wt% in Spiked Sample	Wt% in Original Sample
CeO_2	5.000	5.000	0.000
LiF	0.000	5.104	5.373

Figure E.1. XRD Spectrum of CCC-Treated Glass HFG1-01-1

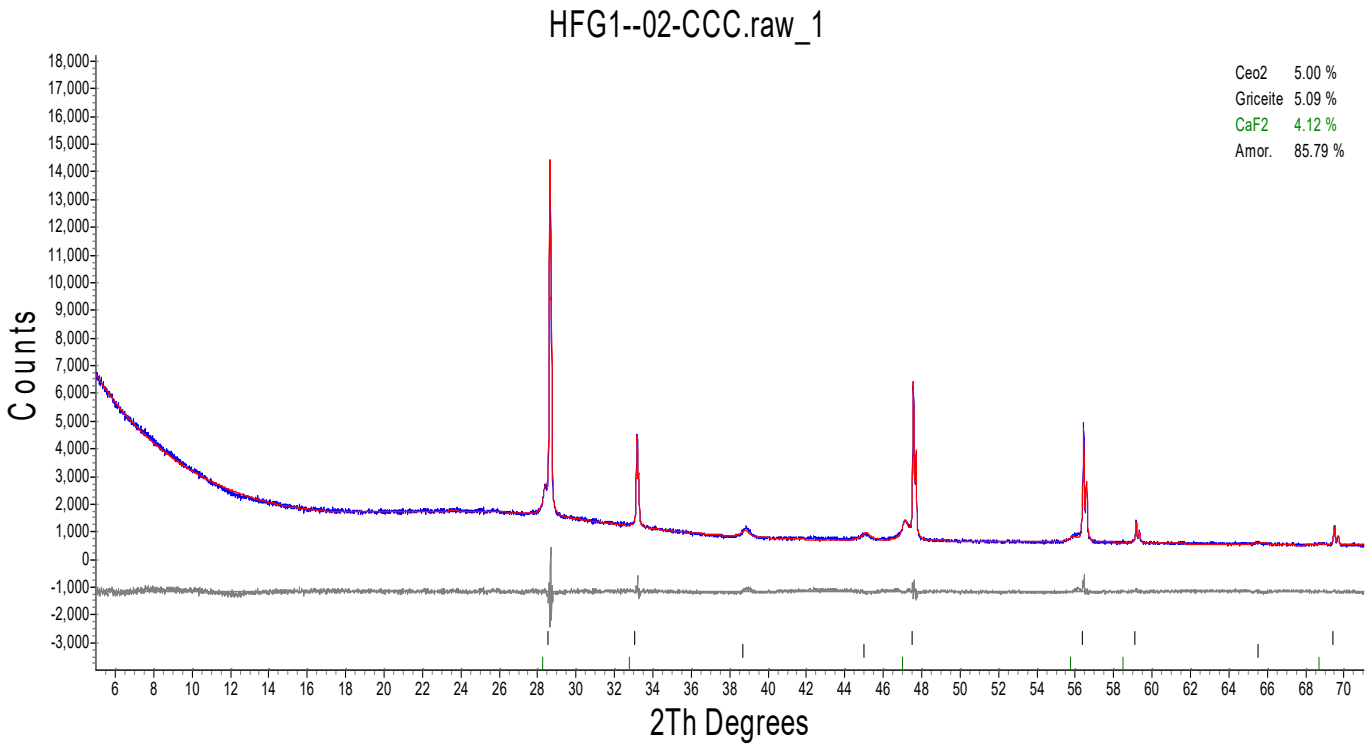

Phase Name	Wt% of Spiked	Wt% in Spiked Sample	Wt% in Original Sample
CeO_2	5.000	5.000	0.000
LiF	0.000	5.090	5.358
CaF_2	0.000	4.125	4.342

Figure E.2. XRD Spectrum of CCC-Treated Glass HFG1-02

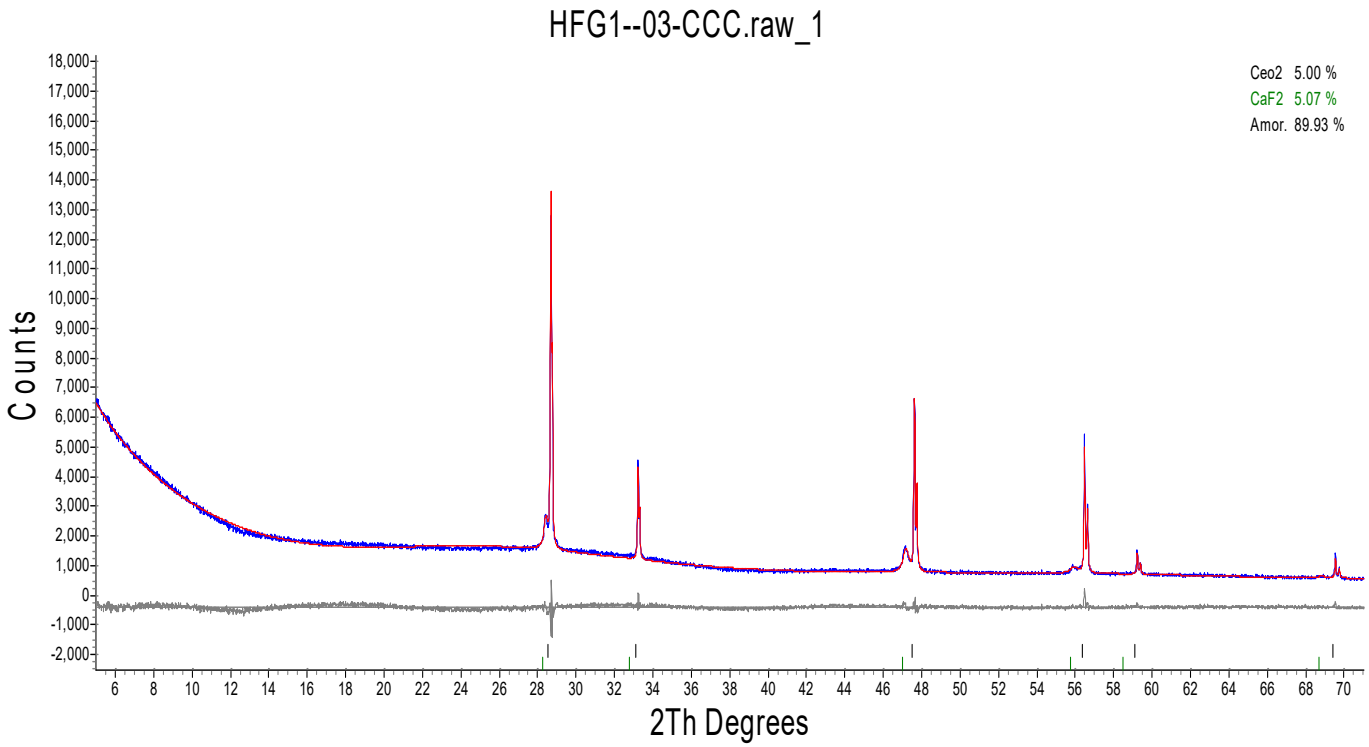

Phase Name	Wt% of Spiked	Wt% in Spiked Sample	Wt% in Original Sample
CeO_2	5.000	5.000	0.000
CaF_2	0.000	5.075	5.342

Figure E.3. XRD Spectrum of CCC-Treated Glass HFG1-03

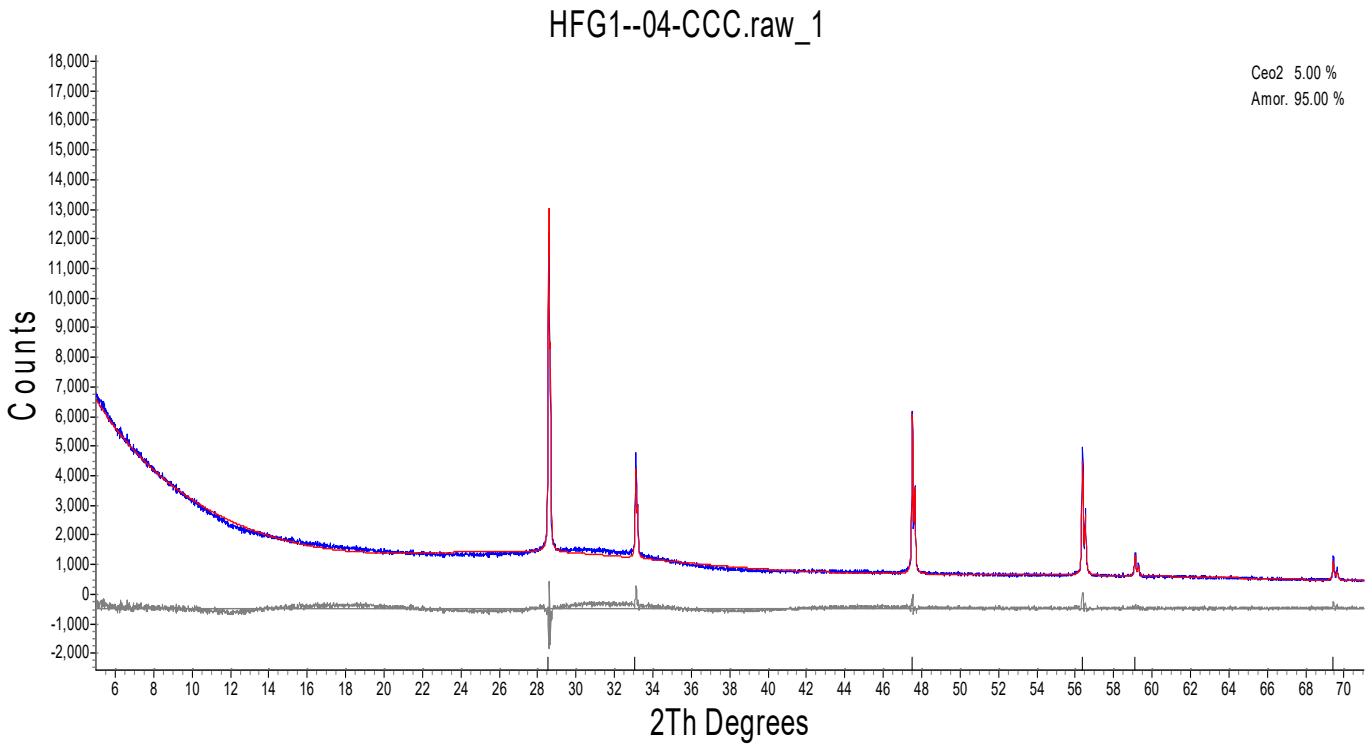

Figure E.4. XRD Spectrum of CCC-Treated Glass HFG1-04

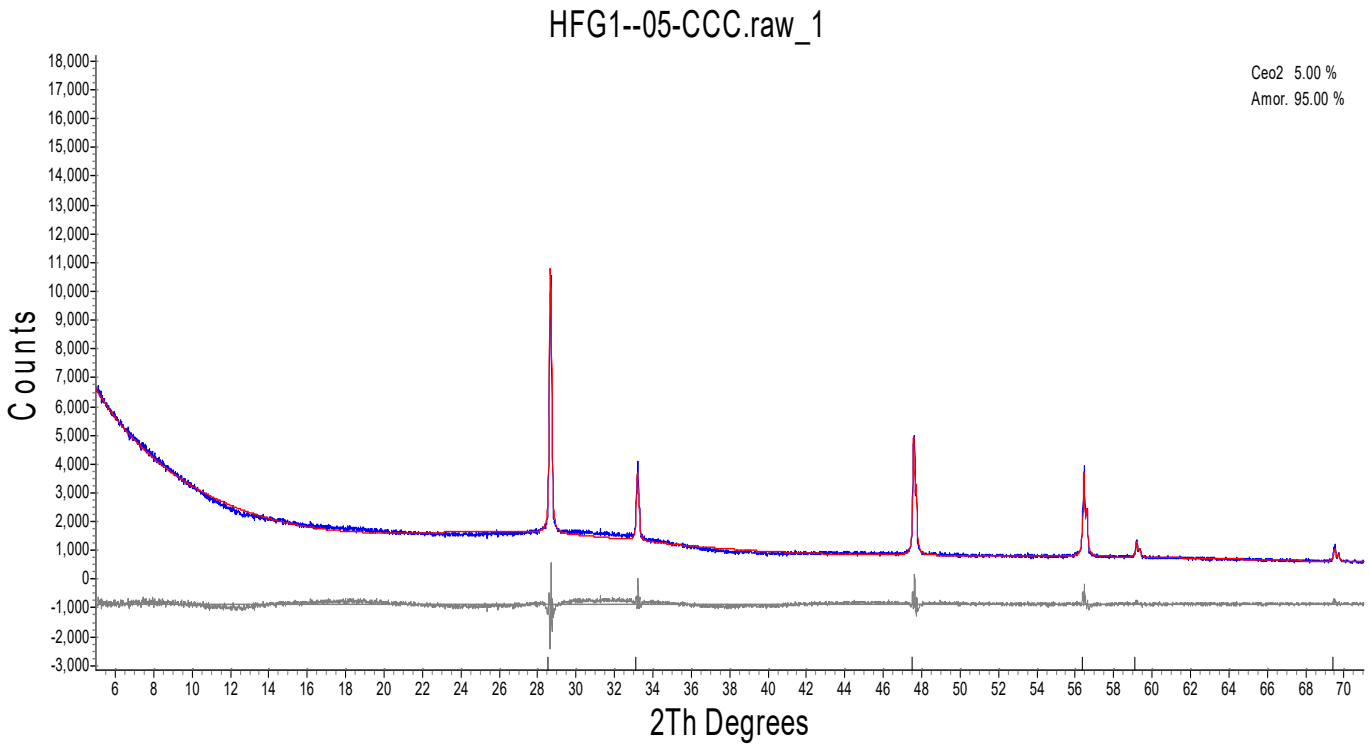

Figure E.5. XRD Spectrum of CCC-Treated Glass HFG1-05

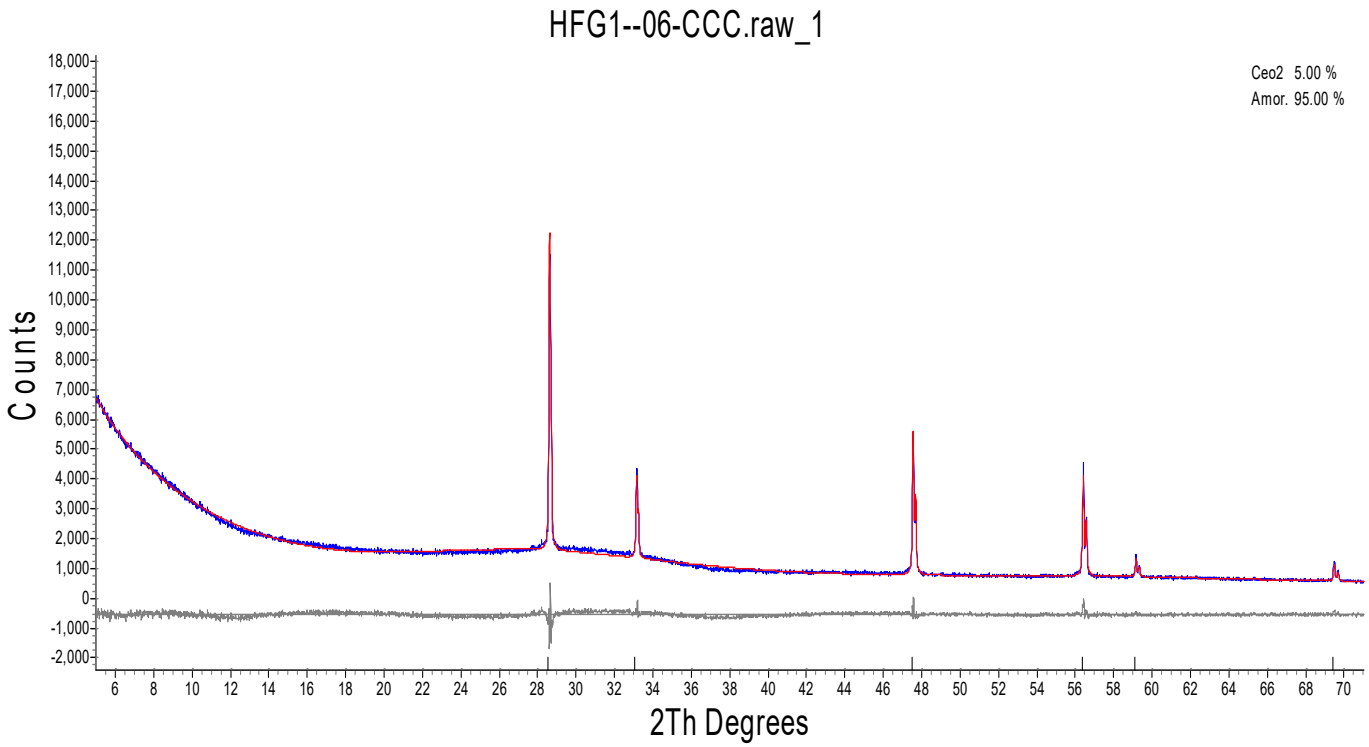

Figure E.6. XRD Spectrum of CCC-Treated Glass HFG1-06

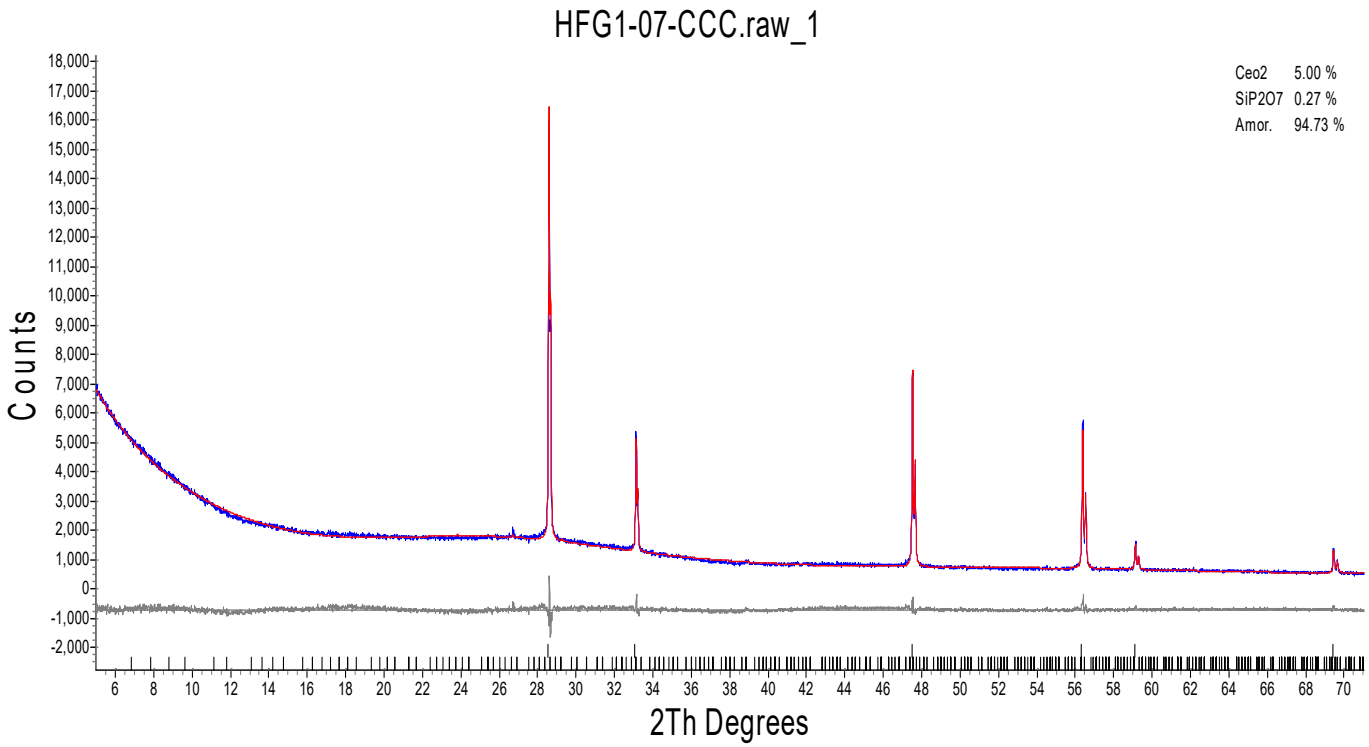

Phase Name	Wt% of Spiked	Wt% in Spiked Sample	Wt% in Original Sample
CeO_2	5.000	5.000	0.000
SiP_2O_7	0.000	0.268	0.282

Figure E.7. XRD Spectrum of CCC-Treated Glass HFG1-07

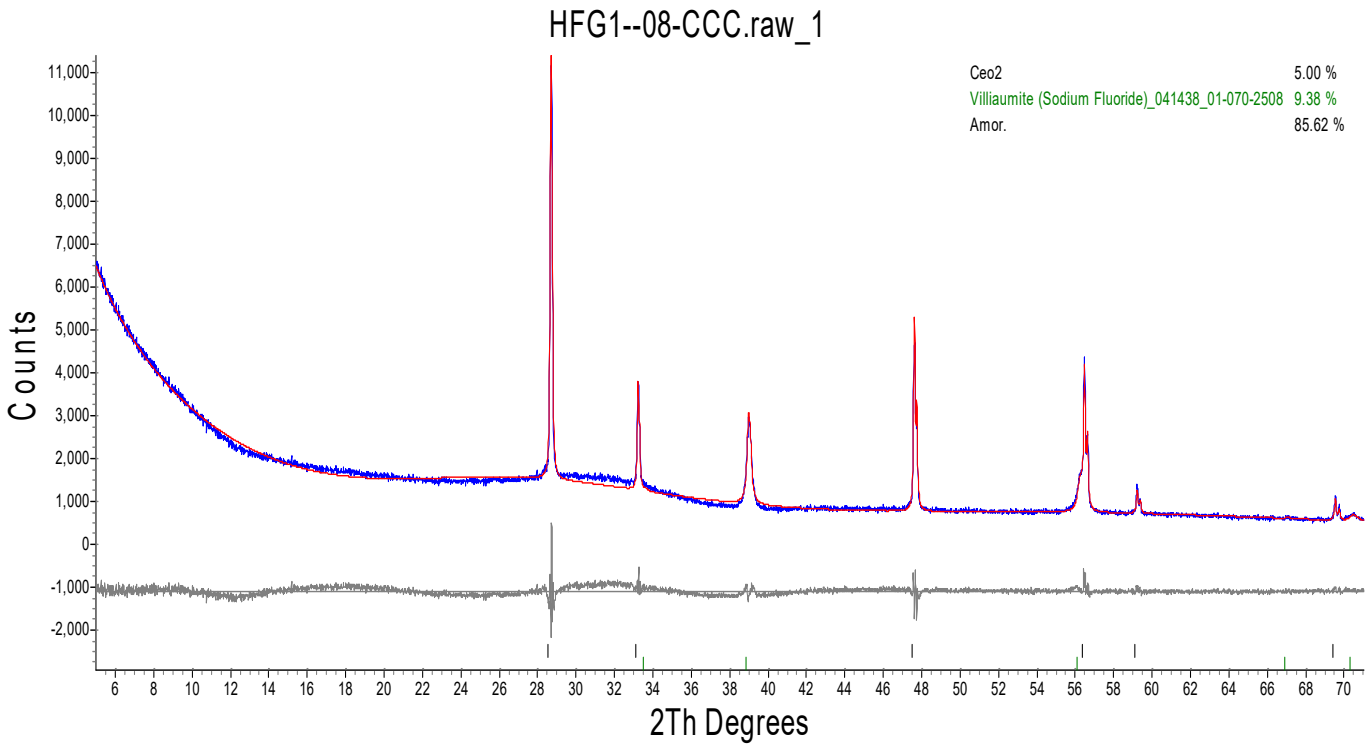

Phase Name	Wt% of Spiked	Wt% in Spiked Sample	Wt% in Original Sample
CeO_2	5.000	5.000	0.000
NaF	0.000	9.380	9.873

Figure E.8. XRD Spectrum of CCC-Treated Glass HFG1-08

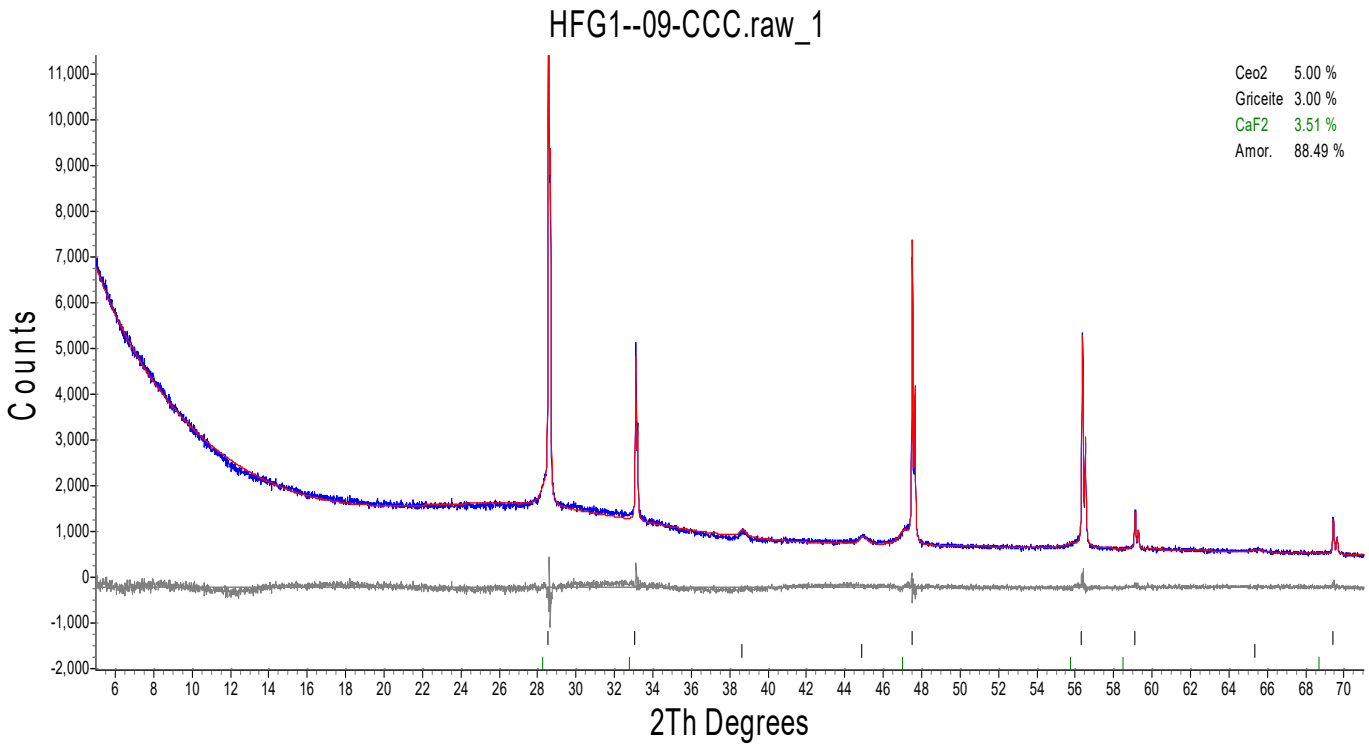

Phase Name	Wt% of Spiked	Wt% in Spiked Sample	Wt% in Original Sample
CeO_2	5.000	5.000	0.000
LiF	0.000	2.998	3.156
CaF_2	0.000	3.508	3.693

Figure E.9. XRD Spectrum of CCC-Treated Glass HFG1-09

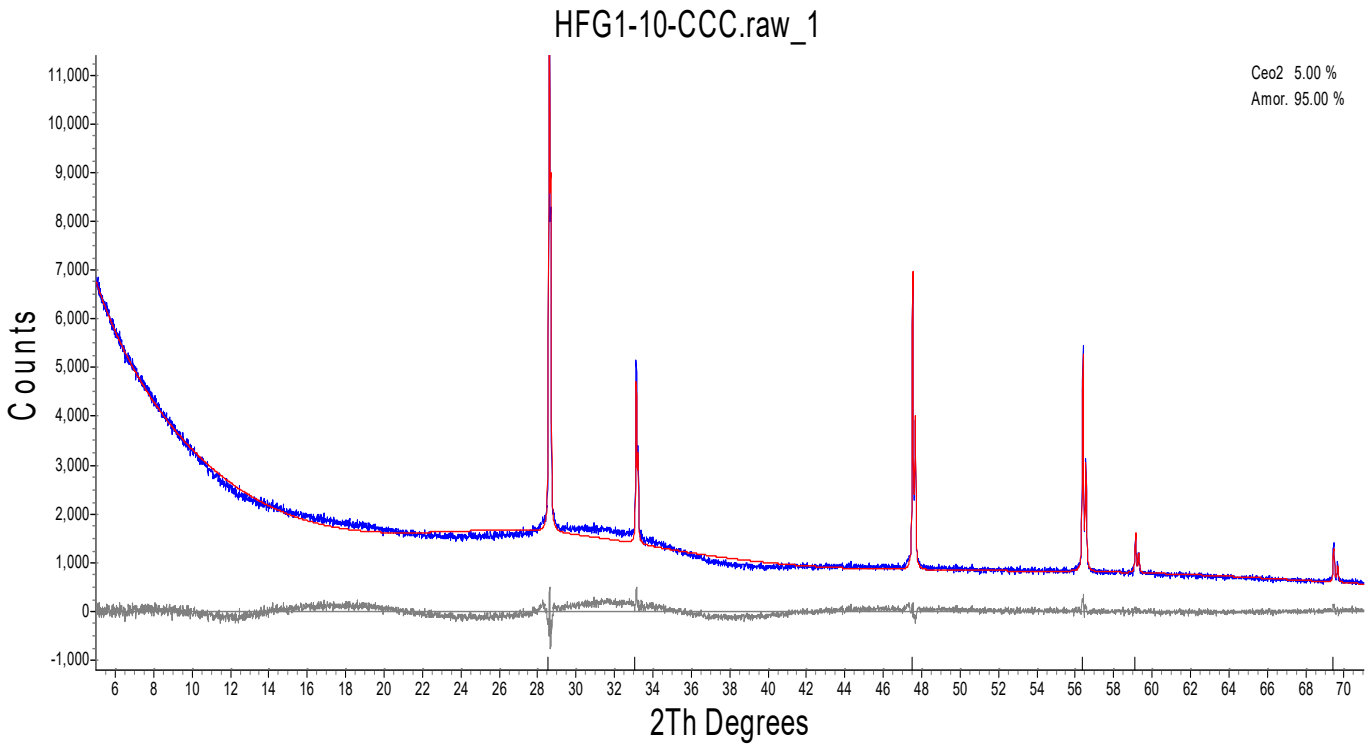

Figure E.10. XRD Spectrum of CCC-Treated Glass HFG1-10

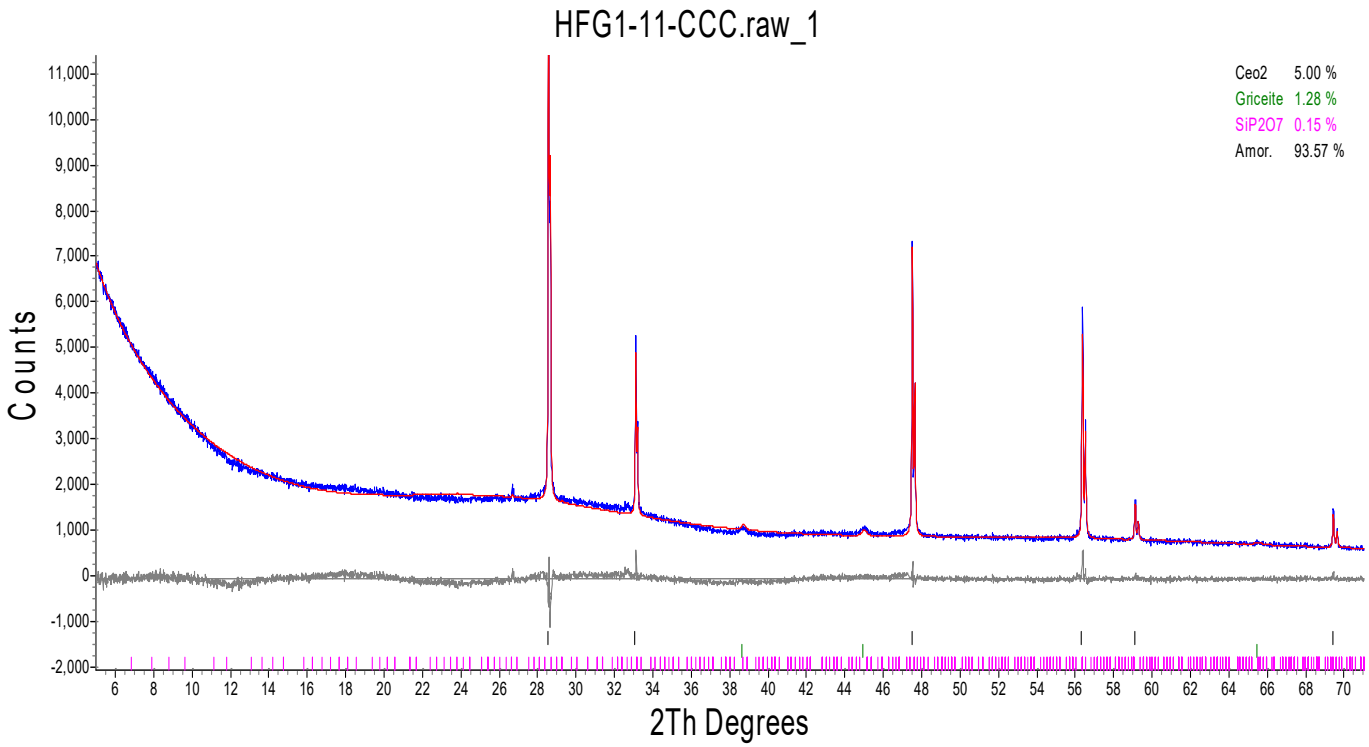

Phase Name	Wt% of Spiked	Wt% in Spiked Sample	Wt% in Original Sample
CeO_2	5.000	5.000	0.000
LiF	0.000	1.276	1.343
SiP_2O_7	0.000	0.153	0.161

Figure E.11. XRD Spectrum of CCC-Treated Glass HFG1-11

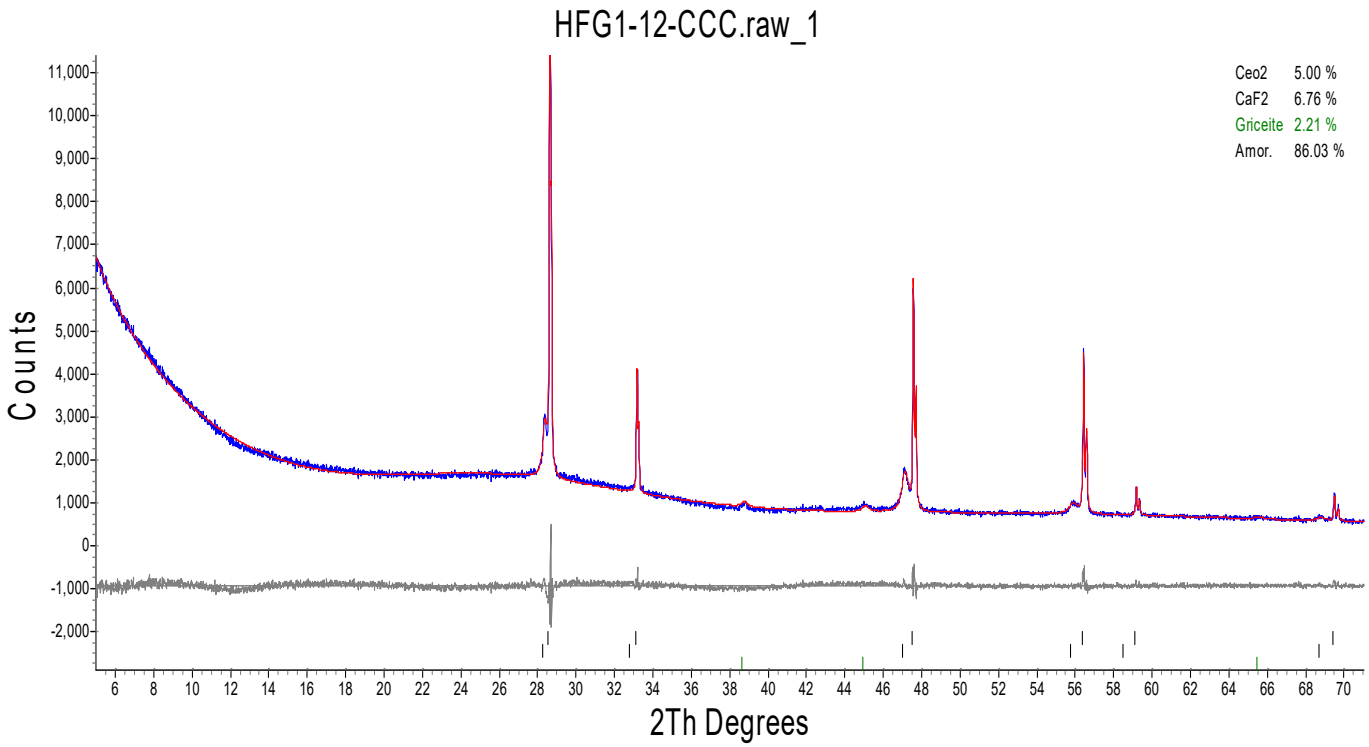

Phase Name	Wt% of Spiked	Wt% in Spiked Sample	Wt% in Original Sample
CeO_2	5.000	5.000	0.000
CaF_2	0.000	6.760	7.116
LiF	0.000	2.208	2.324

Figure E.12. XRD Spectrum of CCC-Treated Glass HFG1-12

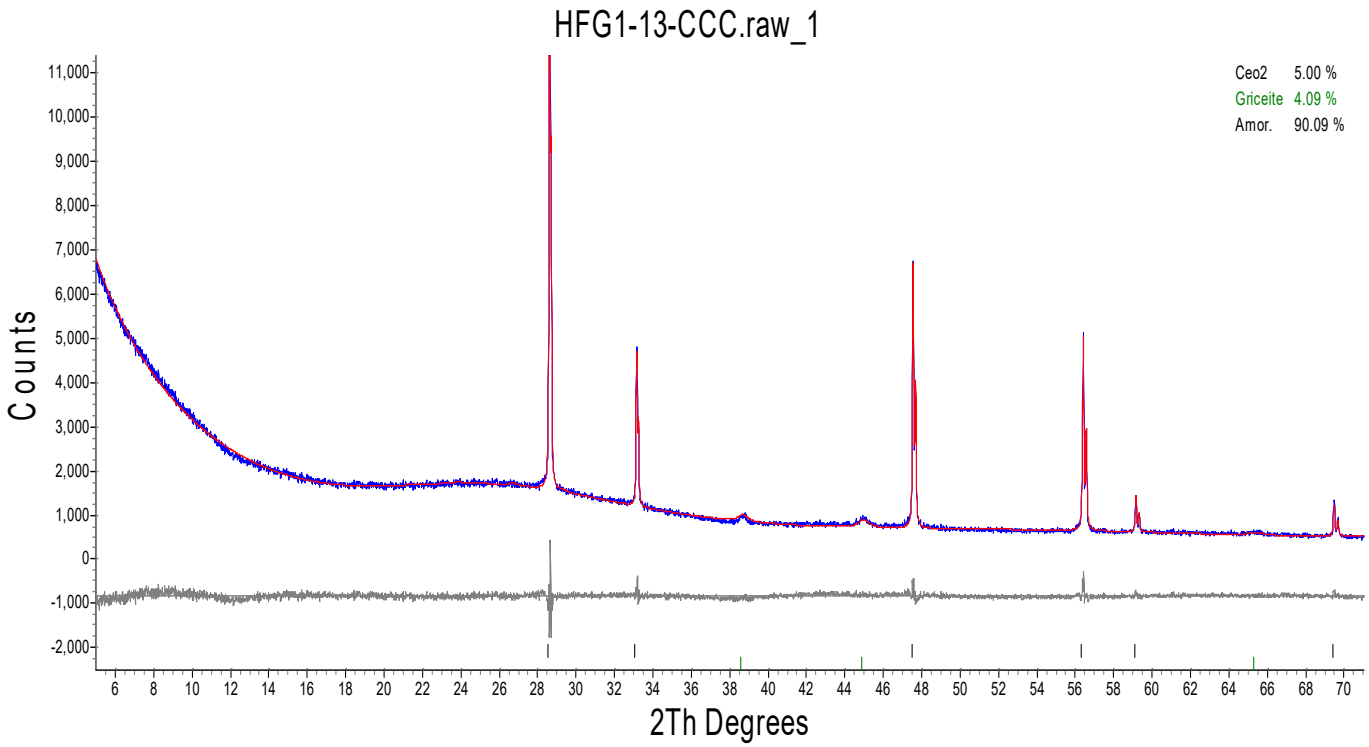

Phase Name	Wt% of Spiked	Wt% in Spiked Sample	Wt% in Original Sample
CeO_2	5.000	5.000	0.000
LiF	0.000	4.085	4.338

Figure E.13. XRD Spectrum of CCC-Treated Glass HFG1-13

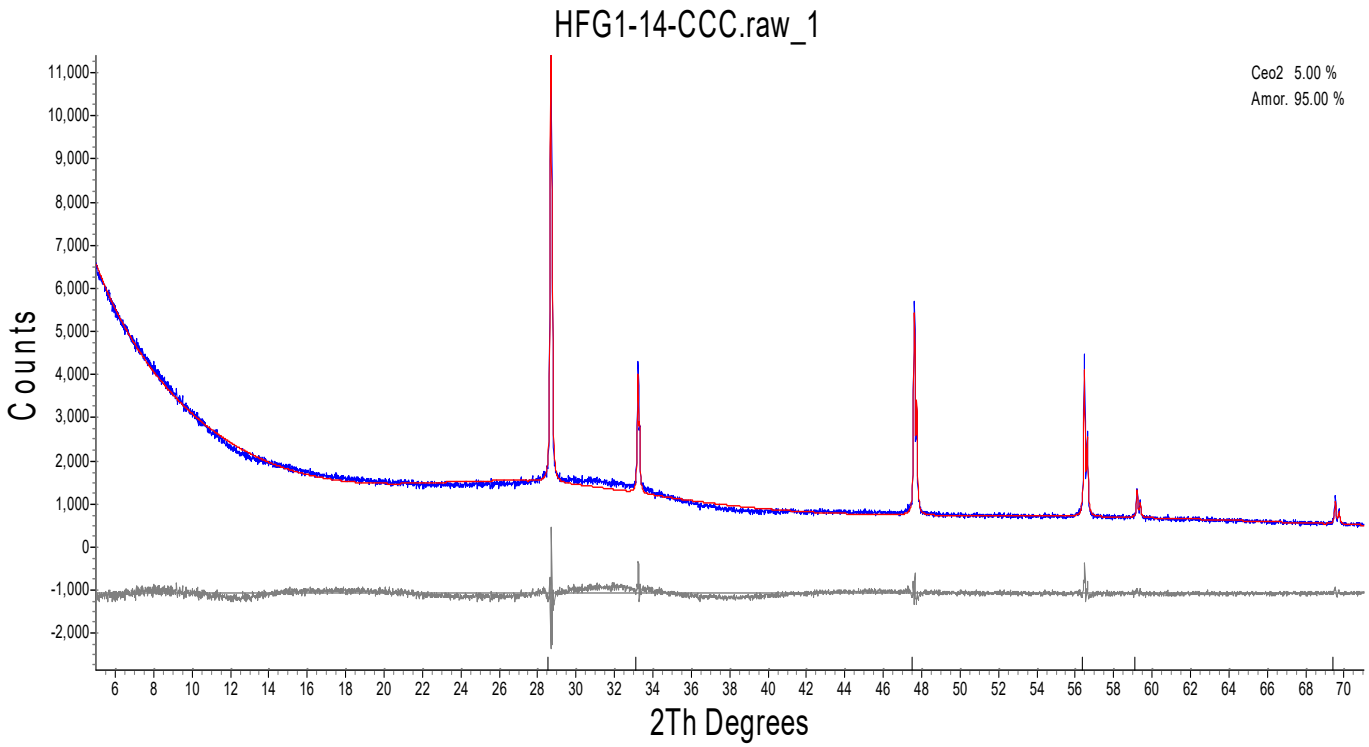

Figure E.14. XRD Spectrum of CCC-Treated Glass HFG1-14

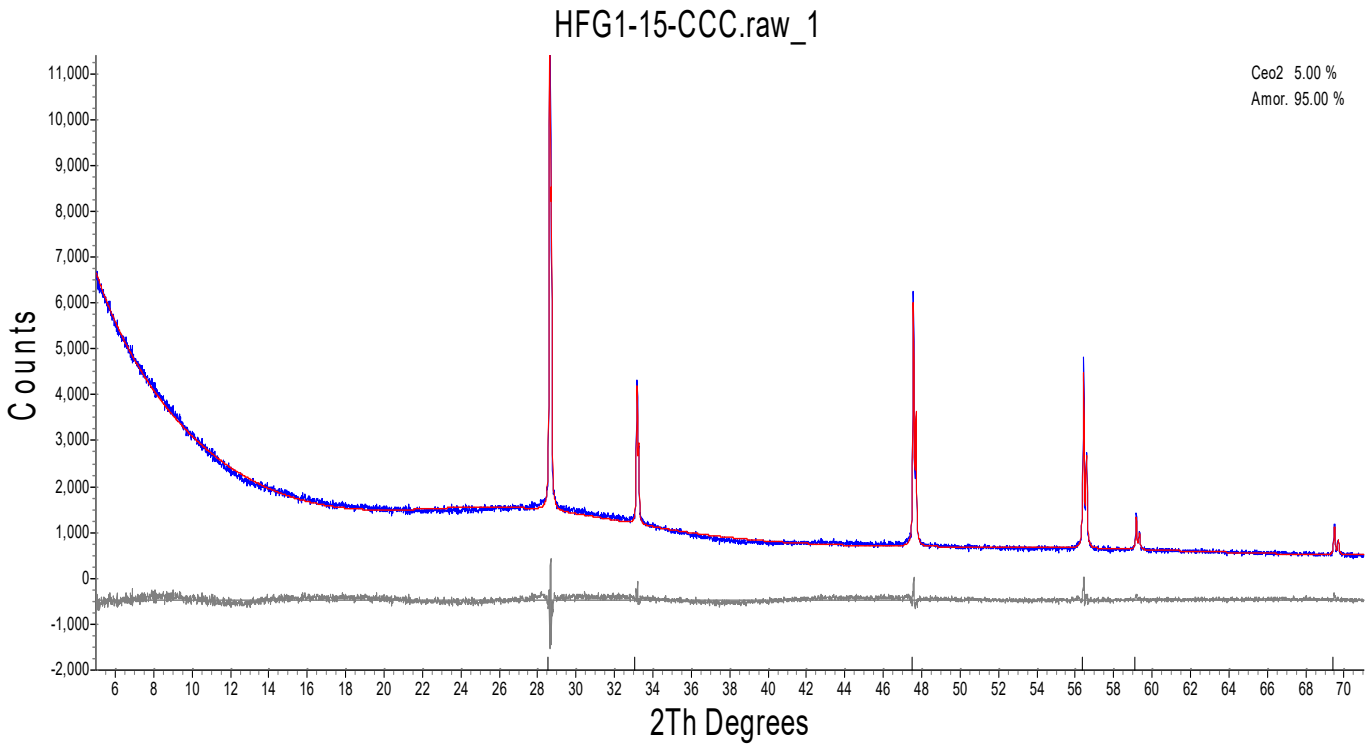

Figure E.15. XRD Spectrum of CCC-Treated Glass HFG1-15

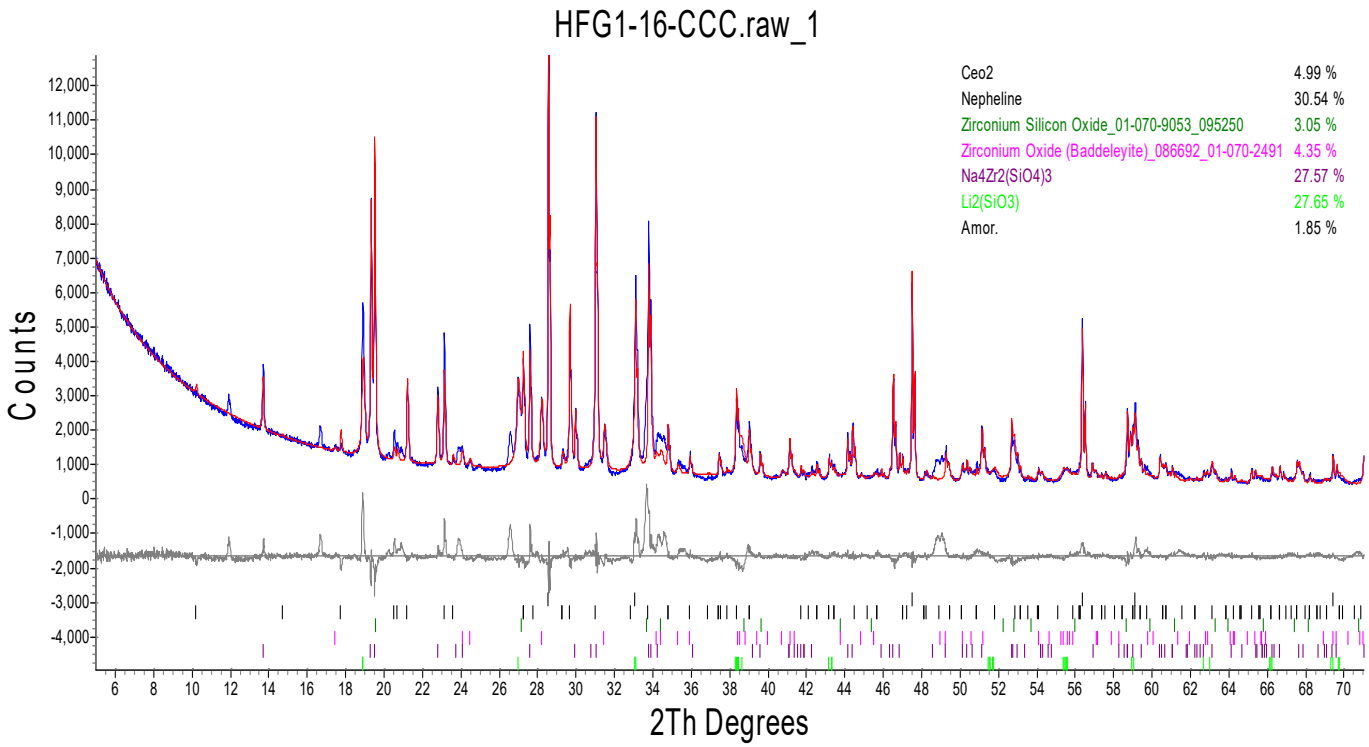

Phase Name	Wt% of Spiked	Wt% in Spiked Sample	Wt% in Original Sample
CeO_2	4.994	4.994	0.000
Nepheline	0.000	30.541	32.146
$ZrSiO_4$	0.000	3.048	3.209
ZrO_2	0.000	4.350	4.578
$Na_4Zr_2(SiO_4)_3$	0.000	27.571	20.020
$Li_2(SiO_3)$	0.000	27.646	29.099

Figure E.16. XRD Spectrum of CCC-Treated Glass HFG1-16

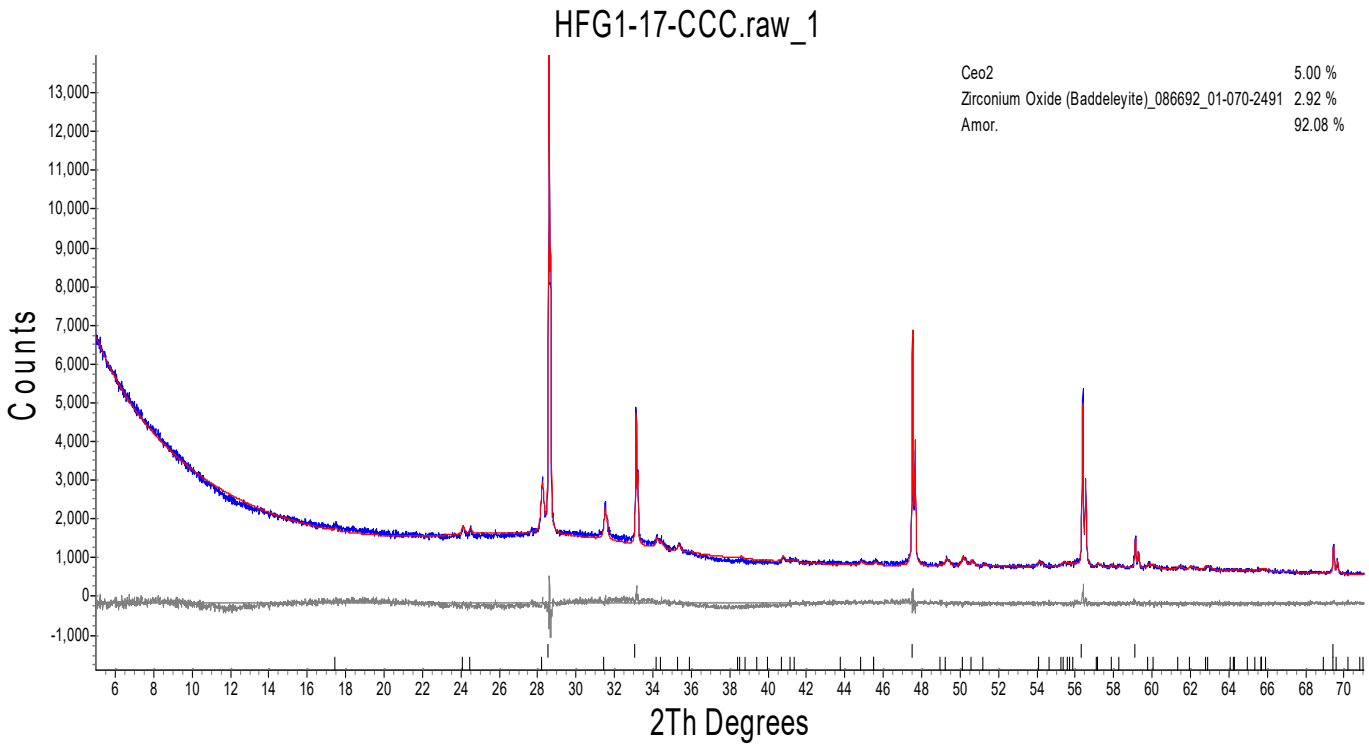

Phase Name	Wt% of Spiked	Wt% in Spiked Sample	Wt% in Original Sample
CeO_2	5.000	5.000	0.000
ZrO_2	0.000	2.916	3.070

Figure E.17. XRD Spectrum of CCC-Treated Glass HFG1-17

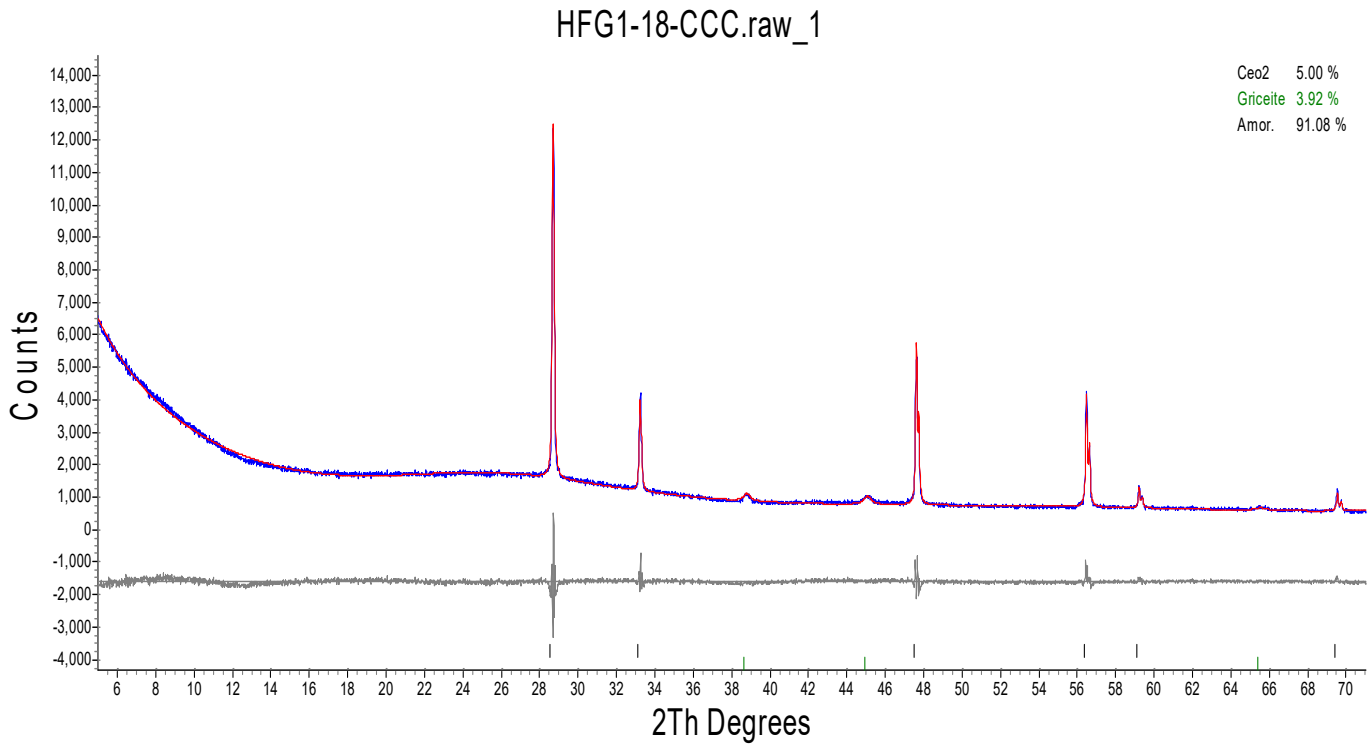

Phase Name	Wt% of Spiked	Wt% in Spiked Sample	Wt% in Original Sample
CeO_2	5.000	5.000	0.000
LiF	0.000	3.925	4.132

Figure E.18. XRD Spectrum of CCC-Treated Glass HFG1-18

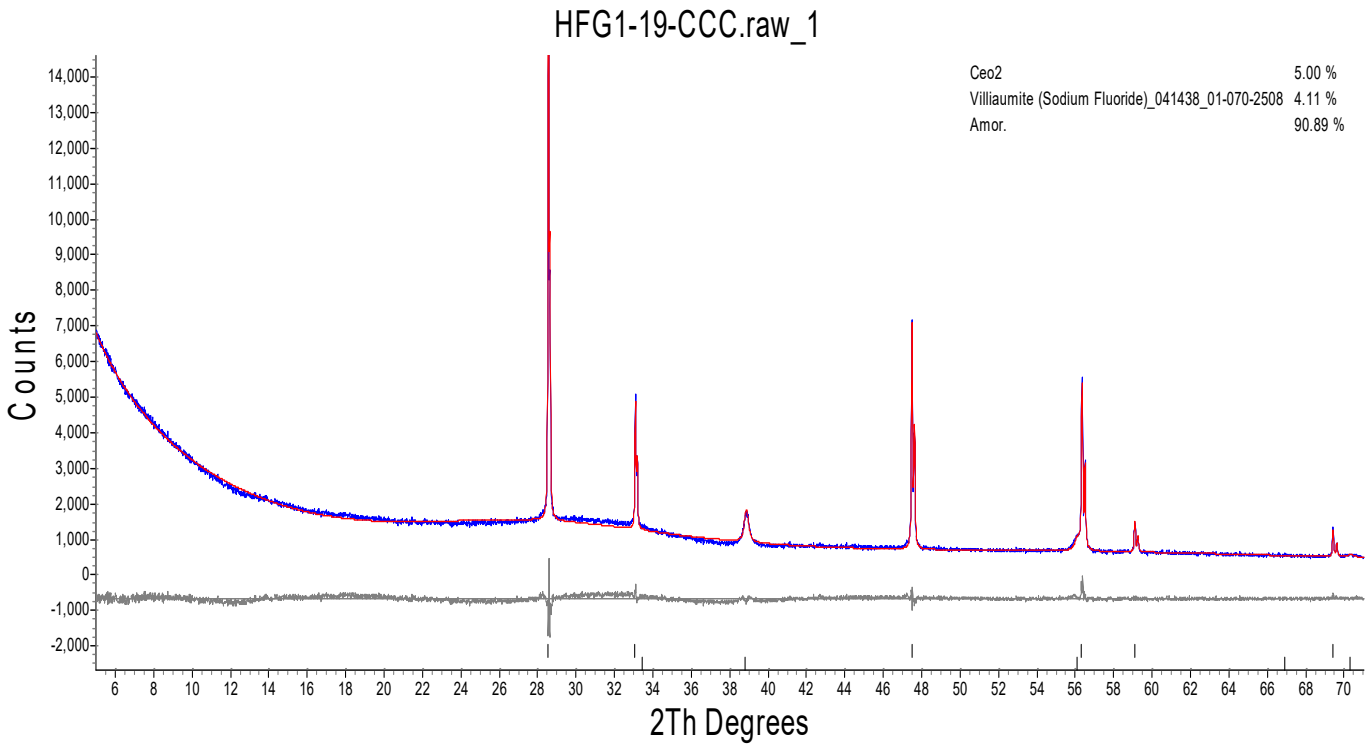

Phase Name	Wt% of Spiked	Wt% in Spiked Sample	Wt% in Original Sample
CeO_2	5.000	5.000	0.000
NaF	0.000	4.108	4.324

Figure E.19. XRD Spectrum of CCC-Treated Glass HFG1-19

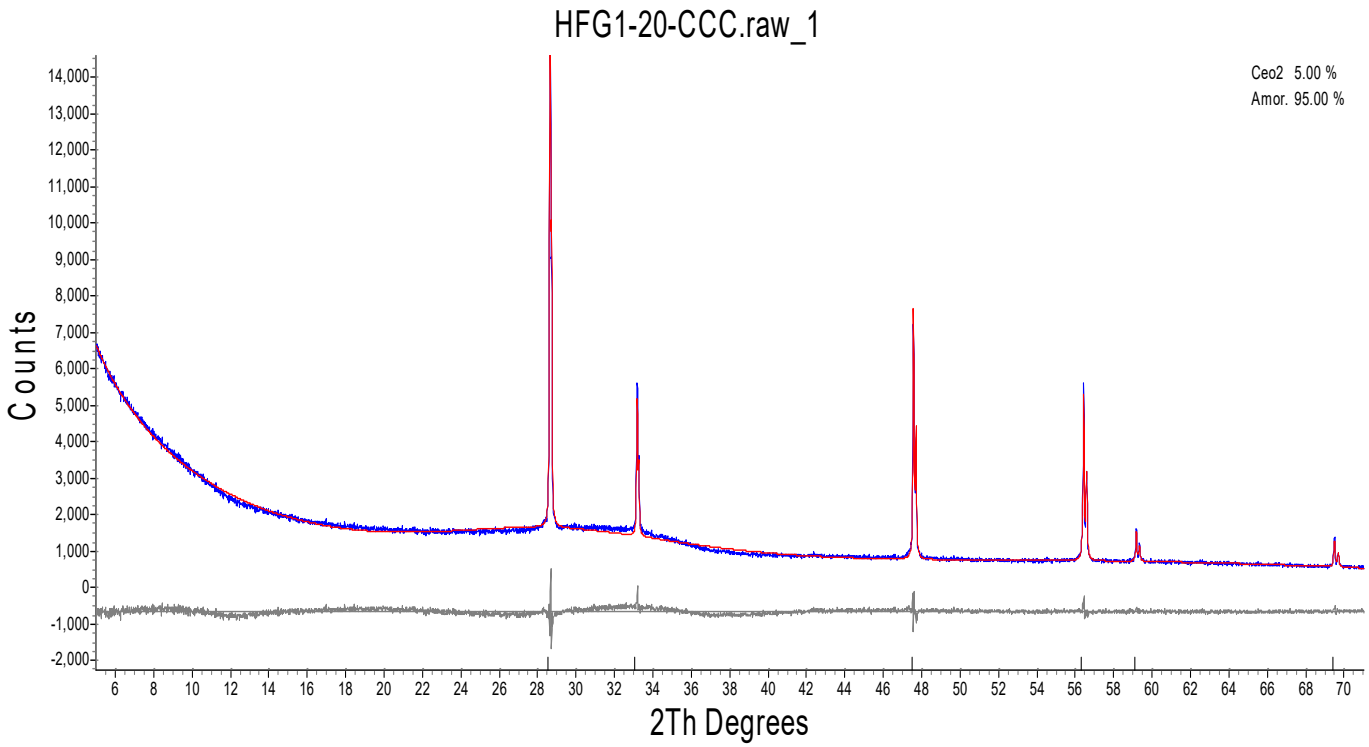

Figure E.20. XRD Spectrum of CCC-Treated Glass HFG1-20

Appendix F – Viscosity Data

This appendix contains the measured viscosity data for each of the glasses in this matrix. The plots shown in this appendix are fitted to the Arrhenius equation:

$$\ln(\eta) = A + \frac{B}{T_K} \tag{F.1}$$

where A and B are independent of temperature and temperature (T_K) is in K (T(°C) + 273.15). If the plots showed curvature, they would be better fit to the Vogel- Fulcher-Tamman (VFT) model:

$$\ln(\eta) = E + \frac{F}{T_k - T_0} \tag{F.2}$$

where E, F, and T_0 are temperature independent and composition dependent coefficients and T_K is the temperature in K (T(°C) + 273.15).

There was insufficient glass remaining to measure the viscosity of glasses HFG1-05 and HFG1-20. Therefore, there are no results shown for these two glasses.

F.1 Glass HFG1-01-1 Viscosity Data

Table F.1. Viscosity Data for Glass HFG1-01-1

Measured Temp., °C	Viscosity, Pa-s	1/T x10000, K^{-1}	ln η, Pa-s
1150	4.03	7.027	1.3941
1050	9.35	7.558	2.2355
950	27.91	8.176	3.3288
1150	4.07	7.027	1.4047
1200	3.13	6.788	1.1412
1150	4.38	7.027	1.4759

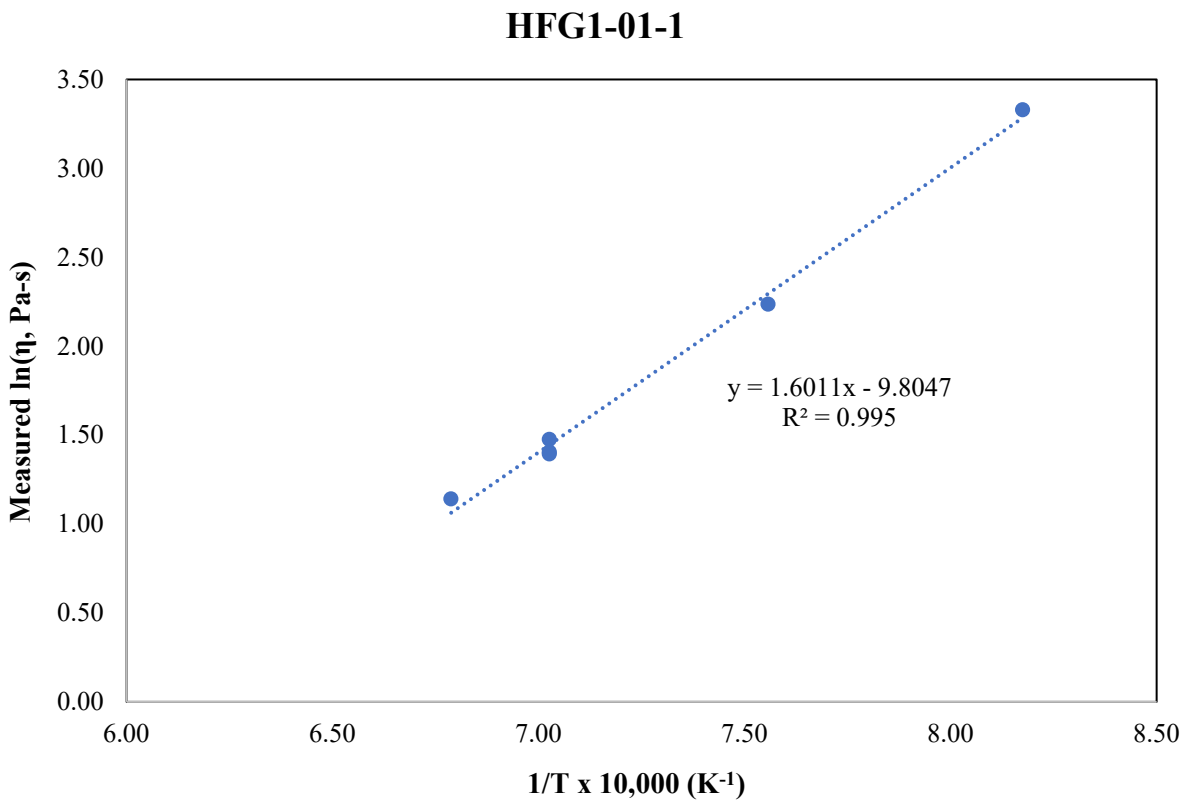

Figure F.1. Viscosity-Temperature Data and Arrhenius Equation Fit for Glass HFG1-01-1

F.2 Glass HFG1-02 Viscosity Data

Table F.2. Viscosity Data for Glass HFG1-02

Measured Temp., °C	Viscosity, Pa-s	1/T x10000, K^{-1}	ln η, Pa-s
1150	8.03	7.027	2.0831
1050	21.61	7.558	3.0731
950	78.80	8.176	4.3669
1150	8.25	7.027	2.1104
1200	5.42	6.788	1.6893
1150	8.19	7.027	2.1034

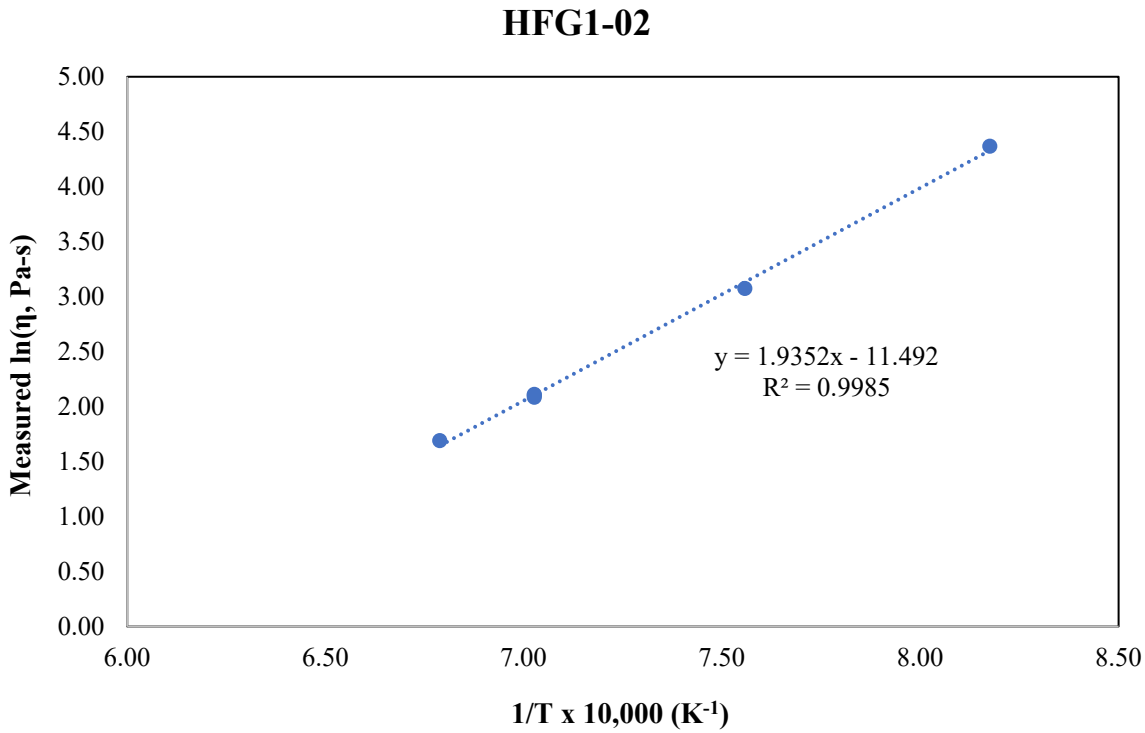

Figure F.2. Viscosity-Temperature Data and Arrhenius Equation Fit for Glass HFG1-02

F.3 Glass HFG1-03 Viscosity Data

Table F.3. Viscosity Data for Glass HFG1-03

Measured Temp., °C	Viscosity, Pa-s	1/T x10000, K^{-1}	ln η, Pa-s
1150	10.70	7.027	2.3702
1050	35.87	7.558	3.5800
950	173.84	8.176	5.1581
1150	10.81	7.027	2.3802
1200	6.50	6.788	1.8717
1150	10.90	7.027	2.3888

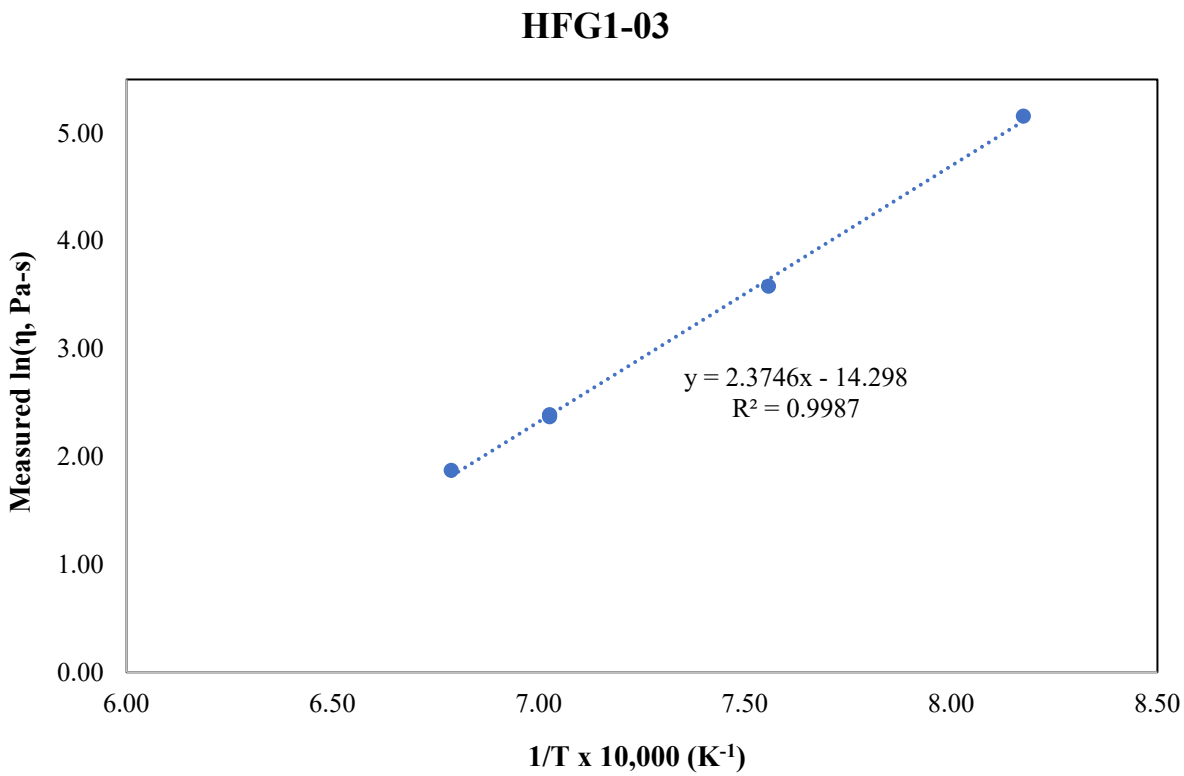

Figure F.3. Viscosity-Temperature Data and Arrhenius Equation Fit for Glass HFG1-03

F.4 Glass HFG1-04 Viscosity Data

Table F.4. Viscosity Data for Glass HFG1-04

Measured Temp., °C	Viscosity, Pa-s	1/T x10000, K-1	ln η, Pa-s
1150	1.99	7.027	0.6895
1050	4.65	7.558	1.5376
950	13.80	8.176	2.6250
1150	1.83	7.027	0.6055
1200	1.28	6.788	0.2434
1150	1.88	7.027	0.6308

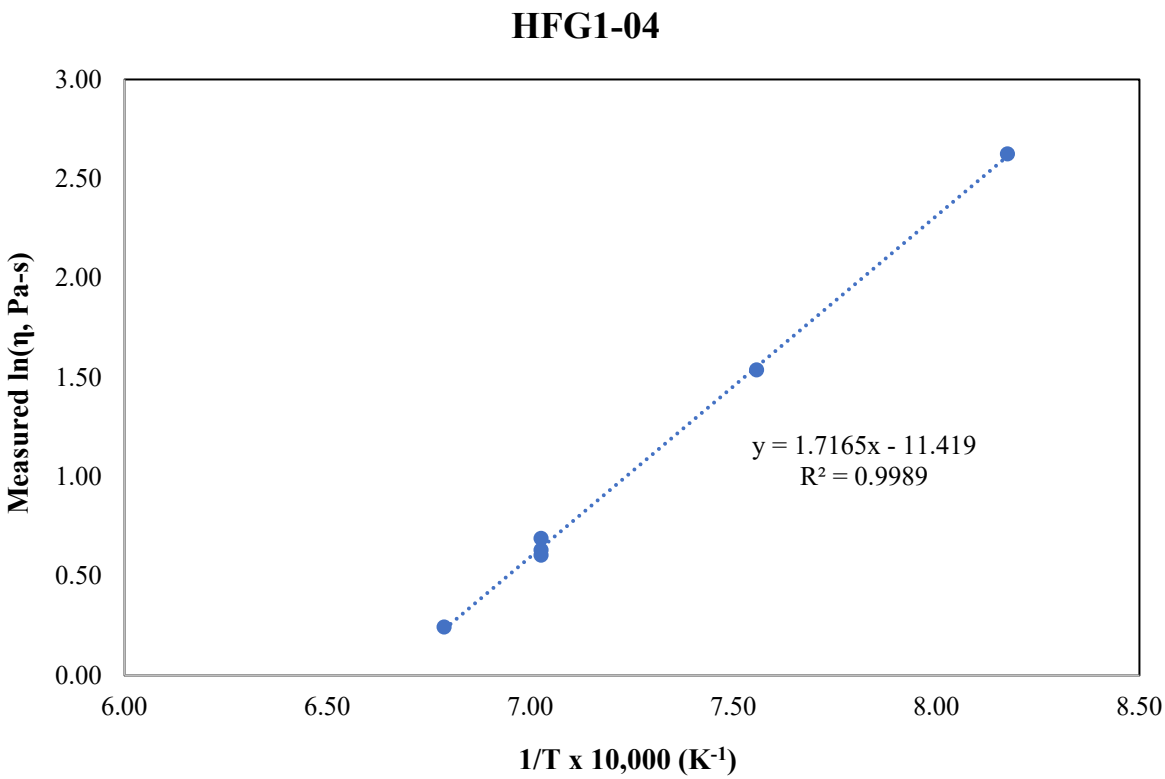

Figure F.4. Viscosity-Temperature Data and Arrhenius Equation Fit for Glass HFG1-04

F.5 Glass HFG1-06 Viscosity Data

Table F.5. Viscosity Data for Glass HFG1-06

Measured Temp., °C	Viscosity, Pa-s	1/T x10000, K^{-1}	ln η, Pa-s
1150	2.44	7.027	0.8924
1050	4.92	7.558	1.5929
950	14.35	8.176	2.6640
1150	2.43	7.027	0.8891
1200	1.90	6.788	0.6404
1150	2.47	7.027	0.9024

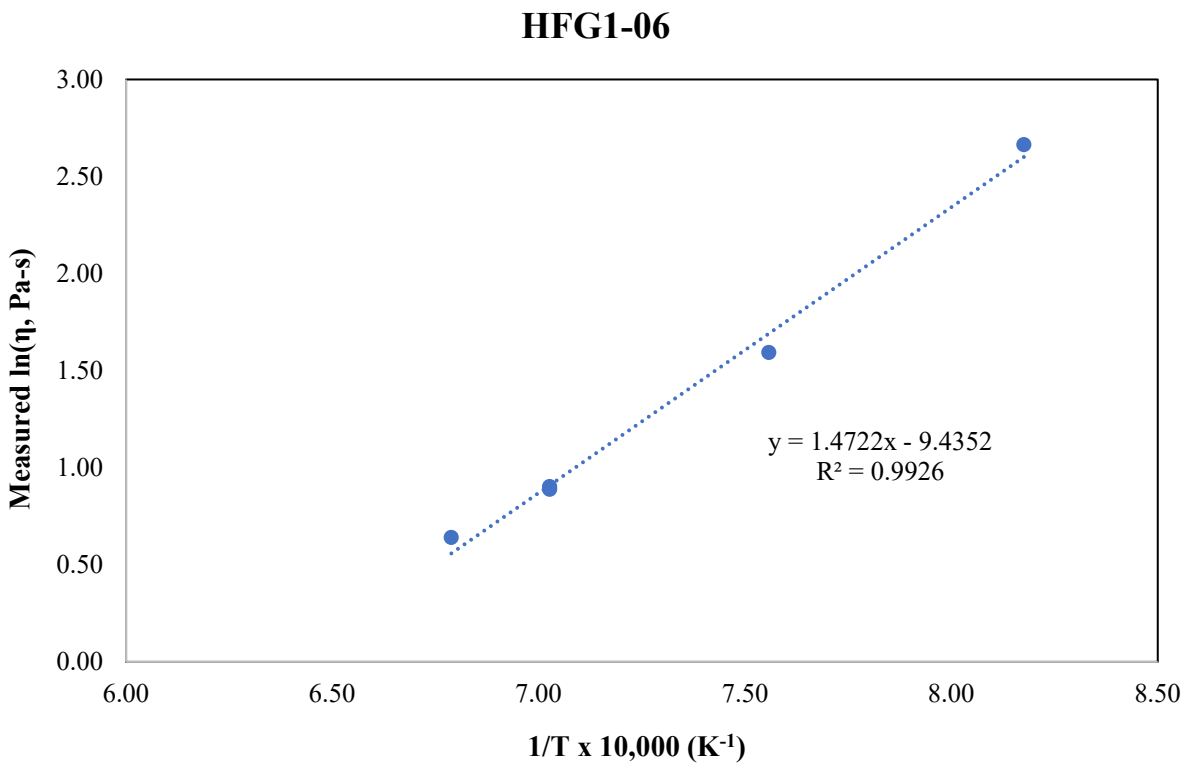

Figure F.5. Viscosity-Temperature Data and Arrhenius Equation Fit for Glass HFG1-06

F.6 Glass HFG1-07 Viscosity Data

Table F.6. Viscosity Data for Glass HFG1-07

Measured Temp., °C	Viscosity, Pa-s	1/T x10000, K^{-1}	ln η, Pa-s
1150	7.30	7.027	1.9875
1050	18.67	7.558	2.9270
950	66.96	8.176	4.2041
1150	7.25	7.027	1.9812
1200	4.97	6.788	1.6029
1150	7.39	7.027	2.0001

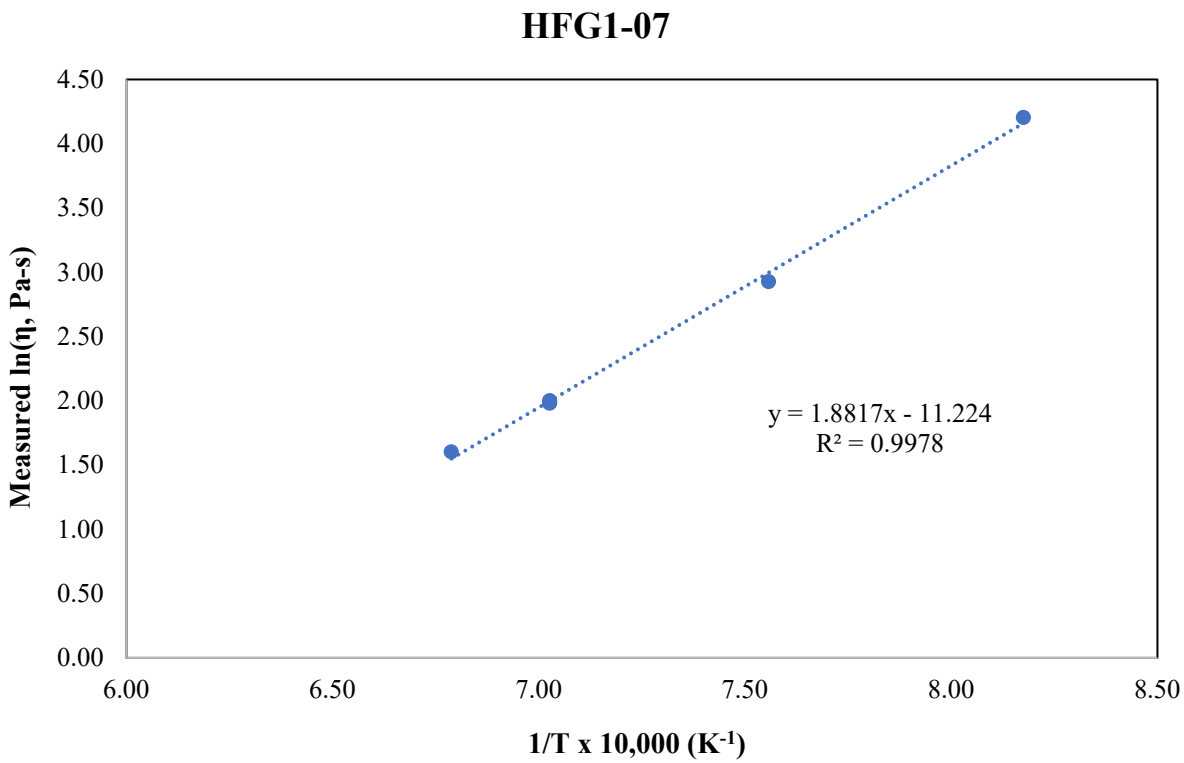

Figure F.6. Viscosity-Temperature Data and Arrhenius Equation Fit for Glass HFG1-07

F.7 Glass HFG1-08 Viscosity Data

Table F.7. Viscosity Data for Glass HFG1-08

Measured Temp., °C	Viscosity, Pa-s	1/T x10000, K^{-1}	ln η, Pa-s
1150	3.03	7.027	1.1077
1050	7.44	7.558	2.0072
950	28.25	8.176	3.3411
1150	2.97	7.027	1.0895
1200	2.27	6.788	0.8203
1150	2.97	7.027	1.0885

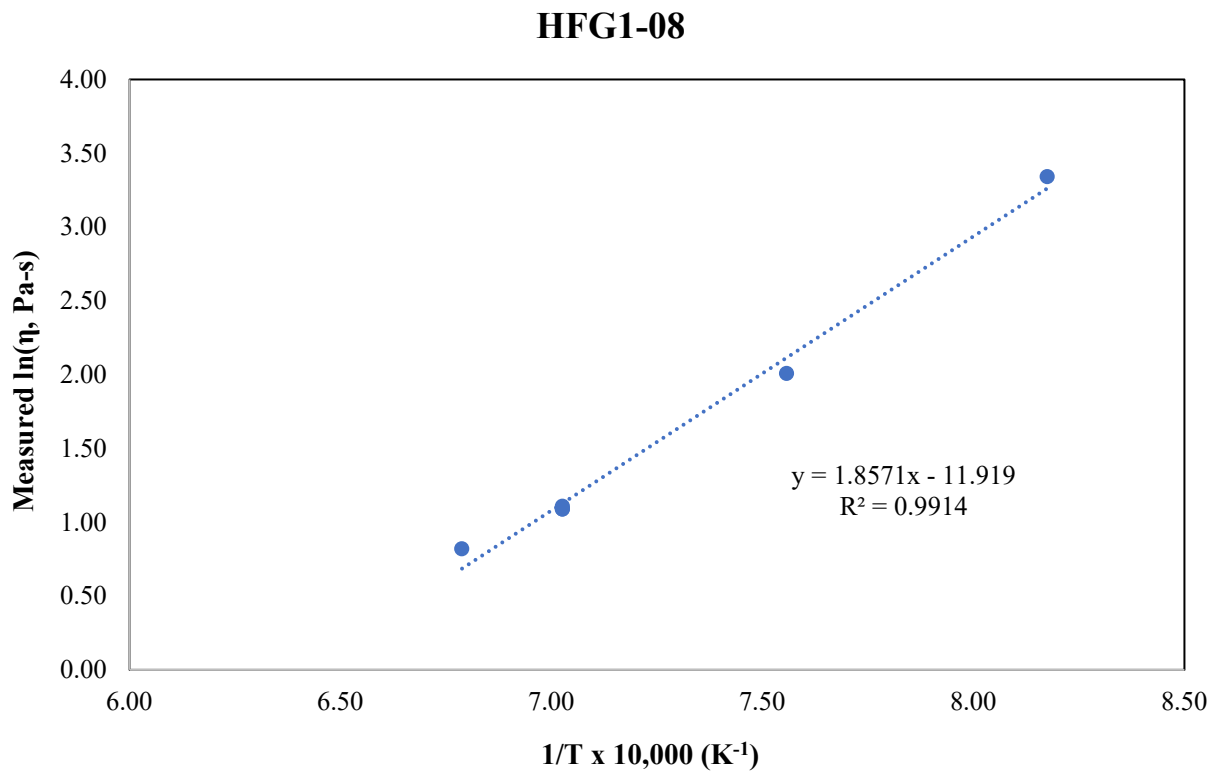

Figure F.7. Viscosity-Temperature Data and Arrhenius Equation Fit for Glass HFG1-08

F.8 Glass HFG1-09 Viscosity Data

Table F.8. Viscosity Data for Glass HFG1-09

Measured Temp., °C	Viscosity, Pa-s	1/T x10000, K^{-1}	ln η, Pa-s
1150	2.70	7.027	0.9927
1050	5.55	7.558	1.7141
950	16.35	8.176	2.7942
1150	2.73	7.027	1.0051
1200	2.22	6.788	0.7975
1150	2.78	7.027	1.0217

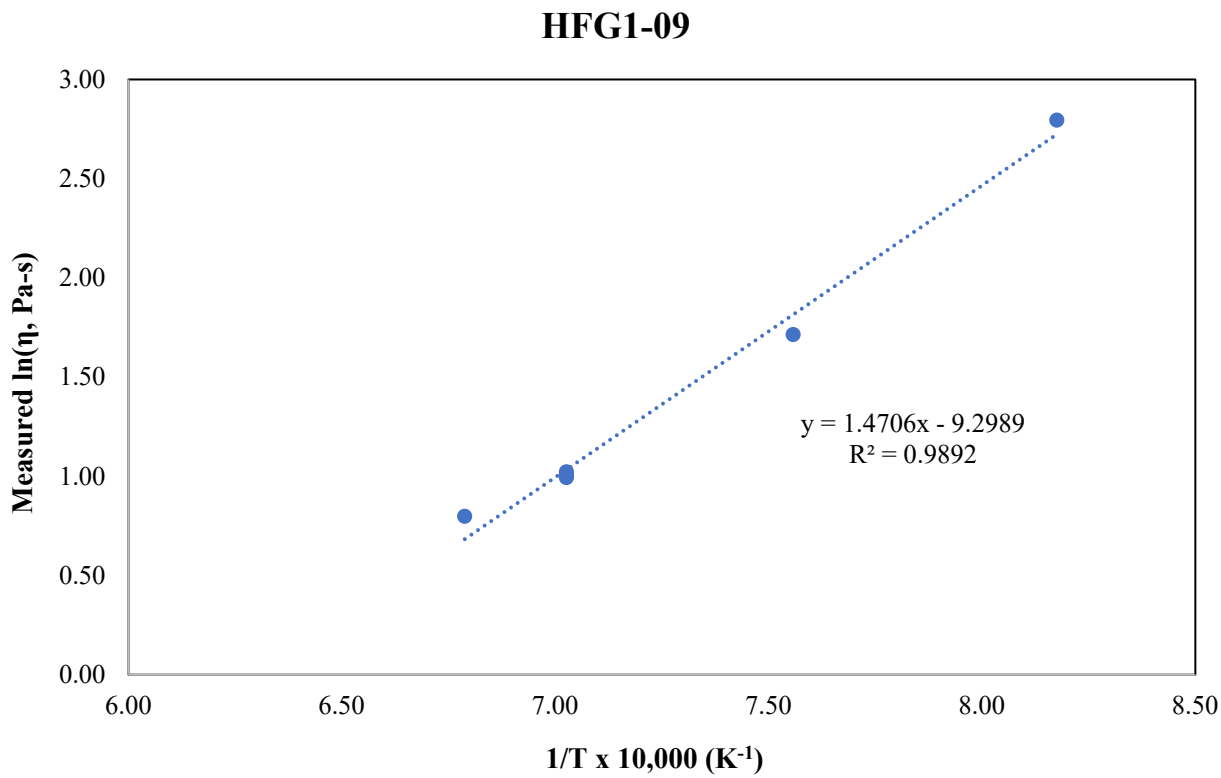

Figure F.8. Viscosity-Temperature Data and Arrhenius Equation Fit for Glass HFG1-09

F.9 Glass HFG1-10 Viscosity Data

Table F.9. Viscosity Data for Glass HFG1-10

Measured Temp., °C	Viscosity, Pa-s	1/T x10000, K^{-1}	ln η, Pa-s
1150	2.13	7.027	0.7544
1050	4.39	7.558	1.4784
950	13.43	8.176	2.5973
1150	2.20	7.027	0.7896
1200	1.39	6.788	0.3286
1150	2.15	7.027	0.7664

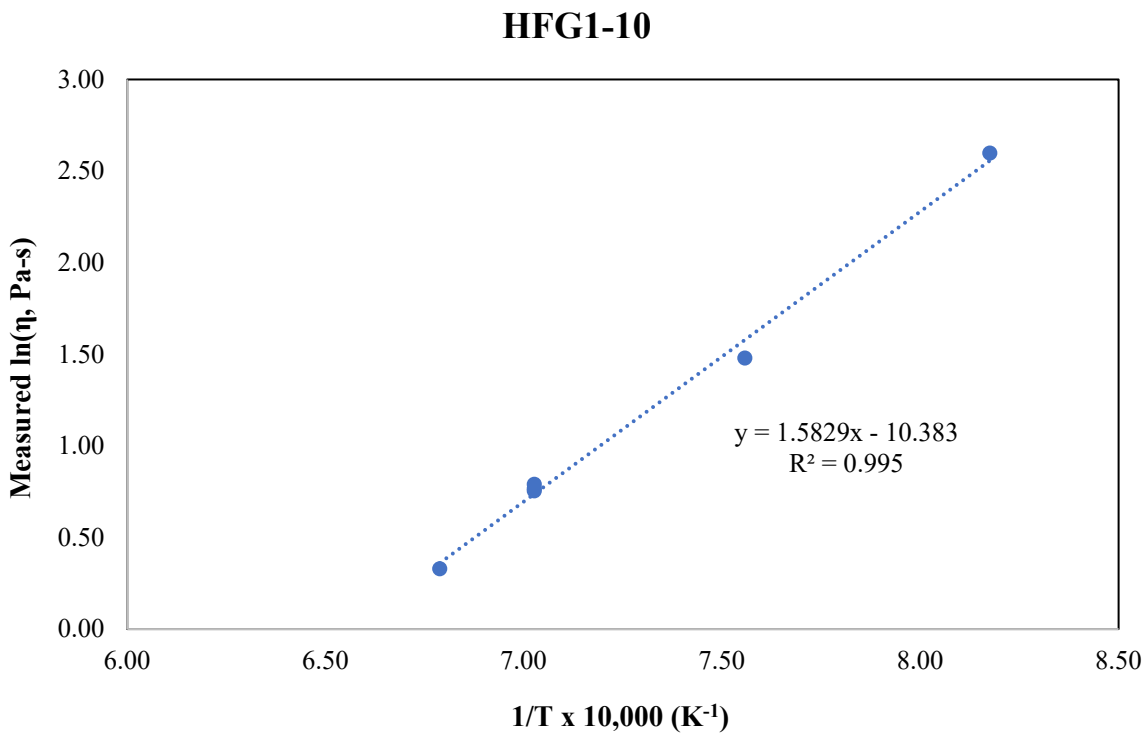

Figure F.9. Viscosity-Temperature Data and Arrhenius Equation Fit for Glass HFG1-10

F.10 Glass HFG1-11 Viscosity Data

Table F.10. Viscosity Data for Glass HFG1-11

Measured Temp., °C	Viscosity, Pa-s	1/T x10000, K^{-1}	ln η, Pa-s
1150	3.58	7.027	1.2754
1050	9.02	7.558	2.1995
950	32.40	8.176	3.4782
1150	3.70	7.027	1.3083
1200	2.53	6.788	0.9264
1150	3.76	7.027	1.3239

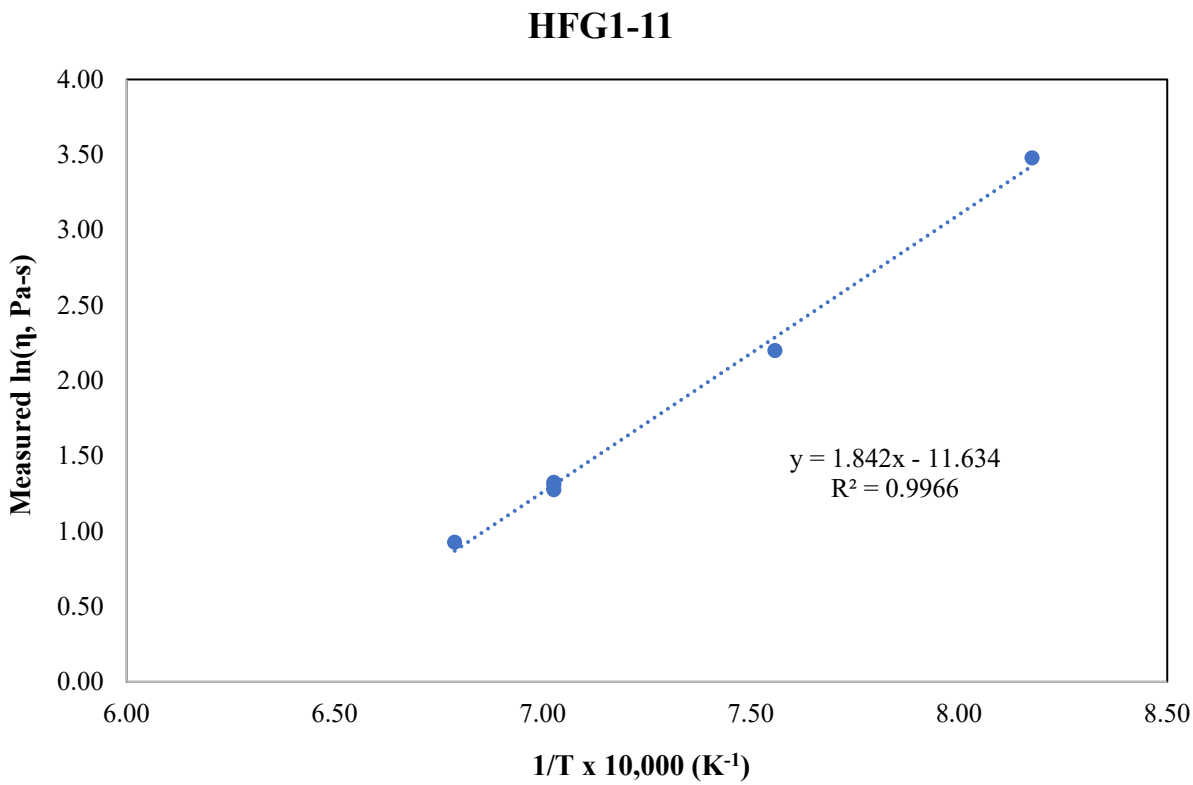

Figure F.10. Viscosity-Temperature Data and Arrhenius Equation Fit for Glass HFG1-11

F.11 Glass HFG1-12 Viscosity Data

Table F.11. Viscosity Data for Glass HFG1-12

Measured Temp., °C	Viscosity, Pa-s	1/T x10000, K^{-1}	ln η, Pa-s
1150	2.80	7.027	1.0296
1050	6.32	7.558	1.8440
950	22.53	8.176	3.1146
1150	2.94	7.027	1.0776
1200	2.30	6.788	0.8340
1150	2.96	7.027	1.0864

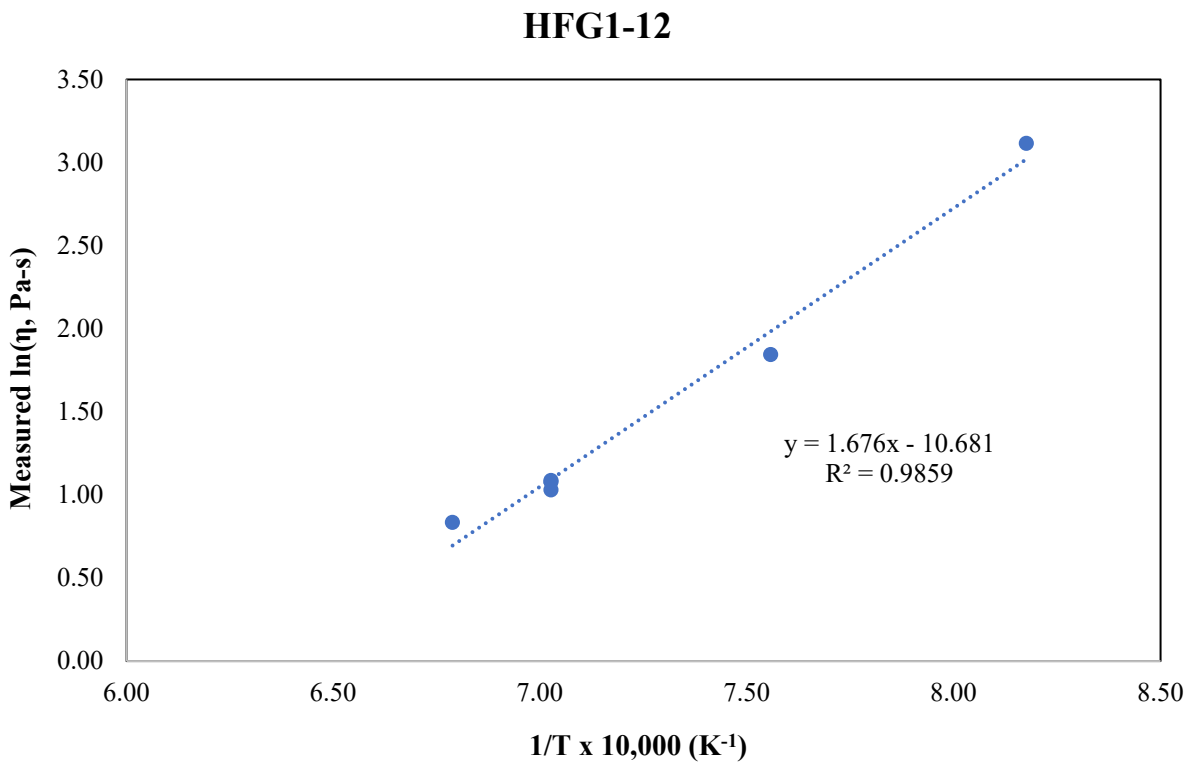

Figure F.11. Viscosity-Temperature Data and Arrhenius Equation Fit for Glass HFG1-12

F.12 Glass HFG1-13 Viscosity Data

Table F.12. Viscosity Data for Glass HFG1-13

Measured Temp., °C	Viscosity, Pa-s	1/T x10000, K^{-1}	ln η, Pa-s
1150	3.77	7.027	1.3263
1050	8.42	7.558	2.1304
950	26.24	8.176	3.2672
1150	3.74	7.027	1.3188
1200	2.86	6.788	1.0515
1150	3.80	7.027	1.3349

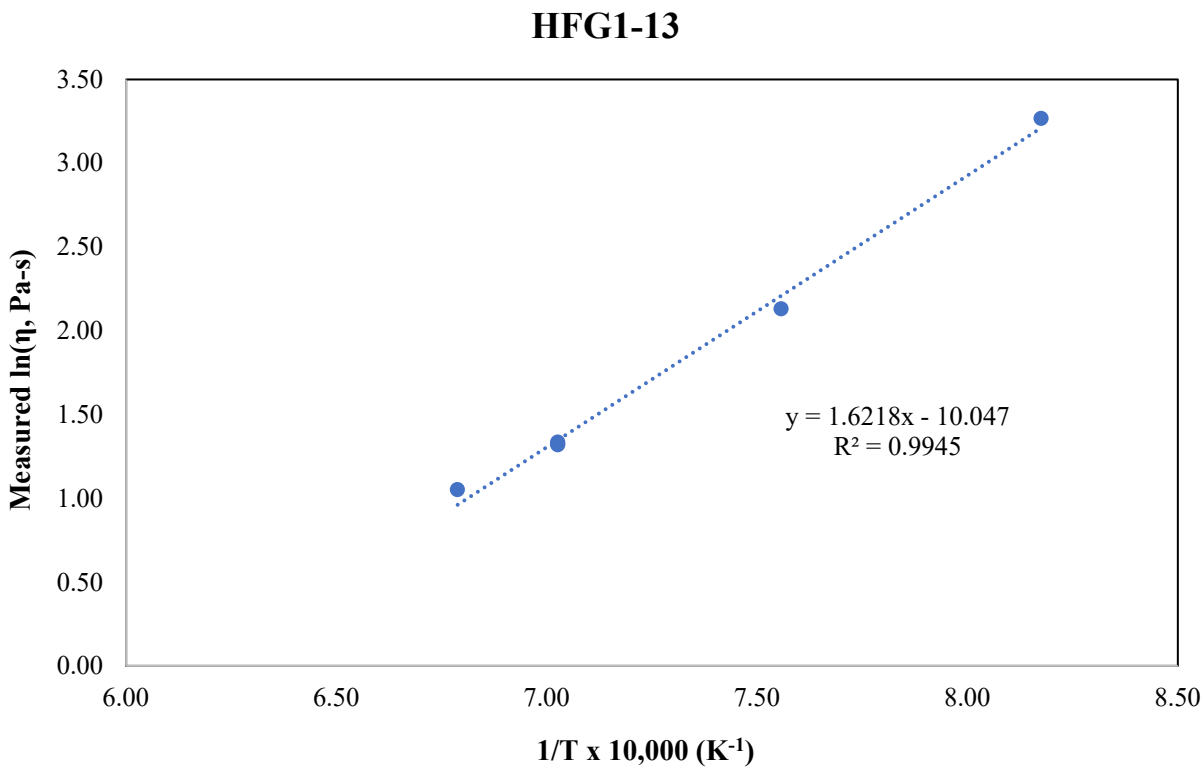

Figure F.12. Viscosity-Temperature Data and Arrhenius Equation Fit for Glass HFG1-13

F.13 Glass HFG1-14 Viscosity Data

Table F.13. Viscosity Data for Glass HFG1-14

Measured Temp., °C	Viscosity, Pa-s	1/T x10000, K^{-1}	ln η, Pa-s
1150	3.97	7.027	1.3787
1050	9.96	7.558	2.2983
950	36.21	8.176	3.5892
1150	3.92	7.027	1.3656
1200	2.79	6.788	1.0267
1150	3.95	7.027	1.3749

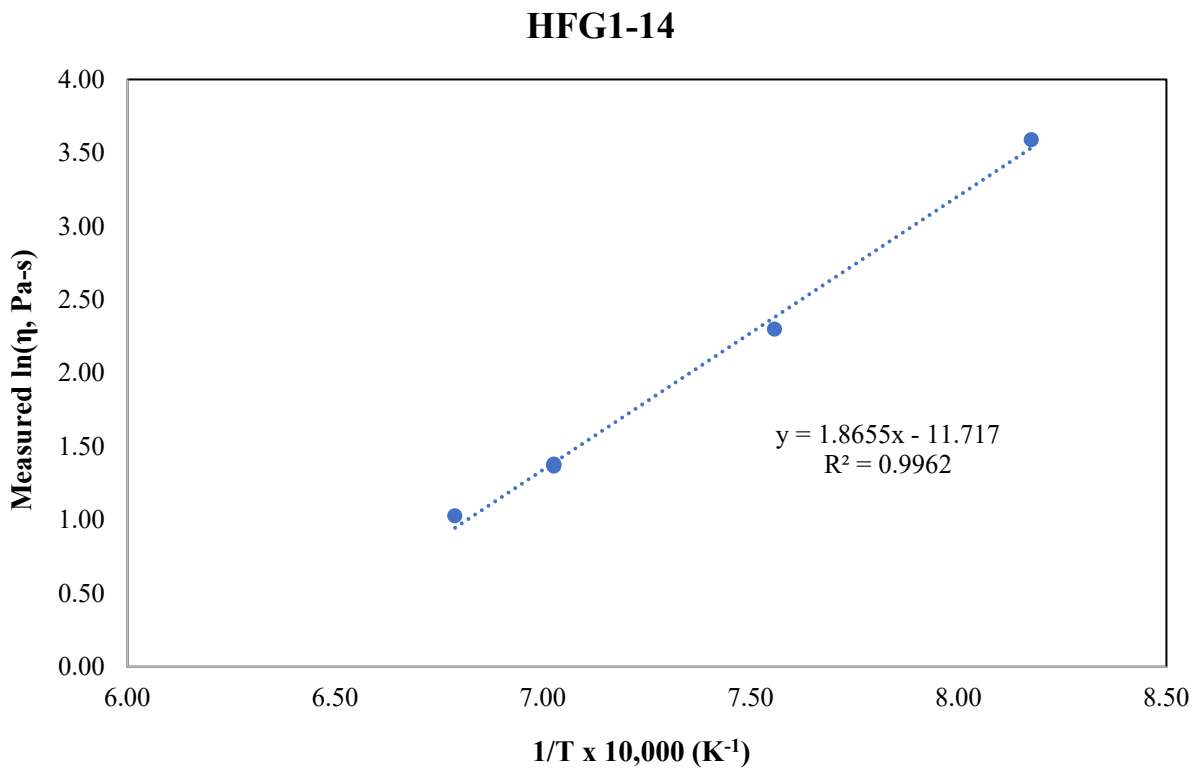

Figure F.13. Viscosity-Temperature Data and Arrhenius Equation Fit for Glass HFG1-14

F.14 Glass HFG1-15 Viscosity Data

Table F.14. Viscosity Data for Glass HFG1-15

Measured Temp., °C	Viscosity, Pa-s	1/T x10000, K^{-1}	ln η, Pa-s
1150	4.16	7.027	1.4254
1050	10.00	7.558	2.3022
950	33.43	8.176	3.5094
1150	4.17	7.027	1.4273
1200	3.02	6.788	1.1064
1150	4.20	7.027	1.4359

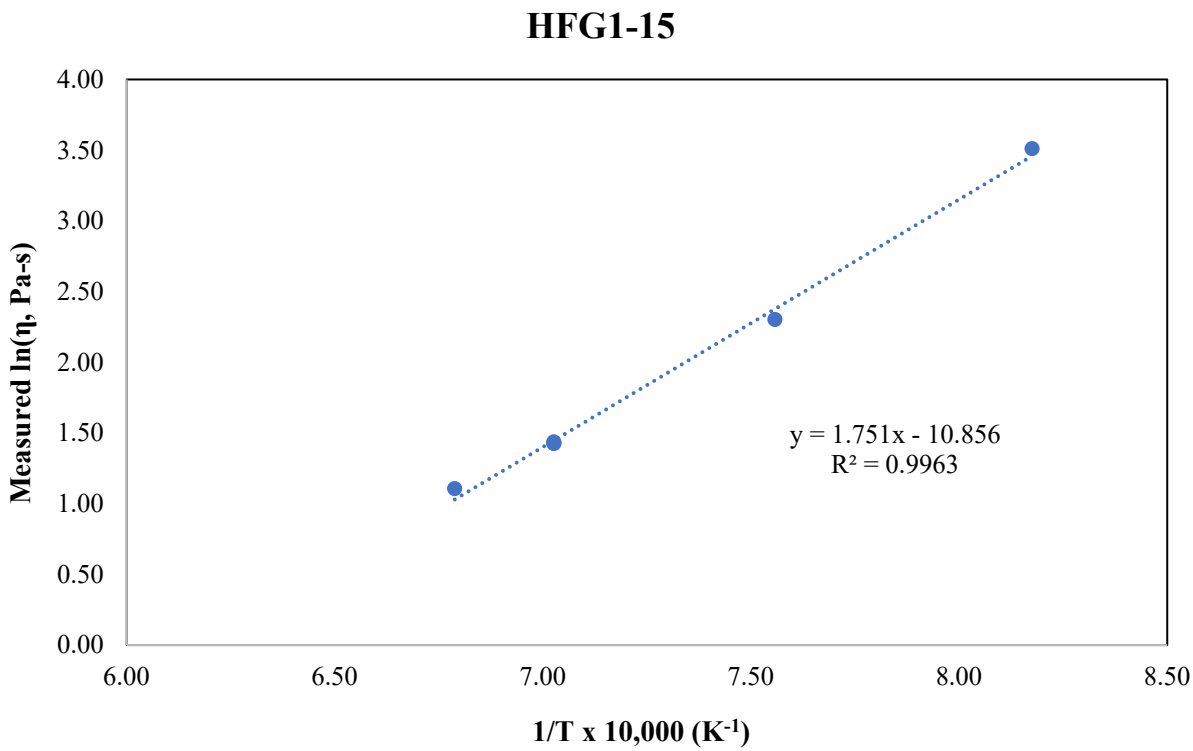

Figure F.14. Viscosity-Temperature Data and Arrhenius Equation Fit for Glass HFG1-15

F.15 Glass HFG1-16 Viscosity Data

Table F.15. Viscosity Data for Glass HFG1-16

Measured Temp., °C	Viscosity, Pa-s	1/T x10000, K^{-1}	ln η, Pa-s
1150	1.80	7.027	0.5893
1050	4.17	7.558	1.4272
950	11.31	8.176	2.4258
1150	1.67	7.027	0.5144
1200	1.09	6.788	0.0874
1150	1.77	7.027	0.5693

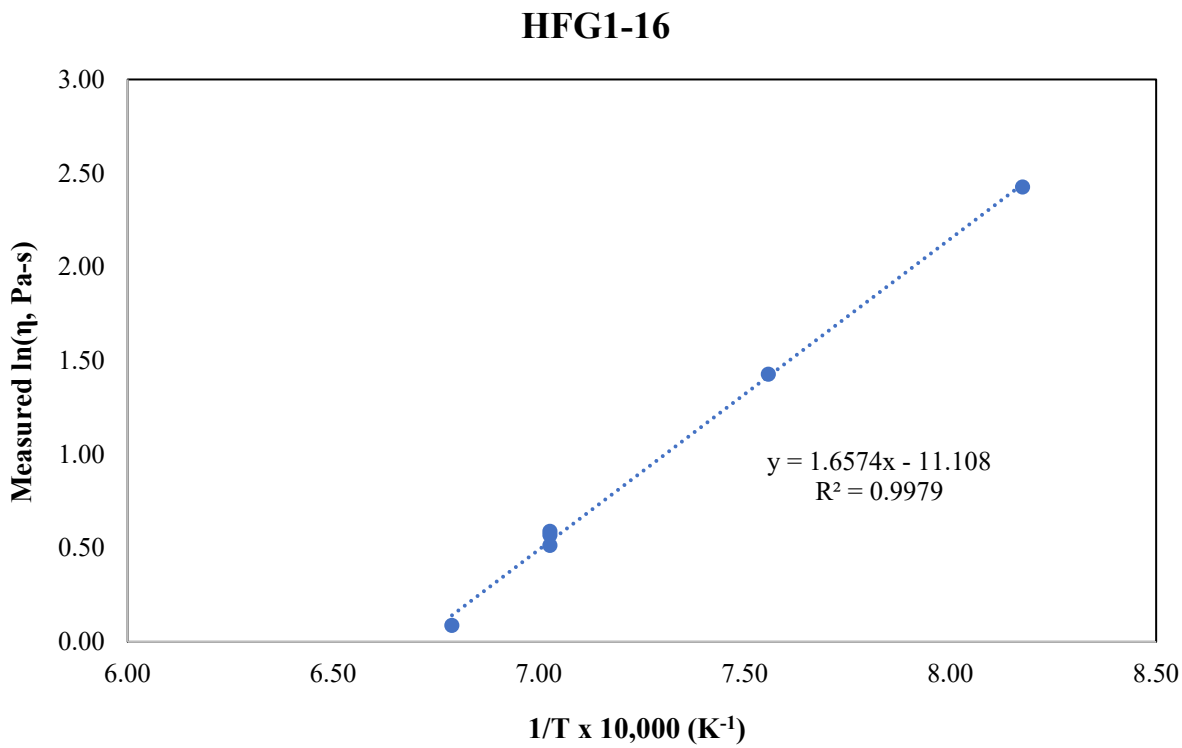

Figure F.15. Viscosity-Temperature Data and Arrhenius Equation Fit for Glass HFG1-16

F.16 Glass HFG1-17 Viscosity Data

Table F.16. Viscosity Data for Glass HFG1-17

Measured Temp., °C	Viscosity, Pa-s	1/T x10000, K^{-1}	ln η, Pa-s
1150	3.60	7.027	1.2804
1050	11.80	7.558	2.4679
950	40.58	8.176	3.7032
1150	3.74	7.027	1.3195
1200	2.22	6.788	0.7975
1150	3.56	7.027	1.2685

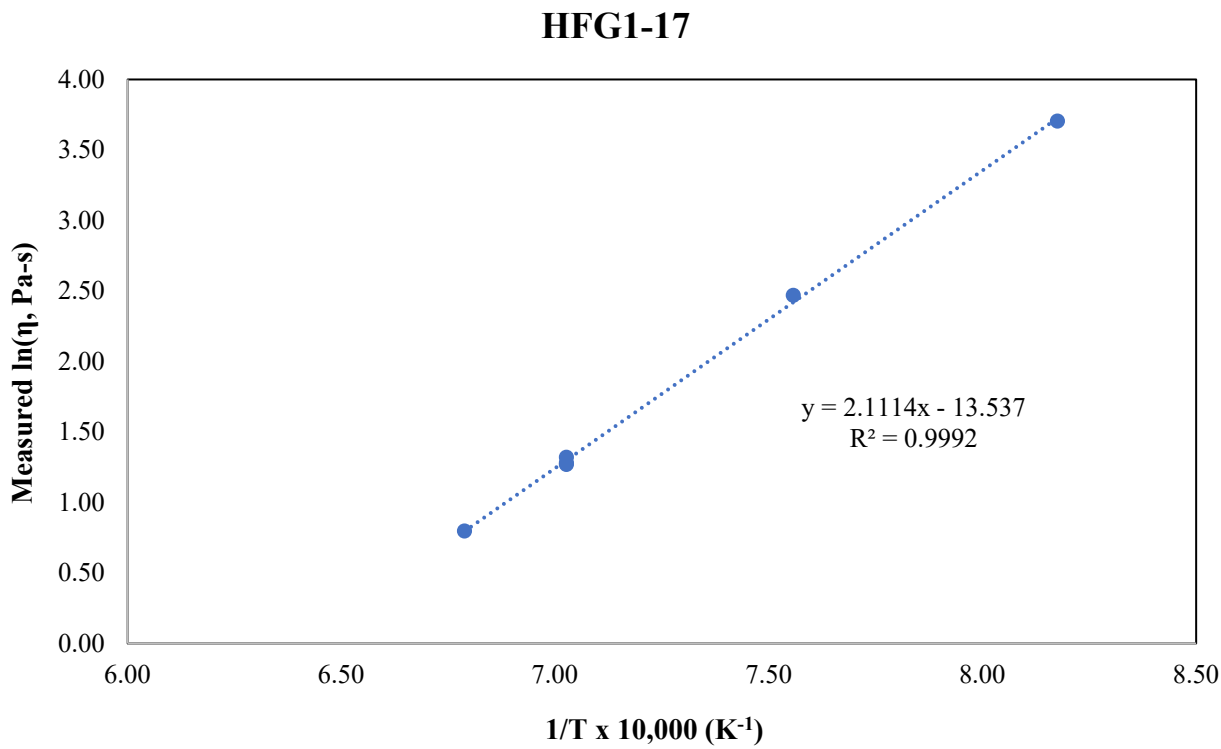

Figure F.16. Viscosity-Temperature Data and Arrhenius Equation Fit for Glass HFG1-17

F.17 Glass HFG1-18 Viscosity Data

Table F.17. Viscosity Data for Glass HFG1-18

Measured Temp., °C	Viscosity, Pa-s	1/T x10000, K^{-1}	ln η, Pa-s
1150	4.74	7.027	1.5566
1050	12.76	7.558	2.5463
950	40.31	8.176	3.6967
1150	4.77	7.027	1.5614
1200	3.23	6.788	1.1732
1150	4.73	7.027	1.5541

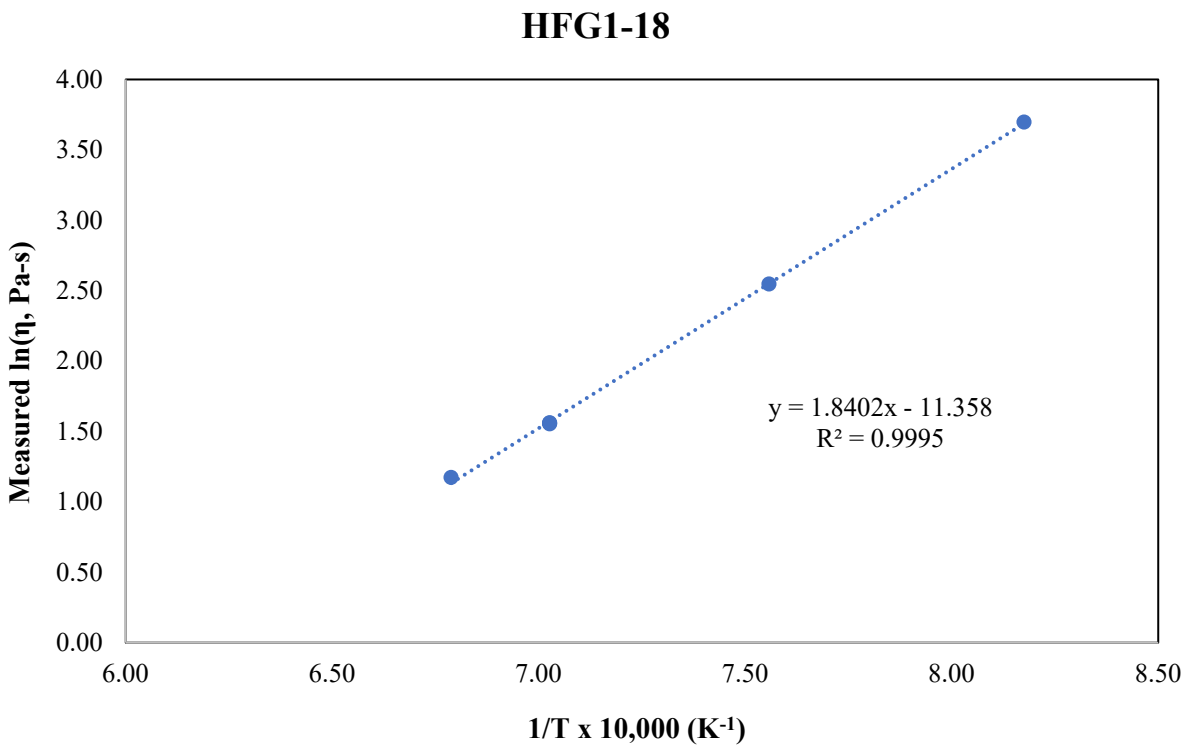

Figure F.17. Viscosity-Temperature Data and Arrhenius Equation Fit for Glass HFG1-18

F.18 Glass HFG1-19 Viscosity Data

Table F.18. Viscosity Data for Glass HFG1-19

Measured Temp., °C	Viscosity, Pa-s	1/T x10000, K^{-1}	ln η, Pa-s
1150	6.35	7.027	1.8483
1050	8.48	7.558	2.1378
950	12.34	8.176	2.5130
1150	7.89	7.027	2.0656
1200	7.85	6.788	2.0601
1150	8.22	7.027	2.1070

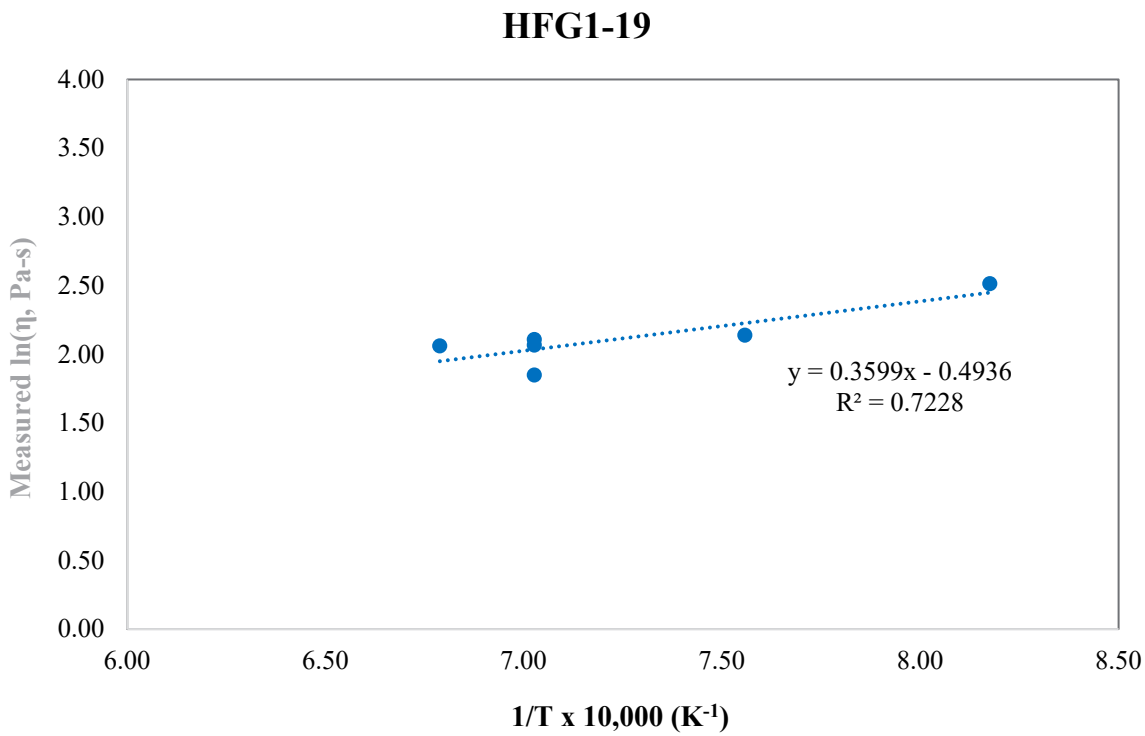

Figure F.18. Viscosity-Temperature Data and Arrhenius Equation Fit for Glass HFG1-19

Appendix G – Electrical Conductivity Data

This appendix contains the measured electrical conductivity (EC) data for each of the glasses in this matrix.

The plots shown in this appendix are fitted to the Arrhenius equation, which is shown below:

$$\ln(\varepsilon) = A + \frac{B}{T_K} \tag{G.1}$$

where *A* and *B* are independent of temperature (T_K) is in K (T(°C) + 273.15)**.** If some of the plots showed curvature, they would be better fit to the Vogel-Fulcher-Tamman (VFT) model:

$$\ln(\varepsilon) = \mathrm{E} + \frac{\mathrm{F}}{T_K - T_0} \tag{G.2)}$$

where *E, F, and* T_0 are temperature independent coefficients. The intent of the figures and Arrhenius equation fits shown in this appendix are mainly to assess trends of the data and provide some observations about whether there may be sufficient curvature in the data to consider VFT fits in the subsequent work that will decide between fitting the data to the Arrhenius or VFT equations for the electrical conductivity-temperature data for each glass that is being made.

There was insufficient glass remaining to measure the electrical conductivity of glasses HFG1-05, HFG1-16, and HFG1-20. Therefore, there are no results shown for these two glasses. The results for glass HFG1-08 were removed due to problems with the data and insufficient glass for more measurements.

G.1 Glass HFG1-01-1 Electrical Conductivity Data

Table G.1. Electrical Conductivity Data for Glass HFG1-01-1

Temperature, °C	Conductivity, S/m	1/T, K^{-1}	ln ε (S/m)
950	29.35	0.000818	3.3793
1200	74.06	0.000679	4.3049
1150	73.72	0.000703	4.3003
1050	46.13	0.000756	3.8314

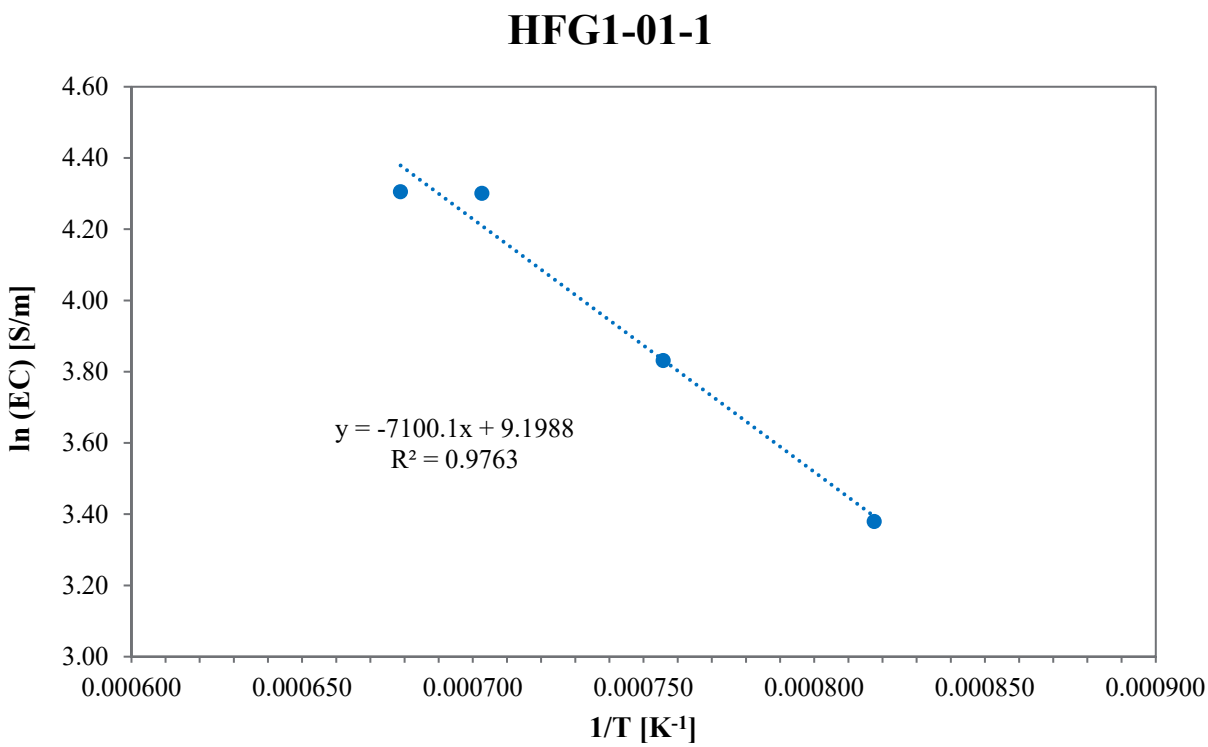

Figure G.1. Electrical Conductivity-Temperature Data and Arrhenius Equation Fit for Glass HFG1-01-1

G.2 Glass HFG1-02 Electrical Conductivity Data

Table G.2. Electrical Conductivity Data for Glass HFG1-02

Temperature, °C	Conductivity, S/m	1/T, K^{-1}	ln ε, S/m
950	12.67	0.000818	2.5393
1200	24.00	0.000679	3.1781
1150	19.69	0.000703	2.9799
1050	16.82	0.000756	2.8227

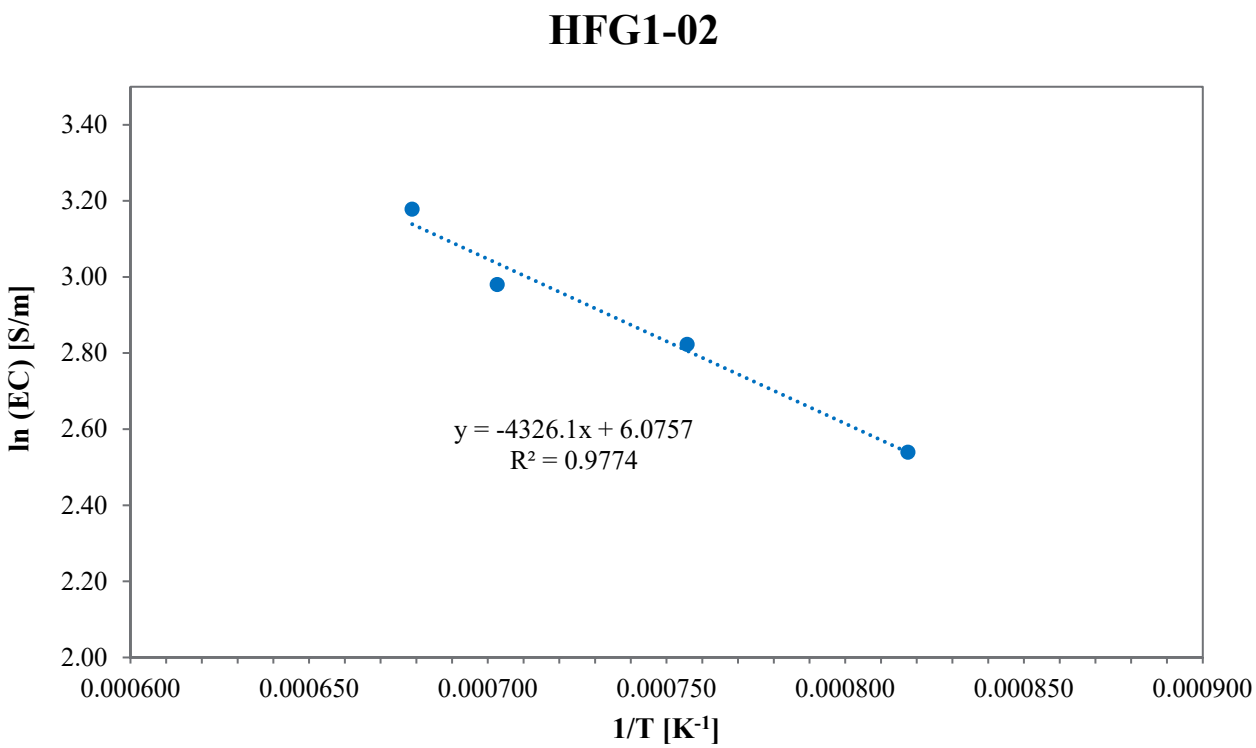

Figure G.2. Electrical Conductivity-Temperature Data and Arrhenius Equation Fit for Glass HFG1-02

G.3 Glass HFG1-03 Electrical Conductivity Data

Table G.3. Electrical Conductivity Data for Glass HFG1-03

Temperature, °C	Conductivity, S/m	1/T, K^{-1}	ln ε, S/m
941	30.49	0.000824	3.4174
980	33.08	0.000798	3.4988
1189	81.06	0.000684	4.3951
1150	65.81	0.000703	4.1867
1127	63.04	0.000714	4.1438
1046	49.86	0.000758	3.9092
1016	45.00	0.000776	3.8066

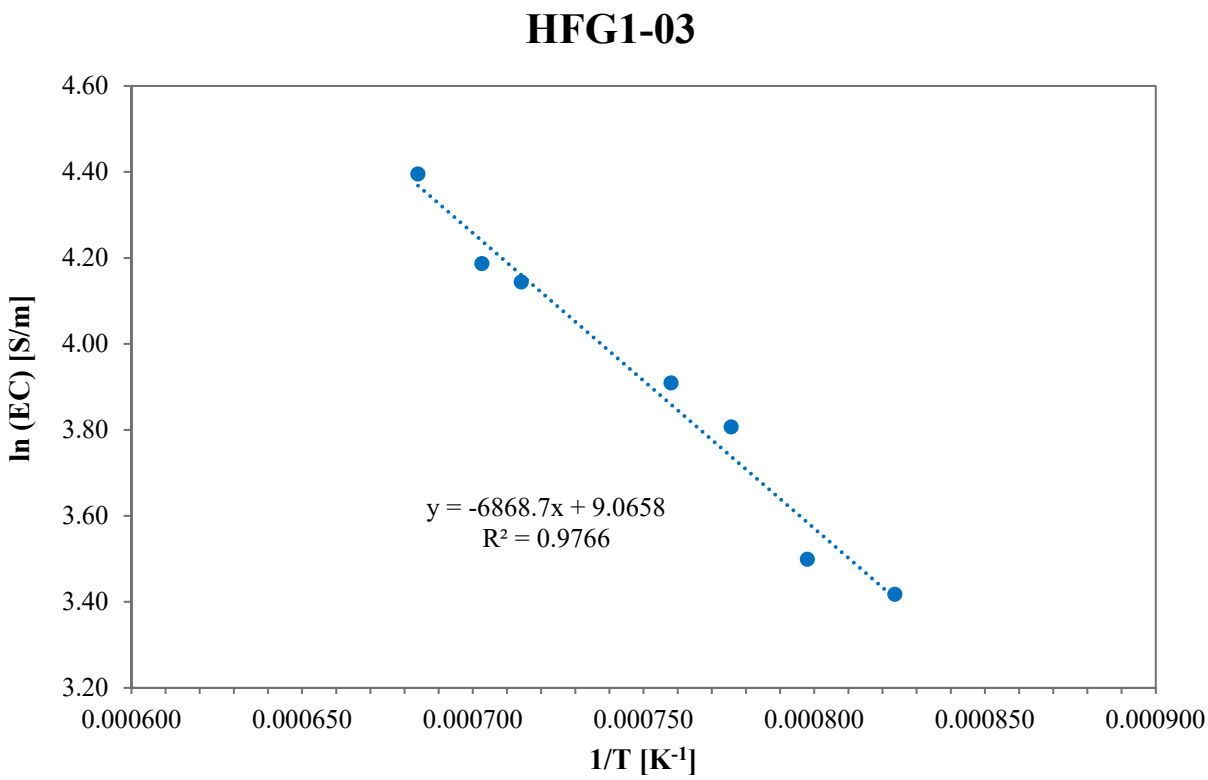

Figure G.3. Electrical Conductivity-Temperature Data and Arrhenius Equation Fit for Glass HFG1-03

G.4 Glass HFG1-04 Electrical Conductivity Data

Table G.4. Electrical Conductivity Data for Glass HFG1-04

Temperature, °C	Conductivity, S/m	1/T, K^{-1}	ln ε, S/m
950	67.64	0.000818	4.2142
1200	129.75	0.000679	4.8656
1150	118.37	0.000703	4.7738
1050	94.43	0.000756	4.5479

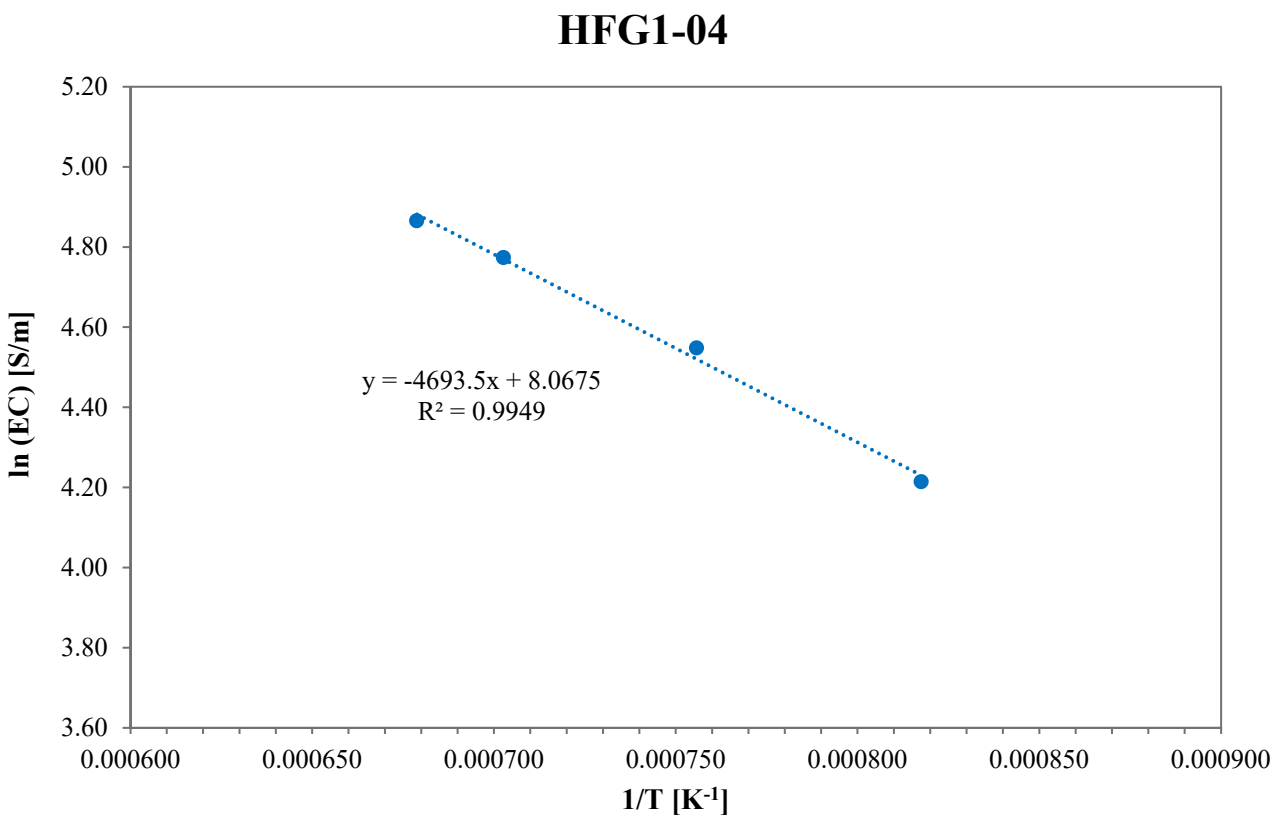

Figure G.4. Electrical Conductivity-Temperature Data and Arrhenius Equation Fit for Glass HFG1-04

G.5 Glass HFG1-06 Electrical Conductivity Data

Table G.5. Electrical Conductivity Data for Glass HFG1-06

Temperature, °C	Conductivity, S/m	1/T, K^{-1}	ln ε, S/m
950	11.68	0.000818	2.4575
1200	63.46	0.000679	4.1504
1150	57.39	0.000703	4.0498
1050	32.77	0.000756	3.4894

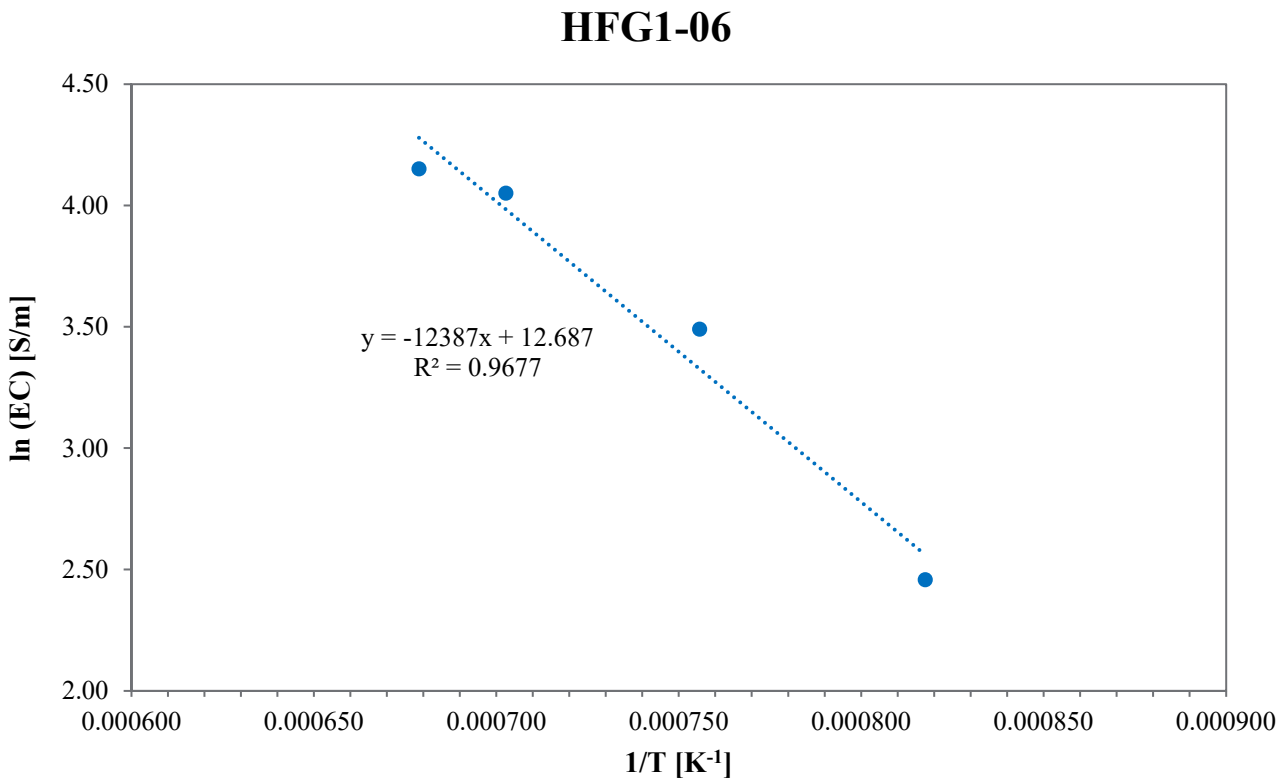

Figure G.5. Electrical Conductivity-Temperature Data and Arrhenius Equation Fit for Glass HFG1-06

G.6 Glass HFG1-07 Electrical Conductivity Data

Table G.6. Electrical Conductivity Data for Glass HFG1-07

Temperature, °C	Conductivity, S/m	1/T, K^{-1}	ln ε, S/m
950	17.32	0.000818	2.8518
1200	44.23	0.000679	3.7894
1150	34.28	0.000703	3.5346
1050	27.91	0.000756	3.3289

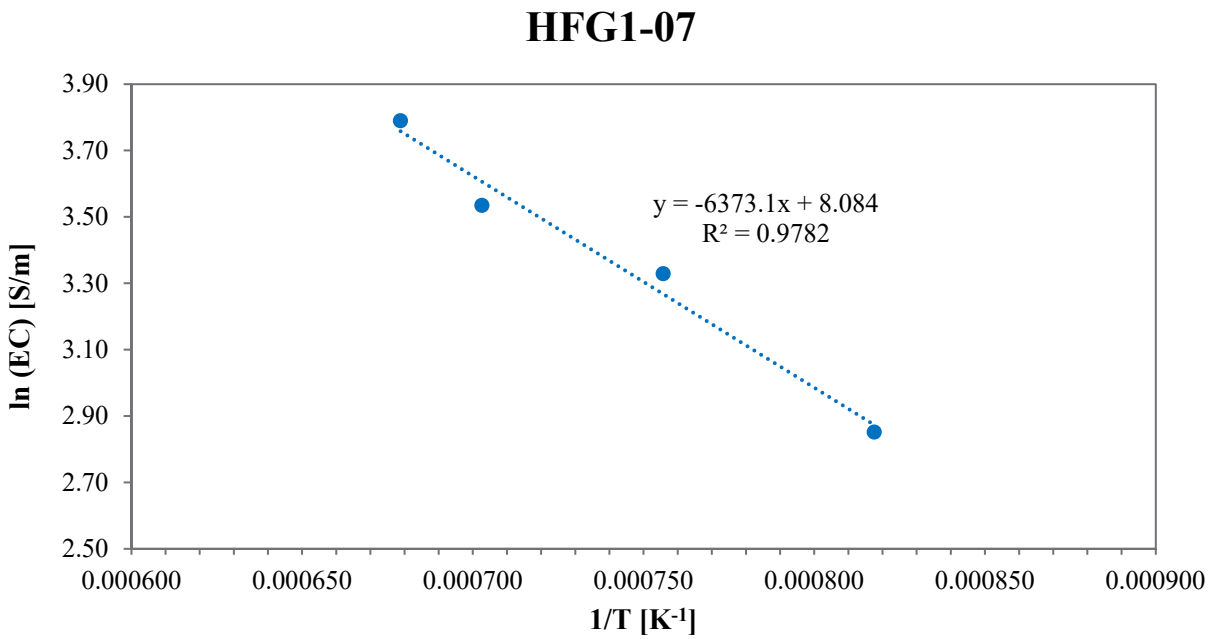

Figure G.6. Electrical Conductivity-Temperature Data and Arrhenius Equation Fit for Glass HFG1-07

G.7 Glass HFG1-09 Electrical Conductivity Data

Table G.7. Electrical Conductivity Data for Glass HFG1-09

Temperature, °C	Conductivity, S/m	1/T, K^{-1}	ln ε, S/m
950	45.26	0.000818	3.8125
1200	77.47	0.000679	4.3498
1150	92.06	0.000703	4.5225
1050	75.21	0.000756	4.3203

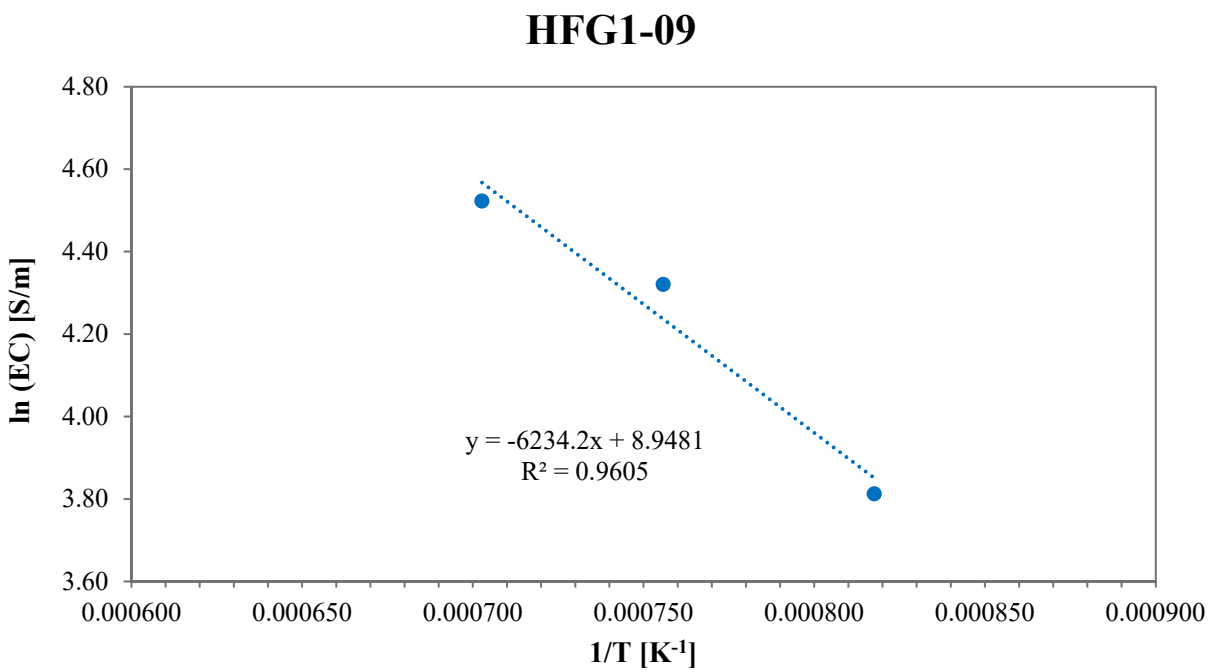

Figure G.7. Electrical Conductivity-Temperature Data and Arrhenius Equation Fit for Glass HFG1-09

G.8 Glass HFG1-10 Electrical Conductivity Data

Table G.8. Electrical Conductivity Data for Glass HFG1-10

Temperature, °C	Conductivity, S/m	1/T, K^{-1}	ln ε, S/m
950	30.84	0.000818	3.4287
1200	57.70	0.000679	4.0552
1150	53.68	0.000703	3.9830
1050	47.85	0.000756	3.8681

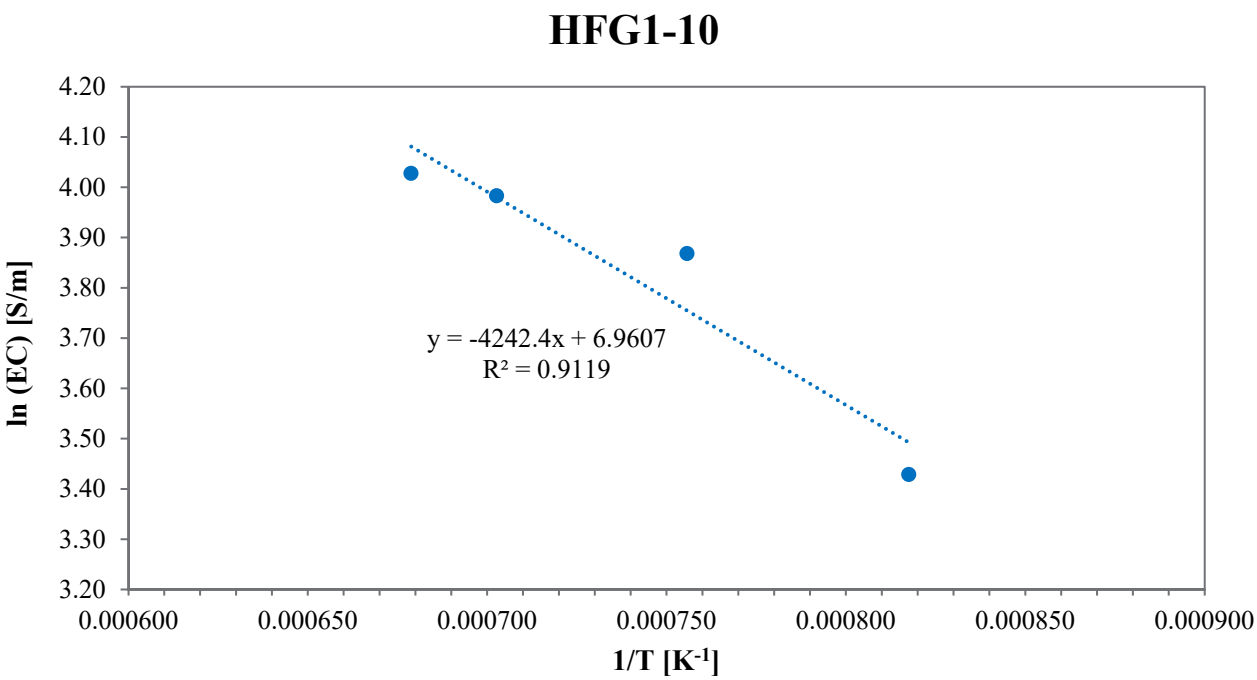

Figure G.8. Electrical Conductivity-Temperature Data and Arrhenius Equation Fit for Glass HFG1-10

G.9 Glass HFG1-11 Electrical Conductivity Data

Table G.9. Electrical Conductivity Data for Glass HFG1-11

Temperature, °C	Conductivity, S/m	1/T, K^{-1}	ln ε, S/m
950	35.26	0.000818	3.5627
1200	96.35	0.000679	4.5680
1150	86.44	0.000703	4.4595
1050	69.74	0.000756	4.2448

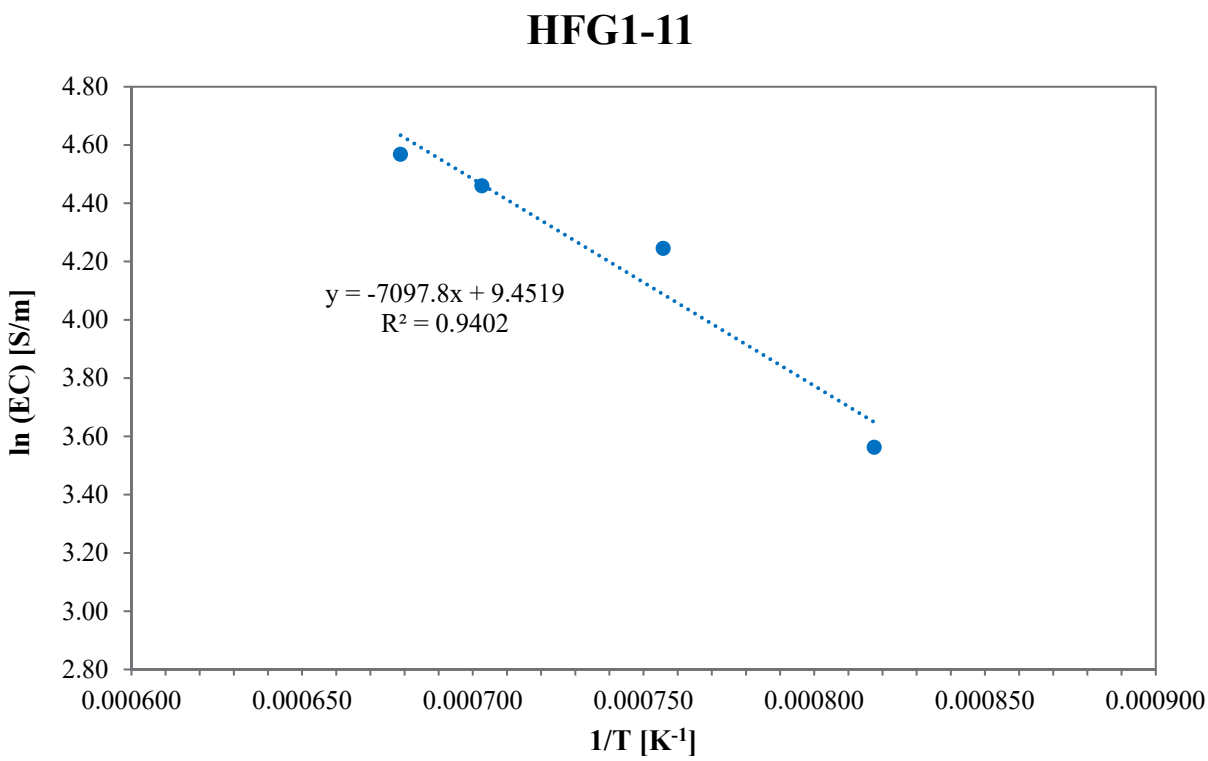

Figure G.9. Electrical Conductivity-Temperature Data and Arrhenius Equation Fit for Glass HFG1-11

G.10 Glass HFG1-12 Electrical Conductivity Data

Table G.10. Electrical Conductivity Data for Glass HFG1-12

Temperature, °C	Conductivity, S/m	1/T, K^{-1}	ln ε, S/m
950	16.41	0.000818	2.7979
1200	22.05	0.000679	3.0934
1150	27.20	0.000703	3.3031
1050	25.62	0.000756	3.2435

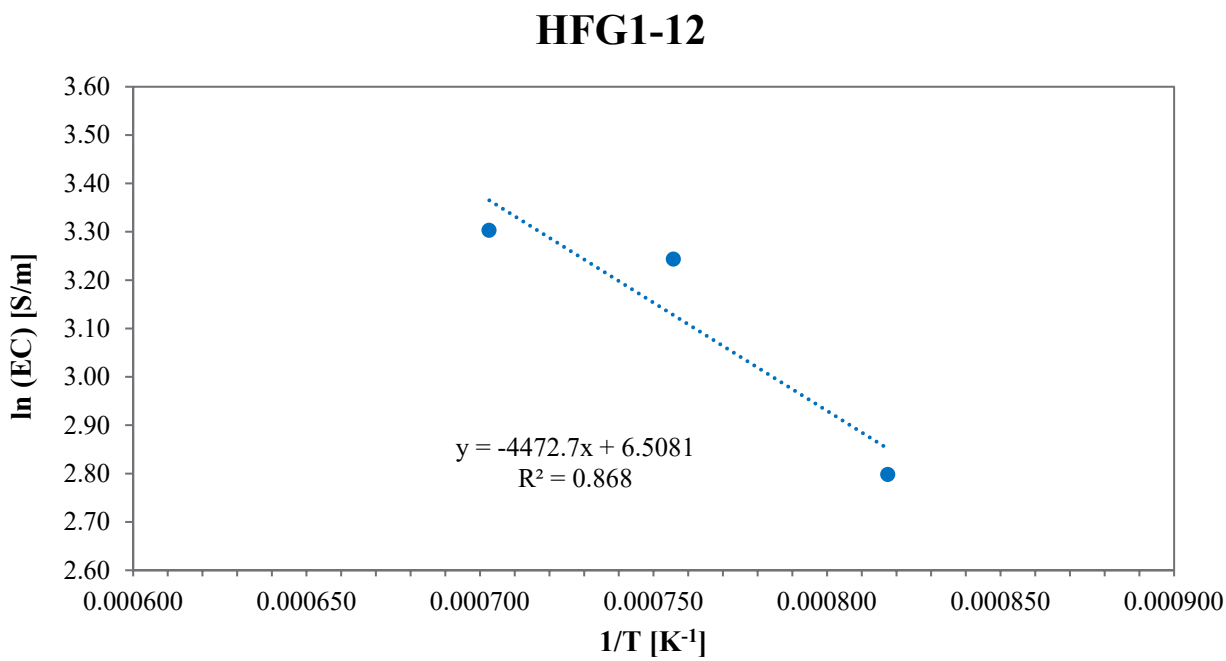

Figure G.10. Electrical Conductivity-Temperature Data and Arrhenius Equation Fit for Glass HFG1-12

G.11 Glass HFG1-13 Electrical Conductivity Data

Table G.11. Electrical Conductivity Data for Glass HFG1-13

Temperature, °C	Conductivity, S/m	1/T, K^{-1}	ln ε, S/m
950	30.23	0.000818	3.4087
1200	93.27	0.000679	4.5355
1150	81.34	0.000703	4.3986
1050	46.21	0.000756	3.8332

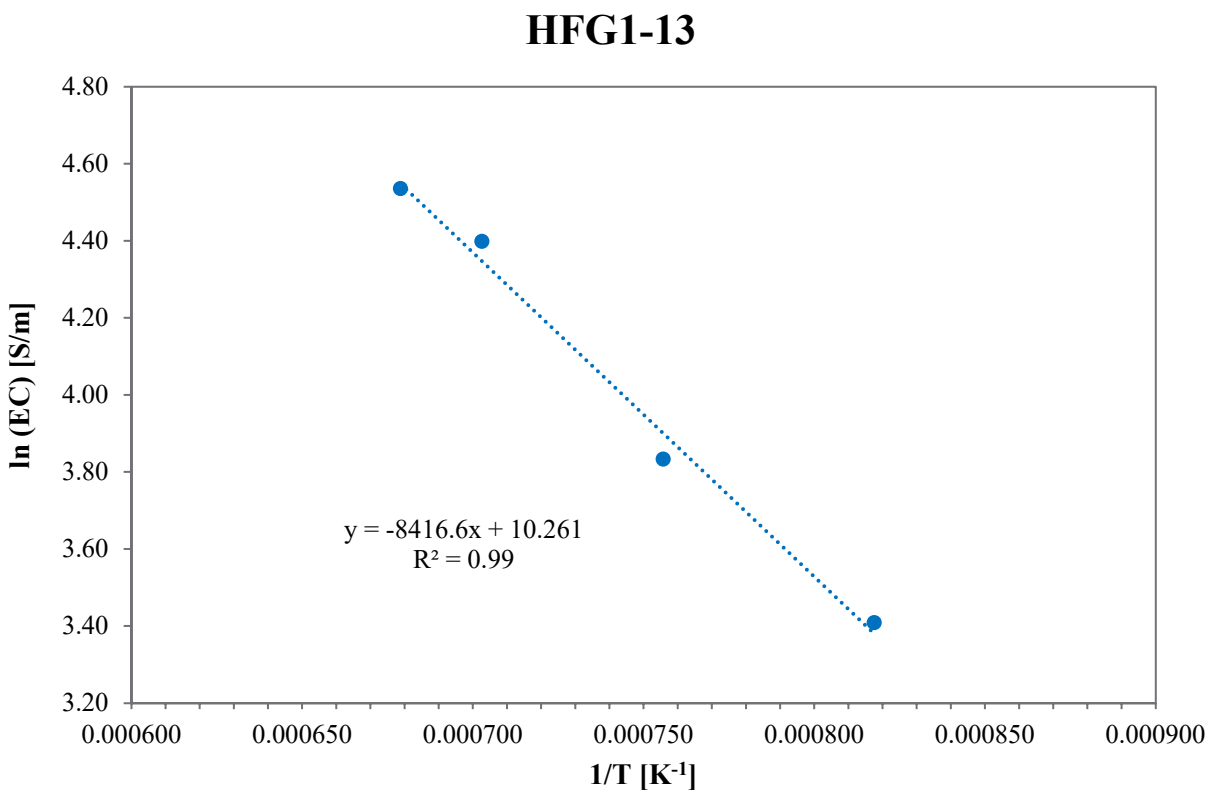

Figure G.11. Electrical Conductivity-Temperature Data and Arrhenius Equation Fit for Glass HFG1-13

G.12 Glass HFG1-14 Electrical Conductivity Data

Table G.12. Electrical Conductivity Data for Glass HFG1-14

Temperature, °C	Conductivity, S/m	1/T, K^{-1}	ln ε, S/m
950	20.34	0.000818	3.0125
1200	28.04	0.000679	3.3337
1150	27.77	0.000703	3.3240
1050	23.36	0.000756	3.1509

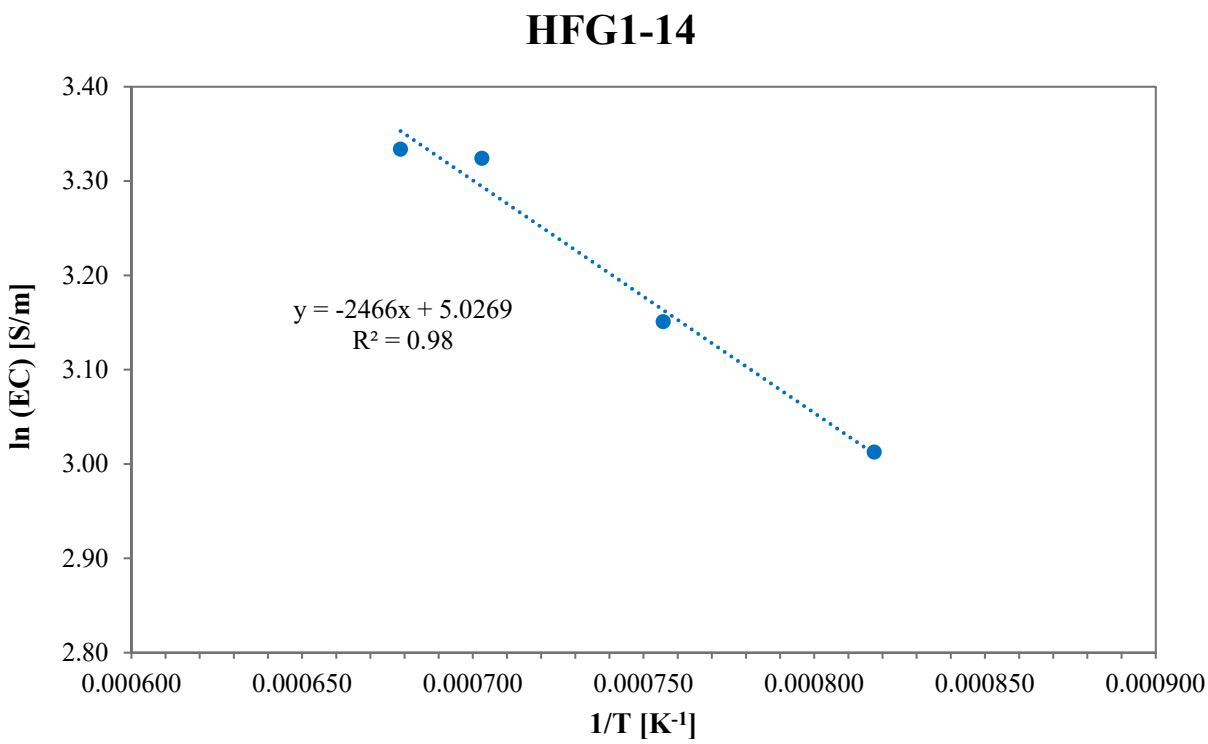

Figure G.12. Electrical Conductivity-Temperature Data and Arrhenius Equation Fit for Glass HFG1-14

G.13 Glass HFG1-15 Electrical Conductivity Data

Table G.13. Electrical Conductivity Data for Glass HFG1-15

Temperature, °C	Conductivity, S/m	1/T, K^{-1}	ln ε, S/m
950	27.53	0.000818	3.3154
1200	38.47	0.000679	3.6499
1150	45.95	0.000703	3.8275
1050	38.65	0.000756	3.6546

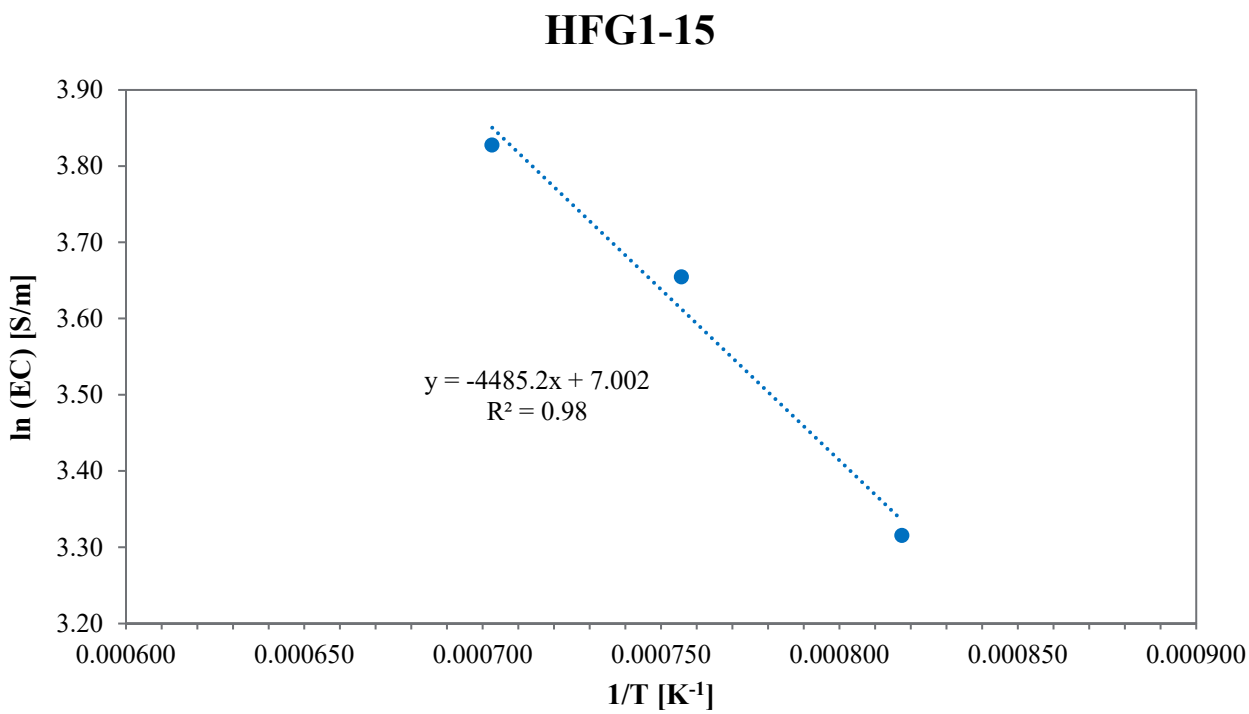

Figure G.13. Electrical Conductivity-Temperature Data and Arrhenius Equation Fit for Glass HFG1-15

G.14 Glass HFG1-17 Electrical Conductivity Data

Table G.14. Electrical Conductivity Data for Glass HFG1-17

Temperature, °C	Conductivity, S/m	1/T, K^{-1}	ln ε, S/m
950	21.16	0.000818	3.0522
1200	50.57	0.000679	3.9233
1150	45.49	0.000703	3.8176
1050	31.81	0.000756	3.4599

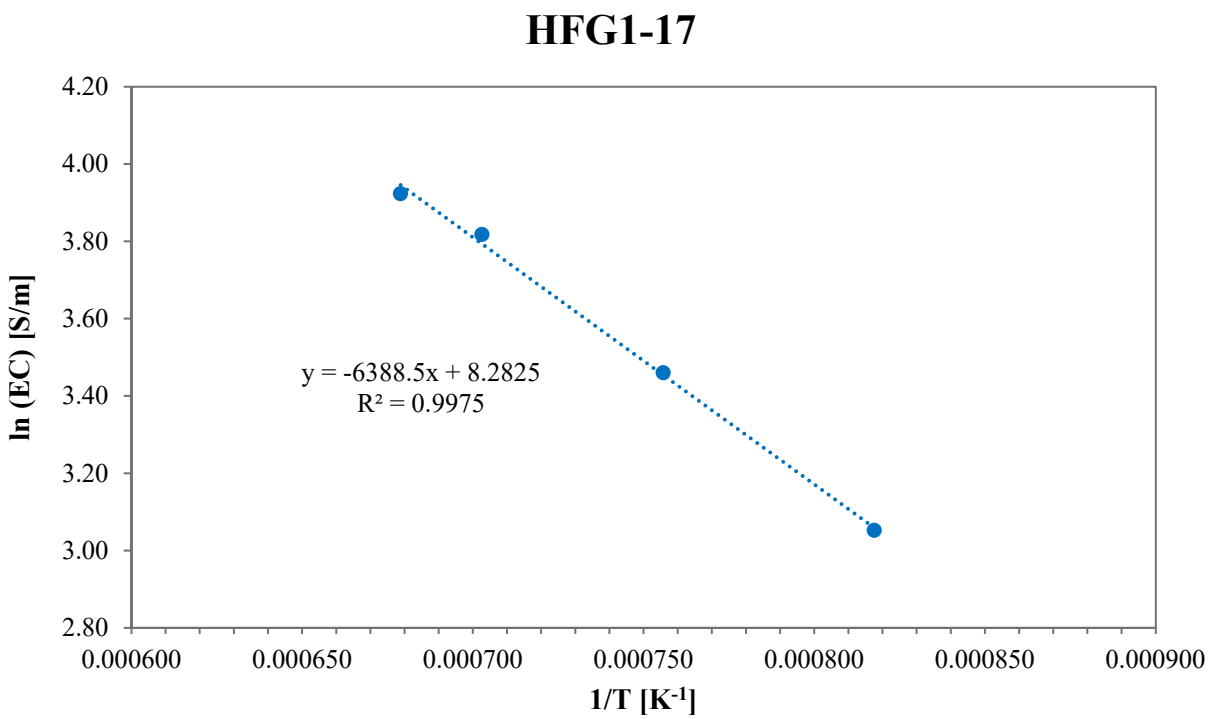

Figure G.14. Electrical Conductivity-Temperature Data and Arrhenius Equation Fit for Glass HFG1-17

G.15 Glass HFG1-18 Electrical Conductivity Data

Table G.15. Electrical Conductivity Data for Glass HFG1-18

Temperature, °C	Conductivity, S/m	1/T, K^{-1}	ln ε, S/m
950	23.11	0.000818	3.1404
1200	45.27	0.000679	3.8126
1150	43.24	0.000703	3.7668
1050	34.13	0.000756	3.5301

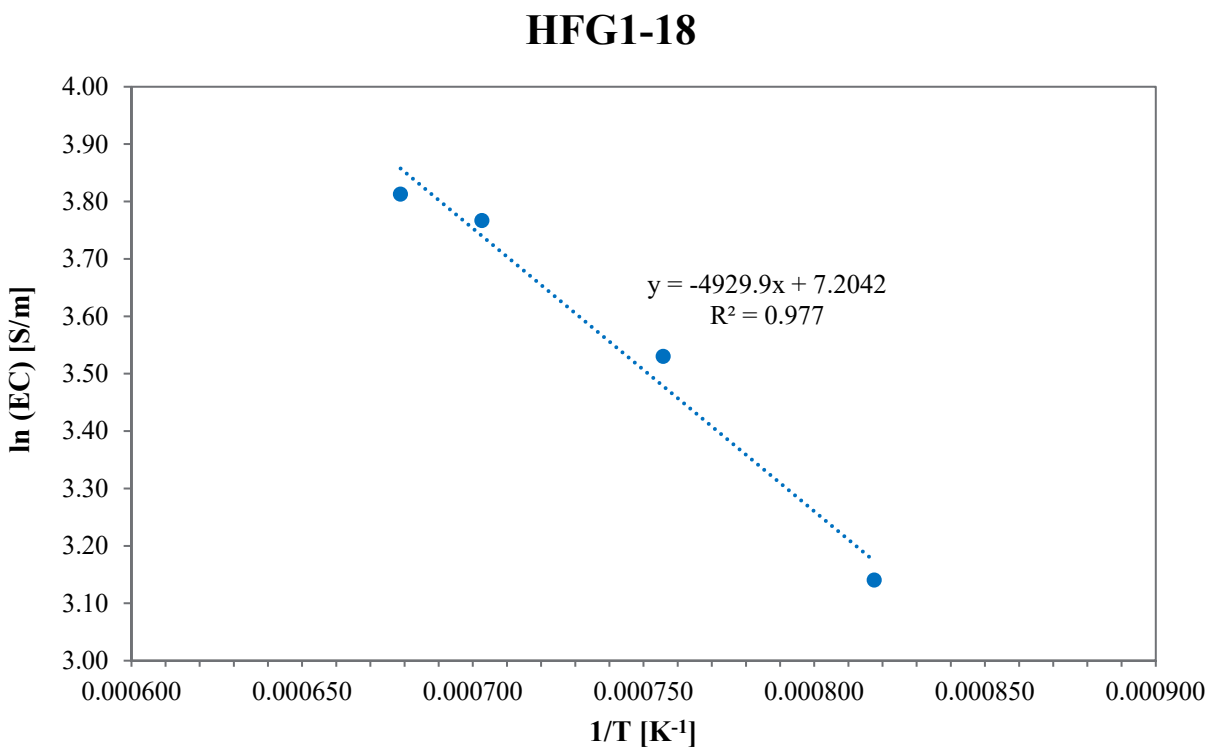

Figure G.15. Electrical Conductivity-Temperature Data and Arrhenius Equation Fit for Glass HFG1-18

G.16 Glass HFG1-19 Electrical Conductivity Data

Table G.16. Electrical Conductivity Data for Glass HFG1-19

Temperature, °C	Conductivity, S/m	1/T, K^{-1}	ln ε, S/m
950	27.72	0.000818	3.3221
1200	53.13	0.000679	3.9727
1150	52.94	0.000703	3.9691
1050	31.94	0.000756	3.4637

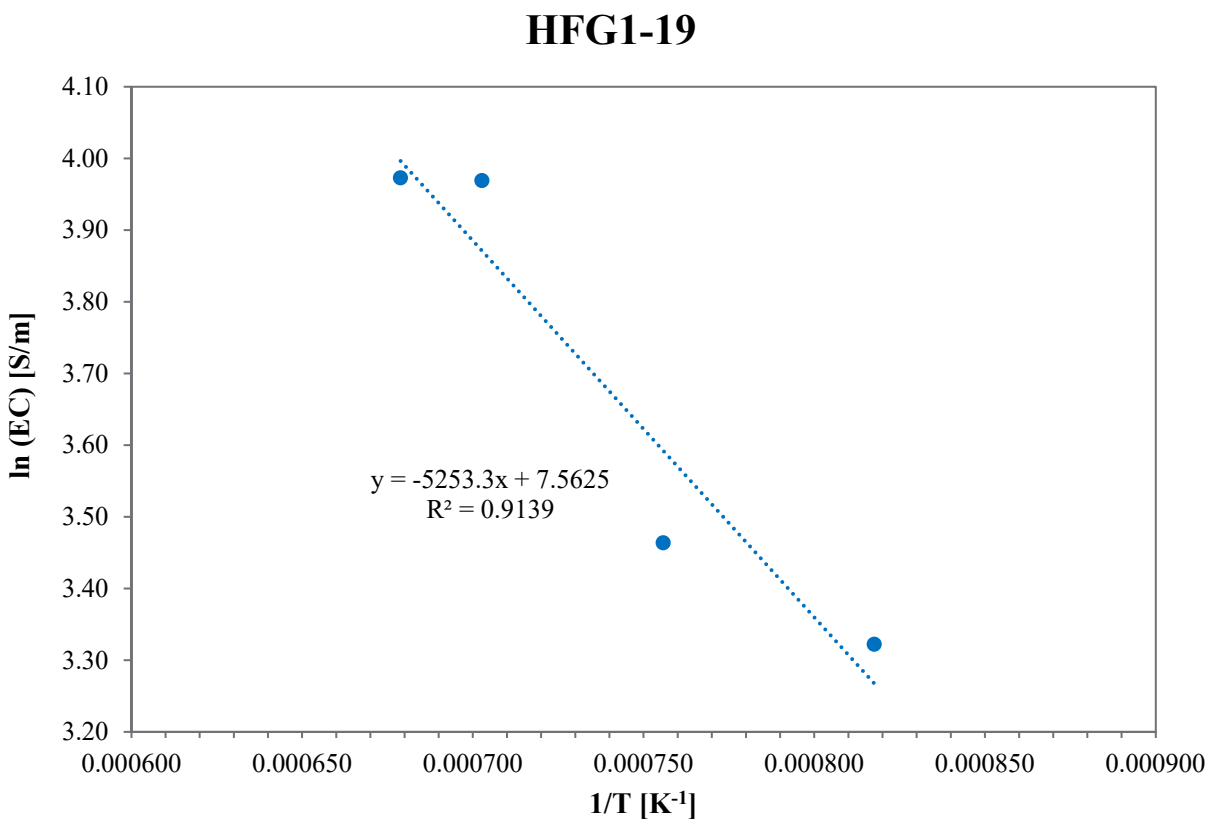

Figure G.16. Electrical Conductivity-Temperature Data and Arrhenius Equation Fit for Glass HFG1-19

Appendix H – Crystal Fraction of Heat-Treated Glasses Photographs

This appendix contains photos of glasses after they were heat-treated at 950 °C for 24 hours. Each showed different responses to the heat- treatment as indicated by these photos.

Figure H.1. Photograph of Glass HFG1-01-1 after CF Heat Treatment at 950 °C for 24 h

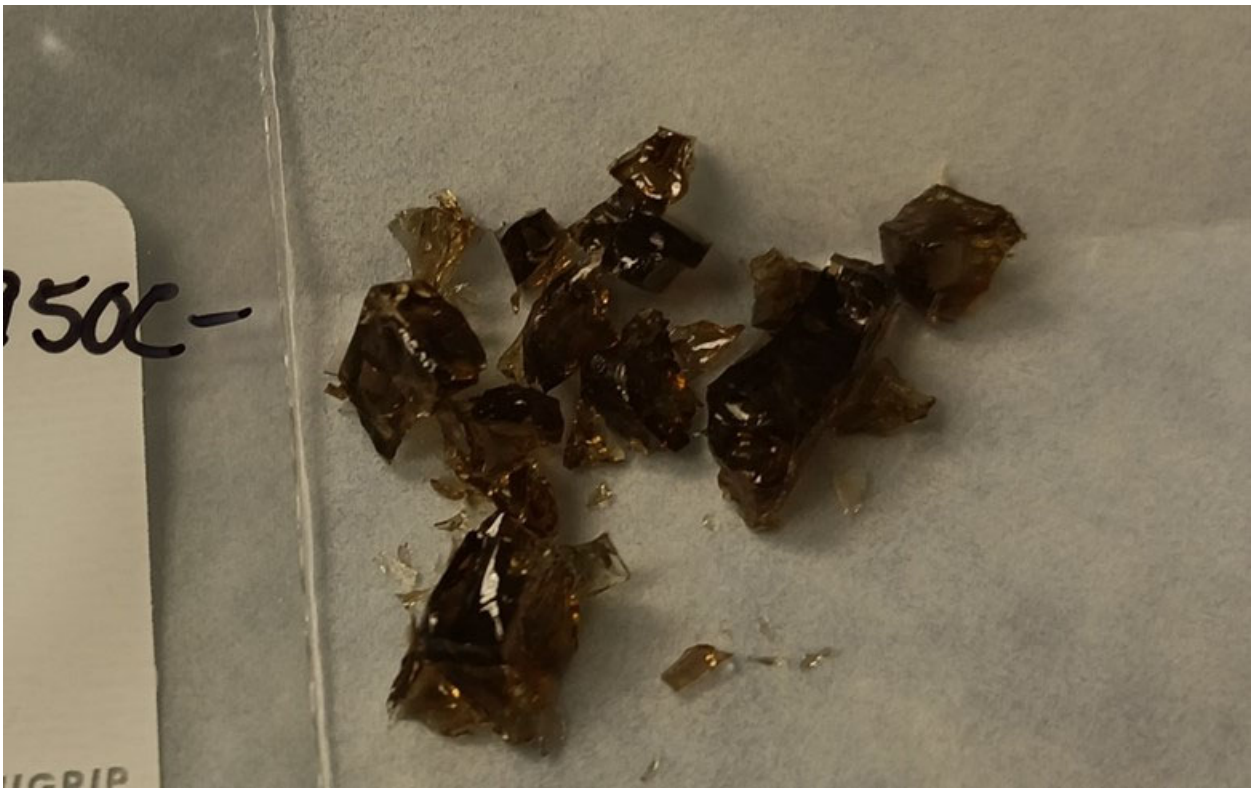

Figure H.2. Photograph of Glass HFG1-02 after CF Heat Treatment at 950 °C for 24 h

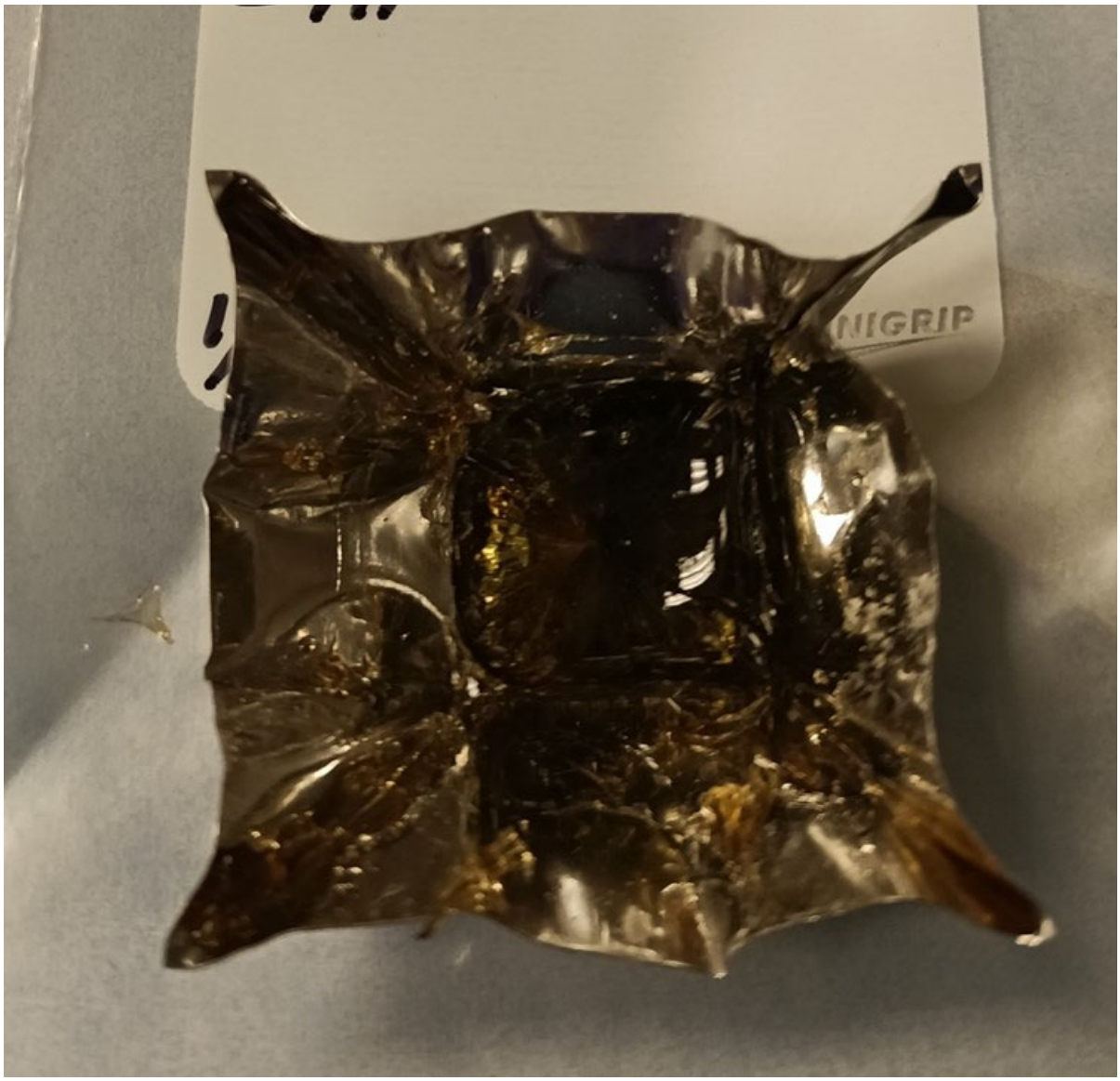

Figure H.3. Photograph of Glass HFG1-03 after CF Heat Treatment at 950 °C for 24 h

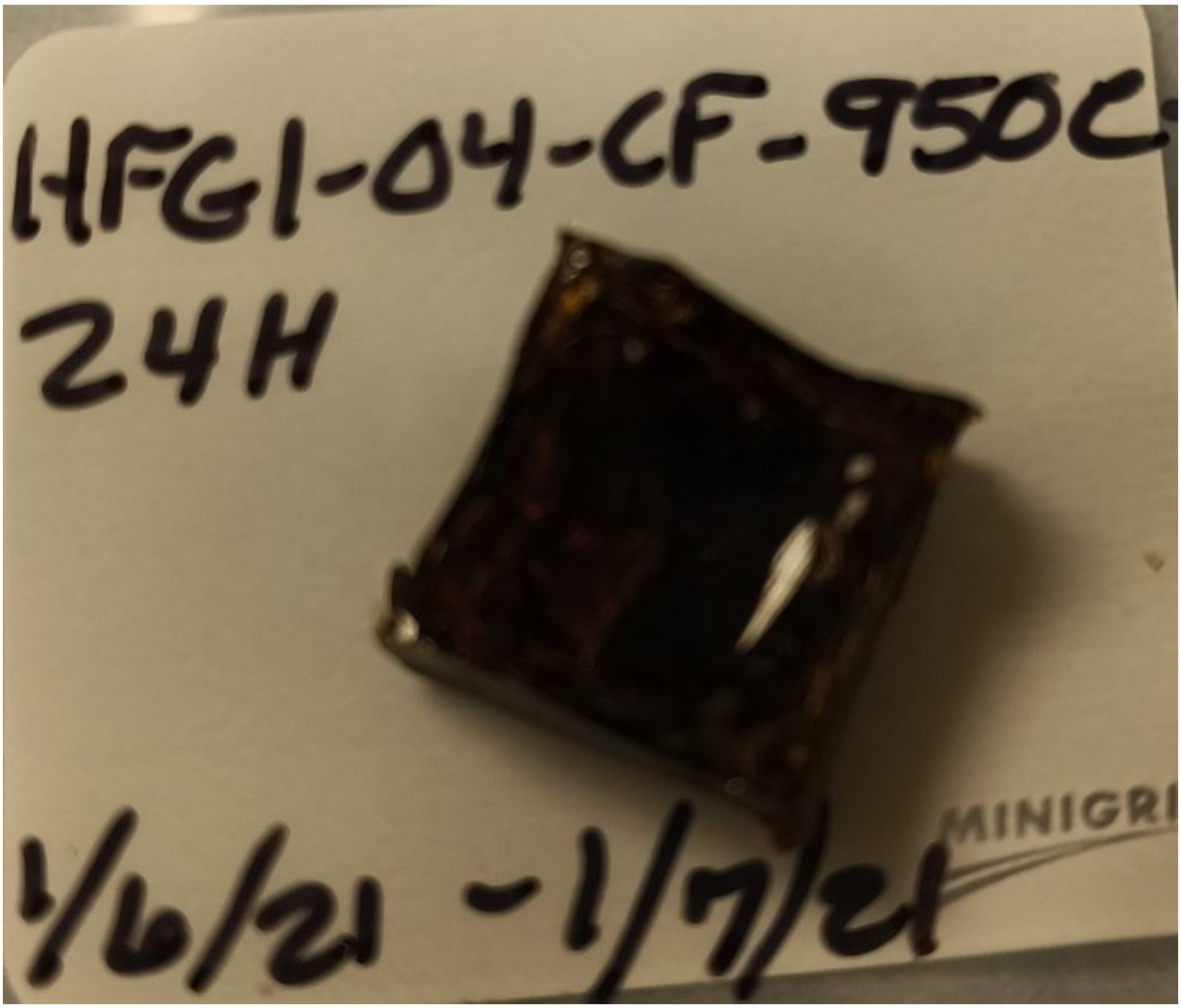

Figure H.4. Photograph of Glass HFG1-04 after CF Heat Treatment at 950 °C for 24 h

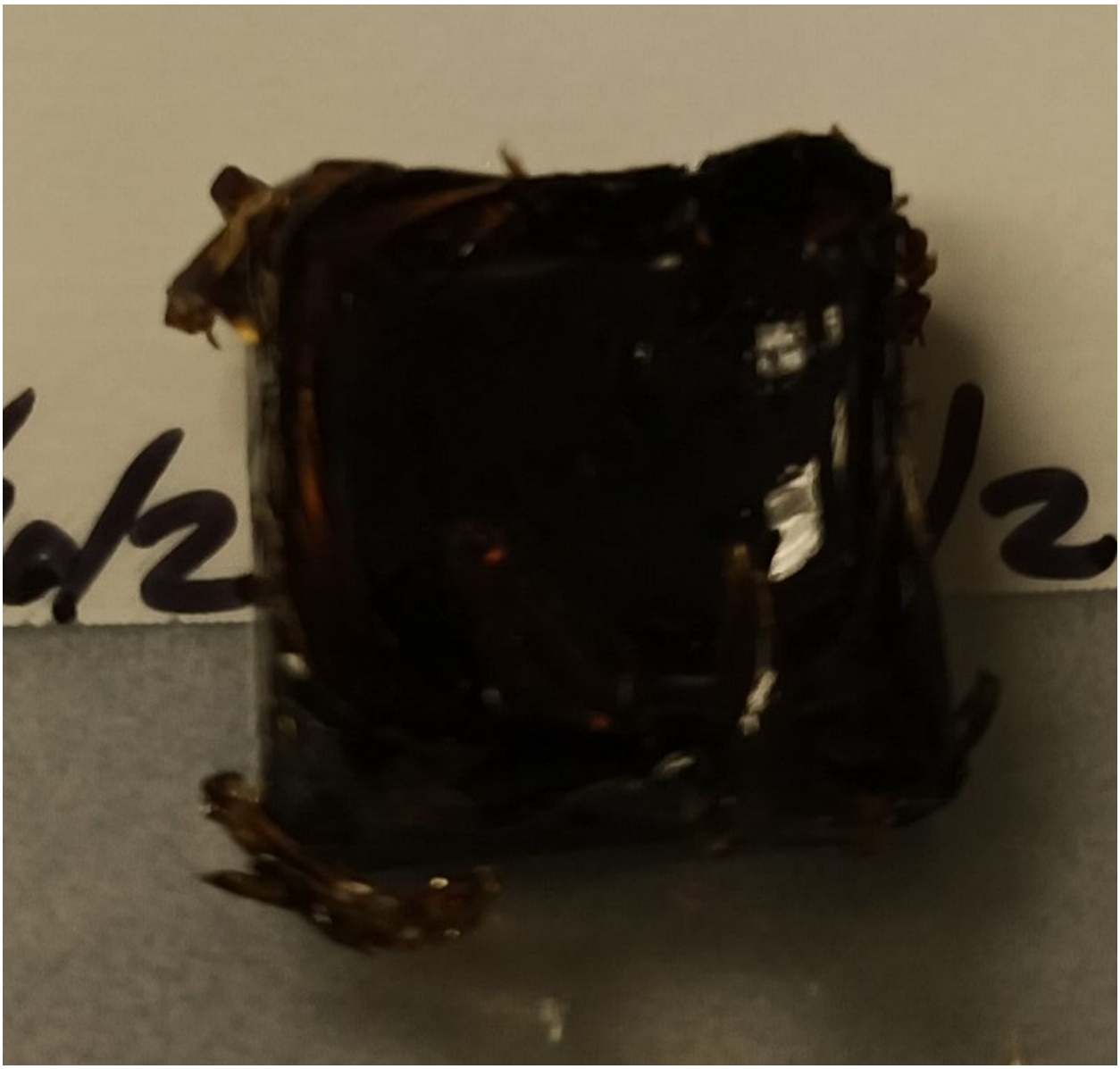

Figure H.5. Photograph of Glass HFG1-05 after CF Heat Treatment at 950 °C for 24 h

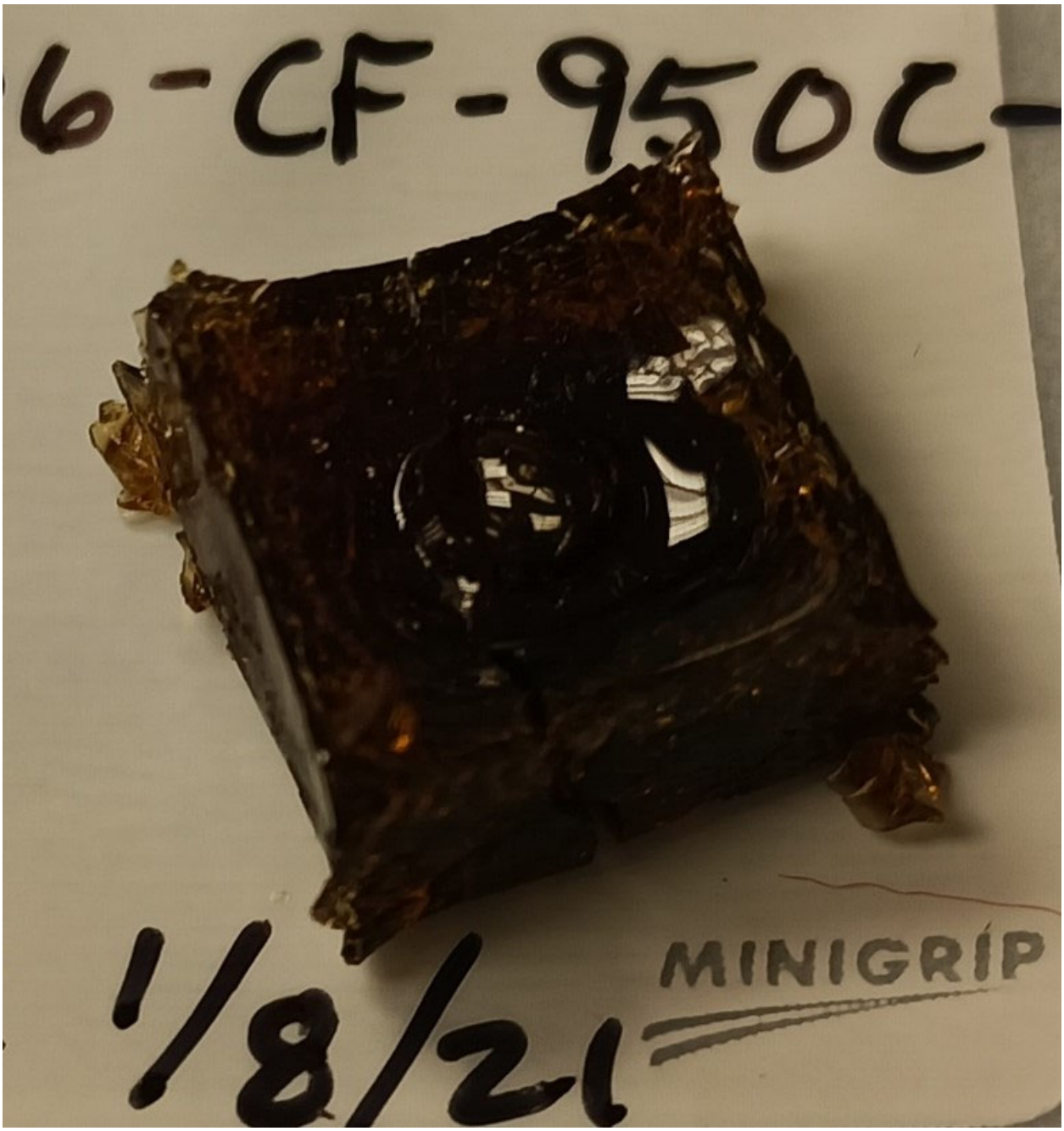

Figure H.6. Photograph of Glass HFG1-06 after CF Heat Treatment at 950 °C for 24 h

Figure H.7. Photograph of Glass HFG1-07 after CF Heat Treatment at 950°C for 24 h

Figure H.8. Photograph of Glass HFG1-08 after CF Heat Treatment at 950°C for 24 h

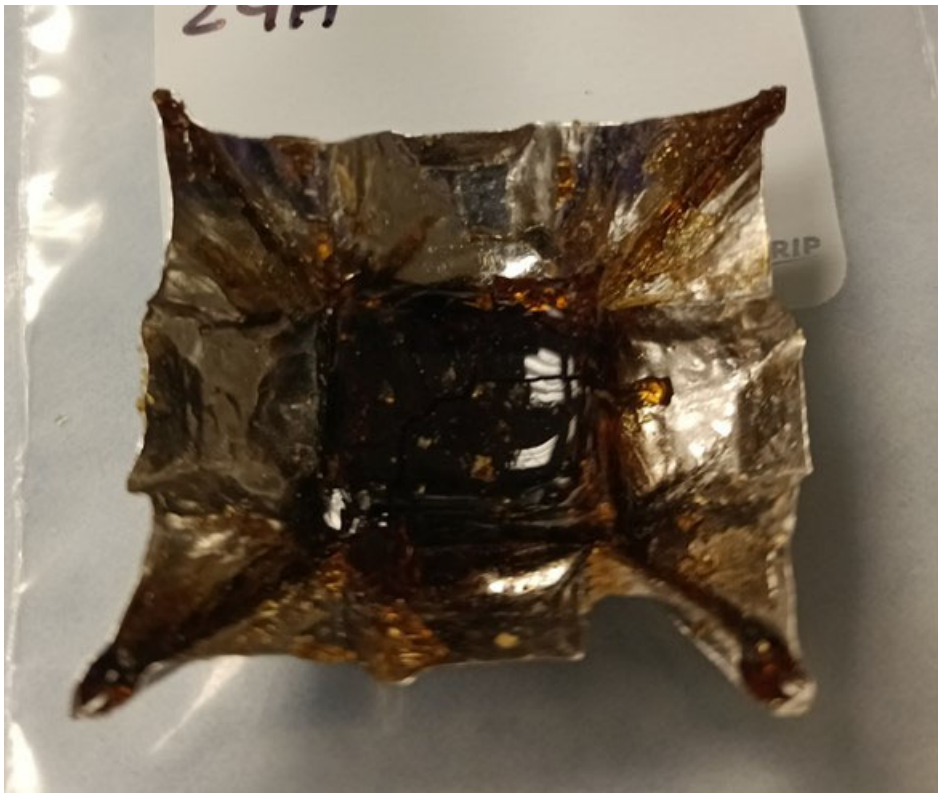

Figure H.9. Photograph of Glass HFG1-09 after CF Heat Treatment at 950 °C for 24 h

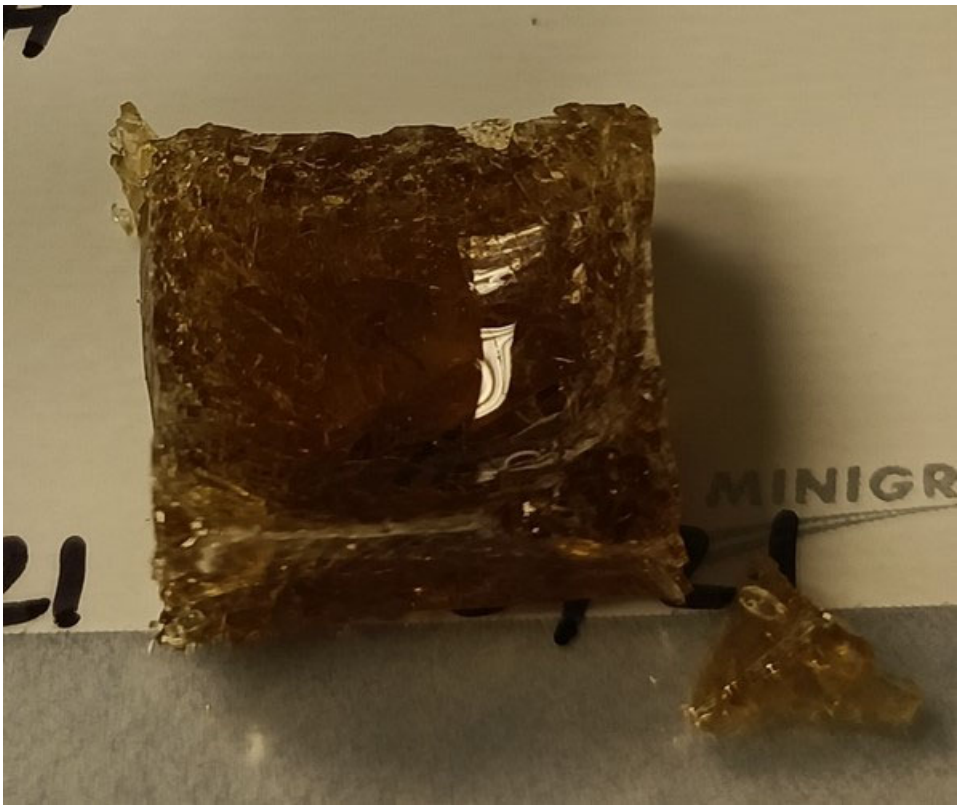

Figure H.10. Photograph of Glass HFG1-10 after CF Heat Treatment at 950 °C for 24 h

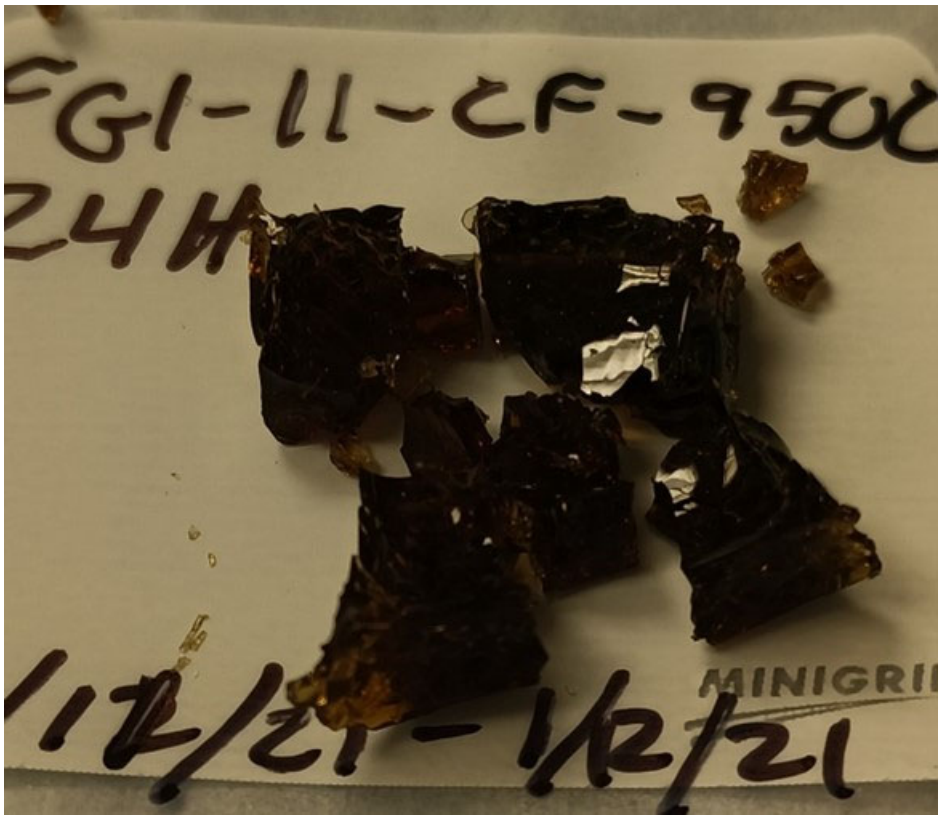

Figure H.11. Photograph of Glass HFG1-11 after CF Heat Treatment at 950 °C for 24 h

Figure H.12. Photograph of Glass HFG1-12 after CF Heat Treatment at 950 °C for 24 h

Figure H.13. Photograph of Glass HFG1-13 after CF Heat Treatment at 950 °C for 24 h

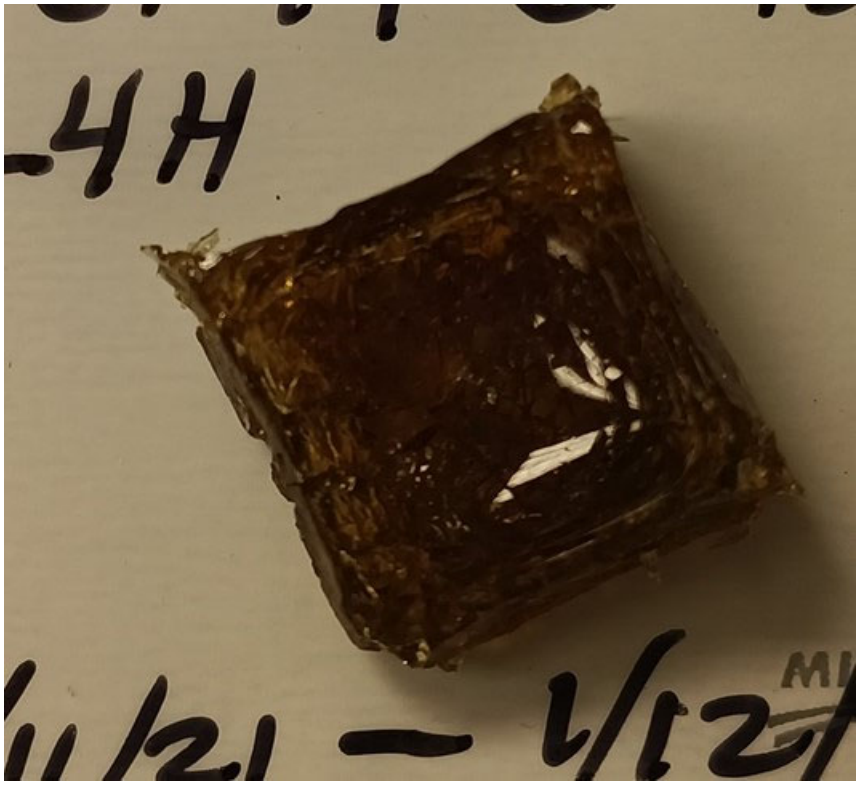

Figure H.14. Photograph of Glass HFG1-14 after CF Heat Treatment at 950 °C for 24 h

Figure H.15. Photograph of Glass HFG1-15 after CF Heat Treatment at 950 °C for 24 h

Figure H.16. Photograph of Glass HFG1-16 after CF Heat Treatment at 950°C for 24 h Magnified 30X

Figure H.17. Photograph of Glass HFG1-17 after CF Heat Treatment at 950°C for 24 h Magnified 20X

Figure H.18. Photograph of Glass HFG1-18 after CF Heat Treatment at 950 °C for 24 h

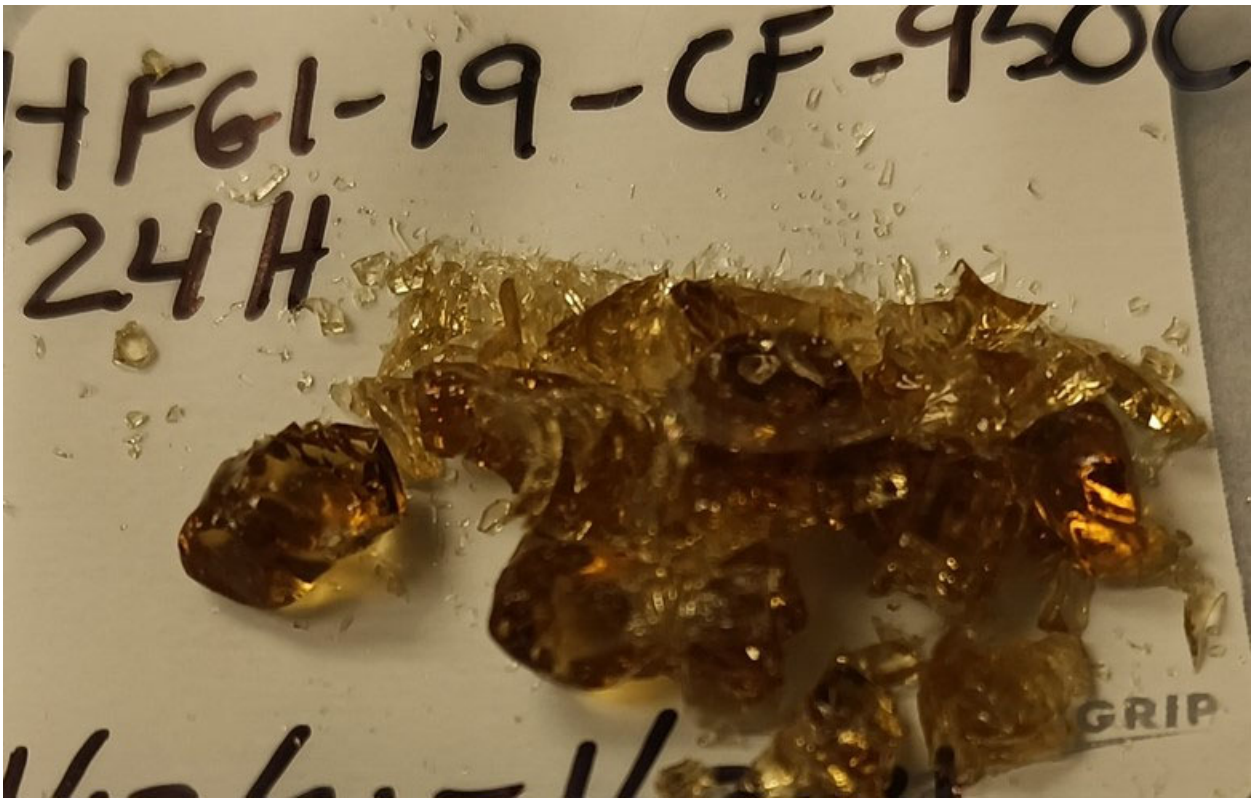

Figure H.19. Photograph of Glass HFG1-19 after CF Heat Treatment at 950 °C for 24 h

Figure H.20. Photograph of Glass HFG1-20 after CF Heat Treatment at 950 °C for 24 h

Appendix I – XRD of Crystal Fraction Heat-Treated Glasses

This appendix shows the XRD plots of several glasses after CF heat-treating at 950 °C. The majority of the glasses remained amorphous with only four glasses developing crystals. These crystals were mainly a Zr containing crystal or a silicate.

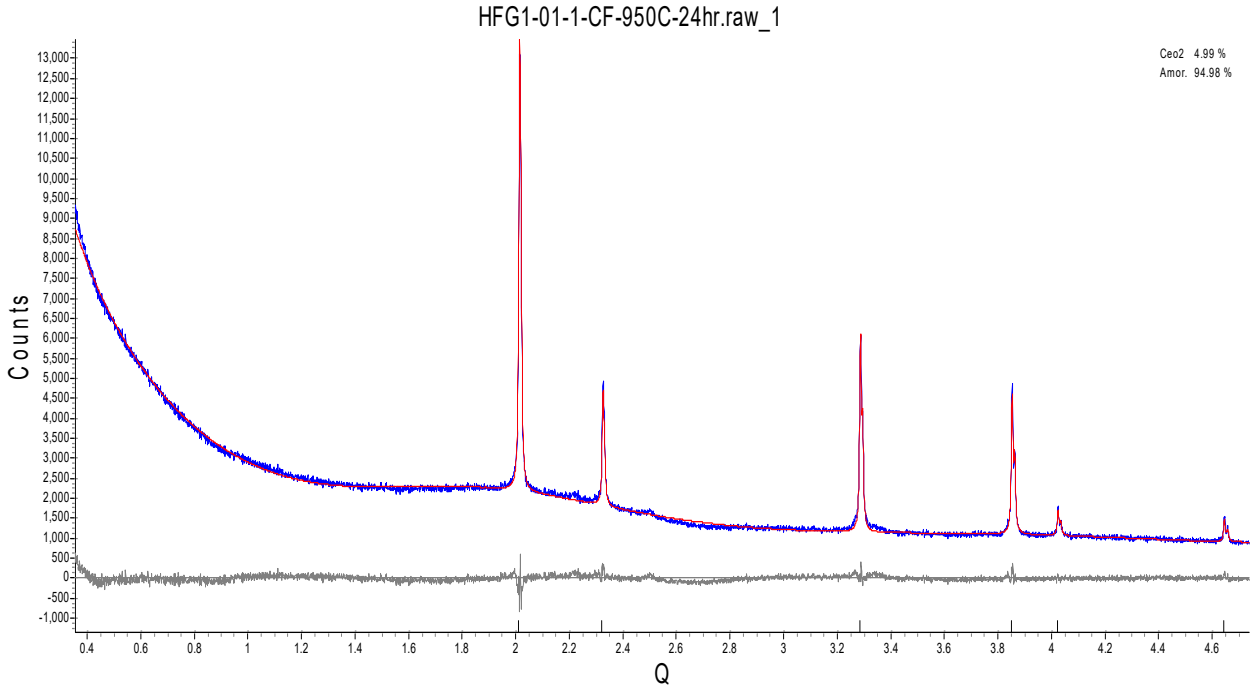

Figure I.1. XRD Spectrum of CF Heat-Treated Glass HFG1-01-1

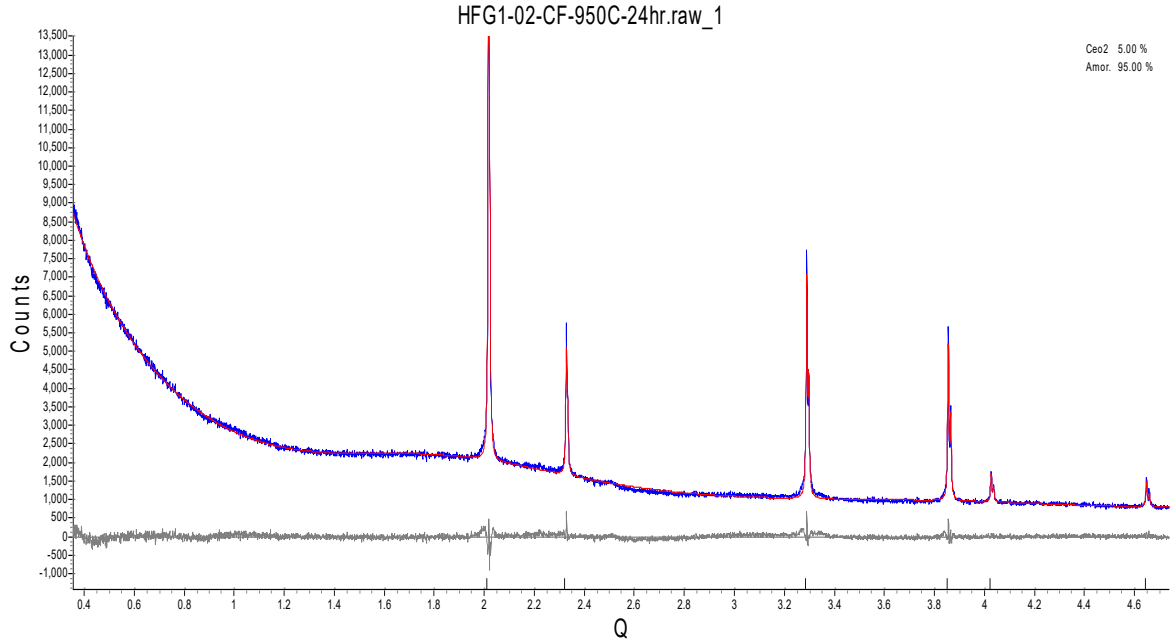

Figure I.2. XRD Spectrum of CF Heat-Treated Glass HFG1-02

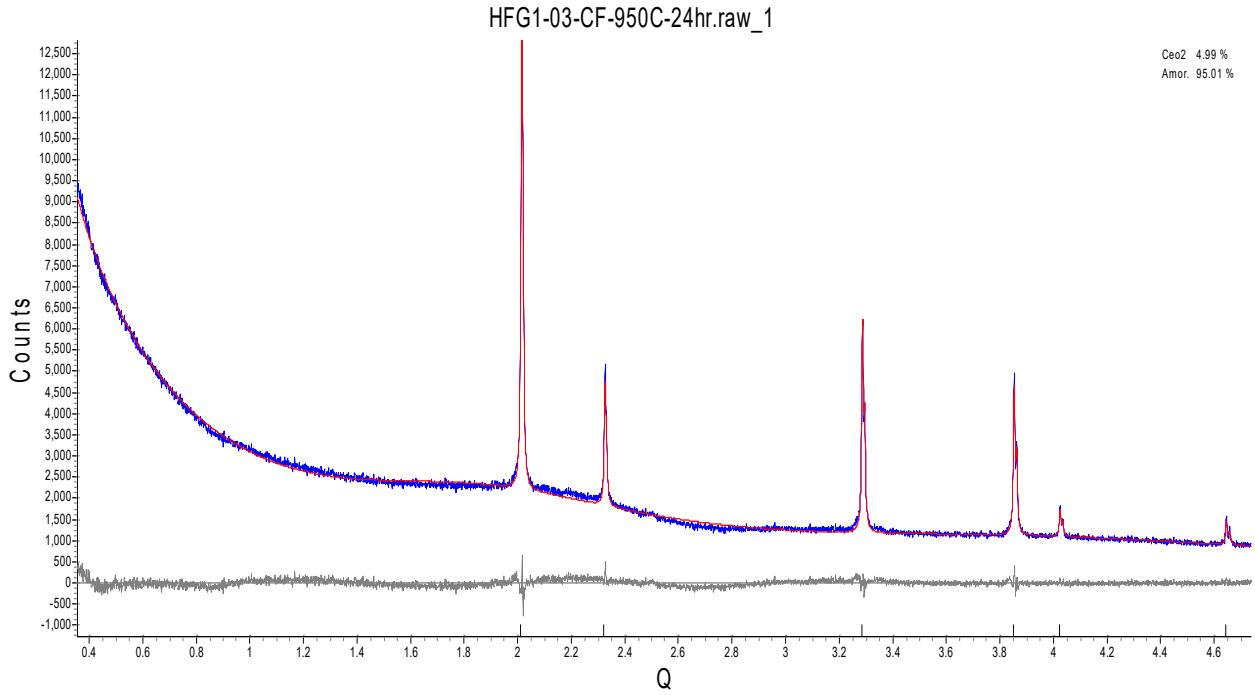

Figure I.3. XRD Spectrum of CF Heat-Treated Glass HFG1-03

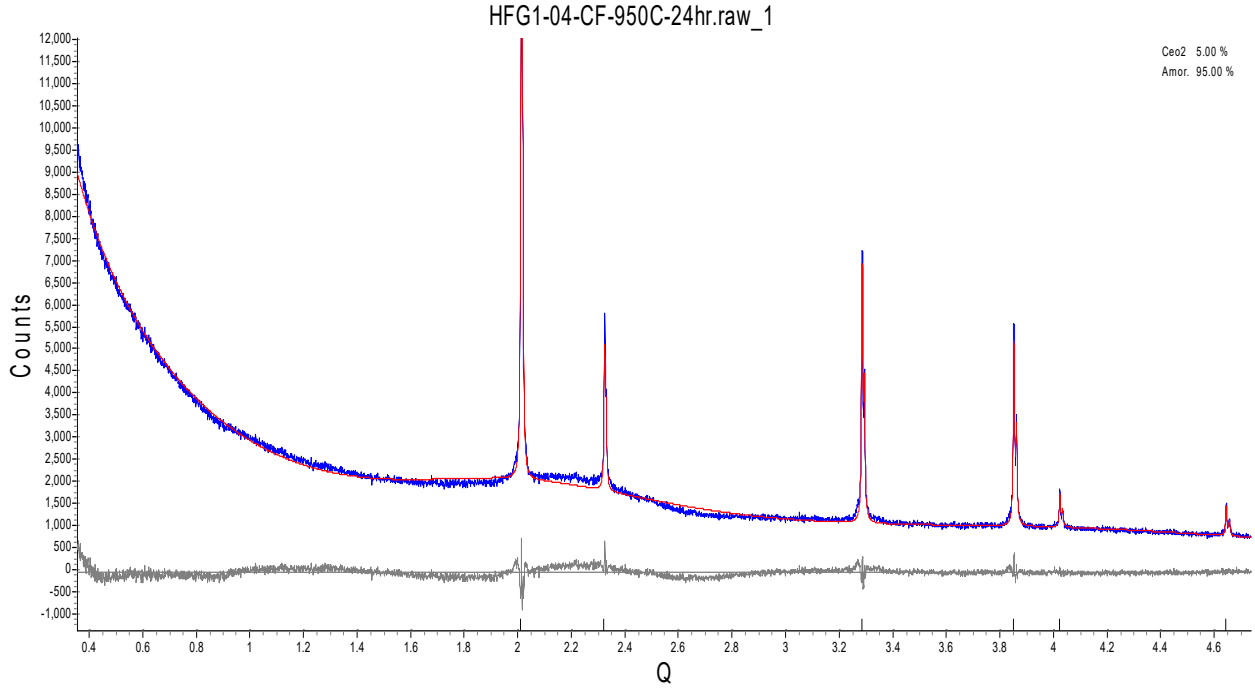

Figure I.4. XRD Spectrum of CF Heat-Treated Glass HFG1-04

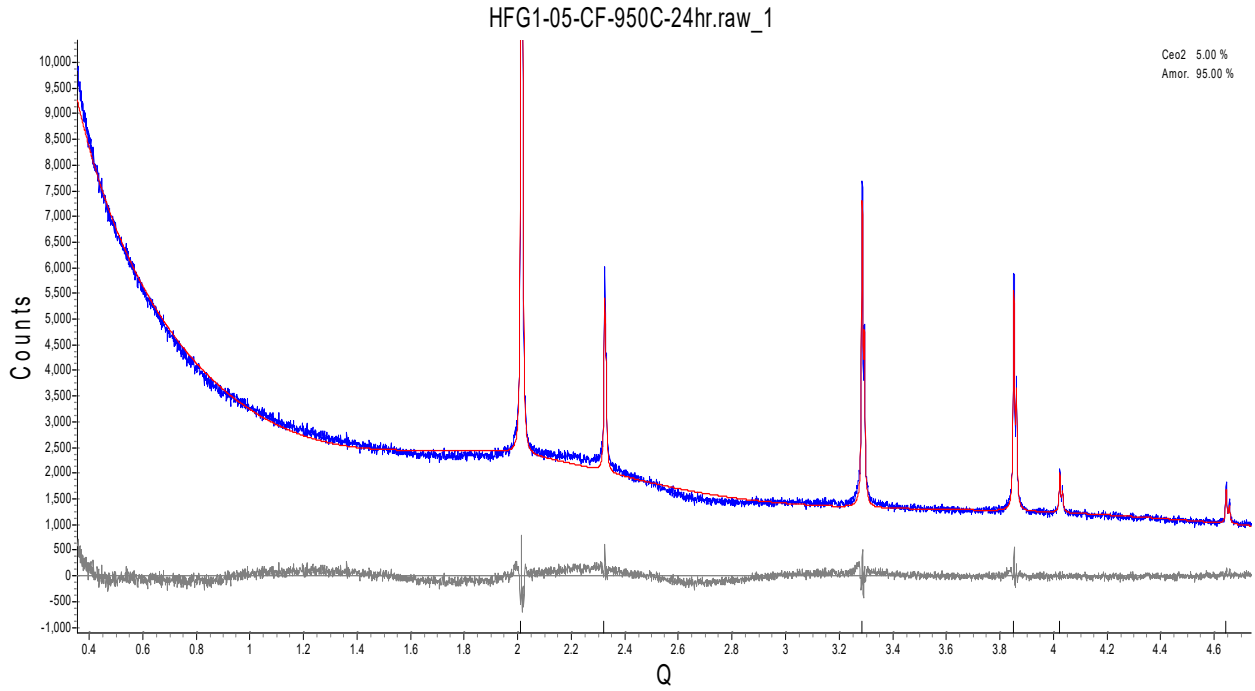

Figure I.5. XRD Spectrum of CF Heat-Treated Glass HFG1-05

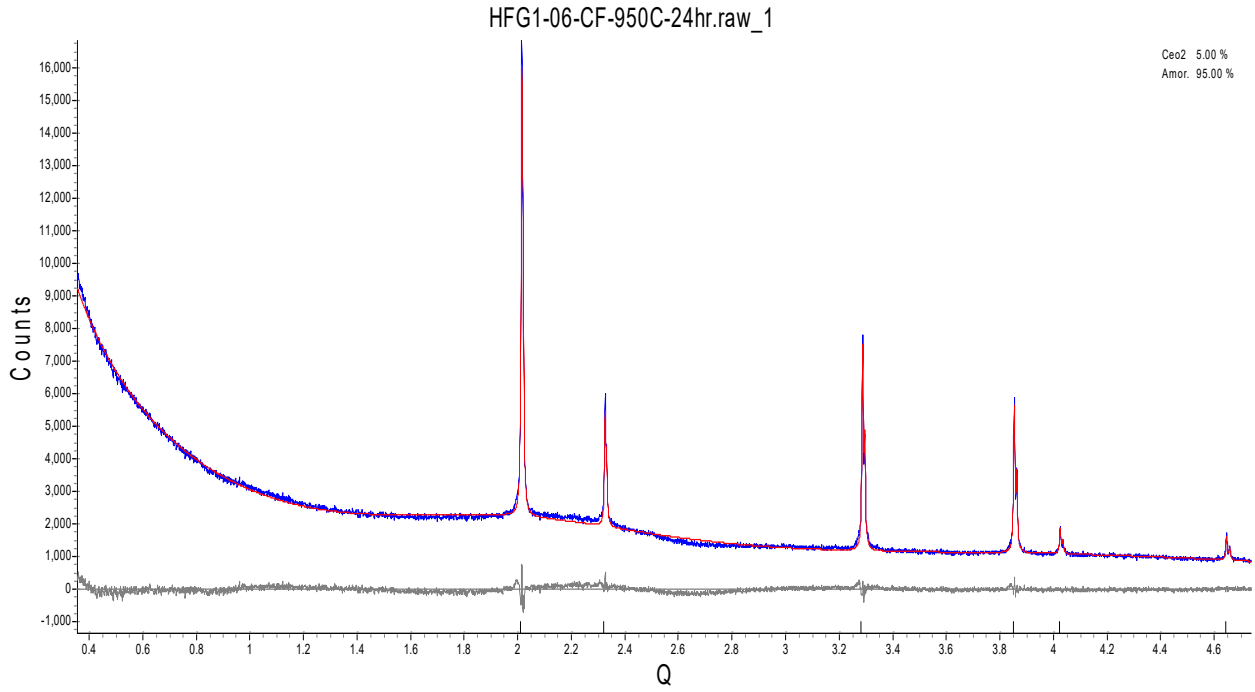

Figure I.6. XRD Spectrum of CF Heat-Treated Glass HFG1-06

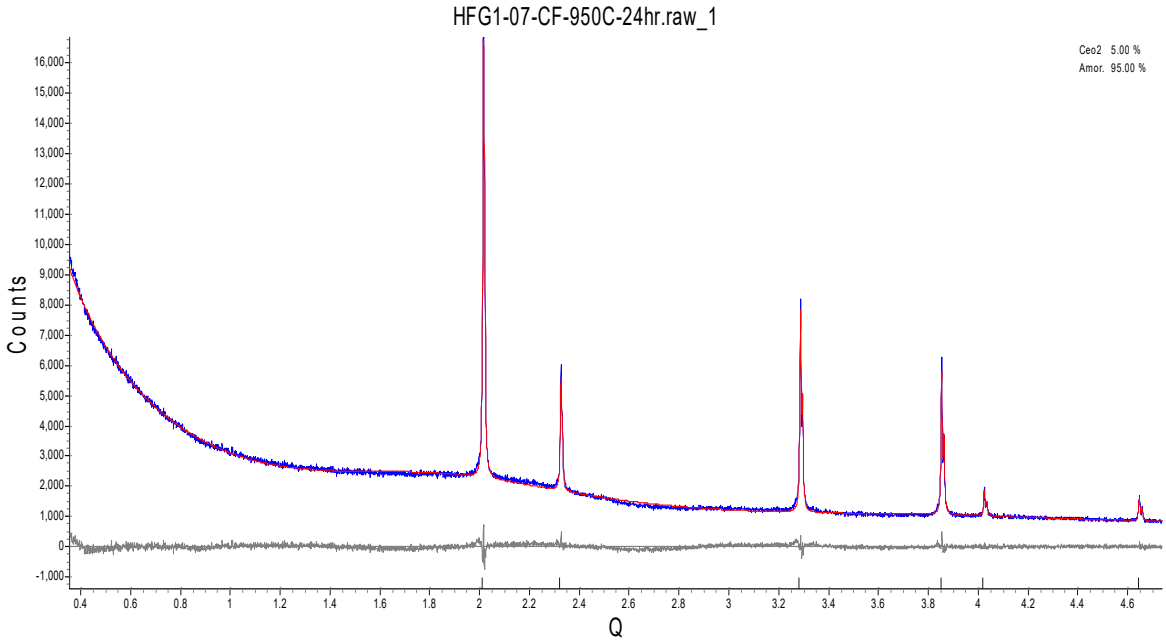

Figure I.7. XRD Spectrum of CF Heat-Treated Glass HFG1-07

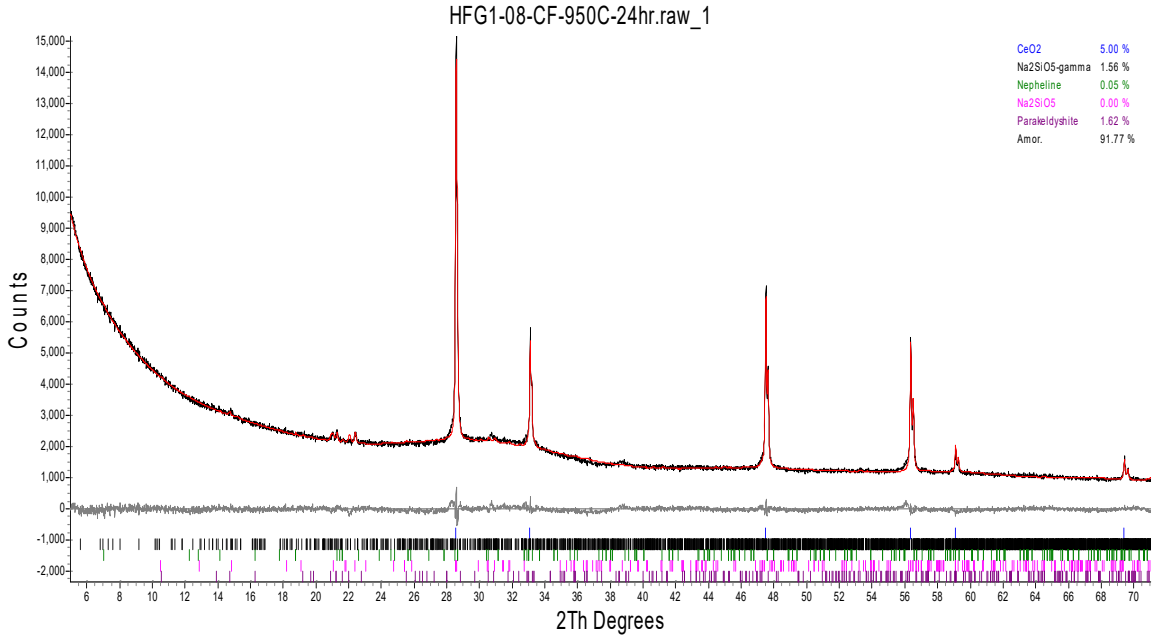

Phase Name	Wt% of Spiked	Wt% in Spiked Sample	Wt% in Original Sample
CeO_2	5.000	5.000	0.000
Na_2SiO_5-gamma	0.000	1.560	1.642
Nepheline	0.000	0.053	0.056
Na_2SiO_5	0.000	0.004	0.004
Parakeldyshite	0.000	1.618	1.703

Figure I.8. XRD Spectrum of CF Heat-Treated Glass HFG1-08

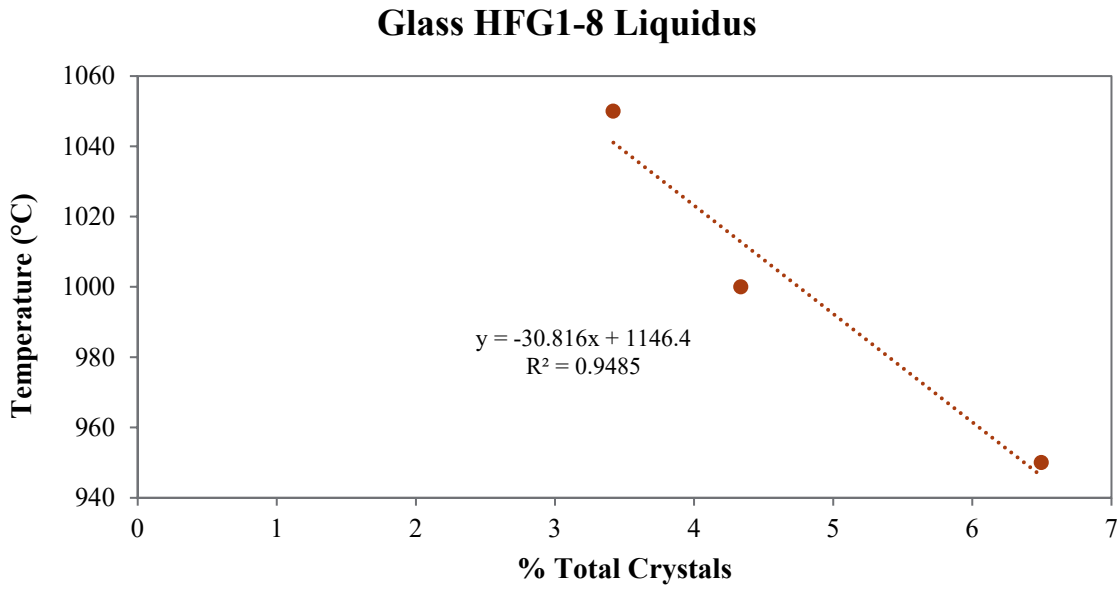

Figure I.9. Liquidus Temperature Determination Plot for Glass HFG1-08

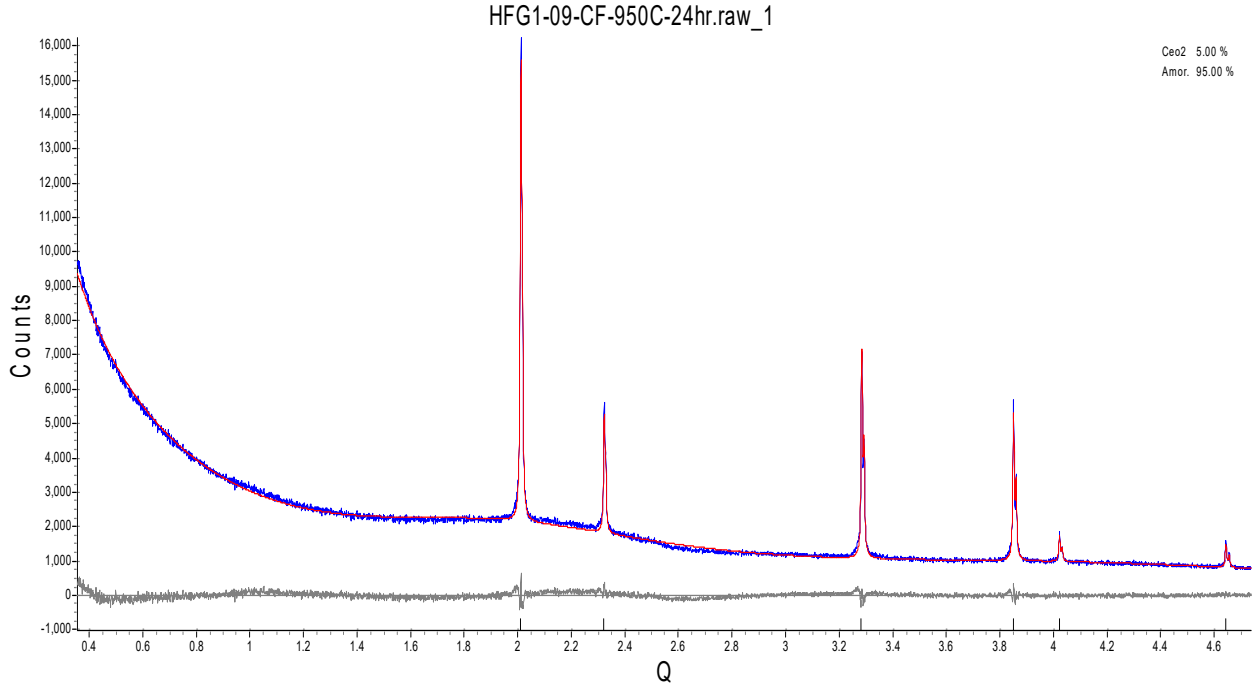

Figure I.10. XRD Spectrum of CF Heat-Treated Glass HFG1-09

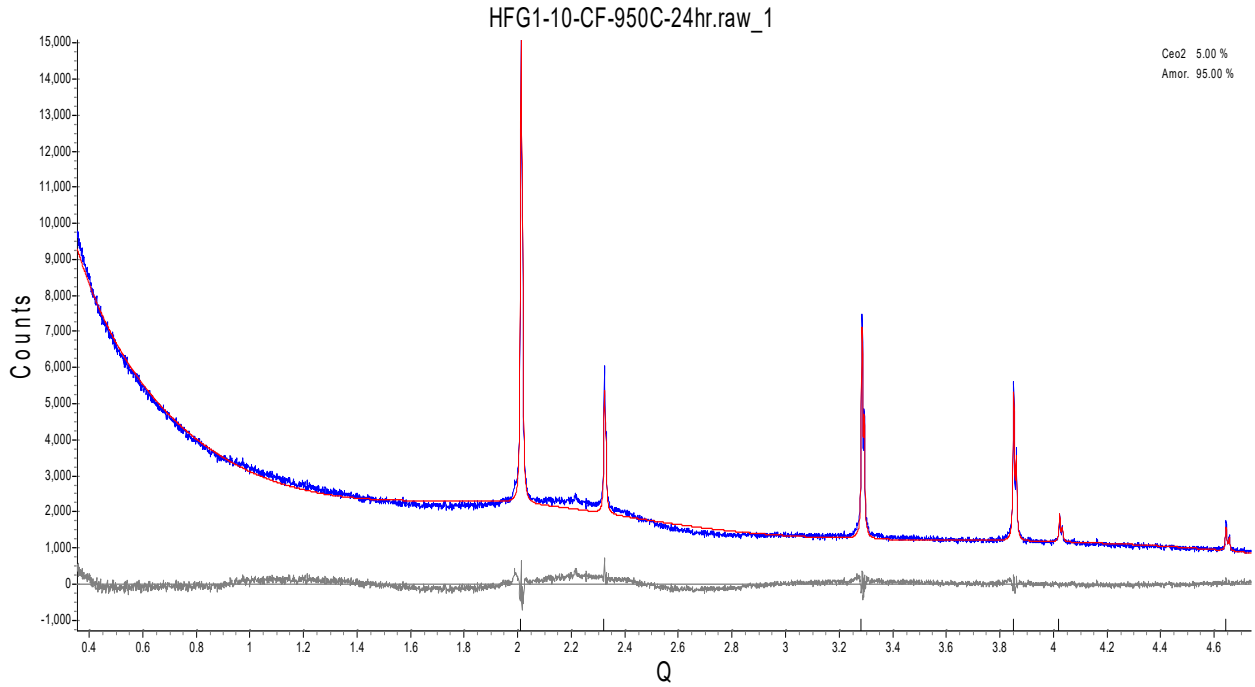

Figure I.11. XRD Spectrum of CF Heat-Treated Glass HFG1-10

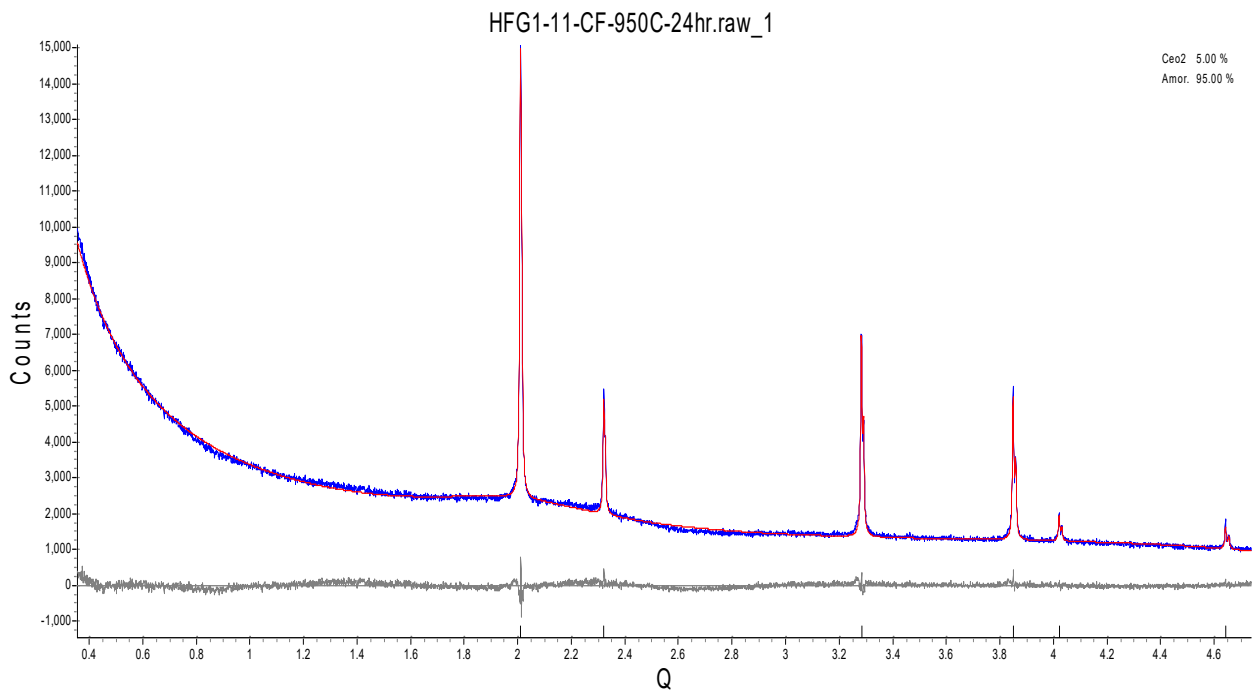

Figure I.12. XRD Spectrum of CF Heat-Treated Glass HFG1-11

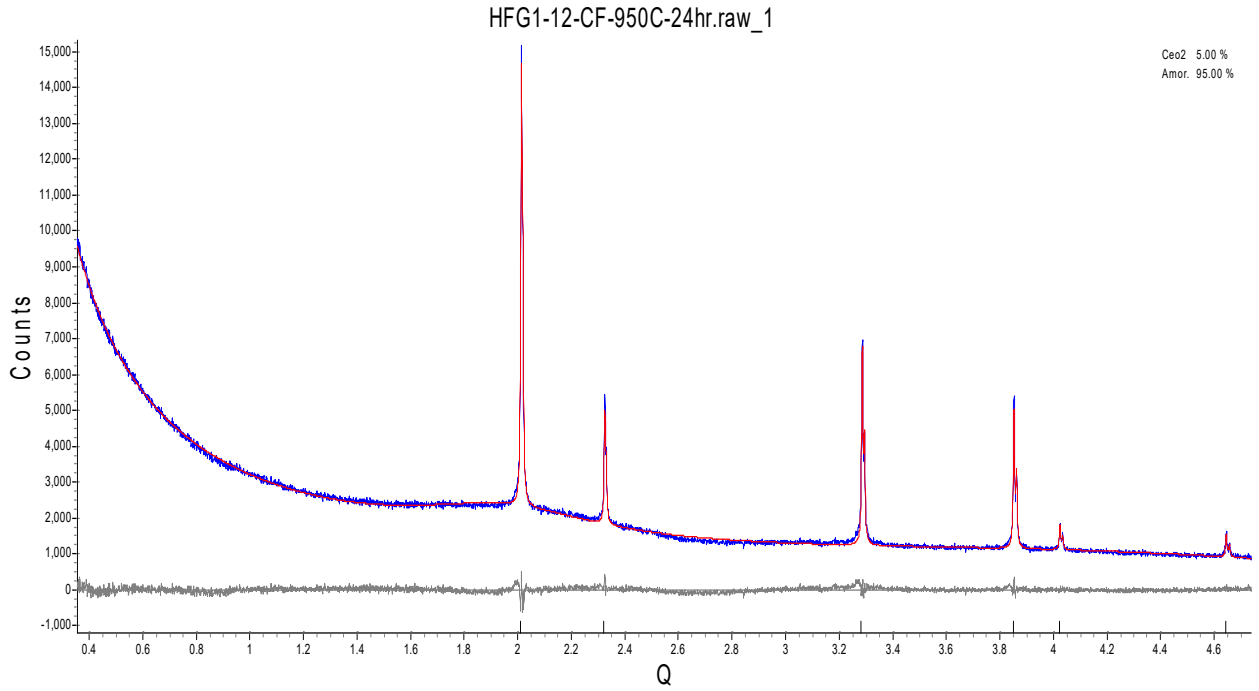

Figure I.13. XRD Spectrum of CF Heat-Treated Glass HFG1-12

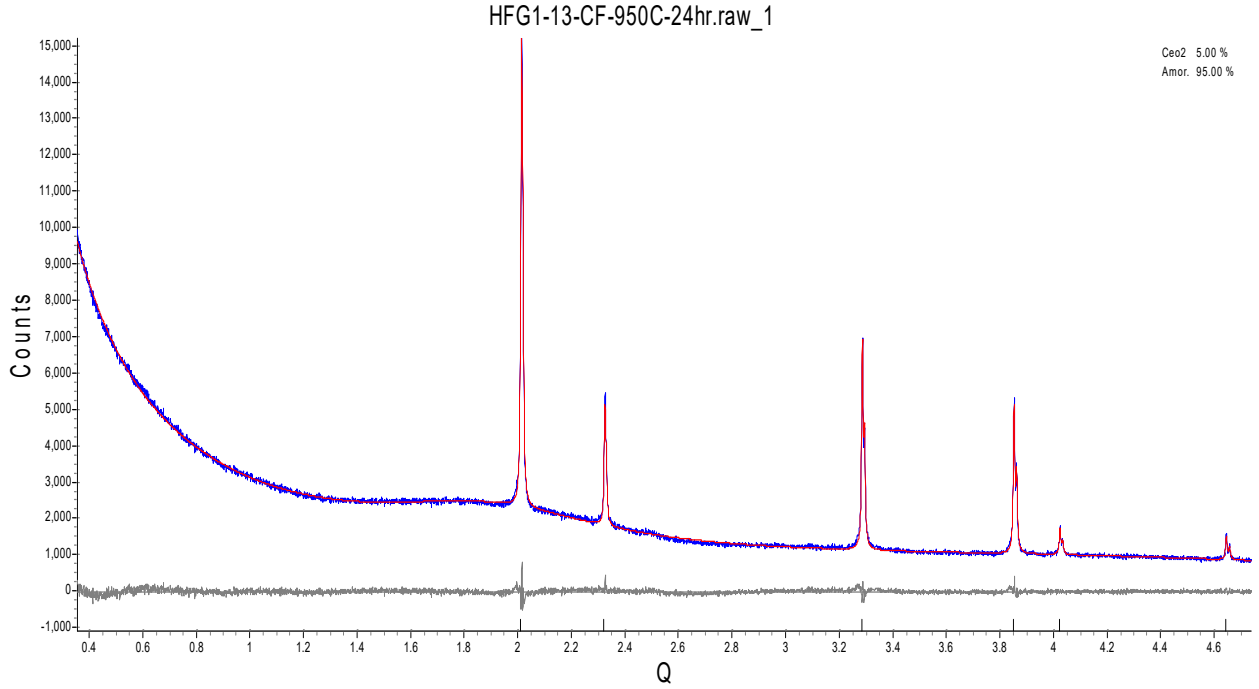

Figure I.14. XRD Spectrum of CF Heat-Treated Glass HFG1-13

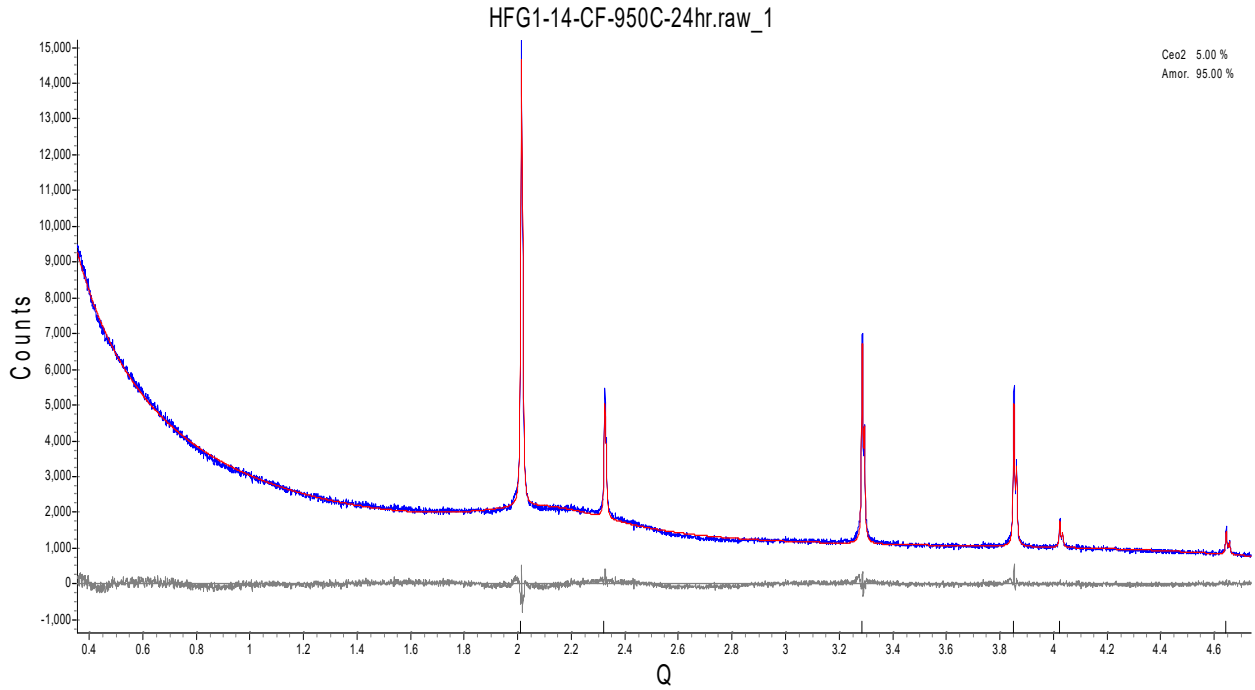

Figure I.15. XRD Spectrum of CF Heat-Treated Glass HFG1-14

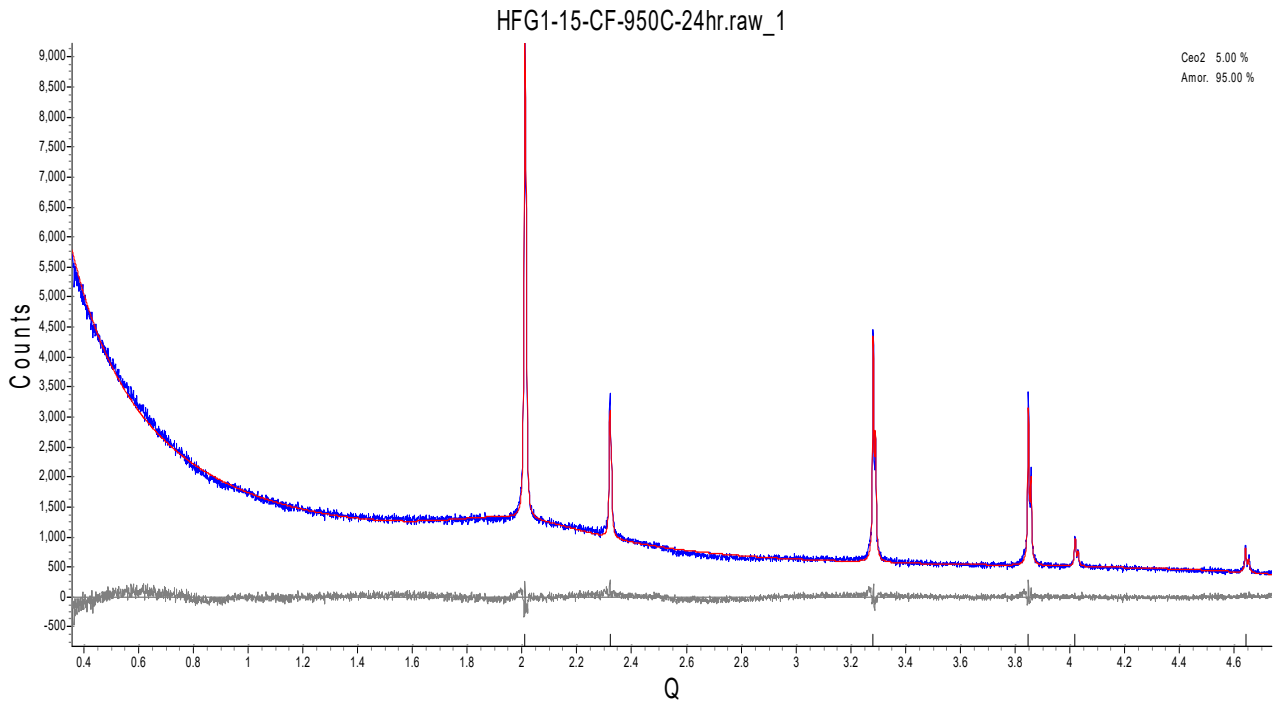

Figure I.16. XRD Spectrum of CF Heat-Treated Glass HFG1-15

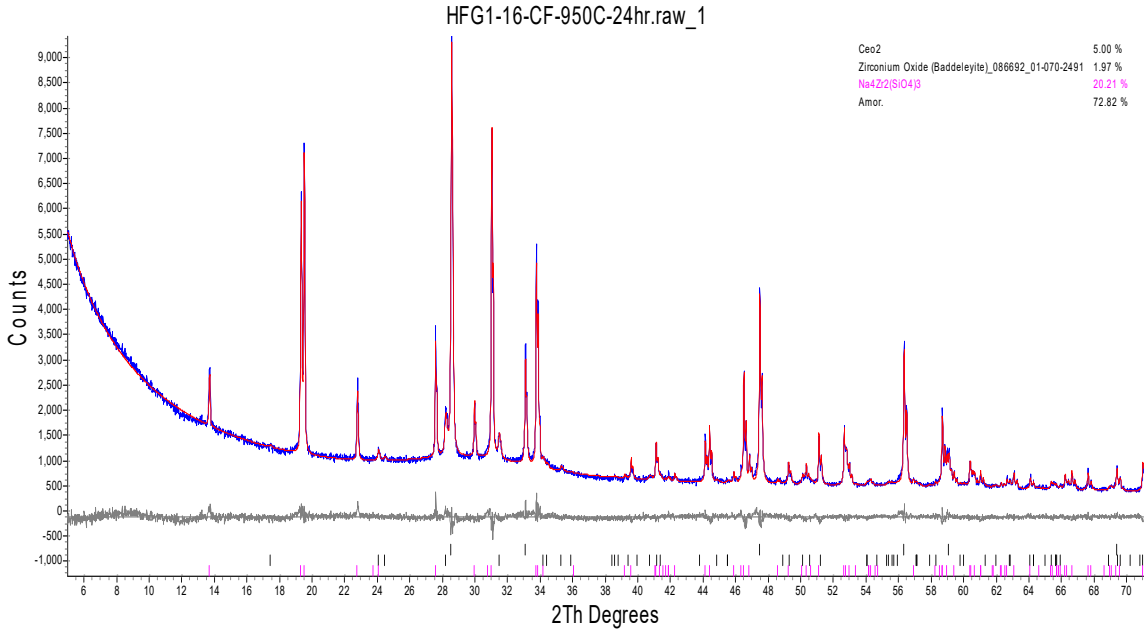

Phase Name	Wt% of Spiked	Wt% in Spiked Sample	Wt% in Original Sample
CeO_2	5.000	5.000	0.000
Baddeleyite	0.000	1.975	2.079
$Na_4Zr_2(SiO_4)_3$	0.000	20.206	21.270

Figure I.17. XRD Spectrum of CF Heat-Treated Glass HFG1-16

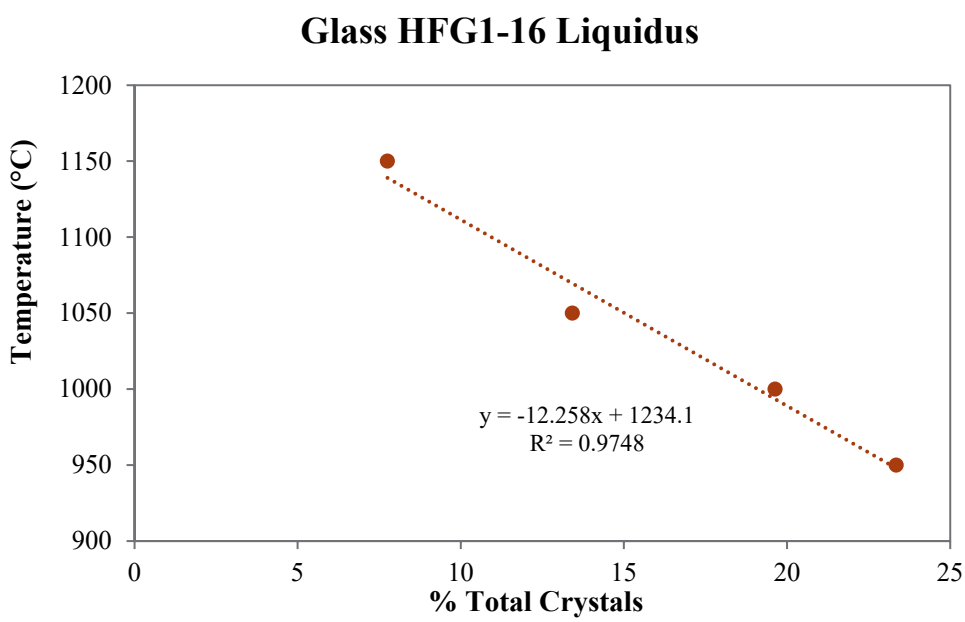

Figure I.18. Liquidus Temperature Determination Plot for Glass HFG1-16

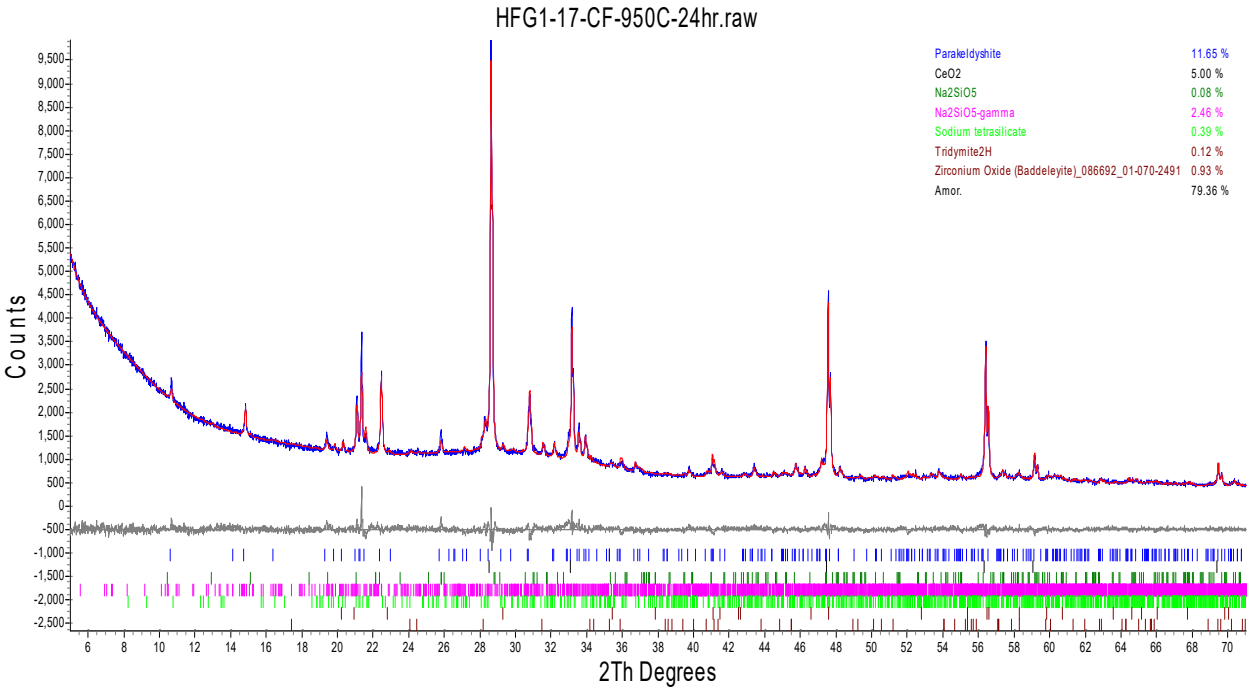

Phase Name	Wt% of Spiked	Wt% in Spiked Sample	Wt% in Original Sample
CeO_2	5.000	5.000	0.000
Parakeldyshite	0.000	11.400	12.000
Na_2SiO_5	0.000	0.090	0.095
Na_2SiO_5-gamma	0.000	2.415	2.542
Sodium tetrasilicate	0.000	0.403	0.424
Tridymite2H	0.000	0.128	0.134

Figure I.19. XRD Spectrum of CF Heat-Treated Glass HFG1-17

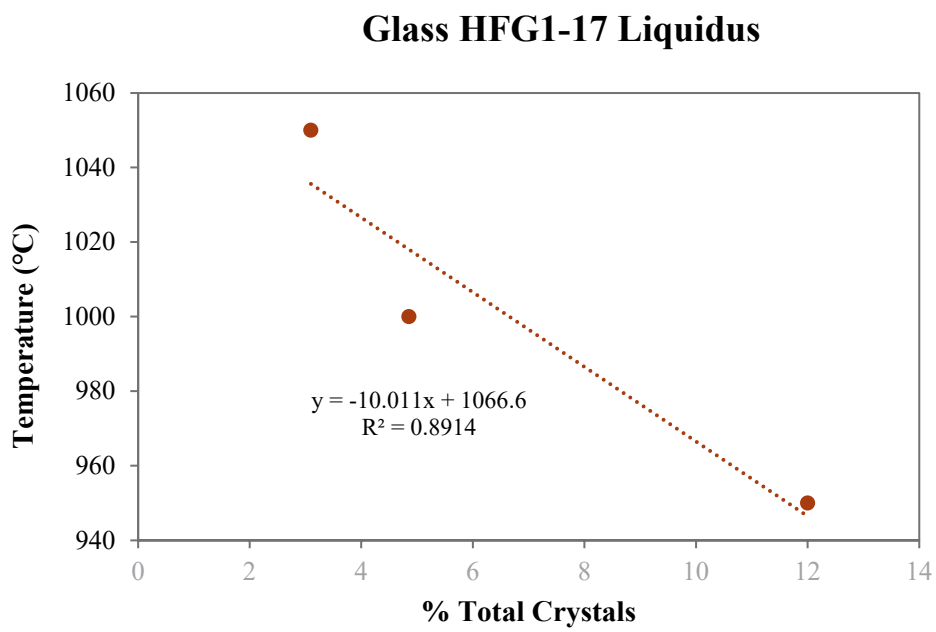

Figure I.20. Liquidus Temperature Determination Plot for Glass HFG1-17

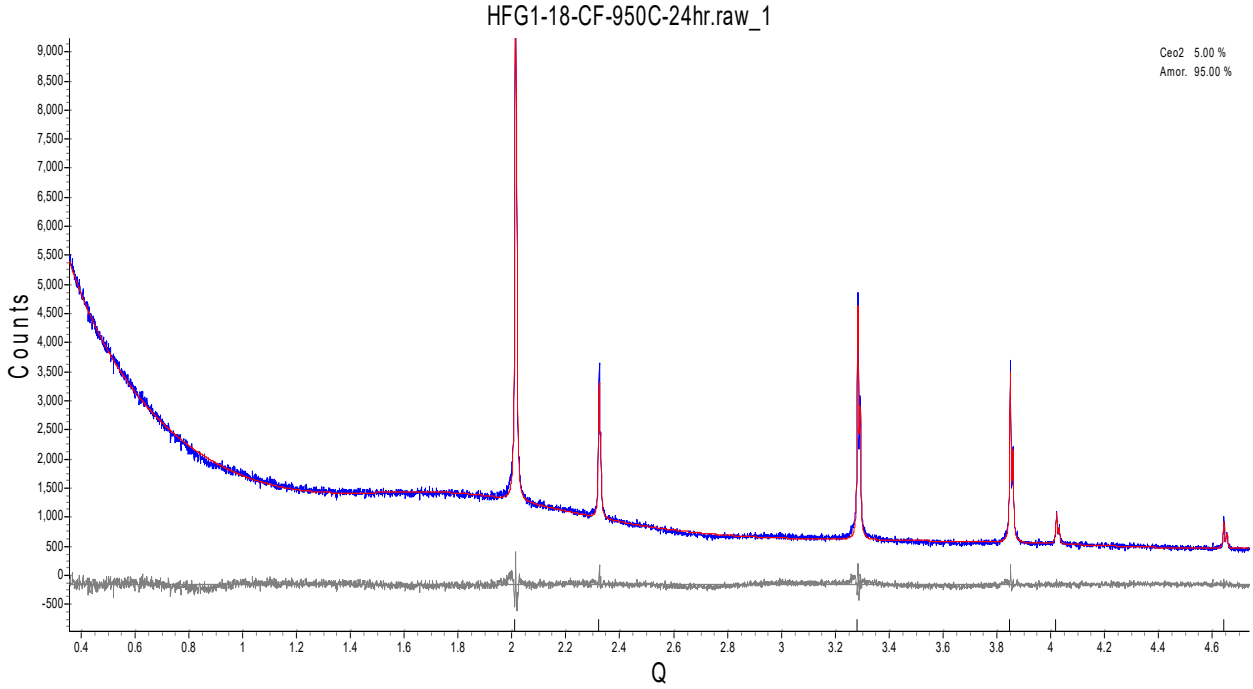

Figure I.21. XRD Spectrum of CF Heat-Treated Glass HFG1-18

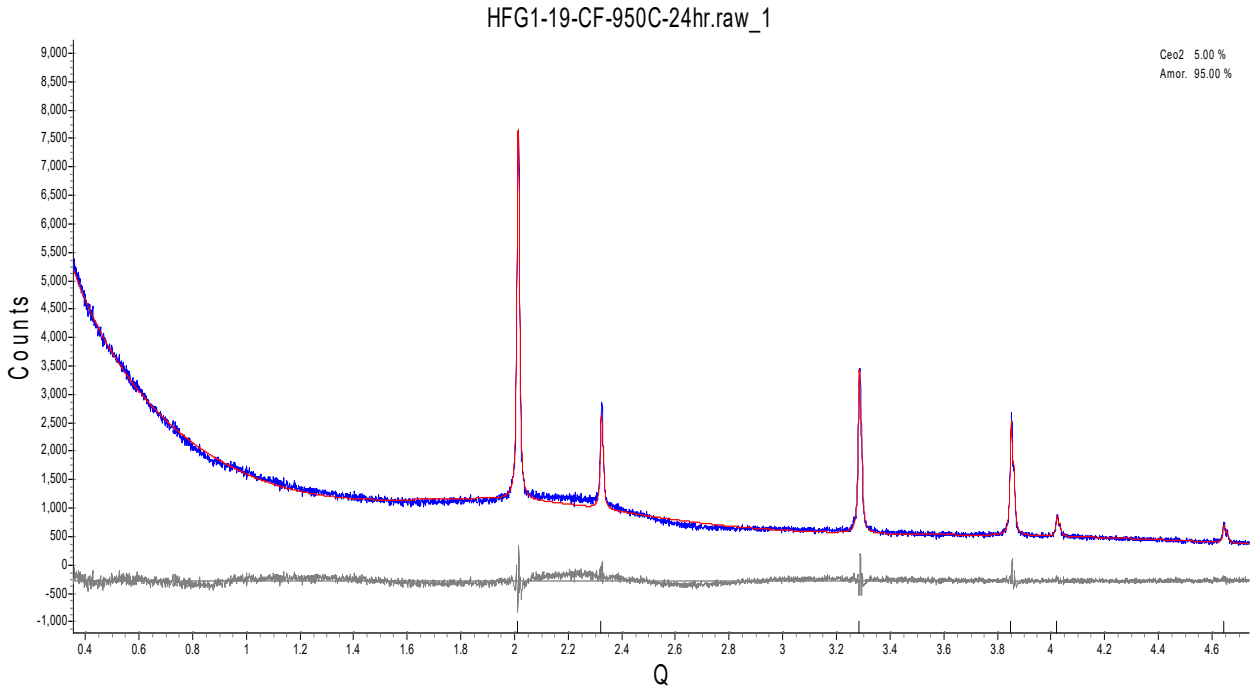

Figure I.22. XRD Spectrum of CF Heat-Treated Glass HFG1-19

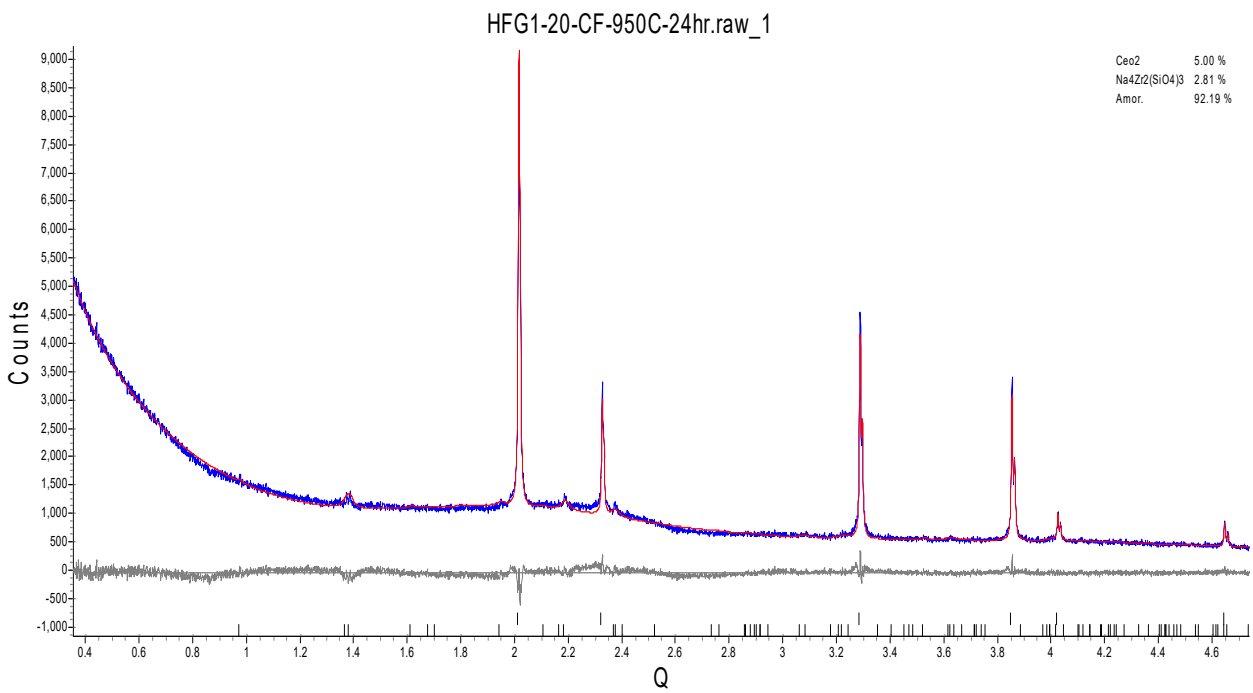

Phase Name	Wt% of Spiked	Wt% in Spiked Sample	Wt% in Original Sample
CeO_2	5.000	5.000	0.000
$Na_4Zr_2(SiO_4)_3$	0.000	2.810	2.958

Figure I.23. XRD Spectrum of CF Heat-Treated Glass HFG1-20

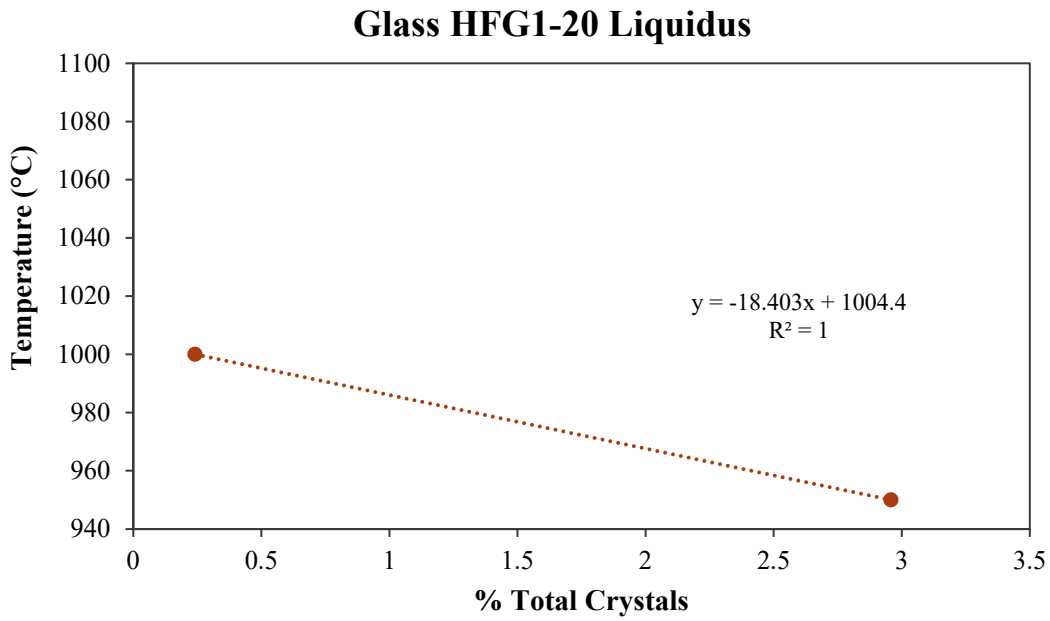

Figure I.24. Liquidus Temperature Determination Plot for Glass HFG1-20

Appendix J – Analyses for Baseline and Sulfur Saturated Glasses and Sulfur Wash Solutions

This appendix presents and compares the normalized compositional analyses of the baseline and sulfur-saturated glasses and wash solutions using ICP-OES and IC. This shows how much sulfur was retained in the glass as well as what was lost from the glass.

Table J.1. Normalized Measured Compositions (mass fractions) for Baseline and Sulfur-Saturated Versions of the High-Fluoride Waste Glasses

	Glass ID											
	HFG1-01-1			HFG1-02			HFG1-03			HFG1-04		
Components	Measured Baseline	Sulfur-saturated	% Diff	Measured Baseline	Sulfur-saturated	% Diff	Measured Baseline	Sulfur-saturated	% Diff	Measured Baseline	Sulfur-saturated	% Diff
Al_2O_3	9.339	9.495	1.67	7.893	8.205	3.95	3.817	3.949	3.46	1.956	1.867	-4.55
B_2O_3	6.722	6.713	-0.13	5.723	5.764	0.72	8.179	8.146	-0.40	9.032	8.967	-0.72
CaO	0.822	0.760	-7.54	2.991	2.700	-9.73	2.165	2.137	-1.29	5.723	5.415	-5.38
Cr_2O_3	<0.146	<0.146	--	<0.146	<0.146	--	<0.146	<0.146	--	<0.146	<0.146	--
F	4.703	3.203	-31.9	5.165	3.623	-25.9	4.513	3.270	-27.5	2.763	2.115	-23.5
Fe_2O_3	0.190	0.200	5.26	0.186	0.197	5.91	0.166	0.180	8.43	0.272	0.274	0.74
K_2O	1.298	1.337	3.00	1.109	0.980	-11.6	0.808	0.727	-10.0	1.358	1.229	-9.50
Li_2O	5.764	5.522	-4.20	1.830	1.526	-16.6	<0.215	<0.215	--	0.683	0.659	-3.51
MnO	<0.129	<0.129	--	<0.129	<0.129	--	<0.129	<0.129	--	<0.129	<0.129	--
Na_2O	13.75	14.424	4.90	14.909	15.266	2.39	17.052	15.465	-9.31	22.916	22.579	-1.47
P_2O_5	<0.229	<0.229	--	<0.229	<0.229	--	<0.229	<0.229	--	<0.229	<0.229	--
SiO_2	44.551	44.016	-1.20	52.627	54.071	2.74	48.134	48.455	0.67	45.139	45.460	0.71
SO_3	0.186	0.891	379	0.137	0.795	480	<0.150	0.695	--	0.241	2.123	781
ZnO	3.327	3.482	4.66	1.344	1.388	3.27	3.121	3.218	3.11	3.333	3.358	0.75
ZrO_2	8.270	7.892	-4.57	4.387	4.248	-3.17	10.600	10.175	-4.01	4.758	4.475	-5.95
Total	99.425	97.935	-1.50	98.301	98.763	0.47	98.555	96.417	-2.17	98.172	98.521	0.36

Table J.1 (cont.)

	Glass ID											
	HFG1-05			HFG1-06			HFG1-07			HFG1-08		
Components	Measured Baseline	Sulfur-saturated	% Diff	Measured Baseline	Sulfur-saturated	% Diff	Measured Baseline	Sulfur-saturated	% Diff	Measured Baseline	Sulfur-saturated	% Diff
Al_2O_3	3.774	3.935	4.27	5.428	5.423	-0.09	9.504	9.476	-0.29	3.278	3.222	-1.71
B_2O_3	9.289	9.217	-0.78	5.941	5.917	-0.40	11.125	11.173	0.43	4.403	4.363	-0.91
CaO	0.338	0.338	0.00	1.377	1.459	5.95	<0.140	<0.140	--	4.523	4.404	-2.63
Cr_2O_3	0.176	<0.147	--	<0.146	<0.146	--	<0.146	<0.146	--	0.163	<0.146	--
F	3.443	2.388	-30.6	4.820	3.520	-27.0	4.008	2.720	-32.1	6.253	4.428	-29.2
Fe_2O_3	0.379	0.404	6.60	0.212	0.209	-1.42	<0.143	<0.143	--	0.371	0.393	5.93
K_2O	0.279	0.242	-13.3	1.221	1.123	-8.03	1.007	1.189	18.1	1.258	1.240	-14.3
Li_2O	3.046	2.847	-6.53	4.048	3.676	-9.19	0.580	0.464	-20.0	0.500	0.503	0.60
MnO	0.186	0.200	7.53	<0.129	<0.129	--	<0.129	<0.129	--	0.183	0.184	0.55
Na_2O	21.534	21.029	-2.35	23.320	22.680	-2.74	18.535	18.198	-1.82	22.748	22.512	-1.04
P_2O_5	0.260	<0.230	--	<0.229	<0.229	--	<0.229	<0.229	--	0.253	<0.229	--
SiO_2	42.465	43.053	1.38	44.551	46.262	3.84	46.423	48.402	4.26	41.930	40.593	-3.19
SO_3	0.381	1.443	279	0.209	1.612	671	<0.125	0.728	--	0.355	1.212	241
ZnO	0.682	0.723	6.01	0.433	0.451	4.16	0.999	1.062	6.31	0.964	0.990	2.70
ZrO_2	11.131	10.752	-3.40	7.298	7.136	-2.22	4.768	4.626	-2.98	12.519	12.123	-3.16
Total	97.363	96.571	-0.81	98.950	99.468	0.52	96.949	98.038	1.12	99.699	96.167	-3.54

Table J.1 (cont.)

	Glass ID											
	HFG1-09			HFG1-10			HFG1-11			HFG1-12		
Components	Measured Baseline	Sulfur-saturated	% Diff	Measured Baseline	Sulfur-saturated	% Diff	Measured Baseline	Sulfur-saturated	% Diff	Measured Baseline	Sulfur-saturated	% Diff
Al_2O_3	5.565	5.971	7.30	6.028	6.089	1.01	7.846	7.794	-0.66	2.806	2.839	1.18
B_2O_3	4.089	4.049	-0.98	9.740	10.304	5.79	9.273	9.153	-1.29	6.697	6.577	-1.79
CaO	5.153	5.282	2.50	3.344	3.505	4.81	<0.140	<0.140	--	5.866	5.894	0.48
Cr_2O_3	0.244	<0.146	--	<0.146	<0.146	--	0.183	<0.146	--	<0.146	<0.146	--
F	6.445	4.585	-28.9	4.090	2.995	-26.8	6.683	4.853	-27.4	6.215	4.520	-27.8
Fe_2O_3	0.364	0.408	12.1	<0.143	<0.143	--	0.356	0.352	-1.12	<0.143	<0.143	--
K_2O	0.386	0.352	-8.81	0.872	0.728	-16.5	0.983	0.866	-11.9	0.678	0.612	-9.73
Li_2O	3.859	3.558	-7.80	3.143	3.052	-2.90	1.560	1.425	-8.65	4.898	4.483	-8.47
MnO	0.175	0.194	10.9	<0.129	<0.129	--	0.174	0.171	1.72	<0.129	<0.129	--
Na_2O	17.996	17.187	-4.50	19.445	19.512	0.34	17.221	17.288	0.39	13.092	13.322	1.76
P_2O_5	<0.229	<0.230	--	<0.229	<0.229	--	0.240	<0.229	--	<0.229	<0.229	--
SiO_2	45.835	46.476	1.40	34.871	37.705	8.13	39.631	40.540	2.29	46.583	47.439	1.84
SO_3	0.359	1.524	325	<0.125	1.266	--	0.313	0.717	129	<0.125	1.313	--
ZnO	3.731	4.011	7.50	3.694	4.027	9.01	2.493	2.511	0.72	0.134	0.142	5.97
ZrO_2	4.177	4.002	-4.19	13.055	13.359	2.33	12.441	11.931	-4.10	12.029	11.485	-4.52
Total	98.608	97.599	-1.02	99.055	102.542	3.52	99.535	97.601	-1.94	99.771	98.626	-1.15

Table J.1 (cont.)

	Glass ID											
	HFG1-13			HFG1-14			HFG1-15			HFG1-16		
Components	Measured Baseline	Sulfur-saturated	% Diff	Measured Baseline	Sulfur-saturated	% Diff	Measured Baseline	Sulfur-saturated	% Diff	Measured Baseline	Sulfur-saturated	% Diff
Al_2O_3	8.389	8.243	-1.74	2.589	2.513	-2.94	4.998	5.040	0.84	8.682	8.337	-3.97
B_2O_3	8.380	8.195	-2.21	4.999	4.604	-7.90	8.235	8.299	0.78	4.257	3.896	-8.48
CaO	3.753	3.533	-5.86	5.737	5.859	2.13	4.852	4.614	-4.91	5.811	5.761	-0.86
Cr_2O_3	<0.146	<0.146	--	<0.146	<0.146	--	0.155	0.147	-5.16	0.139	<0.146	--
F	4.215	2.845	-32.5	4.318	3.133	-27.4	1.958	1.450	-25.9	2.189	1.783	-18.5
Fe_2O_3	0.329	0.326	-0.91	<0.143	<0.143	--	0.355	0.371	4.51	0.278	0.290	4.32
K_2O	0.587	0.565	-3.75	0.164	0.127	-22.6	1.316	1.271	-3.42	1.310	1.139	-13.1
Li_2O	6.486	6.066	-6.48	1.652	1.593	-3.57	4.193	4.177	-0.38	5.842	5.829	-0.22
MnO	0.161	0.156	-3.11	<0.129	<0.129	--	0.172	0.176	2.33	0.139	0.138	-0.72
Na_2O	11.249	13.072	16.21	21.501	21.602	0.47	15.064	15.704	4.25	20.316	19.681	-3.13
P_2O_5	<0.235	<0.229	--	<0.229	<0.229	--	0.247	<0.229	--	0.209	<0.229	--
SiO_2	51.076	50.113	-1.89	49.418	45.941	-7.04	49.257	50.006	1.52	37.396	37.170	-0.60
SO_3	0.297	1.187	300	0.137	1.667	1117	0.330	1.846	459	0.278	1.889	579
ZnO	1.715	1.789	4.31	1.316	1.329	0.99	0.541	0.545	0.74	0.041	<0.124	--
ZrO_2	4.620	4.512	-2.34	8.385	7.693	-8.25	6.322	6.116	-3.26	13.114	11.603	-11.5
Total	100.637	100.602	-0.03	100.862	96.061	-4.76	97.994	99.762	1.80	100.001	97.516	-2.48

Table J.1 (cont.)

	Glass ID											
	HFG1-17			HFG1-18			HFG1-19			HFG1-20		
Components	Measured Baseline	Sulfur-saturated	% Diff	Measured Baseline	Sulfur-saturated	% Diff	Measured Baseline	Sulfur-saturated	% Diff	Measured Baseline	Sulfur-saturated	% Diff
Al_2O_3	4.899	4.804	-1.94	5.069	5.149	1.58	8.791	8.904	1.29	9.325	9.778	4.86
B_2O_3	3.950	3.888	-1.57	11.543	11.849	2.65	8.179	7.985	-2.37	4.299	4.218	-1.88
CaO	3.760	3.855	2.53	0.489	0.477	-2.45	4.845	4.582	-5.43	2.032	2.092	2.95
Cr_2O_3	<0.146	<0.146	--	<0.146	<0.146	--	<0.146	<0.146	--	<0.167	<0.146	--
F	2.463	1.975	-19.8	3.538	2.243	-36.6	5.410	3.733	-31.0	2.683	2.138	-20.3
Fe_2O_3	0.161	0.177	9.94	<0.143	0.161	--	<0.143	<0.143	--	0.236	0.256	8.47
K_2O	0.235	0.190	-19.1	0.407	0.389	-4.42	1.176	1.046	-11.1	<0.120	<0.120	--
Li_2O	6.050	5.565	-8.02	5.178	5.059	-2.30	1.385	1.282	-7.44	4.317	4.177	-3.24
MnO	<0.129	<0.129	--	<0.129	<0.129	--	<0.129	<0.129	--	<0.129	0.131	--
Na_2O	17.153	17.726	3.34	12.958	13.615	5.07	22.141	21.635	-2.29	23.994	22.613	-5.76
P_2O_5	<0.229	<0.229	--	<0.229	<0.229	--	<0.229	<0.229	--	<0.229	<0.229	--
SiO_2	44.141	44.818	1.53	50.648	52.520	3.70	39.631	39.310	-0.81	40.165	41.128	2.40
SO_3	0.166	1.452	775	<0.136	1.019	--	<0.125	1.522	--	0.264	1.613	511
ZnO	2.676	2.763	3.25	2.244	2.387	6.37	3.075	3.103	0.91	3.725	3.868	3.84
ZrO_2	12.828	12.485	-2.67	7.065	6.994	-1.00	5.663	5.376	-5.07	6.768	6.548	-3.25
Total	98.986	99.698	0.72	99.921	101.862	1.94	101.067	98.478	-2.56	98.453	98.560	0.11

Table J.2. Measured Compositions for the High-Fluoride Glass Wash Solutions (mg/L)

Component	HFG-01-1	HFG1-02	HFG1-03	HFG1-04	HFG1-05	HFG1-06	HFG1-07	HFG1-08	HFG1-09	HFG1-10
Al	<1.00	<1.00	<1.00	<1.00	<1.00	<1.00	1.26	<1.00	<1.00	<1.00
B	14.1	10.9	11.6	17.9	27.1	15.8	16.4	15.3	7.38	23.6
Ca	2.52	4.77	11.2	3.88	<1.00	1.69	1.26	1.59	2.26	5.78
Cr	4.77	2.56	2.21	7.81	14.5	8.33	1.12	20.4	11.8	1.27
Fe	<1.00	<1.00	<1.00	<1.00	<1.00	<1.00	<1.00	<1.00	<1.00	<1.00
K	86.8	41.0	30.0	55.7	9.6	42.9	40.7	72.4	16.7	44.2
Li	136.0	68.6	1.52	4.06	27.5	35.1	9.81	8.18	96.5	37.9
Mn	<1.00	<1.00	<1.00	<1.00	<1.00	<1.00	<1.00	<1.00	<1.00	<1.00
Na	811	1030	988	751	1040	967	1060	1410	1020	888
P	<1.00	<1.00	<1.00	<1.00	8.59	4.58	1.68	2.89	<1.00	<1.00
S	625	622	584	412	554	477	600	632	576	524
Si	2.43	4.64	2.93	19.5	12.9	15.1	3.68	9.61	5.59	4.28
Zn	<1.00	<1.00	<1.00	<1.00	<1.00	<1.00	<1.00	<1.00	<1.00	<1.00
Zr	<1.00	<1.00	<1.00	<1.00	<1.00	<1.00	<1.00	<1.00	<1.00	<1.00
F	283	286	115	84.7	168	259	162	446	396	173
PO_4	<10.0	<10.0	<10.0	<10.0	24.9	12.3	<10.0	<10.0	<10.0	<10.0
SO_4	1870	1860	1760	1260	1690	1440	1840	1920	1720	1610

Table J.2 (cont.)

Component	HFG1-11	HFG1-12	HFG1-13	HFG1-14	HFG1-15	HFG1-16	HFG1-17	HFG1-18	HFG1-19	HFG1-20
Al	1.56	<1.00	<1.00	<1.00	<1.00	1.36	<1.00	<1.00	<1.00	1.34
B	16.1	10.8	11.1	8.27	10.7	8.26	6.44	15.4	21.6	10.0
Ca	2.17	1.57	2.63	6.94	7.84	3.3	<1.00	7.49	1.5	1.63
Cr	15.1	1.22	5.75	2.72	6.57	19.7	4.49	1.29	2.41	13.1
Fe	<1.00	<1.00	<1.00	<1.00	<1.00	<1.00	<1.00	<1.00	<1.00	<1.00
K	42	25.5	23.1	5.09	59.3	90.6	12.2	14.5	49.8	2.36
Li	58.9	105	108	12	35.7	36	51.2	97.4	17.4	31.5
Mn	<1.00	<1.00	<1.00	<1.00	<1.00	<1.00	<1.00	<1.00	<1.00	<1.00
Na	1100	666	622	874	642	738	763	625	1030	852
P	2.59	<1.00	<1.00	<1.00	1.23	4.1	<1.00	2.34	<1.00	4.92
S	632	474	510	461	461	466	516	493	507	489
Si	1.58	7.36	5.07	9.86	9.43	12	6.78	5.85	5.89	9.08
Zn	<1.00	<1.00	<1.00	<1.00	<1.00	<1.00	<1.00	<1.00	<1.00	<1.00
Zr	<1.00	<1.00	<1.00	<1.00	<1.00	<1.00	<1.00	<1.00	<1.00	<1.00
F	323	223	157	160	56.6	81.8	96.9	151	257	125
PO_4	<10.0	<10.0	<10.0	<10.0	<10.0	<10.0	<10.0	<10.0	<10.0	13.9
SO_4	1890	1430	1560	1420	1430	1430	1580	1520	1530	1490

Pacific Northwest National Laboratory

902 Battelle Boulevard
P.O. Box 999
Richland, WA 99354
1-888-375-PNNL (7665)

www.pnnl.gov